Theoretical and practical aspects of modelling activated sludge processes

S.C.F. MEIJER
Delft University of Technology, The Netherlands

This study was carried out at the Department of Biotechnological Engineering, Kluyver Laboratory for Biotechnology, Delft University of Technology, the Netherlands.

Front cover layout by Cicero Productions BV, Vught, The Netherlands
Printed by Giethoorn ten Brink BV, Meppel, The Netherlands

ISBN 90-9018027-3

Copyright © 2004 by S.C.F. Meijer

Cover photograph: The mouths of the Ganges delta, Bangladesh.
Photographed from the space shuttle on the 22nd of September 1997, 04:41.
With courtesy of Earth Sciences and Image Analysis Laboratory, NASA Johnson Space Centre (mission STS087, roll 707, frame 92, http://eol.jsc.nasa.gov).

Theoretische en Praktische Aspecten van het Modelleren van Actiefslibprocessen

Proefschrift

ter verkrijging van de graad van doctor aan de Technische Universiteit Delft, op gezag van de Rector Magnificus prof. dr ir J.T. Fokkema, voorzitter van het College voor promoties, in het openbaar te verdedigen op dinsdag 27 april 2004 om 15:30 uur

door

Sebastiaan Carel Fred MEIJER

landbouwkundig ingenieur,
geboren 5 februari 1969, te Leiden

Dit proefschrift is goedgekeurd door de promotoren:

Prof. dr ir J.J. Heijnen

Prof. dr ir M.C.M. van Loosdrecht

Samenstelling promotiecommissie:

Rector Magnificus, voorzitter

Prof. dr ir J.J. Heijnen, Technische Universiteit Delft, promotor

Prof. dr ir M.C.M. van Loosdrecht, Technische Universiteit Delft, promotor

Prof. dr H. Siegrist, ETH, Zürich

Prof. dr ir G. van Straten, Wageningen Universiteit

Prof. dr ir C.J.N. Buisman, Wageningen Universiteit

Prof. ir J.H.J.M van der Graaf, Technische Universiteit Delft

Ing. F.A. Brandse, Waterschap Reest en Wieden, adviseur

Het in dit proefschrift beschreven onderzoek is uitgevoerd in het Kluyverlaboratorium voor Biotechnologie, Technisch Universiteit Delft, Julianalaan 67, 2628 BC te Delft.

to my parents, for their support and encouragement

to Irenka, for her patience and love

Acknowledgements

This research was supervised and facilitated by the Delft University of Technology, department of bio-chemical engineering. The research was financially supported by the Dutch foundation of technical sciences (STW) and the Dutch foundation of applied water research (STOWA). All full-scale analytical measurements were financed and facilitated by the Dutch water-boards Groot Salland, Uitwaterende Sluizen in Hollands Noorderkwartier and Velt en Vecht. Additional funds were supplied by technical consultants Witteveen en Bos.

I would like to thank Frank Brandse of the water board Reest & Wieden, and the technical and analytical staff of the water boards Groot Salland and Velt & Vecht for their technical support and co-operation in obtaining data from the wastewater treatment plant Hardenberg. In addition, I would like to thank Elbert Majoor and Judith van der Wijk for their contribution to the implementation of the full-scale redox control at wastewater treatment plant Hardenberg.

Part of this research was facilitated by the International institute for Hydraulics and Environmental engineering (IHE). I would like to thank Susi Susanti for her scientific contribution and Tineke Hooimans and Hielke van der Spoel for their supervision. Also I would like to thank the technical and analytical staff of the water board Uitwaterende Sluizen in Hollands Noorderkwartier for their co-operation and for obtaining data from wastewater treatment plant Katwoude.

Finally, I would like to thank Jan Willem Mulder (ZHEW), Paul Roeleveld (STOWA), Frank Brandse (Groot Salland), Henry van Veldhuizen (Grontmij), Paul Versteeg (Hoogheemraadschap Rijnland), Peter de Jong (Witteveen en Bos) and Nico Boots (STW) for their contribution to the research supervision committee.

Time

a soliloquy by sir Lawrence of Olivier from the musical "Time"

Stand before me on the sign of infinity, all of you who are of the earth. With the granting of the law of profanation, comes the application of change.

I will give you this key. And with this knowledge, please realise, comes the responsibility of sharing it.

I will show you the way, it is very simple.

Throughout the universe there is order, in the movement of the planets, in nature and in the functioning of the human mind.

A mind that is in it's natural state of order, is in harmony with the universe. Such a mind is timeless.

Your life is an expression of your mind. You are the creator of your own universe, for as a human being, you are free to will whatever state of being you desire through the use of your thoughts and words.

Now, there is a great power in here. It can be a blessing or a curse, it is entirely up to you. For the quality of your life, is brought about by the quality of your thinking. Think about that.

Thoughts produce actions. Look at what you are thinking. See the pettiness, and the envy, and the greed, and the fear, and all other attitudes that cause you pain and discomfort.

Realise that the one thing you have absolute control over is your attitude.

See the effect it has on those around you. For each life is linked to all life, and your words carry with them chain reactions, like a stone that is thrown into a pond.

If your thinking is in order, your words will flow directly from the hart, creating ripples of love.

If you truly want to change your world, you must change your thinking.

Reason is your greatest tool, as it creates an atmosphere of understanding, which leads to caring, which is love.

Choose your words with care, and go forth, with love…

Table of Contents

1

General Introduction

In the field of domestic wastewater treatment, there is an increasing requirement to improve effluent quality for the benefit of receiving surface waters. Additionally, it is required to minimise energy consumption and reduce the use of chemicals in the treatment process. Research at the department of bio-engineering of the Delft university of technology has shown that biological phosphorus removal in wastewater treatment contributes to a more efficient nitrogen and phosphorus removal. Hereby energy consumption and the use of chemicals are reduced considerably. Since 1990, a metabolic model describing this process was developed. This largely was done in the framework of the task group for modelling activated sludge systems of the International Association for Water Quality (IAWQ). The metabolic model, is a mathematical description of the cell-internal metabolism of the total microbial population capable of biological phosphorus removal. In previous research it was shown that the metabolic modelling approach leads to a more consistent model with less model parameters.

1.1 Introduction

The most common method for treatment of domestic wastewater is the activated sludge process. In this process pollutants are degraded by a bacterial suspension (the activated sludge). The first activated sludge processes mainly removed organic pollutants (COD) and pathogenic organisms. Improved process designs facilitated the biological removal of phosphorus and nitrogen. Historically, the discharge of nutrients via domestic wastewater was the main cause for eutrophication, which is the excessive growth of algae in surface and coastal waters. In the past two decades, several new wastewater treatment concepts have been developed. Development of an optimal process for enhanced biological phosphorus removal (EBPR or BioP), especially proved a challenge. This is mainly caused by the complex metabolism of the micro-organisms capable of EBPR. A review on the development of nutrient removing wastewater treatment processes was published by Jeppsson (1996), and is briefly discussed in the following paragraph.

1.1.1 Enhanced biological phosphorus removal

The main requirement for EBPR is the recycle of activated sludge through anaerobic and aerobic (or anoxic) phases. Hereby, substrate is taken up by phosphorus accumulating micro-organisms (PAO's) under anaerobic conditions (fig. 1.1). On the basis of this observation it was concluded that to achieve EBPR, an anaerobic reactor should be introduced in front of a conventional activated sludge process (fig. 1.1a). This process is known as the "two-stage Phoredox process" or the "A/O process" (Hong *et al.*, 1982). To remove organic carbon (TOC), nitrogen (N) and phosphorus (P) within a single-sludge system, several designs were proposed. A process with good EBPR properties and a low effluent nitrate concentration is the "modified Bardenpho process" or "five-stage Phoredox process" (Barnard, 1975) (fig. 1.1b). When only partial N removal is required, this process can be reduced to three stages. This process is often referred to as the "three-stage Phoredox process" or "A2/O process" (Barnard, 1983) (fig. 1.1c). When it was recognised that recycle of nitrate to the anaerobic reactor had an inhibiting effect on the BioP process (Nicholls, 1975; Barnard, 1976), several improved WWTP designs were proposed. These processes are the "University of Cape Town" or UCT process (Ekama *et al.*, 1984) (fig. 1.1d), the "modified UCT" or MUCT process (fig. 1.1f) and the "Johannesburg process" (Dold *et al.*, 1991) (fig. 1.1e). Based on the MUCT process, Brandse of the Waterboard "Groot Salland" (the Netherlands), proposed a WWTP design optimised for denitrifying EBPR (van Loosdrecht *et al.*,

1998). This process is referred to as the "BCFS® process" (fig. 1.1g) and is described in more detail in chapter 3.

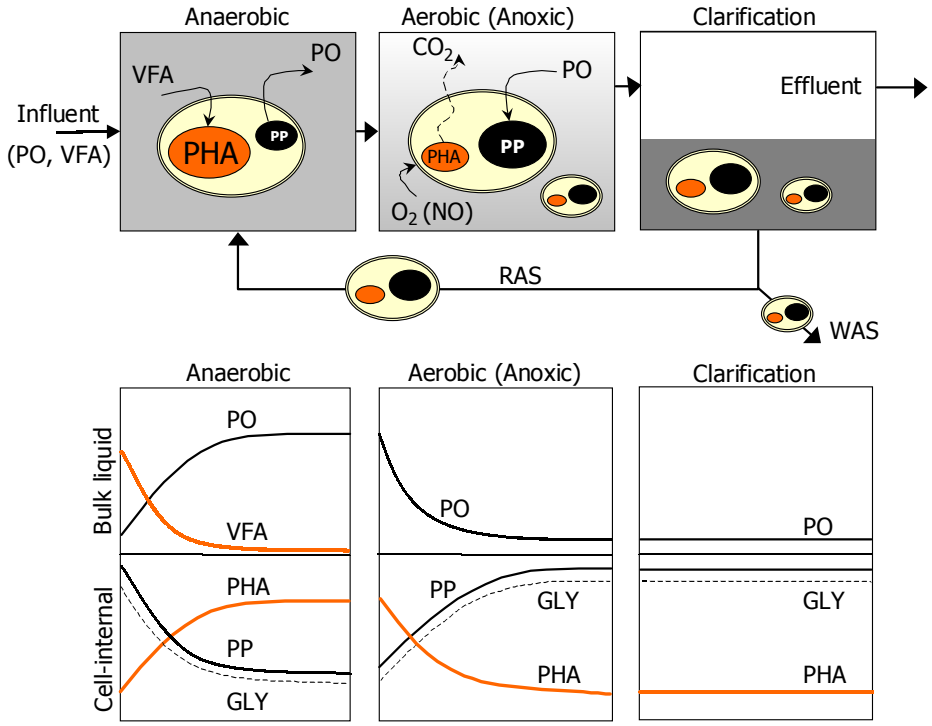

Figure 1.1 **Schematic representation of the BioP process.** A typical EBPR process layout is shown with in the graphs the typical concentration dynamics in the bulk liquid (top) and inside the biomass (bottom). EBPR depends on alternating anaerobic, anoxic and aerobic conditions. The process is cyclic, provided by the return activated sludge (RAS). Phosphorus (P) is removed from the system with the waste activated sludge (WAS). Provided by the storage polymers, PAO's are capable of taking up substrate under anaerobic conditions, which is their competitive advantage in the bacterial suspension.

1.1.2 Model development and refinement

A model is a description of reality, used to understand and predict certain aspects of reality. Often processes in nature are far to complex to be understood in all detail (e.g. the activated sludge process). For the sake of understanding, simplification often is necessary. A simplified description of a natural process, can be the first step towards a process model. The perspective and the extent of simplification, will determine the application of the model.

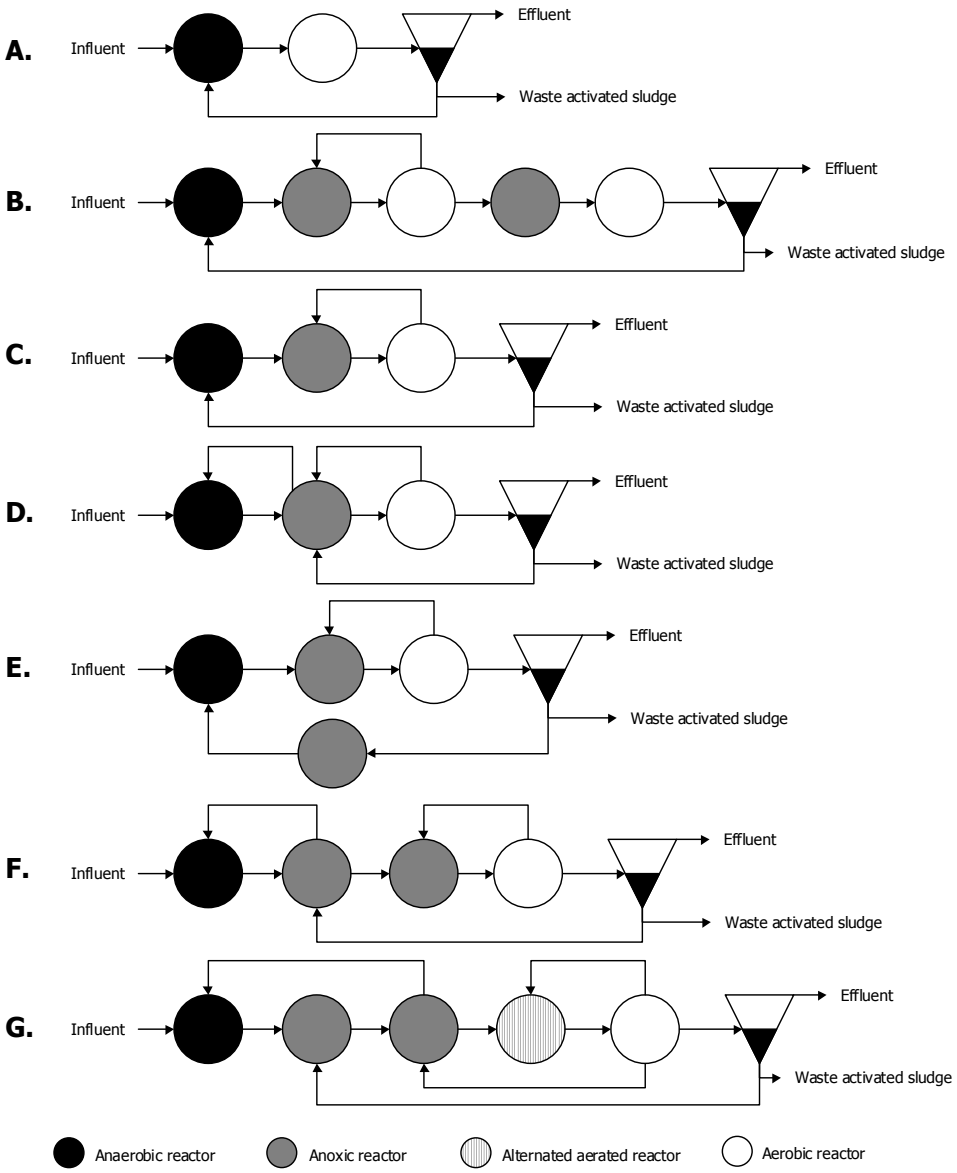

Figure 1.2 **Schematic representation of seven BNR processes.** All examples are continuos mainstream single sludge process and to a certain extent equipped for EBPR. **A**: two stage Phoredox (A/O) process, **B**: five stage Phoredox (modified Bardenpho) process, **C**: three stage Phoredox (A2/O) process, **D**: UCT process, **E**: Johannesburg process, **F**: MUCT process and **G**: BCFS® process.

In activated sludge, a wide variety of micro-organisms are responsible for conversion of pollutants. A comprehensive model that intends to describe all processes will be complicated and impractical in use. On the other hand, oversimplification leads to a model that lacks refinement and does not give additional information. A compromise therefore has to be found between these two extremes. A well known method for functional model design is based on the macroscopic system description. Hereby, systems are treated in terms of macroscopic variables, e.g. mass and energy.

A well known example of a macroscopic system description is the 'black-box' model. In a black-box model the actual process is unknown. What is observed from the process (black-box) is the exchange of compounds, e.g. substrate and reaction products, with the environment. A black-box model only describes the system behaviour under specified conditions. What happens in the actual process remains unknown.

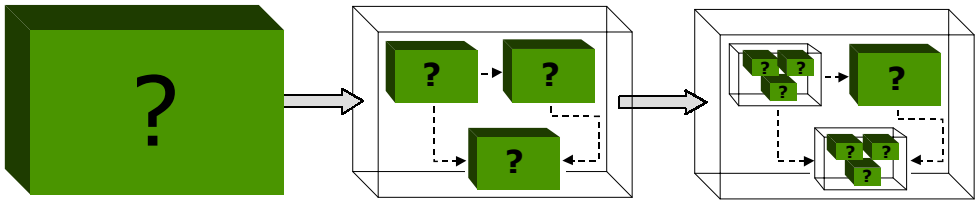

Figure 1.3 Schematic representation of the step-wise refinement of a model. The Black-box (left) is refined towards a grey-box model (right). The grey-box model consists of an ensemble of black-box models. By increasing the model refinement, more details can be studied. Such models will however also be more complex, expressed by an increase of modelled processes and parameters (Smolders, 1995a).

If one starts investigating a system, the system as a whole will be unknown (fig. 1.3). The system therefore is considered as a black box. After some experimentation, possibly mechanisms or sub-systems are elucidated. These subsystems will be considered as new black-boxes, and so forth. An example for this, is the description of the microbial cell. In a general description, the whole cell can be considered as a black-box. A model that relies on this description is the Monod model for microbial growth. With advance of knowledge, certain aspects of the cell-internal metabolism were elucidated. When these new aspects were included in the model, this resulted in a grey-box model in which parts of the cell-internal metabolism were described explicitly. Such a model is called a metabolic model. The main topic of this research is the development and evaluation of a metabolic model for enhanced biological P removal.

In nature, all organisms share a limited number of universal metabolic pathways. It could therefore be more direct to model these common pathways, than to model each type of micro-organism separately. The metabolic BioP model is based on this principle. Although there are possibly several types of micro-organisms capable of EBPR, one general metabolic pathway can be used to describe the total PAO population.

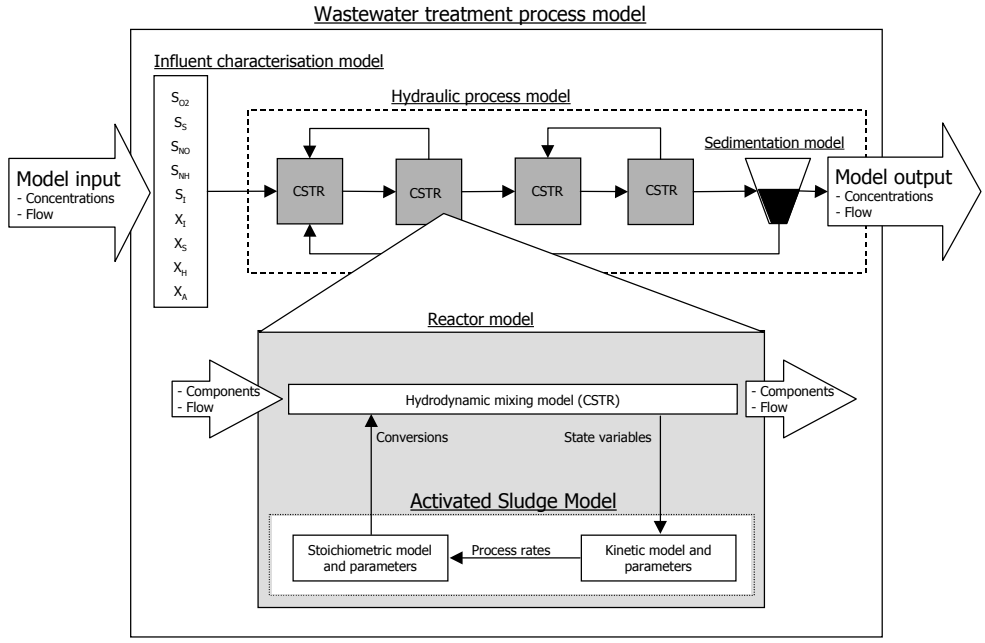

Figure 1.4 Schematic representation of a WWTP model. An ensemble of sub-models is shown whereof a WWTP model is constructed. The model input is calculated from the influent characterisation model. For each reactor model, a hydrodynamic mixing model describes mass transport. The activated sludge model describes biological conversions. Mass transport between the different reactors is described by the process model. A sedimentation tank model describes the separation of sludge from the liquid phase. The individual sub-models are all linked by their in- and outputs.

1.1.3 Wastewater treatment process models

A model of a WWTP is an ensemble of sub-models, together describing the overall treatment process (fig. 1.4). In this ensemble, the activated sludge model describes the biological conversions in the activated sludge. Reactor models describe mass transport and hydraulic behaviour of the separate reactors (e.g. ideally mixed or plug flow, constant versus variable volume,

etc.). The hydraulic process model describes the flows between separate reactors, such as return activated sludge (RAS) and recycle flows. Finally, a sedimentation tank model describes the separation by gravity of solids from the liquid phase in the clarifier tank. Furthermore, there is the influent characterisation model, which calculates the model input based on the chemical wastewater composition.

1.2 General Context

There is an increasing need to improve the effluent quality of domestic wastewater treatment processes. National and international regulation requires a decrease of nutrients being discharged on surface waters. To meet this requirement, a large number of existing WWTP's need to be optimised and extended in the near future. Also the use of energy and chemicals in the treatment process should be minimised. An application that meets these requirements is EBPR.

Research at the department of bio-chemical engineering of the Delft University of Technology in the Netherlands, has shown that EBPR under mainly denitrifying conditions, contributes to a more efficient removal of nutrients and requires less energy and additional chemicals. It was shown that the micro-organisms responsible for this process are commonly present in most WWTP's. Therefore, by improving WWTP designs, better use of the potential of EBPR can be made.

Activated sludge is a comprehensive microbial ecosystem in which a range of pollutants is degraded under alternating anaerobic, anoxic and aerobic conditions. To understand and control such a complex biotechnological process, reliable process models are required. On the bases of such models, new treatment and control concepts can be developed and existing WWTP's can be optimised.

Compared to biological N removal, EBPR is a more complex. PAO's have a cyclic anaerobic, anoxic and aerobic metabolism based on three cell internal storage compounds; poly-phosphate (PP), poly-hydroxyalkanoate (PHA) and glycogen. For an accurate description of EBPR, the cell internal conversions and formations of these storage compounds have to be modelled. Since 1990, the department of bio-chemical engineering of the Delft University of Technology has been working on such a metabolic model. The first partial models, describing the anaerobic, aerobic and anoxic metabolism of PAO's were developed on the basis of lab-scale (sequencing batch reactor) experiments (Smolders *et al.*, 1995b, Kuba *et al.*, 1996 and Murnleitner *et al.*, 1997). Based on their research, WWTP Holten (the Netherlands) was optimised for denitrifying EBPR. Here the

metabolic EBPR model was tested for the first time at full-scale conditions (van Veldhuizen *et al.*, 1999). A second full-scale simulation of WWTP Haarlem-Waarderpolder by Brdjanovic *et al.* (2000), showed shortcomings in the kinetic structure of the metabolic model. It is from this point on, that we continue the research in this thesis.

The research at the Delft University of Technology was associated with the IAWQ (International Association for Water Quality) task group for modelling of activated sludge systems. The metabolic modelling concept is fundamentally different from the approach used in the IAWQ activated sludge models (ASM). The more black-box modelling approach used for the IAWQ-models, has shown to be successful for description of COD and N removal (i.e. heterotrophic growth, nitrification and denitrification). For EBPR however, this approach is less suitable. Modelling EBPR based on a metabolic description results in a model with less model parameters and is more consistent. Owed to the standard IAWQ model matrix notation, it was possible to combine both model concepts in one integrated model. On itself, the metabolic phosphorus model describes enriched (lab-scale) PAO cultures. When combined with the COD and nitrogen models of the IAWQ ASM-1, -2, -2d or -3, also EBPR in (full-scale) activated sludge processes can be described.

1.3 Problem Definition

In 1999, the metabolic EBPR model was integrated with ASM2d (Henze *et al.*, 1999). This model (the TUD model) was tested on three full-scale WWTP's (van Veldhuizen *et al.*, 1999; Wichern *et al.,* 1999 and Brdjanovic *et al.*, 2000). Although the first full-scale simulations were promising, several questions arose concerning the reliability of the model kinetics. It was concluded that the applicability of the model was poor, and that a better method for model calibration was needed. Moreover, the necessity was shown for a method to handle and evaluate large quantities of (input) data used for simulation purposes. Brdjanovic *et al.* (2000), showed that errors in measurements and operational data caused ambiguous simulation results. This brought up questions concerning the reliability of the model and reproducibility of the simulation results.

1.4 Research Objectives

The general objective of activated sludge research is to understand and master the biological processes and interactions in full-scale activated sludge systems. This requires a dynamic process model that describes the

physiology of the individual micro-organisms, as well as the ecological interactions in activated sludge processes. Improved process knowledge eventually should result in the development of more efficient wastewater treatment processes.

The goal of this research is to improve the full-scale performance of the integrated metabolic BioP model. In previous publications, the model was tested at full-scale. In this research the testing is continued. To gain experience with the integrated model, the model will be used to simulate a range of lab- and full-scale conditions. Hereby, it is a specific goal to identify the bottlenecks in modelling full-scale wastewater treatment processes. A major known bottleneck is the model calibration. It is intended to find a more straightforward and practical method to calibrate the model. Furthermore, it will be needed to specify the model reliability, and make more explicit under which conditions and for what purposes the model should and should not be used. In this evaluation process, the model will be refined were needed. Also possibilities will be investigated to simplify and reduce the model and to improve the practical applicability. Eventually, it is the goal to improve the model as a tool for the development, design and optimisation of wastewater treatment plants.

1.5 Structure and Outline of the Thesis

The thesis consists of 9 chapters and several appendices. Generally in chapters 1 and 2 the metabolic model is described, in chapters 3 to 6 the model is tested and in chapters 7 and 8 the model is put into practice. In chapter 9 the conclusions and outlook are presented. Chapter 1 is a general introduction to this research. Chapter 2 is a more specific introduction to the metabolic BioP model. The goal of this introduction is to obtain a better understanding of the stoichiometric and kinetic structure of the metabolic model. In chapters 3 and 4, the model is validated at full-scale conditions. Chapter 3 describes the simulation of a full-scale nutrient removing WWTP at steady state conditions. In chapter 4, the start-up of a full-scale WWTP is simulated. Under start-up conditions model kinetics can be tested more extensively than is possible at steady state conditions. In chapter 5, a method presented for data evaluation and model calibration. The method is tested in a full-scale simulation study. In chapter 6, all previous modelling experiences with the metabolic BioP model are evaluated. The adapted model is tested on the basis of several lab-scale experiments. The updated version of the integrated model is presented in appendix III. In chapters 7 and 8, the model is put into practice. In a case study, a process control based on the

oxidation reduction potential was evaluated. On the basis of a literature study, in chapter 7 the physical meaning of measuring the oxidation reduction potential in activated sludge is discussed. In chapter 8, it is demonstrated how the model can be used for (ORP related) process control and control design.

References

Barnard J. L. (1975) Biological nutrient removal without the addition of chemicals. *Wat. Res.* **9**, 485-490.

Barnard J. L. (1976) A review of biological phosphorus removal in the activated sludge process. *Water SA.* **2**(3), 126-144.

Barnard J. L. (1983) Background to Biological Phosphorus Removal. *Wat. Sci. Tech.*, **15**(3-4), 1-13.

Brdjanovic D., van Loosdrecht M. C. M., Versteeg P., Hooijmans C. M., Alaerts G. J. and Heijnen J. J. (2000) Modeling COD, N and P removal in a full-scale WWTP Haarlem Waarderpolder. *Wat. Res.* **34**(3), 846-858.

Dold P. L., Wentzel M. C., Billing A. E., Ekama G. A. and Marais G. v. R. (1991) Activated Sludge System Simulation Programs. Water Research Commission, Pretoria, South Africa.

Ekama G. A., Marais G. v. R. and Siebritz I. P. (1984) Biological excess phosphorus removal. *Theory design and operation of nutrient removal activated sludge processes* **7**, 1-32. Water Research Commission, Pretoria, South Africa.

Henze M., Gujer W., Mino T., Matsuo T., Wentzel M. C., Marais G. v. R. and van Loosdrecht M. C. M. (1999) Activated Sludge Model No.2d, ASM2d. *Wat. Sci. Tech.* **39**(1), 165-182.

Hong S. -N., Krichten D. J., Kisenbauwer K. S. and Sell R. L. (1982) A biological wastewater treatment system for nutrient removal. EPA Workshop on Biological Phosphorus Removal in municipal wastewater treatement, Annapolis, Md.

Jeppsson U. (1996) Modelling aspects of wastewater treatment processes. Ph.D. thesis, Lund University, Sweden, ISBN 91-88934-00-4.

Kuba T., Murnleitner E., van Loosdrecht M. C. M. and Heijnen J. J. (1996) A Metabolic Model for Biological Phosphorus Removal by Denitrifying Organisms. *Biotechnol. Bioeng.* **52**(6), 685-695.

Murnleitner E., Kuba T., van Loosdrecht M. C. M. and Heijnen J. J. (1997) An integrated metabolic model for the aerobic and denitrifying biological phosphorous removal. *Biotechnol. Bioeng.* **54**, 434-450.

Nicholls H. A. (1975) Full Scale Experimentation of the New Johannesburg Aeration Plants. *Water SA.* **1**(3), 121.

Smolders G. L. F. (1995a) A metabolic model of the biological phosphorus removal; stoichiometry, kinetics and dynamic behaviour. Ph.D. Thesis Delft University of Technology, Delft, the Netherlands, 208 p.

Smolders G. L. F., van der Meij J., van Loosdrecht M. C. M. and Heijnen J. J. (1995b) Structured Metabolic model for anaerobic and aerobic stoichiometry and kinetics of the biological phosphorus removal process. *Biotechnol. Bioeng.* **47**, 277-287.

Van Loosdrecht M. C. M., Brandse F. A. and de Vries A. C. (1998) Upgrading of wastewater treatment processes for integrated nutrient removal – The BCFS® process. *Water Sci. Technol.* **37**(9), 209-217.

Van Veldhuizen H. M., van Loosdrecht M. C. M. and Heijnen J. J. (1999) Modelling biological phosphorus and nitrogen removal in a full scale activated sludge process. *Wat. Res.* **33**(16), 3459-3468.

Wichern M., Obenaus F. and Rosenwinkel K. -H. (1999) Comparison of the models ASM2d and TU-Delft in simulation praxis, 6. Simba-Anwendertreffen, Magdenburg, Germany.

2

An Integrated Metabolic Activated Sludge Model for BioP and Nitrogen Removal

This chapter starts with a literature overview of the development of the metabolic BioP model. The metabolic model is rather different from other activated sludge models. Therefore the model structure and development is discussed in detail. Also the model stoichiometry and kinetics are discussed. The main purpose of this chapter is to give insight in the metabolic modelling concept, as this is required for a proper application of the model. The chapter concludes by discussing the integration of the metabolic BioP with ASM2d. The integrated model will be further investigated in this research.

2.1 Introduction

The development of mathematical models describing biological nutrient removal (BNR) in activated sludge processes, started around 1976 with the study of enhanced biological phosphorus (P) removal (EBPR or BioP) by Barnard in South Africa. The various models becoming available at that time were little used due to a lack of trust in their predictions, limitations in computing power and the complicated way these models were presented. The International Association on Water Pollution Research and Control (since 2000 the International Water Association, IWA) introduced the first Activated Sludge Model for biological carbon and nitrogen removal (ASM1) in 1986. This model was presented in the matrix notation for chemical reactions as used by Petersen (1965), and became a common way of presenting activated sludge models since. The common representation and nomenclature facilitated the communication and allowed the focusing of discussions on essential aspects of bio-kinetic modelling (Henze *et al.*, 2000). The insights in the BioP process since the mid-1980s, were included in the second version of the activated sludge model (ASM2), which was published in 1995 by Henze *et al.*. This model included EBPR and a simple model for chemical P removal. A further extension with denitrifying EBPR was published as ASM2d (Henze *et al.*, 1999).

Increasing knowledge of the cell-internal biochemistry of phosphorus accumulating micro-organisms (PAO's), in 1994 resulted in the development of a metabolic model describing EBPR. Up till now, several versions of this model have been published. The first publications focussed on specific aspects of BioP (Smolders *et al.*, 1994a/b, 1995 and Kuba *et al.*, 1996). In later publications, the partial models were combined (Smolders *et al.*, 1995b and Murnleitner *et al.*, 1997). More recent, the metabolic BioP model was integrated with the heterotrophic, hydrolytic and autotrophic reactions of ASM2d. This model is referred to as the Technical University of Delft integrated metabolic BioP model or TUD model (van Veldhuizen *et al.*, 1999).

In succeeding publications, several improvements of the TUD model were proposed. Most of these changes were not properly validated, others were never incorporated. Also previously published models contained rounding and typesetting errors. This thesis therefore presents a complete and updated version of the TUD model (appendix III), based on previous publications and supplemented with new insights. In this particular chapter, the development of the metabolic model is discussed. Hereby, it is the objective to improve the understanding of the stoichiometric and kinetic model structure and hereby get to know the model limitations.

2.2 History of the Model Development

The first metabolic model describing the anaerobic and aerobic phases of EBPR was proposed by Smolders *et al.* (1994a/b, and 1995a/b). The model was developed on the basis of lab-scale anaerobic/aerobic (A/O) Sequencing Batch Reactor experiments (SBR) with a Sludge Retention Time (SRT) of 8 days (fig. 6.3). The model was validated on two similar experiments with a SRT of 5 and 20 days. Additionally, the start-up of an enriched culture of PAO's was used to validate the model stoichiometry (Smolders *et al.*, 1995c). Initially, the model kinetics were chosen as simple as possible. A kinetic structure was proposed in which the poly-hydroxybuterate (PHA) consumption rate was the net result of biomass growth, poly-phosphate (PP) and glycogen formation (fig. 2.2).

On the basis of these publications, Kuba *et al.* (1996) proposed a metabolic model for denitrifying EBPR. The kinetic structure of this model was according to Smolders *et al.* (1995a). Suggestions were made to improve the kinetics. The anoxic model was calibrated on the basis of four batch experiments with different initial phosphate (PO_4^{2-}) concentrations (fig. 6.2). Two lab-scale anaerobic-anoxic (A2) SBR experiments (SRT of 8 and 14 days) were used to validate this model (fig. 6.1).

The anaerobic, aerobic and anoxic models were combined by Murnleitner *et al.* (1997). It was tested on the basis of original SBR experiments by Smolders *et al.* and Kuba *et al.*. The tests showed that the kinetic structure proposed by Smolders *et al.*, was not suited to describe all SBR experiments with a single set of model parameter values. Therefore, Murnleitner *et al.* proposed a different kinetic structure, in which growth was the net result of PHA consumption and PP and glycogen formation (fig. 2.2). Also the kinetic rate equations were adjusted. In the model presented by Murnleitner *et al.*, a metabolic model for anoxic acetate uptake according to Kuba *et al.* (1995) was included. More recently, Filipe *et al.* (1999) proposed improvements for the anoxic acetate uptake model according to Smolders *et al.* (1994a). These improvements were however not incorporated in the TUD model.

In 1999, the metabolic BioP model was integrated with the heterotrophic, hydrolytic and autotrophic processes from ASM2d (Henze *et al.*, 1999) by van Veldhuizen *et al.*. With this model a full-scale MUCT process for COD, N and P removal was simulated. This study showed that the TUD model was capable of describing full-scale conditions, without significant adjustments. In the same year, Wichern *et al.* (1999) compared the full-scale performance of the TUD model, ASM2d and ASM3p (Koch *et al.*, 2000; Rieger *et al.*, 2000 and 2001). They observed that the TUD model

predicted accumulation of cell-internal glycogen, hereby underestimating growth of PAO's. With the same model, Brdjanovic *et al.* (2000) simulated a full-scale side-stream P-removing process. Also Brdjanovic *et al.*, observed irregularities in the modelled glycogen kinetics, especially with increasing SRT. The model only could be fitted, by strongly decreasing the maximum glycogen formation rate. It was therefore suggested that glycogen formation is a function of the SRT. After calibrating glycogen formation, the model described the studied process without significant parameter adjustments.

Brdjanovic *et al.* (1998a) studied the effect of temperature on EBPR. Their results were incorporated in the TUD model, that was used to simulate a full-scale MUCT process optimised for denitrifying EBPR (this thesis, chapters 3 and 4). Modifications were made to solve the kinetic problems with glycogen formation. On the basis of an extensive model evaluation in chapters 3, 4 and 6, an updated and validated model is presented in appendix III.

From this thesis it is concluded that the stoichiometry of the metabolic model can be extrapolated without calibration. It was shown that operational conditions rather than model kinetics determine the WWTP operation. Careful evaluation of operational data is therefore required. It was concluded that steady state conditions are not suited to calibrate model kinetics. Therefore, in chapter 4, the TUD model was evaluated under start-up conditions. These simulations show that growth of PAO's is mainly determined by the glycogen formation rate. Furthermore, it was concluded that the steady state PAO concentration is strongly influenced by preceding (seasonal) temperature changes. Temperature changes therefore should be modelled. In chapters 3 and 4, a calibration method was developed, which was tested in chapter 5.

In more recent research, Filipe *et al.* (2001a) improved the model for anaerobic acetate uptake. A kinetic PP dependency was included, which improved the description of acetate uptake under varying initial PP concentrations. Also a different pH dependency for anaerobic acetate uptake was suggested. This dependency becomes critical when anaerobic substrate uptake is limiting. In the TUD model, anaerobic acetate uptake was modelled according to Smolders *et al.* (1994a).

2.3 The Metabolic Model

2.3.1 Introduction to BioP

Fig. 1.1 shows a schematic representation of enhanced biological phosphorus removal. EBPR is a cyclic process, depending on alternating anaerobic and aerobic (or anoxic) conditions. Under anaerobic conditions,

Volatile Fatty Acids (VFA) from the influent are taken up by PAO's and stored as poly-hydroxyalkanoate (PHA). When influent VFA is mainly acetate (HAc), the main storage product is poly-hydroxybuterate (PHB). Anaerobic uptake and storage of acetate requires energy. This is generated by degradation of cell internal glycogen and poly-phosphate (PP). As a result, under anaerobic conditions PAO's release a large amount of phosphate into the bulk liquid.

In a subsequent aerobic (or anoxic) phase, PHA is oxidised. The hereby generated energy is mainly is used to restore glycogen and PP. To restore PP, PAO's take up phosphate from the bulk liquid. The remaining energy is used for growth and maintenance of the cell structure.

At steady state, growth of PAO's equals waste of PAO's via the waste activated sludge (WAS) flow (fig. 1.1). The amount of P removed from the WWTP is determined by the P fraction in the WAS flow. Generally WAS contains 1 to 2 % P. In an EBPR process this can be increased to 4 to 8 %, by additional contribution of PP.

After gravitational settling and WAS removal, RAS is recycled to the anaerobic phase (fig. 1.1). This configuration provides the cyclic anaerobic/aerobic (A/O) conditions required for EBPR. What is typically observed from BioP process is the anaerobic phosphate release as shown in fig. 1.1.

2.3.2 Grey box versus metabolic approach

ASM2d and the metabolic BioP model originate from two different modelling concepts. Schematically, this is illustrated in fig. 2.1. ASM2d relies on (observed) macroscopic yields and uses a grey box approach towards cell-internal conversions. The model structure is directly related to the (measured) conversions in the bulk liquid. The cell-internal mechanism is modelled on the basis of PP and a COD storage compound. Model kinetics are described by Monod-type relations for the observed conversions.

The metabolic BioP model is based on the formation and degradation of *all* relevant cell internal storage compounds (PHA, glycogen and PP). All model yields are stoichiometrically related and follow from the metabolic conversions, mediated by ATP and $NADH_2$. The heart of the metabolic model consists of three metabolic yields, being the ATP formation per $NADH_2$ (δ), the biomass production per ATP (κ) and the ATP requirement for maintenance (m_{ATP}) (fig. 2.1). These yields were determined experimentally, which is further discussed in the following sections.

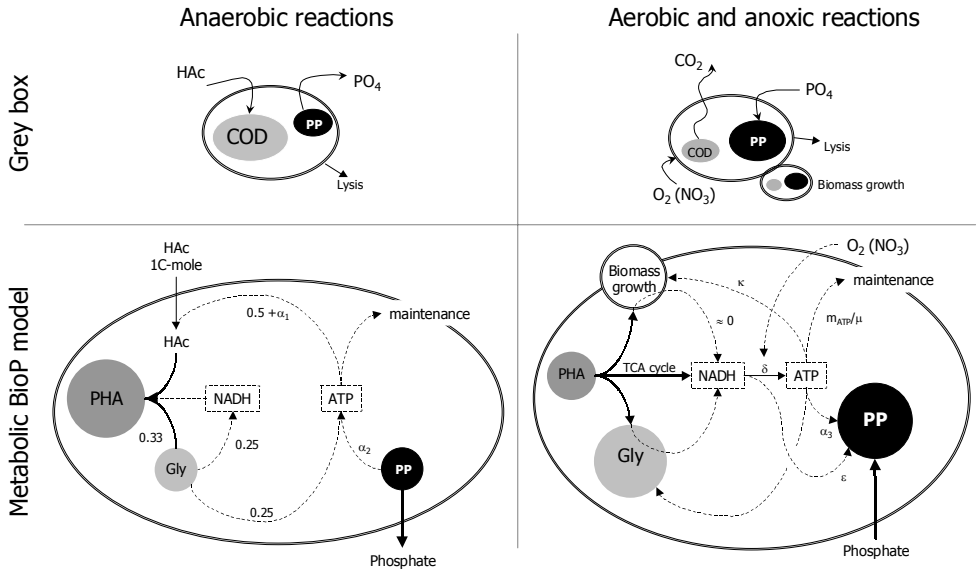

Figure 2.1 **Different modelling concepts for EBPR.** On top, the grey box approach of ASM2d is presented. One COD storage is modelled. Below the metabolic concept presented. All reactions are listed in tables 2.1 and 2.2. **Bold** lines are phosphate mass flows, thin solid lines carbon mass flows and dashed lines mass flows of ATP and $NADH_2$. ATP is an energy source, where $NADH_2$ is both energy source and a source to balance the cell-internal reduction potential. The net conversion of $NADH_2$ and ATP is zero. The parameters α_1, α_2, α_3, δ, ε, κ and m_{ATP}, are the efficiencies of the metabolic reactions in tables 2.1 and 2.2.

2.3.3 Anaerobic stoichiometry

The anaerobic stoichiometry of the metabolic model was first proposed by Smolders *et al.* (1994a). The reactions are presented in table 2.1 (eq. 2.1 to 2.3), and schematically represented in fig. 2.1. In these equations, α_1 is the efficiency of transport of acetate over the cell membrane. α_1 is pH dependent (Smolders *et al.*, 1994a; Filipe *et al.*, 2001a) and has a typical value between 0 and 0.5 mole ATP·C-mole^{-1}. α_2 is the efficiency by which ATP is produced from hydrolysis of PP. α_2 has a typical value of 1 mole ATP/P-mole (Smolders *et al.*, 1994a). Under the assumption that the metabolic intermediates ATP and $NADH_2$ are in steady state, an overall anaerobic stoichiometry was formulated according to eq. 2.4 and 2.5 (table 2.1). If the conversion factors in eq. 2.4 and 2.5 are recalculated from moles to grams, the anaerobic model yields are obtained (appendix III, table 5). The anaerobic yield for acetate uptake is a function of the pH. Smolders *et al.* and Filipe *et al.* both found linear, however different

relations; Smolders *et al.* (1994a) $Y_{P/HAc} = 0.19 \times pH_{out} - 0.85$ (P-mole/C-mole) and Filipe *et al.* (2001a) $Y_{P/HAc} = 0.16 \times pH_{out} - 0.55$. This difference could be caused by the presence of glycogen accumulating micro-organisms (GAO's). Moreover, the presence of propionate and butyrate in wastewater will result in a different value for $Y_{P/HAc}$. It is therefore advised to experimentally determine the anaerobic yield for the operational pH value.

	Anaerobic metabolic reactions (in moles C and P)	
2.1	Acetate uptake	$-\underset{\text{acetic acid}}{CH_2O} - \left(\frac{1}{2}+\alpha_1\right)ATP - \frac{1}{4}NADH_2 + \underset{\text{PHA}}{CH_{1.5}O_{0.5}} + \frac{1}{2}H_2O = 0$
2.2	PP degradation	$-\underset{\text{poly P}}{HPO_3} - H_2O + \alpha_2 ATP + \underset{\text{phosphate}}{H_3PO_4} = 0$
2.3	$NADH_2$ production	$-\underset{\text{glycogen}}{CH_{10/6}O_{5/6}} - \frac{1}{6}H_2O + \frac{2}{3}\underset{\text{PHA}}{CH_{1.5}O_{0.5}} + \frac{1}{3}CO_2 + \frac{1}{2}NADH_2 + \frac{1}{2}ATP = 0$
	Overall anaerobic stoichiometry (in moles C and P)	
2.4	Acetate uptake	$-\underset{\text{acetic acid}}{CH_2O} - 0.5\underset{\text{glycogen}}{CH_{10/6}O_{5/6}} - 0.44\underset{\text{poly P}}{HPO_3} + 1.33\underset{\text{PHA}}{CH_{1.5}O_{0.5}} + 0.17CO_2 + 0.44\underset{\text{phosphate}}{H_3PO_4} - 0.023H_2O = 0$
2.5	Maintenance	$-\underset{\text{poly P}}{HPO_3} - H_2O + \underset{\text{phosphate}}{H_3PO_4} = 0$

Table 2.1 **Anaerobic metabolic reactions and derived stoichiometry.** The overall reactions are valid when the net conversions of ATP and $NADH_2$ are zero. α_1 is the efficiency of the transport of acetate over the cell membrane and has a typical value between 0 and 0.5 mole ATP·C-mole^{-1}. α_2 is the efficiency by which ATP is produced from the hydrolysis of PP and has a typical value of 1 mole ATP·P-mole^{-1} (Smolders *et al.*, 1994a).

2.3.4 Aerobic and anoxic stoichiometry

The aerobic stoichiometry of the model was proposed by Smolders *et al.* (1994b). Using a similar method, Kuba *et al.* (1996) determined the anoxic stoichiometry. The anoxic metabolic reactions are shown in table 2.2 (eq. 2.6a to 2.11). Schematically this is presented fig. 2.1 (bottom, right). Eq. 2.6a/b and 2.7a/b depend on the electron acceptor in the bulk liquid (nitrate or oxygen) and therefore are located in the cell membrane. The reactions 2.8 to 2.11 are independent of the electron acceptor, and therefore identical for anoxic and aerobic conditions.

In the oxidative phosphorylation (eq. 2.1a and 2.1b), δ is the efficiency by which ATP is produced from $NADH_2$. It is the main stoichiometric parameter in the TUD model, linking all aerobic (and anoxic) yields (appendix III, table 5). To determine δ, Smolders *et al.* (1994b) conducted experiments in which the oxygen consumption was measured with and without phosphate present in the bulk liquid. From these experiments, δ or the P/O ratio was measured to be 1.85 mole ATP·mole^{-1} $NADH_2$. This value was verified under conditions where all PHA was oxidised. Under these (maintenance) conditions, the only energy source for PAO's was produced from hydrolysis of PP (table 2.1, eq. 2.1) being the reverse reaction of eq. 2.10 (table 2.2). For anoxic conditions, Kuba *et al.* (1996) found the relation $\delta_{anoxic}=0.5\times\delta_{aerobic}$.

ε represents the ATP requirement for phosphate transport over the cell membrane (eq. 2.7a/b). PO_4^{2-} is a negative charged ion, and therefore has to be taken up against the electric potential of the cell membrane. A typical value for ε lies between 4.5 and 9 P-mole·mole^{-1}$NADH_2$. In the metabolic model an avg. value for ε was used (7 P-mole·mole^{-1} $NADH_2$, Smolders *et al.*, 1994b). This is allowed, since the model is relative insensitive towards ε. For anoxic conditions, Kuba *et al.* (1996) found the relation $\varepsilon_{anoxic}=0.5\times\varepsilon_{aerobic}$.

In eq. 2.9, κ represents the ATP requirement for biomass polymerisation. κ has a theoretical value of approx. 1.6 mole ATP·C-mole^{-1} PAO (Stouthamer, 1979). On the basis of the oxygen balance, Smolders *et al.* (1994b) calculated κ to be 1.72 mole ATP·C-mole^{-1} PAO, which is in the range of the theoretically expected value. When recalculating the metabolic parameters, a high sensitivity of the calculated value of κ was observed towards the measured value of δ, i.e. the parameter are correlated. An independent parameter estimation therefore was not possible. However, in the metabolic model the sensitivity towards κ is relative low.

m_{ATP} is the ATP requirement for maintenance, and was calculated from the oxygen consumption (OC) under maintenance conditions m_{OC} (appendix III, table 6b). Based on the oxygen balance, Smolders *et al.* (1994b) calculated m_{ATP} to be 0.019 mole ATP·C-mole^{-1}·h^{-1}. On the basis of eq. 2.6a, we propose to use a more direct theoretical relation according to $m_{ATP}=2\cdot\delta\times m_{OC}$, which results in a slightly lower value (0.017 mole ATP·C-mole^{-1}·h^{-1}). Under normal operational conditions (SRT of 10 to 30 days), the model is relative insensitive towards m_{ATP}. The maintenance rates in the TUD model are calculated from m_{OC} and δ (appendix III, tab. 6b).

α_1 is the efficiency of the transport of acetate over the cell membrane and has a typical value between 0 and 0.5 mole ATP·C-mole^{-1} (eq. 2.1). α_2 is the efficiency by which ATP is produced from the hydrolysis of PP and

has a typical value of 1 mole ATP·P-mole^{-1} (eq. 2.10). α_3 is the efficiency for PP synthesis and is assumed to be equal to α_2 (1 ATP·P-mole^{-1}), originating from the reversed reaction eq. 2.2 (Smolders *et al.*, 1994a).

2.3.5 Stoichiometric structure

From the metabolic reactions, an overall anaerobic (table 2.1, eq. 2.4), aerobic (table 2.3) and anoxic (not shown) stoichiometry can be determined. In the model formulation, it is assumed that the cell internal concentrations of metabolites ($NADH_2$, ATP and HPO_4-internal) are in steady state. This implies that the net conversions are zero. The formulation of an overall anaerobic reaction is unambiguous, as there is only one metabolic reaction (eq. 2.4). By measuring one uptake rate, e.g. the acetate uptake rate (eq. 2.3), all other rates are fixed.

For the aerobic and anoxic stoichiometry, five overall reactions (r_X, r_{PP}, r_{GLY}, r_{PHA} and m_{PHA}) are found. The system can be solved if four of the five rates are determined. This means that there are multiple possibilities to formulate a set of overall reactions. Two options are presented in table 2.3. The kinetic structure that is chosen, determines the appearance of the model stoichiometry. Smolders *et al.* (1994b) proposed a kinetic structure in which the oxygen (or nitrate) consumption and PHA degradation are the net result of biomass growth (r_X), PP formation (r_{PP}), glycogen formation (r_{GLY}) and maintenance according to fig. 2.2. The net turnover of PHA and oxygen (dashed lines, r_{PHA} and r_O) is the combined result of the formation of PP, glycogen and biomass (solid lines), which kinetic rate expressions are defined in the model. This kinetic structure is expressed in the linear eq. 2.12 and 2.13, and leads to the set of overall reactions in table 2.3 (eq. 2.16 to 2.19).

$$r_O = \frac{1}{Y_{X/O}} \cdot r_X + \frac{1}{Y_{PP/O}} \cdot r_{PP} + \frac{1}{Y_{GLY/O}} \cdot r_{GLY} + m_O \cdot C_X \qquad (2.12)$$

$$r_{PHA} = \frac{1}{Y_{X/PHA}} \cdot r_X + \frac{1}{Y_{PP/PHA}} \cdot r_{PP} + \frac{1}{Y_{GLY/PHA}} \cdot r_{GLY} + m_{PHA} \cdot C_X \qquad (2.13)$$

In these balances, C_X represents the PAO concentration. m_O and m_{PHA} are the maintenance rates. When expressed in COD, the maintenance rates relate according to $-m_O = m_{PHA}$. Yields are represented by $Y_{a/b}$, following from the metabolic reactions.

2.3.6 Model kinetics

Murnleitner *et al.* (1997), showed that the kinetic model structure proposed by Smolders *et al.* (1994b), required different kinetic parameters to describe aerobic and anoxic conditions. Experimentally, it was verified that the PHA content is independent of the SRT. Eq. 2.12 and 2.13 however assume a intrinsic relation between growth (i.e. the SRT) and the PHA content. Moreover, Filipe *et al.* (1999) showed that the model according to Smolders *et al.* is not suited to simulate the continuous flow systems as operated by Wentzel *et al.* (1989a/b). Filipe *et al.* solved this problem by redefining the kinetic rate equations. Murnleitner *et al.* redefined the total kinetic model structure including the rate equations. In the here presented model, we used the kinetic model proposed by Murnleitner *et al.*. The improved kinetic structure is presented in fig. 2.2 (right hand scheme), and relates to eq 2.14 and 2.15.

	Aerobic metabolic reactions (in moles C and P)	
2.6a	oxidative phosphorylation	$-NADH_2 - \frac{1}{2}O_2 + H_2O + \delta\ ATP = 0$
2.7a	phosphate transport	$-\varepsilon\ \underset{\text{external phosphate}}{H_3PO_4\ out} - NADH_2 - \frac{1}{2}O_2 + \varepsilon\ \underset{\text{int ernal phosphate}}{H_3PO_4\ in} + H_2O = 0$
	Anoxic metabolic reactions (in moles C, P and N)	
2.6b	oxidative phosphorylation	$-NADH_2 - \frac{2}{5}\underset{\text{nitrate}}{HNO_3} + \frac{1}{5}N_2 + \frac{6}{5}H_2O + \frac{\delta}{2}ATP = 0$
2.7b	phosphate transport	$-\frac{\varepsilon}{2}\underset{\text{external phosphate}}{H_3PO_4\ out} - NADH_2 - \frac{2}{5}\underset{\text{nitrate}}{HNO_3} + \frac{\varepsilon}{2}\underset{\text{int ernal phosphate}}{H_3PO_4\ in} + \frac{1}{5}N_2 + \frac{6}{5}H_2O = 0$
	Aerobic and anoxic metabolic reactions (in moles C, P and N)	
2.8	PHA degradation in the TCA cycle	$-\underset{\text{PHA}}{CH_{1.5}O_{0.5}} - \frac{3}{2}H_2O + \frac{9}{4}NADH_2 + \frac{1}{2}ATP + CO_2 = 0$
2.9	growth of PAO	$-1.27\underset{\text{PHA}}{CH_{1.5}O_{0.5}} - 0.2\,NH_3 - 0.015\underset{\text{phosphate}}{H_3PO_4} - \left(\kappa + \frac{m_{ATP}}{\mu}\right)ATP - 0.385\,H_2O + \underset{\text{biomass}}{CH_{2.09}O_{0.54}N_{0.20}P_{0.015}} + 0.615\,NADH_2 + 0.27\,CO_2 = 0$
2.10	PP formation	$-\underset{\text{int ernal phosphate}}{H_3PO_4\ in} - \alpha_3 ATP + \underset{\text{poly P}}{HPO_3} + H_2O = 0$
2.11	glycogen formation	$-\frac{4}{3}\underset{\text{PHA}}{CH_{1.5}O_{0.5}} - \frac{5}{6}ATP - \frac{5}{6}H_2O + \underset{\text{glycogen}}{CH_{1\frac{1}{6}}O_{\frac{5}{6}}} + \frac{1}{3}CO_2 + NADH_2 = 0$

Table 2.2 **Aerobic and anoxic metabolic reactions.** Eq. 2.6a, 2.7a and 2.8 to 2.11 are according to Smolders *et al.* (1994b), Eq. 2.6b, 2.7b and 2.8 to 2.11 are according to Kuba *et al.* (1996).

$$r_O = \frac{-1}{Y_{PHA/O}} \cdot r_{PHA} + \frac{1}{Y_{PP/O}} \cdot r_{PP} + \frac{1}{Y_{GLY/O}} \cdot r_{GLY} + m_O \cdot C_X \tag{2.14}$$

$$r_X = Y_{X/PHA} \cdot r_{PHA} - \frac{Y_{X/PHA}}{Y_{PP/PHA}} \cdot r_{PP} - \frac{Y_{X/PHA}}{Y_{GLY/X}} \cdot r_{GLY} - Y_{X/PHA} \cdot m_{PHA} \cdot C_X \Rightarrow$$

$$r_X = \frac{1}{Y_{PHA/X}} \cdot r_{PHA} - \frac{1}{Y_{PP/X}} \cdot r_{PP} - \frac{1}{Y_{GLY/X}} \cdot r_{GLY} - m_X \cdot C_X \tag{2.15}$$

Eq. 2.15 follows from eq. 2.13. In the model matrix (appendix III, table 1), eq. 2.14 and 2.15 can be derived from the columns of respectively oxygen (S_O) and PAO (X_{PAO}). With the reformulated kinetic structure, Murnleitner *et al.* (1997) described all SBR experiments performed by Smolders *et al.* and Kuba *et al*, with one set of model parameters (fig. 6.1, 6.2 and 6.3). The proposed kinetic structure resulted in the overall model stoichiometry presented in table 2.3 (eq. 2.20 to 2.23). It should be noticed that these reactions can not be read separately, as they are merely the result of the mathematical formulation in eq. 2.14 and 2.15.

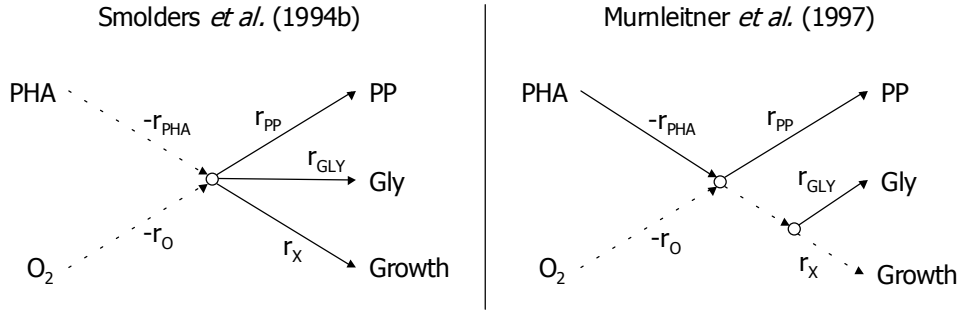

Figure 2.2 Two kinetic BioP model structures. Solid lines are modelled rates, dashed lines are rates resulting from the model. In the definition by Smolders *et al.* (1994b), growth is limited by the maximum growth rate. In the definition by Murnleitner *et al.* (1997), growth is the result of PHA degradation and storage of PP and glycogen.

In the kinetic structure proposed by Smolders *et al.* (1994b), the rates for biomass growth, PP formation and glycogen formation define the rate for PHA degradation. Hereby, growth of PAO's is limited by the maximum growth rate. In the kinetic model proposed by Murnleitner *et al.*, growth is determined by the net result of PHA degradation and PP and glycogen

formation. From an ecological point of view, this structure, in which storage is preferred above growth, seems logical. In the competition with other micro-organisms, PAO's rely on their storage ability. A rapid resupply of storage compounds is a primary condition for long term survival. In this formulation, the maximum growth rate is no longer an intrinsic property of PAO's, but becomes dependent on environmental conditions and the maximum PHA storage capacity (Brdjanovic *et al.*, 1998b).

Overall aerobic stoichiometry by Smolders *et al.* (1994b) (in moles C, P and N)		
2.16	Biomass growth	$-1.37\,\underset{\text{PHA}}{CH_{1.5}O_{0.5}} - 0.2\,NH_3 - 0.015\,\underset{\text{phosphate}}{H_3PO_4} - 0.42\,O_2 + \underset{\text{biomass}}{CH_{2.09}O_{0.54}N_{0.20}P_{0.015}} + 0.37\,CO_2 - 0.305\,H_2O = 0$
2.17	Poly-P formation	$-0.27\,\underset{\text{PHA}}{CH_{1.5}O_{0.5}} - 0.306\,O_2 - \underset{\text{phosphate}}{H_3PO_4} + \underset{\text{poly P}}{HPO_3} + 0.27\,CO_2 + 1.2\,H_2O = 0$
2.18	glycogen formation	$-1.12\,\underset{\text{PHA}}{CH_{1.5}O_{0.5}} - 0.26\,O_2 + \underset{\text{glycogen}}{CH_{10/6}O_{5/6}} + 0.12\,CO_2 + 0.007\,H_2O = 0$
2.19	Maintenance	$-\underset{\text{PHA}}{CH_{1.5}O_{0.5}} - 1.125\,O_2 + CO_2 + 0.75\,H_2O = 0$
Overall aerobic stoichiometry by Murnleitner *et al.* (1997) (in moles C, P and N)		
2.20	PHA degradation	$-\underset{\text{PHA}}{CH_{1.5}O_{0.5}} - 0.14\,NH_3 - 0.011\,\underset{\text{phosphate}}{H_3PO_4} - 0.32\,O_2 + 0.72\,\underset{\text{biomass}}{CH_{2.09}O_{0.54}N_{0.20}P_{0.015}} + 0.28\,CO_2 - 0.23\,H_2O = 0$
2.21	Poly-P formation	$-0.19\,\underset{\text{biomass}}{CH_{2.09}O_{0.54}N_{0.20}P_{0.015}} - 0.218\,O_2 - 0.997\,\underset{\text{phosphate}}{H_3PO_4} + \underset{\text{poly P}}{HPO_3} + 0.038\,NH_3 + 0.19\,CO_2 + 1.14\,H_2O = 0$
2.22	glycogen formation	$-0.78\,\underset{\text{biomass}}{CH_{2.09}O_{0.54}N_{0.20}P_{0.015}} - 0.27\,H_2O - 0.22\,CO_2 + \underset{\text{glycogen}}{CH_{10/6}O_{5/6}} + 0.1\,O_2 + 0.012\,\underset{\text{phosphate}}{H_3PO_4} + 0.156\,NH_3 = 0$
2.23	Maintenance	$-0.89\,\underset{\text{biomass}}{CH_{2.09}O_{0.54}N_{0.20}P_{0.015}} - O_2 + 0.013\,\underset{\text{phosphate}}{H_3PO_4} + 0.178\,NH_3 + 0.89\,CO_2 + 0.64\,H_2O = 0$

Table 2.3 **Aerobic stoichiometry resulting from different kinetic structures.** Eq. 2.16 to 2.19 result from the kinetic structure proposed by Smolders *et al.* (1994b). Eq. 2.20 to 2.23 result from the improved kinetic structure proposed by Murnleitner *et al.* (1997).

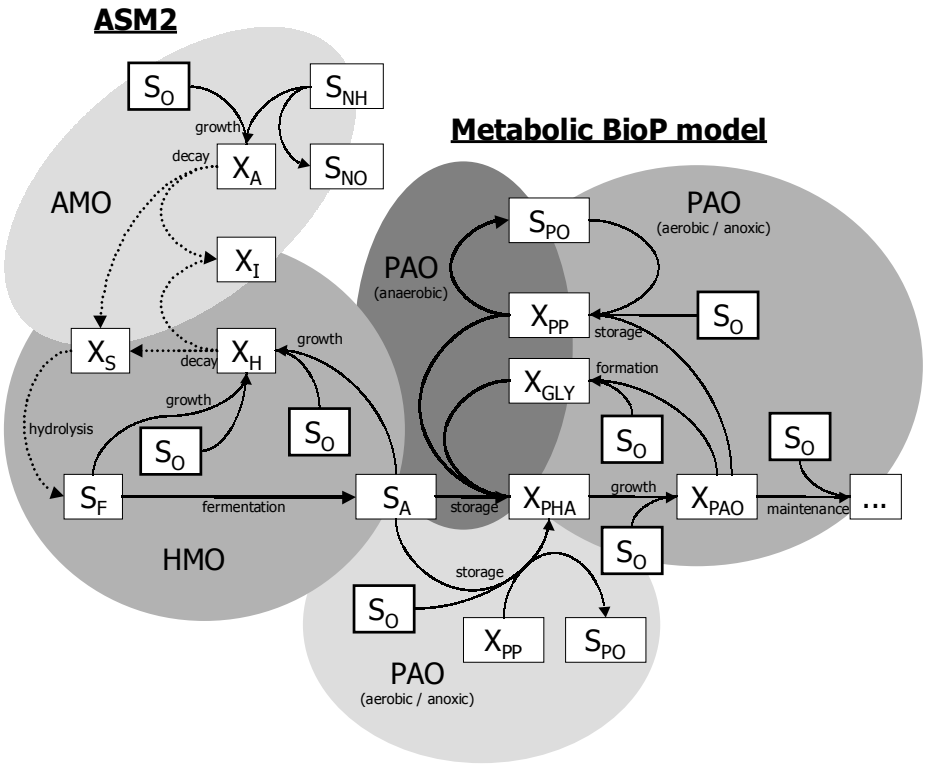

Figure 2.3 Interactions in the integrated TUD Model. Anaerobic conversions are represented by **bold** lines, anoxic and aerobic conversions by thin lines. Conversions independent of oxygen of nitrate are represented by dashed lines. For all boxes with S_O, also S_{NO} can be read. The shaded areas distinguish between different micro-organisms and processes. AMO's and HMO's are linked via particulate substrate (X_S). The decay of AMO's triggers the growth of HMO's. Both anaerobic and aerobic storage of PHA by PAO's is modelled.

2.4 Model Integration

To simulate full-scale EBPR, the metabolic model was combined with the heterotrophic, hydrolytic and autotrophic reactions from ASM2d (Henze *et al.*, 1999). In fig. 2.3 it is shown how the different model structures interact. The model concepts of ASM2d and the metabolic BioP model are quite different, and therefore combination of both concepts may seem inconsequent. It would be possible to reformulate the auto- and heterotrophic processes of ASM2d in a metabolic form. This a model would have a number of yields, identical to the current model ASM2d. Metabolic

reformulation of ASM2d therefore would not lead to a smaller model and moreover, would not improve the model performance. Therefore, in the TUD model, the processes of ASM2d were maintained in their original form. Facilitated by the ASM matrix notation originally proposed by Petersen (1965), integration of the two models was relative simple.

2.4.1 Substrate competition

Soluble substrate (S_F and S_A) is supplied via the influent. Fig. 2.3 shows that PAO's and regular heterotrophic micro-organisms (HMO's) compete for S_A. Hereby, the competitive advantage of PAO's is the ability to store S_A under anaerobic conditions. To facilitate EBPR, a primary anaerobic state is therefore required (fig. 1.2). When anaerobic substrate uptake by PAO's is not possible, PAO's and HMO's compete directly for external substrate (S_A). In time this competition is lost by PAO's, caused by a lower growth yield. Substrate uptake by PAO's under anoxic (and aerobic) conditions causes hydrolysis of PP leading to a immediate deterioration of the P-removal capacity. An proper BioP system therefore should accommodate full anaerobic substrate uptake while minimising anoxic and aerobic substrate uptake.

2.4.2 Fermentation and hydrolysis

S_A is formed from S_F during anaerobic fermentation. If the influent S_A load is limiting, EBPR depends on hydrolysis of X_S and fermentation of S_F (fig. 2.3). Under such conditions, EBPR is sensitive for the modelled fermentation and hydrolysis rates, as these rates determine the availability of substrate. There is however little or no experimental proof for the modelled fermentation and hydrolysis processes. This is mainly caused by the unclear relation between the modelled influent COD fractions (S_A, S_F, S_I, X_S and X_I) and the actual wastewater composition. Koch *et al.* (2000) concluded that hydrolysis is the limiting process in the formation of VFA. They observed that the fermentation rate was insensitive in their model (ASM3p), and therefore suggested to remove this process. This only holds for situations where the bio-degradable fraction of wastewater mainly consists of X_S. This is typically caused by short hydraulic retention time (HRT) in sewer systems (e.g. Swiss conditions). When the sewer HRT allows hydrolysis to occur (e.g. Dutch conditions), wastewater will contain a relative high amount of soluble substrate (S_F and S_A). Hence, the fermentation rate is sensitive and therefore should be modelled (chapter 5). It was proposed to fit the anaerobic phosphate release (i.e. VFA uptake by PAO's) by adjusting the (unknown) fermentation and hydrolysis rates.

Hereby, the anaerobic phosphate release was estimated from a phosphate balance, which is further discussed in chapter 3.

2.4.3 Endogenous respiration

By integrating the metabolic BioP model and ASM2d, two modelling approaches towards endogenous respiration are combined. In ASM2d endogenous respiration is modelled according to the lysis concept. Hereby, biomass degenerates while forming particulate inert material (X_I) and particulate substrate (X_S) (fig. 2.3). X_S is hydrolysed and oxidised, resulting in an endogenous oxygen consumption. Lysis therefore causes an internal recycle of substrate (X_S), which complicates the calibration of the model.

In the metabolic BioP model an COD storage is readily available. This facilitates the more straightforward maintenance concept, which also is used in ASM3p (Koch *et al.*, 2000). PHA is directly oxidised for maintenance purposes. Hereby, no particulate inert matter (X_I) and particulate substrate (X_S) are formed, and therefore X_S recycle is avoided.

The assumption that no inert (or inactive) material is formed in the EBPR process is unlikely. There is however, no sufficient quantitative and mechanistic information on the formation of inert or inactive material. In the model, the unknown production of X_I is compensated by fitting the influent X_I/X ratio to the measured solids balance (COD_X). Because X_I in the wastewater is an estimate, it is justified and convenient to lump both model uncertainties in the influent X_I/X fraction. This method to fit the solids balance in the model is further discussed in chapter 3.

2.4.4 Exemplary versus mathematical description

In the here presented metabolic BioP model, the proposed kinetic structure results in a set of atypical model reactions (table 2.3, reactions 2.20 to 2.23). These reactions are the mathematical result of the kinetic formulation (eq. 2.14 and 2.15), and can not be seen independently. For those not aware, this could easily lead to misinterpretations of the model matrix, as the individual stoichiometric reactions are not exemplarily for the actual EBPR process. This should be realised when the model is used for educational purposes.

In modelling practice however, working with the metabolic concept has important advantages over the grey box descriptions as used in ASM2, ASM2d and ASM3p. The main advantage is the solid stoichiometric base of the metabolic model, which is proven in chapters 3 and 4 and several other studies (Smolders *et al.*, 1994a/b and 1995a; Kuba *et al.*, 1996; Murnleitner *et al.*, 1997; van Veldhuizen *et al.*, 1999; Brdjanovic *et al.*, 2000; Filipe *et al.*, 1999). This solid stoichiometric basis is largely owed to

inclusion of glycogen in the metabolic model. Moreover, Brdjanovic *et al.* (1998c) showed that glycogen potentially can become limiting in EBPR. An additional argument against modelling one lumped carbon pool, comes from a modelling point of view. In ASM2, ASM2d and ASM3p, glycogen and PHA are lumped in one carbon pool. Because glycogen and PHA have counteracting dynamics, the net dynamics of a lumped carbon pool are damped, which reduces the sensitivity and accuracy of the modelled storage.

References

Barnard J. L. (1976) A review of biological phosphorus removal in the activated sludge process. *Water SA.* **2**(3), 126-144.

Brdjanovic D., Logemann S., van Loosdrecht M. C. M., Hooijmans C. M., Alaerts G. J. and Heijnen J. J. (1998a) Influence of temperature on biological phosphorus removal: process and ecological studies. *Wat. Res.* **32**(4), 1035-1048.

Brdjanovic D., van Loosdrecht M. C. M., Hooijmans C. M., Alaerts G. J. and Heijnen J. J. (1998b) Minimal aerobic sludge retention time in biological phosphorus removal systems. *Biotechnol. Bioeng.* **60**(3), 326-332.

Brdjanovic D, van Loosdrecht MCM, Hooijmans CM, Alaerts G. J. and Heijnen J. J. (1998c) Bioassay for glycogen determination in biological phosphorus removal systems. *Wat. Sci. Tech.* **37**(4-5), 541-547.

Brdjanovic D., van Loosdrecht M. C. M., Hooijmans C. M., Alaerts G. J. and Heijnen J. J. (1999) Innovative methods for sludge characterisation in biological phosphorus removal systems. *Wat. Sci. Tech.* **39**(6), 37-43.

Brdjanovic D., van Loosdrecht M. C. M., Versteeg P., Hooijmans C. M., Alaerts G. J. and Heijnen J. J. (2000) Modeling COD, N and P removal in a full-scale wwtp Haarlem Waarderpolder. *Wat. Res.* **34**(3), 846-858.

Filipe C. D. M. and Daigger G. T. (1999) Evaluation of the capacity of phosphorus-accumulating organisms to use nitrate and oxygen as final electron acceptors: A theoretical study on population dynamics. *Wat. Environ. Res.* **71**(6), 1140-1150.

Filipe C. D. M., Daigger G. T. and Grady C. P. L. (2001a) Stoichiometry and kinetics of acetate uptake under anaerobic conditions by an enriched culture of phosphorus-accumulating organisms at different pHs. *Biotechnol. Bioeng.* **76**(1), 32-43.

Filipe C. D. M., Daigger G. T. and Grady C. P. L. (2001b) pH as a key factor in the competition between glycogen-accumulating organisms and phosphorus-accumulating organisms. *Wat. Environ. Res.* **73**(2), 223-232.

Henze M., Gujer W., Mino T., Matsuo T., Wentzel M. C., Marais G. v. R. and van Loosdrecht M. C. M. (1995) Activated Sludge Model No.2, ASM2. *IAWQ Scientific and technical report no.1.* London, UK.

Henze M., Gujer W., Mino T., Matsuo T., Wentzel M. C., Marais G. v. R. and van Loosdrecht M. C. M. (1999) Activated Sludge Model No.2d, ASM2d. *Wat. Sci. Tech.* **39**(1), 165-182.

Henze M., Gujer W., Mino T. and van Loosdrecht M. C. M. (2000) Activated Sludge Models ASM1, ASM2, ASM2d and ASM3. *IAWQ Scientific and technical report no.9.* London, UK.

Koch G., Kühni M., Gujer W. and Siegrist H. (2000) Calibration and validation of Activated Sludge Model No. 3 for Swiss municipal wastewater, *Wat. Res.*, **34**(14), 3580-3590.

Kuba T., Wachtmeister A., van Loosdrecht M. C. M. and Heijnen J. J. (1994) Effect of nitrate on phosphorus release in biological phosphorus removal systems. *Wat. Sci. Tech.* **30**(6), 263-269.

Kuba T., Murnleitner E., van Loosdrecht M. C. M. and Heijnen J. J. (1996) A Metabolic Model for Biological Phosphorus Removal by Denitrifying Organisms. *Biotechnol. Bioeng.* **52**(6), 685-695.

Murnleitner E., Kuba T., van Loosdrecht M. C. M. and Heijnen J. J. (1997) An integrated metabolic model for the aerobic and denitrifying biological phosphorous removal. *Biotechnol. Bioeng.* **54**, 434-450.

Petersen E. E. (1965) Chemical reaction analysis. *Prentice Hall*, Englewood Cliffs, NJ.

Rieger L., Koch G., Kühni M., Gujer W. and Siegrist H. (2001). The EAWAG BioP-Module for Activated Sludge Model No. 3, *Wat. Res.*, **35**(16), 3887-3903.

Smolders G. L. F., van der Meij J., van Loosdrecht M. C. M. and Heijnen J. J. (1994a) Model of the anaerobic metabolism of the biological phosphorous removal process: stoichiometry and pH influence. *Biotechnol.Bioeng.* **43**(6), 461-470.

Smolders G. L. F., van der Meij J., van Loosdrecht M. C. M. and Heijnen J. J. (1994b) Stoichiometric model of the aerobic metabolism of the biological phosphorus removal process. *Biotechnol.Bioeng.* **44**(7), 837-848.

Smolders G. L. F., van der Meij J., van Loosdrecht M. C. M. and Heijnen J. J. (1995a) Structured Metabolic model for anaerobic and aerobic stoichiometry and kinetics of the biological phosphorus removal process. *Biotechnol. Bioeng.* **47**, 277-287.

Smolders G. L. F., Klop J. M., van Loosdrecht M. C. M. and Heijnen J. J. (1995b) A metabolic model for the biological phosphorus removal process: Effect of the sludge retention time. *Biotechnol. Bioeng.* **48**, 222-233.

Smolders G. L. F., Bulstra D. J., Jacobs R., van Loosdrecht M. C. M. and Heijnen J. J. (1995c) A metabolic model for the biological phosphorus removal process II: Validation during start-up conditions. *Biotechnol. Bioeng.* **48**, 234-245.

Stouthamer A. H. (1975) The search for correlation between theoretical and experimental growth yields. Microbial Biochemistry, Vol 21.

Van Veldhuizen H. M., van Loosdrecht M. C. M. and Heijnen J. J. (1999) Modelling biological phosphorus and nitrogen removal in a full scale activated sludge process. *Wat. Res.* **33**(16), 3459-3468.

Wentzel M. C., Dold P. L., Ekama G. A. and Marais G. v. R. (1989a) Enhanced polyphosphate organism cultures in activated sludge. Part III: Kinetic Model. *Water SA*, **15**, 89-102.

Wentzel M. C., Ekama G. A., Loewenthal R. E., Dold P. L. and Marais G. v. R. (1989b) Enhanced polyphosphate organism cultures in activated sludge. Part II: Experimental behavior. *Water SA*, **15**, 71-88.

Wichern M., Obenaus F. and Rosenwinkel K.-H. (1999) Comparison of the models ASM2d and TU-Delft in simulation praxis, 6. Simba-Anwendertreffen, Magdenburg.

3

Metabolic Modelling of Full-Scale Biological Nutrient Removal

In this chapter a full-scale biological nutrient removing wastewater treatment process (WWTP) was simulated. The model output matched the data of the real WWTP with only minor parameter adjustments. A stepwise calibration method was proposed, in which three model parameters were calibrated. These parameters related to less accurate processes in the model. From the evaluation it was concluded that the modelled inert influent fraction and anoxic sludge fraction require calibration for each simulated wastewater treatment process. Also it was observed that under steady state conditions the sensitivity of the model kinetics was low. This generally will apply to all low-loaded WWTP's in (pseudo) steady state. Calibrating model kinetics under these conditions is therefore less accurate. Operational plant conditions were evaluated based on mass balance calculations. The total phosphorus balance showed useful to evaluate the sludge retention time of the system. Because all compounds on the phosphorous balance can be recovered, errors in the operational data become apparent. Errors in operational data strongly effect the model reliability. This data therefore should be checked on consistency or be considered in model calibration.

This chapter was largely based upon Meijer *et al.* (2001) *Water. Res.* **35**(11), 2711-2723

3.1 Introduction

Modelling WWTP's for COD and N removal, has become a standard practice and valuable instrument for design and operation of WWTP's. However, with respect to modelling EBPR, practical use of activated sludge models is still limiting. Partly this is due to the complexity of the BioP process, partly to limited modelling experience. Essentially, there are two models proposed, ASM2d (Henze *et al.*, 1999) from the IAWQ task group, and an in ASM2d integrated metabolic BioP model proposed by Smolders *et al.* (1994a/b), Murnleitner *et al.* (1997) and van Veldhuizen *et al.* (1999). This model is further referred to as the TUD (Technical University Delft) model. ASM2d uses a grey box description towards EBPR, as only one organic storage compound is modelled. In the TUD model, full account is given to the metabolism of PAO and therefore all storage compounds are modelled explicitly. Eight cell-internal processes are described involving three storage polymers: PHA, glycogen and PP. An elaborate description of the TUD model is found in chapter 2.

In two previous studies, the TUD model was used to simulate full-scale EBPR; a side stream P-removal process (WWTP Haarlem Waarderpolder, Brdjanovic *et al.*, 2000) and a mainstream P-removal process (WWTP Holten, van Veldhuizen *et al.*, 1999). In this chapter, a full-scale BNR process, WWTP Hardenberg, was simulated. This MUCT-type WWTP (fig. 1.2, Wentzel *et al.*, 1990) was optimised for denitrifying EBPR according to the BCFS® design. During a three day sampling period, the pseudo steady state of the WWTP was recorded. Pseudo steady state (p.s.s.) conditions imply that the process is determined by recurring 24-hour influent variations. By definition, no significant changes in the activated sludge will occur at such conditions.

In previous research, problems were reported with the metabolic model kinetics (Brdjanovic *et al.*, 2000). In this study, the model is re-evaluated. Hereby focus was on verification of operational data, validation of the model stoichiometry and kinetics, the calibration method and the practical applicability of the TUD model at full-scale conditions.

Flow	Average ± s_D $m^3 \cdot d^{-1}$	Process unit	Volume m^3	Depth m	HRT h
Influent, Q_{IN}	6855 ± 2387	Anaerobic reactor, R1	1480	5.0	1.4
Overflow thickener to R2, Q_{OF}	[1]126	Selector reactor, S	740	5.0	0.5
Effluent, Q_{EF}	6738 ± 2516	Anoxic reactor, R2	2290	5.0	0.8
Waste activated sludge, Q_W	243 ± 299	Alternate aerated carousel, R3	4190	2.5	0.9
Pump-flow A, Q_A	18708 ± 263	Aerated carousel, R4	4190	2.5	0.9
Pump-flow B, Q_B	35236 ± 334	Clarifier, CL (2 × 2625 m^3)	5250	-	6.6
Pump-flow C, Q_C	59174 ± 3021	RAS volume	[2]150	-	0.3
Recycle activated sludge, Q_{RAS}	12126 ± 335				
Internal recycles, Q_{R4IN} and Q_{R3IN}	[3]635040	Total WWTP	18140	6981	62.4

Table 3.1 Operational data and hydraulic design parameters of the WWTP
Average measurements ± standard deviation. The hydraulic retention time (HRT) was calculated from the listed flows and volumes. Measurement [1] was estimated, [2] was estimated from denitrification in the RAS and [3] estimated from superficial flow velocity measurements.

3.2 Materials and Methods

3.2.1 WWTP Hardenberg

Wwtp Hardenberg is one of seven WWTP's managed by the Dutch water board "Groot Salland". In 1998 it was upgraded to a BCFS® process (fig. 3.1), which is a MUCT-type design. Typical process characteristics are SVI below 100 ml/g without addition of chemicals, high activity of denitrifying EBPR and PO_{EF} below 0.5 $gP \cdot m^{-3}$. The chemical phosphate stripper, as shown in fig. 3.1 was not built, however optional. An elaborate description of BCFS® and the upgrading philosophy is found in van Loosdrecht *et al.* (1998).

The WWTP was constructed from an anaerobic reactor (R1) with plug-flow characteristics, a selector reactor (S) and an anoxic reactor (R2), both supposed to be completely mixed, followed by two carrousel reactors (R3 and R4) in line (fig. 3.1). R3 aerated alternately. R4 was fully aerated. The oxygen concentration in R3 and R4 (DO_{R3} and DO_{R4}) was controlled on respectively 0.6 and 2.8 $gO_2 \cdot m^{-3}$ (table 3.3). In both R3 and R4, significant

oxygen gradients were measured (not shown). In the clarifiers (CL), activated sludge was separated from the liquid phase. Cyclic process conditions were provided by the return activated sludge (RAS) from the clarifier underflow (Q_{RAS}) and three recycle pump-flows Q_A, Q_B and Q_C. These flows were ORP controlled on the measurements ORP_{R1}, ORP_{R2} and ORP_{R3} respectively. During the recorded period, dry weather influent caused Q_A, Q_B, Q_C and Q_{RAS} to be more or less constant. In table 3.1 operational data and reactor volumes are listed. Q_A, Q_B and Q_C were measured on-line. Q_W was calculated from the capacity and operation time of the WAS pump. The overflow from the thickener (Q_{OF}) was estimated. The internal carrousel flows Q_{R3IN} and Q_{R4IN} were estimated from the superficial flow velocities in R3 and R4.

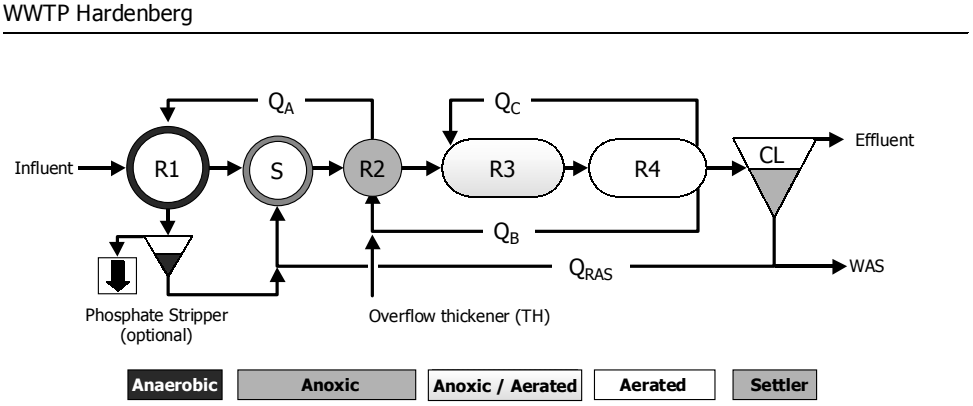

Figure 3.1 Schematic layout of WWTP Hardenberg. Dark grey, light grey, striped grey and white mark respectively anaerobic, anoxic, aerobic/anoxic and aerobic process units. For WWTP Hardenberg, R1, S, R2 and the thickener (not shown) were constructed as one circular reactor. The overflow from the thickener (Q_{OF}) was received by R2.

3.2.2 Measurements

The pseudo steady state (p.s.s.) of the WWTP was recorded during a 60-hour measurement campaign from the 23rd to the 25th of June 1998. Samples were taken every two hours from the influent (fig. 3.2), R1 (fig. 3.4), R2 (fig. 3.5), R3 and R4, WAS, overflow of the thickener and effluent. The samples were analysed on COD, COD_{MF} (COD of the micro-filtrated fraction, 0.45 μ pore diameter, no flocculation), BOD_5 (Biological Oxygen Demand), VFA (Volatile Fatty Acids), NH_4 (ammonium), NO_3 (nitrate), TKN (total Kjeldalh nitrogen), TP (total phosphorus), PO_4 (ortho-phosphate) and MLSS (Mixed Liquor Suspended Solids). Pump-flow rates, control

measurements and energy consumption and operation time of mixers and aerators and were recorded every two hours. Average measurement results are presented in tables 3.2 and 3.3.

3.2.3 The WWTP model

All simulations were performed with the TUD model (appendix III). SIMBA© 3.3+ was used as simulation platform (Alex *et al.*, 1997), which operated under Matlab/Simulink© 5.2. In SIMBA© models are constructed by connecting CSTR's in a desired process configuration. The WWTP was modelled according to the flow scheme in fig. 3.1 and data from table 3.1. R1 was modelled as three CSTR's in series. S and R2 were modelled as single CSTR's. R3 and R4 were modelled as six CSTR's with internal recycle Q_{R3IN} and Q_{R4IN}. With this set-up, longitudinal oxygen gradients in R3 and R4 were simulated sufficiently. CL separated particulate matter from the liquid phase ideally. A residual X_{EF} was modelled as a percentile loss of the RAS. Biological conversions in the RAS volume were simulated by an non-aerated CSTR placed in the RAS flow. DO_{R3} and DO_{R4} were controlled on respectively 0.6 and 2.8 $gO_2 \cdot m^{-3}$ (table 3.3). X_{R4} was controlled on 4693 $gCOD \cdot m^{-3}$ by regulating Q_W (table 3.3). This control simulated manual operation by the plant operators. In the model, Q_A, Q_B, Q_C and Q_{RAS} were constant (table 3.1).

3.2.4 Model adjustments

In the original TUD model, hydrolysis (r_h) was a function of heterotrophic micro-organisms (HMO's). In EBPR processes, PAO's grow at the expense of HMO's as both compete for the same substrate. This study showed a X_{PAO}/X_H ratio of 0.51, whereas in simulations of A_2N processes even higher ratios were observed (Hao *et al.*, 2001). This model set-up therefore caused a reduction of the hydrolysis rate. However, according to Goel *et al.* (1998 and 1999), hydrolysis is associated with the total heterotrophic biomass. Therefore in the TUD model r_h was made a function of $X_{PAO} + X_H$. The fraction particulate biodegradable matter was hereby redefined as $X_S/(X_{PAO}+X_H)$. Except for PO_{R1}, the model sensitivity towards the maximum hydrolysis rate (k_h) was relative low (table 3.6).

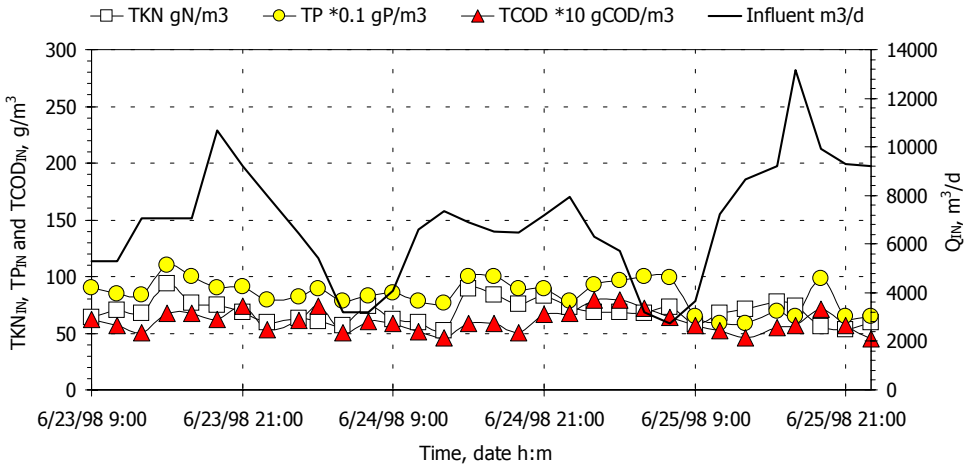

Figure. 3.2. Influent measurements. On the right axis Q_{IN}, on the left TKN_{IN}, TP_{IN} and COD_{IN}.

3.2.5 Influent characterisation

Influent was measured with a flow proportional sample collector. During the recorded period no rain events occurred. The p.s.s. of the WWTP was mainly determined by 24-hour recurring dry weather influent dynamics. Hereby sewage pumping stations caused the typical flow dynamics observed in fig. 3.2. Concentration variations in the measured influent were relative small. Variations in the influent loads (concentration × flow), therefore were primarily caused by flow dynamics. To decrease simulation time, the influent was modelled with average concentrations and actual flow data. The actual influent measurements and model influent composition are presented in table 3.2.

The influent characterisation was performed according to Roeleveld and van Loosdrecht (2001). In this method the influent X_I/X ratio is determined from BOD_5 measurements. If however, a COD_X balance is available from which X_I/X can be estimated, it is suggested not to use this method. Firstly, BOD_5 measurements are laborious and secondly, it is questioned if BOD_5 can be determined with the required accuracy for precise determination of X_I/X. The latter argument is of importance, as the simulated SRT has been found highly sensitive towards X_I/X (Brdjanovic *et al.*, 2000; van Veldhuizen *et al.*, 1999). Instead, it is suggested to use the influent X_I/X ratio to fit the COD_X balance in the model (i.e. calibrate the sludge production).

Measurement	Average± s_D	Unit	Simulation		value	Unit
Influent			**Soluble compounds**			
Total COD, TCOD	603.9 ± 95.5	gCOD·m^{-3}	Dissolved oxygen, DO	S_O	0	gO_2·m^{-3}
Micro filtrated COD, COD_{MF}	240.5 ± 37.9	gCOD·m^{-3}	Fermentable COD	S_F	109	gCOD·m^{-3}
5-day BOD, BOD_5	245.5 ± 48.7	gCOD·m^{-3}	Fatty acid	S_A	91	gCOD·m^{-3}
Tot. Kjeldalh N, TKN	68.8 ± 10.1	gN·m^{-3}	Ammonium	S_{NH}	52	gN·m^{-3}
Ammonium, NH_4	53.4 ± 8.7	gN·m^{-3}	Nitrate	S_{NO}	0	gN·m^{-3}
Nitrate, NO_3	0.1 ± 0.2	gN·m^{-3}	Ortho phosphate	S_{PO}	6.6	gP·m^{-3}
Total phosphorus, TP	8.4 ± 1.4	gP·m^{-3}	Inert COD	S_I	40	gCOD·m^{-3}
Ortho phosphate, PO_4	5.2 ± 0.8	gP·m^{-3}	Alkalinity, HCO_3	S_{HCO}	8	mole/l
Mixed liquor susp. solids, MLSS	308.6 ± 18.2	g·m^{-3}	**Particulate compounds**			
Influent fatty acids, VFA			Inert COD	X_I	174.8	gCOD·m^{-3}
Acetic acid, CH_3COOH	68.3 ± 9.2	gCOD·m^{-3}	Solid COD	X_S	188.7	gCOD·m^{-3}
Propionic acid, C_2H_5COOH	12.3 ± 1.4	gCOD·m^{-3}	Autotrophic micro-organisms	X_A	0.01	gCOD·m^{-3}
Butyric acid, C_3H_7COOH	5.4 ± 0.7	gCOD·m^{-3}	Heterotrophic micro-organisms	X_H	0.01	gCOD·m^{-3}
Valeric acid, C_4H_9COOH	5.2 ± 0.6	gCOD·m^{-3}	P-accumulating micro-organisms	X_{PAO}	0.01	gCOD·m^{-3}
Effluent			Poly-phosphate	X_{PP}	0.001	gP·m^{-3}
Micro filtrated COD, COD_{MF}	41.5 ± 5.8	gCOD·m^{-3}	Poly-hydroxybuterate	X_{PHA}	0.001	gCOD·m^{-3}
5-day BOD, BOD_5	1.9 ± 0.4	gCOD·m^{-3}	Glycogen	X_{GLY}	0.001	gCOD·m^{-3}
Overflow WAS thickener			**Overflow WAS thickener**			
Tot. Kjeldalh N, TKN	55.9 ± 14.6	gN·m^{-3}	Ammonium	S_{NH}	55.9	gN·m^{-3}
Total phosphorus, TP	47.2 ± 8.5	gP·m^{-3}	Ortho phosphate	S_{PO}	47.2	gP·m^{-3}
Ortho phosphate, PO_4	39.8 ± 8.9	gP·m^{-3}	Alkalinity, HCO_3	S_{HCO}	8	mole/l

Table 3.2. In- and effluent data and the characterised model influent. The model influent was calculated according to Roeleveld and van Loosdrecht (2001).

			R1	R2	R3	R4	Q_{EF}	Q_W
$gCOD \cdot m^{-3}$	Total COD	TCOD	3896 ±493	4698 ±522	4610 ±140	4735 ±321	42 ±8	8615 ±1762
	Simulation	**X_T+S_T**	**3954**	**4756**	**4736**	**4732**	**44**	**8468**
	Particulate COD	COD_X	3839	4654	4570	4693 ±320	0.8 ±6.4	8574 ±1762
	Simulation	**X_T**	**3898**	**4714**	**4696**	**4692**	**5**	**8428**
	Micro-filtrated COD	COD_{MF}	57 ±10	44 ±5	40 ±2	42 ±8	42 ±6	42 ±8
	Simulation	**$S_A+S_F+S_I$**	**56**	**42**	**40**	**40**	**40**	**40**
	Volatile fatty acids	COD_{VFA}	0 ±1	0	-	-	-	-
	Simulation	**S_A**	**0**	**0**	**0**	**0**	**0**	**0**
	Fermentable COD	-	17	4	-	-	-	-
	Simulation	**S_F**	**16**	**2**	**1**	**0**	**0**	**0**
$gP \cdot m^{-3}$	Total phosphorus	TP	-	-	-	155 ±6	0.2 ±0	268 ±17
	Simulation	**$S_{PO}+X_{PP}+iP$**	**124**	**152**	**152**	**152**	**0.4**	**274**
	Ortho-phosphate	PO_4	24 ±5	7.4 ±3.9	1.6 ±2.5	-	0.4 ±0.8	-
	Simulation	**S_{PO}**	**24**	**7.1**	**1.2**	**0.3**	**0.3**	**0**
$gN \cdot m^{-3}$	Tot. Kjeldalh nitrogen	TKN	-	-	-	-	2 ±1	-
	Simulation	**S_{NH} + iN**	**158**	**178**	**173**	**171**	**1**	**307**
	Ammonium	NH_4	-	6.4 ±2.6	-	0.6 ±1.8	0.3	-
	Simulation	**S_{NH}**	**19**	**6.7**	**2**	**0.4**	**0.4**	**0**
	Nitrate	NO_3	0	0.2 ±0.1	1 ±1	2.8 ±1.6	3.2 ±0.5	3.0
	Simulation	**S_{NO}**	**0**	**0.2**	**1.9**	**3.0**	**3.0**	**3.0**
$g \cdot m^{-3}$	Dissolved oxygen	DO	-	-	0.6 ±0.2	2.8 ±0.9	-	-
	Simulation	**S_O**	**0**	**0**	**0.4**	**3.0**	**3.0**	**0.1**

Table 3.3. Measurements and simulation results. Avg. measurements ± standard deviations. Values printed **bold** are simulation results.

3.3 Data Evaluation

3.3.1 Initial simulation

On the basis of the original operational data it was not possible to simulate the WWTP performance. It was observed that (i), the overall TP and solids (COD_X) balance could not be fitted simultaneously (ii), the COD_X balance over the anaerobic reactor R1 and the clarifier (CL) could not be closed and (iii), internal ammonium, nitrate and phosphate concentration profiles

could not be simulated. It was therefore concluded that operational data and or measurements contained gross errors. These data therefore were checked by evaluating the mass balances over the WWTP.

3.3.2 Evaluation of the SRT

The RAS concentration is a crucial operational parameter. In the model, via Q_W, RAS determines solids in the aeration tank (X_{AT}) and eventually the SRT. Brdjanovic *et al.* (2000) showed that the model is highly sensitive towards the SRT. For a proper simulation, the SRT should be known within 95 % accuracy. Often much lower accuracy is obtained, especially when the SRT is calculated from the RAS concentration (initially in this study 88 %, table 3.4). RAS measurements are generally inaccurate, especially when grab-samples are used. This is caused by the dynamic operation of the clarifier. Moreover, RAS samples taken from distribution works and transport-pipes with valves and bends, are known to be inaccurate caused by non homogeneous distribution of MLSS. In this study the SRT was estimated from mass balance calculations. According to fig. 3.3, four balances were formulated:

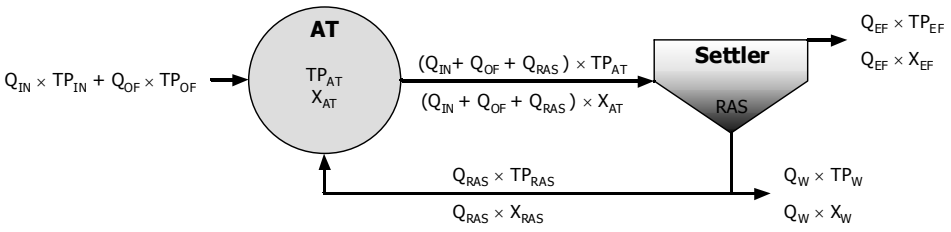

Figure. 3.3. Mass balances for SRT estimation. TP and COD_X balances over the WWTP and clarifier ($kg \cdot d^{-1}$). The mass balances are presented in eq. 3.1 to 3.4. Concentrations and flows are used from tables 3.1, 3.2 and 3.3. Table 3.4 presents the results of the balance calculations.

(i) the overall TP balance,

$$Q_{IN} \times TP_{IN} + Q_{OF} \times TP_{OF} = Q_{EF} \times TP_{EF} + Q_W \times TP_W \quad (3.1)$$

(ii) the overall flow balance

$$Q_{IN} + Q_{OF} = Q_{EF} + Q_W \quad (3.2)$$

(iii) the clarifier TP balance

$$(Q_{IN} + Q_{OF} + Q_{RAS}) \times TP_{AT} = Q_{EF} \times TP_{EF} + (Q_{RAS} + Q_W) \times TP_W \quad (3.3)$$

(iv) the clarifier solids (COD_X) balance

$$(Q_{IN} + Q_{OF} + Q_{RAS}) \times X_{AT} = Q_{EF} \times X_{EF} + (Q_{RAS} + Q_W) \times X_W \quad (3.4)$$

These mass balances only hold for steady state conditions. Concentrations and flows are obtained from tables 3.1 and 3.3. The system of four eq. (n=4), had one unknown u (Q_{OF}) and thereby n-u=3 degrees of freedom. Therefore three operational parameters could be estimated. The least reliable parameters were chosen, being Q_W, TP_W and X_W (table 3.3). For the calculations, the equation solver "Maple V" was used (Char *et al.*, 1991). Initially no satisfactory solutions were found. It was however possible to solve eq. 3.1 and 3.2, hereby finding solutions for Q_W and TP_W. We relied on accurate measurement of solids (X_{AT}) and TP in R4. Therefore, a gross error in Q_{RAS} was assumed. By adjusting Q_{RAS} to 1.2 times Q_{IN}, as specified in the original plant design (Q_{RAS} = 8226 $m^3 \cdot d^{-1}$), it was possible to balance the system within the error of measurements (table 3.4).

3.3.3 Evaluation of recycle flow A

Because it was not possible to simulate the solids concentration in the anaerobic tank R1 (X_{R1}), the solids balance over R1 (eq. 3.5) was formulated.

$$Q_{IN} \times X_{IN} + Q_A \times X_{QA} = (Q_{IN} + Q_A) \times X_{R1} \quad (3.5)$$

In this balance, formation and degradation of PAO storage polymers and anaerobic hydrolysis are neglected. Solving eq. 3.5 for Q_A resulted in 29012 $m^3 \cdot d^{-1}$, being well above the maximum pump capacity of 18000 $m^3 \cdot d^{-1}$. Therefore, an additional balance was formulated.

$$Q_{IN} \times PO_{IN} + Q_A \times PO_{R2} + Q_{IN} \times VFA_{IN} \times Y_{PO} = (Q_{IN} + Q_A) \times PO_{R1} \quad (3.6)$$

Eq. 3.6 is the phosphate balance over R1. In this balance the anaerobic PO_4 release is calculated based on VFA_{IN} and the yield according to Smolders *et al.* (1994a, Y_{PO}=0.36 gP/$gCOD_{Ac}$). Hereby formation of VFA by hydrolysis was neglected. Solving eq. 3.5 and 3.6 simultaneously, resulted in a minimal flow Q_A of 22415 $m^3 \cdot d^{-1}$ and a solids concentration in flow Q_A (X_{QA}) of 4895 $gCOD \cdot m^{-3}$. The high calculated value of X_{QA} could be caused by settling of particulate matter in R2. Therefore, retention of solids in R2 was modelled. Applying the estimated values for X_{QA} and Q_A, the solid and phosphate concentration in the anaerobic reactor were simulated satisfactory (fig. 3.4).

Mass balance calculations (eq. 3.1 to 3.7)	Average ± s_D	Balanced	Unit
Estimation of the SRT			
Return activated sludge flow, Q_{RAS} (Q_{RAS}=1.2*Q_{IN})	12126 ± 335	8226	$m^3 \cdot d^{-1}$
Overflow thickener, Q_{OF}	[1]126	102	$m^3 \cdot d^{-1}$
Waste activated sludge flow, Q_W	244 ± 299	219	$m^3 \cdot d^{-1}$
Total phosphorus in WAS, TP_W	268 ± 17	278	$gP \cdot m^{-3}$
Total particulate in WAS, X_W	8574 ± 1762	8411	$gCOD \cdot m^{-3}$
Sludge retention time, SRT	28.9	32.8	d
Estimation of Q_A			
Pump-flow A, Q_A	18708 ± 263	22415	$m^3 \cdot d^{-1}$
MLSS in flow A, X_{QA}	4654 ± 522	4895	$gCOD \cdot m^{-3}$
Estimation of Q_B			
Pump-flow B, Q_B	35236 ± 334	44536	$m^3 \cdot d^{-1}$

Table 3.4. Results of SRT and flow estimations. Average measurements ± standard deviation and balanced operational data according to eq. 3.1 to 3.7. [1] was estimated from grab samples.

3.3.4 Evaluation of recycle flow B

Because ammonium and nitrate in reactor R2 could not be simulated, a ammonium balance over R2 was formulated (eq. 3.7).

$$Q_{IN} \times NH_{IN} + Q_{OF} \times NH_{OF} + Q_B \times NH_{R4} + Q_{RAS} \times NH_{EF} = (Q_{IN} + Q_{OF} + Q_B + Q_{RAS}) \times NH_{R2} \quad (3.7)$$

In this balance, nitrification, ammonification and biomass growth in R2 were neglected. From eq. 3.7, flow Q_B was estimated under the assumptions that (i), ammonium in R2 was accurate (6.4 ± 2.6 $gN \cdot m^{-3}$) (ii), ammonium in the effluent and R4 were negligible and (iii), Q_{RAS}=1.2×Q_{IN}. From eq. 3.7 it was calculated that Q_B was 44536 $m^3 \cdot d^{-1}$, which is 1.27 times higher than the original value (35000 $m^3 \cdot d^{-1}$). Because the measurement of Q_B showed unreliable, in the simulation Q_B was used to calibrate ammonium and nitrate in R2 (table 3.3, fig. 3.5). This resulted in a calibrated flow of Q_B=44300 $m^3 \cdot d^{-1}$.

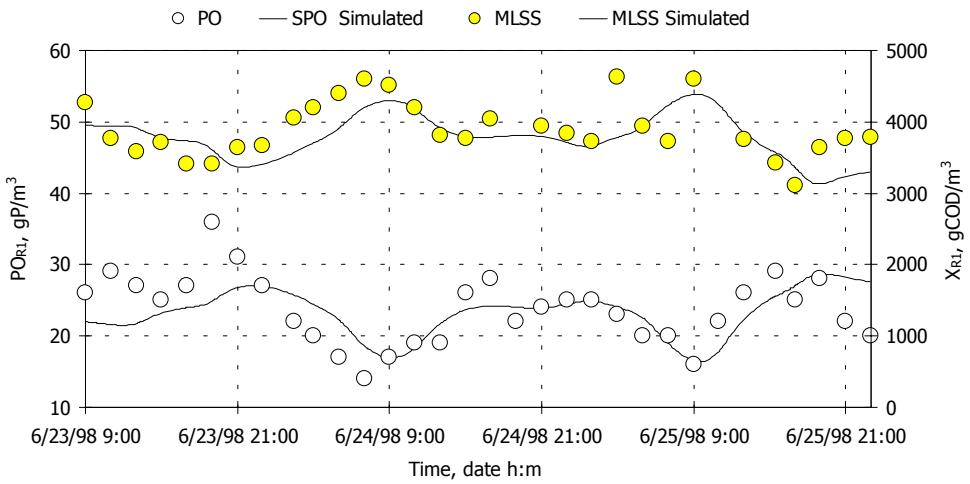

Figure 3.4 Measurement and simulation of X_{R1} and PO_{R1}. Measurements are markers, simulations lines.

3.4 Model Calibration

After the operational data were checked and measurements were balanced, the model was ready for calibration. Hereby a stepwise approach was used. Simulation time was reduced by starting with static simulations. The model was fitted on the average measurements presented in table 3.3.

Step 1. Calibrating the COD_X balance. X_{R4} was controlled on 4693 ± 320 gCOD·m^{-3} by regulating Q_W. Assuming the yield of the process was constant, the SRT is a function of the influent X_I/X ratio according to fig. 3.6. Roeleveld and van Loosdrecht (2001) proposed to estimate the influent X_I/X ratio based on influent BOD_5 measurements. The author however proposes a more accurate method, in which the WAS production is estimated from the overall TP balance (eq. 3.1). On the basis of the WAS production, the COD_X balance was closed by calibrating the influent X_I/X ratio. The calibrated ratio was found to be 0.507.

Step 2. Calibrating nitrification. The overall nitrified load (^{L}NIT kgN·d^{-1}) could be simulated without calibration. However, during the calibration procedure unrealistic low phosphate in R4 caused growth limitation of autotrophic micro-organisms (AMO's). Therefore, temporarily the phosphate affinity for growth of AMO's ($K_{N,PO}$) was reduced to 0.001 gP·m^{-3}.

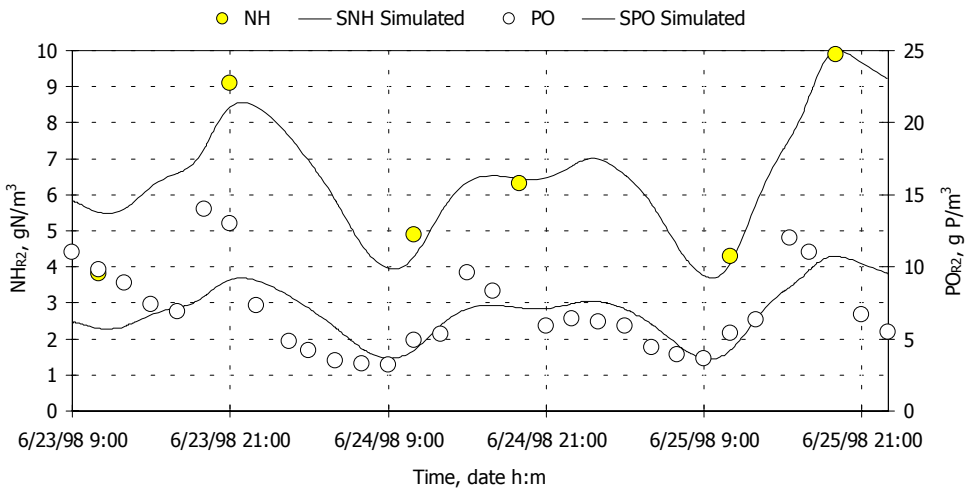

Figure 3.5 Measurement and simulation of NH_{R2} and PO_{R2}. Measurements are markers, simulations lines.

Step 3a. Calibrating denitrification in the RAS volume. Some denitrification occurred in the RAS volume (0.3 $gN \cdot m^{-3}$, table 3.3). From the calculated denitrified load ($^{L}NO_{RAS}$), the RAS volume was estimated to be 150 m^3.

3.4.1 Simultaneous Nitrification and Denitrification

Simultaneous nitrification and denitrification (SND) often occurs in full-scale WWTP's. Non ideal mixing and (partial) settling of activated sludge in the aeration tank causes oxygen gradients and diffusion limitations. Therefore, the actual anoxic volume often is higher than the designed anoxic volume. With the COD & N balance, the overall denitrified load (^{L}DEN, $kgN \cdot d^{-1}$) is calculated (Nowak *et al*, 1999a). To fit denitrification and thereby correct for the actual anoxic volume, the calibration parameter K_O was introduced. In the model, K_O replaces the oxygen affinity for PAO's ($K_{P,O}$) and HMO's ($K_{H,O}$). The sensitivity of K_O towards nitrate in the effluent (NO_{EF}) is a function of X_I/X. This relation is shown in fig. 3.7. The net effect of increasing K_O is an increase of the anoxic activated sludge fraction (fig. 3.8), as if the oxygen penetration depth in the sludge flocs is decreased, hereby causing an anoxic zone in the centre of the floc (Pochana and Keller, 1999).

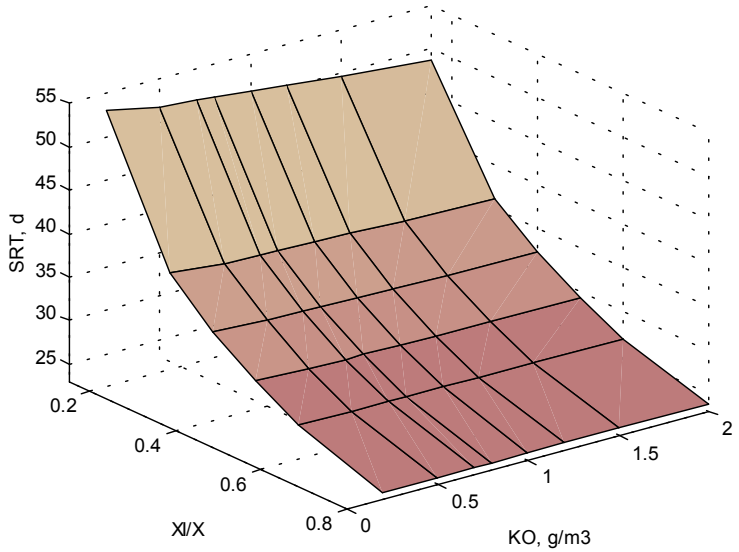

Figure. 3.6 SRT as a function of the influent X_I/X ratio and K_O. With X_I/X the COD_X balance is fitted. This process is also effected by K_O.

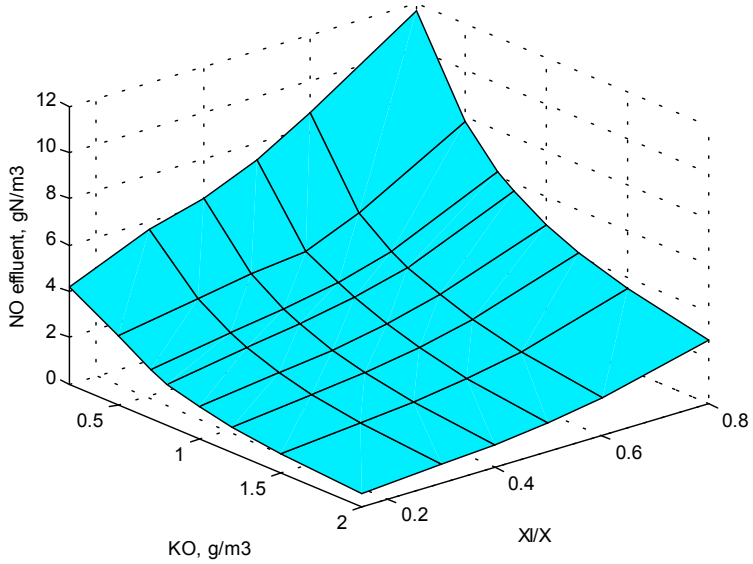

Figure. 3.7 NO_{EF} as a function of the influent X_I/X ratio and K_O. K_O is used to fit ^{L}DEN. This process is also effected by X_I/X.

Step 3b. Calibrating the anoxic sludge fraction. After the nitrified load (^{L}NIT) was fitted and solid COD fraction (COD_X) was balanced (step 1 and 2), the denitrified load (^{L}DEN) was fitted (i.e. the anoxic sludge fraction was fitted). Therefore K_O was increased from 0.2 to 0.7 $gO_2 \cdot m^{-3}$. Fig. 3.7 shows how this caused NO_{EF} to decrease from 6.5 to 3.2 $gN \cdot m^{-3}$ in relation to X_I/X=0.507.

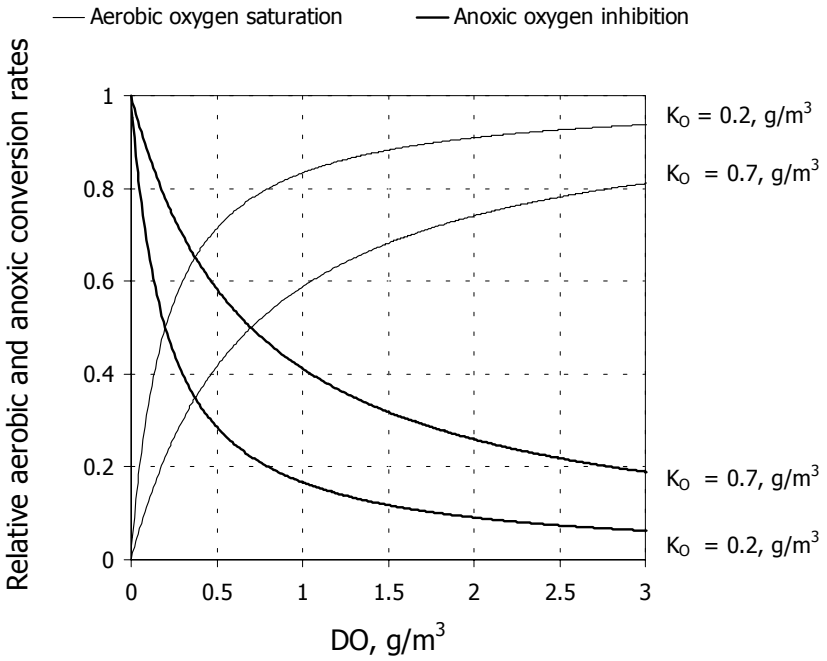

Figure. 3.8 The aerobic and anoxic conversion rate as function of K_O. The aerobic oxygen saturation is plotted in thin lines, the anoxic oxygen inhibition in bold lines. K_O was increased from 0.2 to 0.7 $gO_2 \cdot m^{-3}$ to increase ^{L}DEN.

Step 4. Calibrating the anoxic phosphate uptake. Because EBPR has a limited influence on other processes in the model, the phosphate profile over the WWTP was calibrated last. The anaerobic phosphate concentration (PO_{R1}) was simulated correctly with the adjusted kinetics for hydrolysis. PP formation depends on the electron acceptor (oxygen or nitrate). Murnleitner *et al.* (1997) however, observed a reduced electron acceptor affinity for PP formation. In the model this is expressed in the reduction factor g_{PP} (<1). Originally for g_{PP} a value of 0.1 was proposed, hereby increasing the affinity for oxygen according to $g_{PP} \times K_O$ and $g_{PP} \times K_{P,NO}$.

In this study the oxygen affinity for PP formation was reduced by increasing g_{PP} to 0.25. Hereby the phosphate profile over the WWTP (PO_{R2}, PO_{R3} and PO_{R4}) was simulated sufficiently (table 3.3).

Step 5. Calibrating the net oxygen consumption. The COD_X balance was fitted by adjusting the influent X_I/X ratio. There is however, a second (independent) balance related to COD_X, being the COD & N balance (Nowak *et al.*, 1999a). COD and N balances are linked via denitrification and therefore have to be solved simultaneously. From the COD & N balance it was calculated that the net oxygen consumption OC_{NET} was 2631 $kgO_2 \cdot d^{-1}$ (table 3.5). The simulated OC_{NET} was 2597 $kgO_2 \cdot d^{-1}$, which indicated that the calibration was sufficient.

COD & N mass balance calculation		Balanced	Unit
Oxygen for NH_4 oxidation (nitrification)	OC_{NIT}	1595	$kgO_2 \cdot d^{-1}$
Oxygen for COD oxidation	OC_{COD}	1037	$kgO_2 \cdot d^{-1}$
Total oxygen consumption	OC_{NET}	2631	$kgO_2 \cdot d^{-1}$
COD oxidised with NO_3 (denitrification)	$^{L}COD_{DEN}$	958	$kgCOD \cdot d^{-1}$
Total COD oxidised	$^{L}COD_{BD}$	1995	$kgCOD \cdot d^{-1}$
Nitrification rate	^{L}NIT	349	$kgN \cdot d^{-1}$
Denitrification rate	^{L}DEN	334	$kgN \cdot d^{-1}$

Table 3.5. The COD & N mass balance calculation. (Nowak *et al.*, 1999a).

3.5 Discussion

3.5.1 Fitting models on faulty data

The P balance is a closed balance, indicating that all in and outgoing TP loads can be recovered in the liquid phase. In contrast to the P balance, the COD & N balance has compounds in the gaseous phase (O_2 and N_2). Usually this is not measured. When a model is fitted on faulty data, the COD & N balance is "closed" by over- or underestimating O_2 and N_2. The P balance however, can not be fitted on faulty data unnoticed, as all loads are generally measured. Consequently, BioP models can not be fitted on faulty measurements (ASM2d, TUD), whereas models lacking this balance can (ASM1, ASM3). The P-balance is an extra independent balance coupled to the solids balance (COD_X), and therefore useful for error detection and estimation of the SRT. For a proper simulation, the SRT has to be known with an accuracy higher than 95 % (Brdjanovic *et al.*, 2000). In modelling practice, this means that the P balance should fit.

		Calibration parameters				Operational data			
y\p	Reactor	g_{PP}	K_O	k_h	X_I/X	Q_A	Q_B	Q_W	Q_{RAS}
PO_4	1	0.1	0.2	0.1	-0.4	-1.1	-0.3		
	2	0.3	0.5	0.2	-0.8	-0.4	-1.3		-0.3
	3	0.4	0.5		-0.3		-0.4		-0.4
	4	0.5	0.5			0.4			-0.5
NO_3	1		-11.0		2.7				
	2		-7.7		1.7		1.5		-0.2
	3		-2.3		1.1		-0.5		-0.2
	4		-1.6		0.7		-0.5		-0.2
NH_4	1					-0.6	-0.3		
	2					-0.1	-0.9		-0.1
	3					-0.2	-0.4		-0.2
	4		-0.1			-0.4			-0.1
COD_S	1		0.1	0.2					
	2								
	3								
	4								
COD_X	1				0.5	-1.4		-0.7	0.4
	2				0.5	-0.1		-0.7	0.4
	3				0.5	-0.1		-0.7	0.4
	4				0.5	-0.1		-0.7	0.4
X_{PAO}	1		0.2	0.2	-0.6	-1.9		-0.6	0.2
	2		0.2	0.2	-0.6	-0.5		-0.6	0.2
	3		0.2	0.2	-0.6	-0.5		-0.6	0.2
	4		0.2	0.2	-0.6	-0.5		-0.6	0.2
X_A	1					-1.12		-0.2	0.1
	2					0.2		-0.2	0.1
	3					0.2		-0.2	0.1
	4					0.2		-0.2	0.1

Table 3.6 Sensitivity analysis of model parameters and operational data. The most sensitive parameters are presented (top row). The sensitivity was calculated according to eq. 3.8. Only sensitivity above 0.1 is shown.

3.5.2 Sensitivity analysis

To evaluate the sensitivity of the estimated operational data (table 3.4) and calibrated parameters, a sensitivity-analysis was performed. Eq. 3.8 shows the sensitivity (s) expressed as relative change of the modelled concentration (y) divided by the relative change of the calibrated parameter (p) according to van Veldhuizen *et al.* (1999).

$$s = \frac{dy/y}{dp/p} \tag{3.8}$$

Results of the analysis are presented in table 3.6. It is seen that the proposed calibration parameters (g_{PP}, K_O, k_h, X_I/X) are sensitive to specific processes. This simplifies the calibration procedure. The estimated operational data however, show a more general sensitivity (Q_A, Q_B, Q_W and Q_{RAS}). The high sensitivity of operational data is expressed by the inability to calibrate the model while using erroneous data. Performing simulations with erroneous data generally leads to laborious and unjust calibrations of kinetic and/or stoichiometric model parameters. It was also observed that model kinetics generally are less sensitive than stoichiometric parameters and operational data (not shown).

3.5.3 A heuristic calibration approach

The proposed calibration method is rather qualitative than quantitative. Calibration parameters were selected on the basis of process knowledge rather than mathematical sensitivity analysis. This approach resulted in the introduction of the black box calibration parameter K_O that was introduced to correct for hydrodynamic and physical shortcomings of the plant model. Additionally the calibration parameter X_I/X was introduced to balance COD_X for a given SRT.

Several mathematical parameter calibration methods were developed (Weijers *et al.*, 1997; Yuan *et al.*, 1997; von Sperling, 1993; Wanner *et al.*, 1992). In this study however, a largely heuristic approach was used for several reasons. Firstly, it was observed that the model was more sensitive towards operational data than towards model parameters. Therefore, evaluation of input data was preferred over calibration of model parameters. Secondly, mathematical calibration procedures usually neglect the influence of faulty operational data, and instead, focus on model kinetics and stoichiometric parameters. Finally, it was observed that after balancing faulty operational data and measurements, only minor calibration was required to fit the model.

It is the opinion of the author that model calibration in first instance should be focused on the evaluation of operational data. From previous experience with the TUD model (van Veldhuizen *et al.*, 1999; Brdjanovic *et al.*, 2000; this study) it was concluded that only minor calibration was needed after correcting errors in the operational data. Table 3.7 gives an overview of model parameters that were calibrated for simulation of WWTP

Haarlem Waarderpolder (Hrlm), WWTP Holten (Hltn) and WWTP Hardenberg (Hdbg). For none of these studies the model stoichiometry required calibration. Caused by shortcomings of the activated sludge model (ASM1, ASM2d, TUD and ASM3), the parameters K_O and X_I/X will need adjustment for each simulated WWTP. This should be considered when extrapolating the model to new conditions.

In this simulation study, model (EBPR) kinetics were found to be less sensitive. This generally will be the case for low loaded WWTP's at p.s.s. conditions. Under such conditions, only kinetic rates that are limiting, will be sensitive for calibration. Therefore, such conditions are not suitable for a proper kinetic model evaluation.

Calibration parameters	Hltn	Hrlm	Hdbg	default	reference
Maximum fermentation rate, q_{fe}	1	1	[4]3	3	Henze, 1999
PP storage rate, K_{PP}	0.07	0.05	0.05	0.05	Murnleitner, 1997
Glycogen storage rate, K_{GLY}	1.09	0.15	1.09	1.09	Murnleitner, 1997
Anoxic PAO reduction factor, η_{PNO}	0.7	0.8	0.8	[2]0.5	Murnleitner, 1997
X_I influent fraction, X_I/X	[1]0.57	[1]0.67	[1]0.49	-	This chapter
Affinity reduction factor, g_{PP}	0.1	0.1	0.25	0.1	Murnleitner, 1997
DO affinity, K_O	[3]0.2	[3]0.2	0.7	0.2	Henze, 1999

Table 3.7 **Full scale calibration parameters.** Calibration results of simulations of Hltn (WWTP Holten by van Veldhuizen *et al.*, 1999), Hrlm (WWTP Haarlem Waarderpolder by Brdjanovic *et al.*, 2000), and Hdbg (WWTP Hardenberg). **[1]** COD_X balance calibrated based on the influent X_I/X ratio, **[2]** default value proposed to be set to 0.8, **[3]** denitrification calibrated by adjusting aeration, **[4]** after redefinition of the hydrolysis kinetics.

3.5.4 The calibration procedure

The proposed stepwise calibration resulted in a orderly and relative quick calibration. The most sensitive parameters were calibrated first (X_I/X, K_O, k_h, g_{PP}). The sensitivity analysis in table 3.6 shows that the selected calibration parameters primarily affected the intended processes, leaving other process more ore less unaffected. Therefore the amount of iteration loops could be reduced. Iteration is however inevitable, as processes in the model are linked. Fig. 3.6 shows this effect for the COD_X balance, which is effected by calibration of denitrification (K_O). Increasing denitrification results in a decrease of the SRT, caused by different anoxic and aerobic yields. This should then be corrected by readjusting X_I/X, which again affects denitrification etc.. However, because this effect, was relative small, only one iteration was required.

3.5.5 Balancing solids

Fig. 3.6 shows the sensitivity of X_I/X towards the SRT. X_I is not converted and therefore accumulates in the WWTP. When X_{AT} is controlled, increasing X_I/X leads to a increase of ^{L}WAS (i.e. decreasing SRT). The relation between SRT and X_I/X is not linear, caused by a increasing contribution of lysis and maintenance at higher SRT. Extrapolation of the model to a higher SRT, causes a shift in the COD_X balance as was described by Nowak *et al.* (1999b). In the model, X_I is defined as being inert. In practice however, hydrolysis of the inert fraction will take place very slowly. In the model this effect should be corrected by lowering the influent X_I/X ratio.

3.5.6 Calibrating K_O

In the TUD model, K_O is used to fit ^{L}DEN and thereby correct for the actual anoxic volume, which is caused by oxygen diffusion limitations in sludge flocs and concentration gradients in the aeration tank caused by non-ideal mixing. In an attempt to model these processes explicitly, Alex *et al.* (1999) proposed a hydrodynamic mixing model. Such a model will be of limited use as long as (i), diffusion limitations in flocs are not properly described and (ii), the proposed mixing model requires new (unknown) parameters for vertical liquid exchange. Instead, the aeration tank was simulated with a relative simple hydrodynamic set-up and approximation of the actual (fuzzy-logic) oxygen control. Hereby, the modelling error that was introduced in the anoxic sludge fraction was corrected by calibrating K_O. According to fig. 3.8, increasing K_O from 0.2 to 0.7 caused an increase of denitrification of approx. 30 % in R3 and 10 % in R4. Hereby aerobic conversions decreased proportionally. This resulted in a decrease of NO_{EF} from 6.5 to 3.2 $gN \cdot m^{-3}$ for X_I/X=0.507 (fig. 3.7).

3.5.7 The COD & N balance

The final calibration step (5), was a check on the calibrated model. The COD & N balance is related to the COD_X balance via ^{L}NIT, ^{L}DEN, OC_{COD} and OC_{NET}. This relation is shown in fig. 3.9. Calculation of the COD & N balance corresponded with the modelled OC_{NET}, providing a check on the calibrated model.

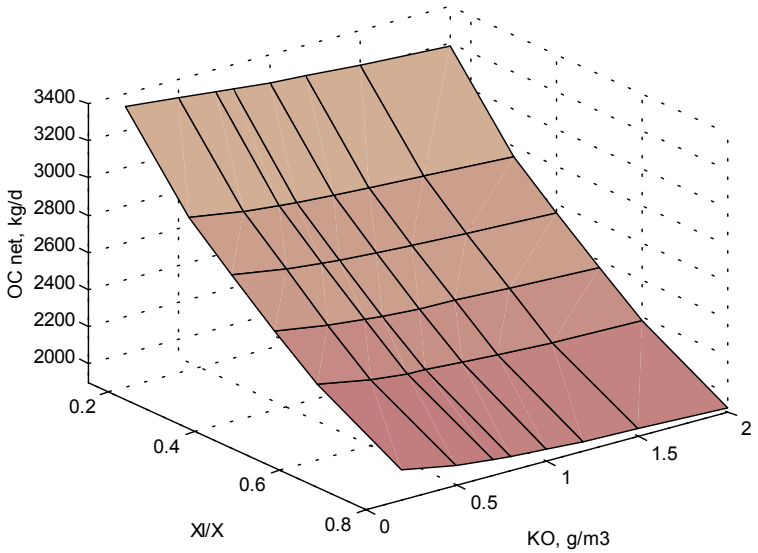

Figure 3.9 OC_{NET} as a function of the influent X_I/X ratio and K_O. Increasing K_O enlarges the anoxic conversion rate while aerobic rates are decreased accordingly, which slightly effects OC_{NET}.

3.6 Conclusions

Without changing the stoichiometric matrix of the TUD model, the pseudo steady state of WWTP Hardenberg was simulated, hereby predicting effluent as well as process internal concentration profiles correctly. Based on this and previous research, it is concluded that the stoichiometric matrix of the TUD model, that was developed from lab experiments, can be extrapolated to full-scale conditions without calibration.

Correct estimation of operational data, in particular the SRT, showed decisive for an accurate simulation. This was caused by high model sensitivity towards operational data. Adjustment of erroneous operational data was therefore preferred over calibration of model parameters. Based on mass balance calculations, five process flows and three measured concentrations were estimated. Model (EBPR) kinetics were found less sensitive and therefore less suitable for model calibration. This will generally be the case for low loaded (i.e. over dimensioned) WWTP's at p.s.s. conditions. Two calibration parameters were introduced, K_O and X_I/X. Both require calibration for each simulated system. Calibration of K_O proved a straightforward black box solution to modelling diffusion

limitations in activated sludge processes. The influent ratio X_I/X was calibrated to balance solids in the model for a given SRT.

The calibration method that was proposed in this chapter was rather qualitative than quantitative, selecting calibration parameters on the basis of processes knowledge, rather than on sensitivity analysis. The stepwise calibration method provided an orderly and relative quick calibration, minimising iteration loops. Only three model parameters were changed, each parameter calibrating a specific balance in the model. Calculation of the COD & N balance proved an useful final check on the calibrated model.

References

Alex J., Tschepetzki R. and Bitter U. (1997) SIMBA Simulation of biological waste water treatment. Users manual, Institute of Automation and Communication e. V., Magdeburg.

Alex J., Tschepetzki R., Jumar U., Obenaus F. and Rosenwinkel K. H. (1999) Analysis and design of suitable model structures for activated sludge tanks with circulating flow. *Water Sci. Technol.* **39**(4), 55-60.

Brdjanovic D., van Loosdrecht M. C. M., Versteeg P., Hooijmans C. M., Alaerts G. J. and Heijnen J. J. (2000) Modelling COD, N and P removal in a full-scale WWTP Haarlem Waarderpolder. *Water Res.* **34**(3), 846-858.

Char B.W., Geddes K.O., Gonnet G.H., Leong B.L., Monagan M.B. and Watt S.M. (1991) Maple V Language reference manual. Springer Verlag, ISBN 0-387-94124-X, 267p.

Goel R., Mino T., Satoh H. and Matsuo T. (1998) Comparison of hydrolytic enzyme systems in pure culture and activated sludge under different electron acceptor conditions. *Water Sci. Technol.* **37**(4-5), 335-343.

Goel R., Mino T., Satoh H. and Matsuo T. (1999) Modeling hydrolysis processes considering intracellular storage. *Water Sci. Technol.* **39**(1), 97-105.

Gujer W., Henze M., Mino T. and van Loosdrecht M. (1999) Activated Sludge Model No. 3. *Water Sci. Technol.* **39**(1), 183-193.

Henze M., Gujer W., Mino T., Matsuo T., Wentzel M. C., Marais G. v. R. and van Loosdrecht M. C. M. (1999) Activated Sludge Model No.2d, ASM2d. *Water Sci. Technol.* **39**(1), 165-182.

Hao X., van Loosdrecht M. C. M., Meijer S. C. F. and Qian Y. (2001) Model Based Evaluation of two BNR processes – UCT and A_2N. *Wat. Res.* **35**(12), 2851-2860.

Murnleitner E., Kuba T., van Loosdrecht M. C. M. and Heijnen J. J. (1997) An integrated metabolic model for the aerobic and denitrifying biological phosphorous removal. *Biotechnol. Bioeng.* **54**, 434-450.

Nowak O., Franz A., Svardal K., Muller V. and Kuhn V. (1999a) Parameter estimation for activated sludge models with the help of mass balances. *Water Sci. Technol.* **39**(4), 113-120.

Nowak O., Svardal K., Franz A. and Kuhn V. (1999b) Degradation of particulate organic matter - A comparison of different model concepts. *Water Sci. Technol.* **39**(1), 119-127.

Pochana K. and Keller J. (1999) Study of factors affecting simultaneous nitrification and denitrification (SND). *Water Sci. Technol.* **39**(6), 61-68.

Roeleveld P.J and Van Loosdrecht M.C.M. (2001) Experiences with guidelines for wastewater characterisation in The Netherlands. *Wat. Sci. Technol.* **45**(6), 145-156.

Smolders G. L. F., van der Meij J., van Loosdrecht M. C. M. and Heijnen J. J. (1994a) Model of the anaerobic metabolism of the biological phosphorous removal process: stoichiometry and pH influence. *Biotechnol. Bioeng.* **43**(6), 461-470.

Smolders G. L. F., van der Meij J., van Loosdrecht M. C. M. and Heijnen J. J. (1994b) Stoichiometric model of the aerobic metabolism of the biological phosphorus removal process. *Biotechnol. Bioeng.* **44**(7), 837-848.

Van Loosdrecht M.C.M., Brandse F.A. and de Vries A.C. (1998) Upgrading of wastewater treatment processes for integrated nutrient removal – The BCFS® process. *Water Sci. Technol.* **37**(9), 209-217.

Van Veldhuizen H. M., van Loosdrecht M. C.M. and Heijnen J. J. (1999) Modelling biological phosphorus and nitrogen removal in a full scale activated sludge process. *Water Res.* **33**(16), 3459-3468.

Von Sperling M. (1993) Parameter estimation and sensitivity analysis of an activated sludge model using Monte Carlo simulation and the analyst's involvement. *Water Sci. Technol.* **28**(11-12), 219-229.

Wanner O., Kappeler J. and Gujer W. (1992) Calibration of an activated sludge model based on human expertise and on a mathematical optimisation technique, a comparison. *Water Sci. Technol.* **25**(6), 141-148.

Wentzel M. C., Ekama G. A. and Marais G. v. R. (1992) Processes and modelling of nitrification denitrification biological excess phosphorus removal systems - a review. *Water Sci. Technol.* **25**(6), 59-82.

Wentzel M. C., Ekama G. A., Dold P. L., Marais G. v. R. (1990) Biological excess phosphorus removal. Steady state process design. *Water SA.* **16**(1), 29-48.

Weijers S. R. and Vanrolleghem P. A. (1997) Procedure for selecting best identifiable parameters in calibrating Activated Sludge Model No. 1 to full-scale plant data. *Water Sci. Technol.* **36**(5), 69-79.

Yuan Z., Vanrolleghem P. A. and Vansteenkiste G. C. (1997) Modelling error identification of activated sludge models. *Water Sci. Technol.* **36**(5), 81-88.

4

Modelling the Start-Up of a Biological Nutrient Removing WWTP

In the previous chapter it was shown that wastewater treatment plants simulated at (pseudo) steady state have a low kinetic sensitivity. An increased sensitivity of the model kinetics was expected at start-up conditions. Therefore a full-scale start-up was evaluated in a simulation study. A kinetic sensitivity analysis showed that the model converged to identical steady states, disregarding the kinetic parameter values. This observation underlined that the BioP process is largely determined by stoichiometry. The sensitivity analysis showed that the glycogen formation rate and the temperature were most sensitive in the model. By including a temperature profile in the model, simulation results improved significantly. It was shown that in the metabolic model growth is mainly determined by the by the glycogen formation rate. By carefully fitting this process, good simulation results were obtained. The glycogen formation rate was found to be highly sensitive in the model. A maximum glycogen fraction was introduced to avoided model instability. With this practical adjustment, unrealistic accumulation of glycogen in the model could be avoided.

This chapter was largely based upon Meijer *et al.* (2002) *Water. Res.* **36**, 4667-4682.

4.1 Introduction

In the previous chapter and studies by van Veldhuizen *et al.*, 1999 and Brdjanovic *et al.*, 2000, the metabolic model was used to simulate full-scale WWTP's at pseudo steady state. Such conditions imply that the process is determined by recurring 24-hour influent dynamics, whereas the activated sludge composition remains unchanged. In chapter 3, it was demonstrated that under such conditions the model kinetics are insensitive. Kinetics however, become sensitive when a shift of the microbiological population is induced. This would be the case under start-up conditions. To evaluate the model kinetics, the start-up of a full-scale UCT-system was evaluated in a simulation study.

4.2 Material and Methods

4.2.1 The start-up procedure

WWTP Hardenberg, managed by the Dutch water board 'Groot Salland', is one of seven WWTP's upgraded according to the BCFS®-design. BCFS® is a MUCT-type design, optimised for denitrifying EBPR. The process scheme of the original plant, WWTP Hardenberg-Old (H-Old), and the upgraded process are shown in fig. 4.1. A detailed description of BCFS® and the upgrading philosophy is found in chapter 3 and van Loosdrecht *et al.* (1998).

The old WWTP was originally designed for COD removal and nitrification, however some denitrification and BioP were measured. In 1998, WWTP H-Old was upgraded by introducing three additional process units, R1, S and R2, with new process flows Q_A, Q_B and Q_C. During the construction, WWTP H-Old remained in operation. The existing carrousel reactors R3 and R4, and the clarifier units (CL) were integrated in the newly built configuration. The start-up was initiated instantly by redirection of the process flows.

A start-up is a transition from an initial to a final (pseudo steady) state. For the start-up of WWTP Hardenberg, the initial state was the p.s.s. of WWTP H-Old (t=0, the 4th of February 1998). The final state was measured after 140 days, corresponding with the p.s.s. of WWTP Hardenberg recorded on the 23rd to the 25th of June 1998 (chapter 3). The inoculum for the start-up was activated sludge from WWTP H-Old. At that time, R1, S and R2 were filled with effluent.

4.2.2 Recording the original WWTP

The pseudo steady state of the original WWTP (H-Old) was recorded during 60-hours (the 20th to the 22nd of January 1998). Every two hours, samples were collected from the influent, contact tank (S), aeration tank (R4), WAS, thickener overflow and effluent. The samples were analysed on MLSS, TCOD, COD_{MF}, BOD_5, VFA, TKN, NH_4^+, NO_3^-, TP and PO_4^{2-}. Pump flow rates (table 4.1), dissolved oxygen (DO) and the oxidation reduction potential (ORP) and energy use and operation time of mixers and aerators were recorded every two hours. The average measurement results are presented in table 4.2.

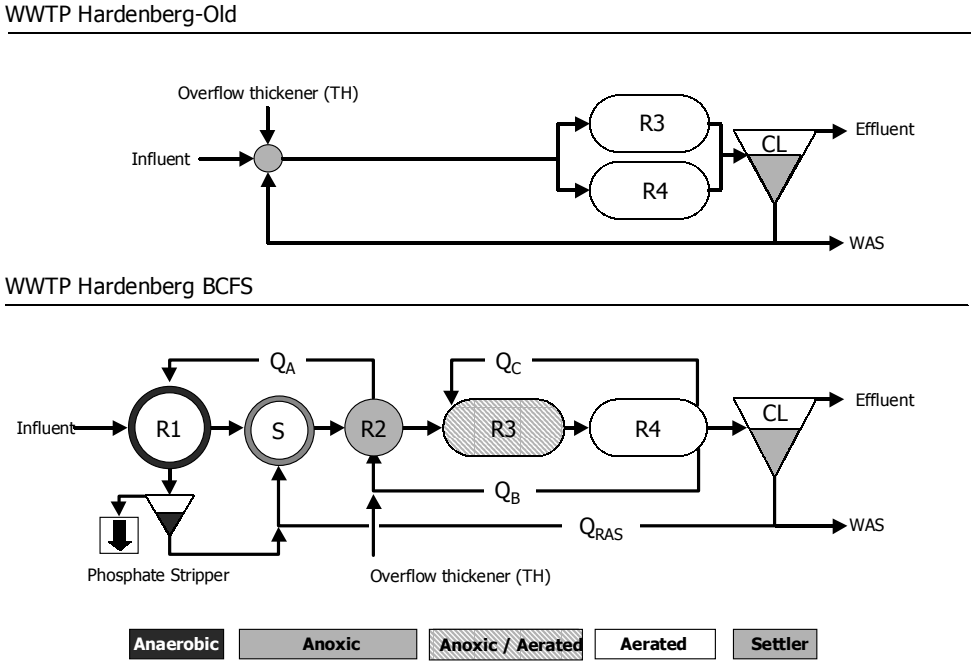

Figure 4.1 Basic plant scheme of the old and new WWTP. White represents aerobic conditions, grey scales (dark to light) anaerobic, anoxic, and anoxic/aerobic conditions. Carrousels R3 and R4 were integrated in the new process. R1, S, R2 and the thickener (not shown), were constructed as one circular reactor (van Loosdrecht *et al.*, 1998). R1 was a plug flow reactor. S, R2 and R3 and R4 were completely mixed. The phosphate stripper was not applied. R2 received an internal loading from the overflow of the thickener (Q_{OF}). Q_A, Q_B and Q_C were ORP set-point controlled (van Loosdrecht *et al.*, 1998).

4.2.3 Measuring the start-up

During the 140-day start-up (the 4th of February to the 22nd of June 1998), influent, R1, R2, R3 and R4, effluent, WAS and thickener were sampled. Samples were analysed on MLSS, TP, phosphate, ammonium and nitrate During the first 60 days, phosphate, ammonium and nitrate in R2 (NH_{R2}, NO_{R2} and PO_{R2}) were measured on-line. Every two hours, process control measurements (DO and ORP) and energy use and operation time of mixers and aeration and were recorded. Growth of PAO's was estimated regularly from phosphate release batch-tests (Brdjanovic *et al.*, 1997).

Flow	Average ± s_D $m^3 \cdot d^{-1}$	Process unit	Volume m^3	Depth m	HRT h
Influent, Q_{IN}	5761 ± 2788	Selector reactor, S	40	2.5	0.06
Overflow thickener, Q_{OF}	97	Aerated carousel, R3	4190	2.5	11.7
Effluent, Q_{EF}	5313 ± 2817	Aerated carousel, R4	4190	2.5	11.7
Waste Activated Sludge, Q_W	452 ± 331	Clarifiers, CL	2625	-	3.7
Return Activated Sludge, Q_{RAS}	11362 ± 3487	RAS volume	+1000	-	2.1
Internal recycle R4, Q_{R4IN}	635040				
Internal recycle R3, Q_{R3IN}	635040	Total WWTP	11045	-	46

Table (4.1) WWTP H-Old operational and hydraulic data. Average flows are presented with standard deviation (s_D). (+) is estimated. Hydraulic retention times (HRT) were calculated from the flows and volumes.

4.2.4 Models

For all simulations SIMBA© 3.3+ was used as simulation platform, operating under Matlab/Simulink© 5.2 (Alex *et al.*, 1997). Biological conversions were calculated with the TUD model (chapter 2). The influent was characterised according to Roeleveld and van Loosdrecht *et al.* (2001). For the simulation of WWTP H-Old, the measurements from table 4.2 were used. For the start-up simulation, the influent compositions measured in January and June were averaged (chapter 3).

Model of the old WWTP. The old WWTP was modelled according to the flow scheme in fig. 4.1. The contact tank was modelled as one CSTR. R3 and R4 were modelled as 6 CSTR's in series with internal recycle flows Q_{R3IN} and Q_{R4IN} (table 4.1). DO_{R3} and DO_{R4} were both controlled on 3.7 $gO_2 \cdot m^{-3}$ in the third CSTR (table 4.2), hereby approximating the longitudinal DO gradients in the aeration tanks (not shown). The solids concentration in R4 (X_{R4}) was controlled on 4113 $gCOD \cdot m^{-3}$ by regulating the waste flow (Q_W table 4.2).

Meas.	$FePO_4$	$Fe(OH)_3$	DO	NO_3^-	NH_4^+	TKN	PO_4^{2-}	TP	-	VFA	COD_{MF}	COD_X	TCOD
Sim.	X_{MeP}	X_{MeOH}	S_O	S_{NO}	S_{NH}	S_{NH}+iN	S_{PO}	S_{PO}+X_{PP}+iP	S_F	S_A	S_T	X_T	X_T+S_T
	g·m^{-3}	g·m^{-3}	gO$_2$·m^{-3}	gN·m^{-3}	gN·m^{-3}	gN·m^{-3}	gP·m^{-3}	gP·m^{-3}	gCOD·m^{-3}	gCOD·m^{-3}	gCOD·m^{-3}	gCOD·m^{-3}	gCOD·m^{-3}
Q_{IN}				0.1		67		7.7	137	69	239	388	627
± s_D		-	0	± 0.0	-	± 7	-	± 1.0	± 26	± 9	± 30	± 67	± 77
sim.	**0**	**0**	**0**	**0**	**51**	**67**	**4**	**7.8**	**137**	**69**	**240**	**388**	**628**
Q_{OF}				0.1	57	93		30			623	1126	1749
± s_D	-	-	0	± 0.0	± 5	± 14	-	± 8	295	295	± 52	± 327	± 344
sim.	**0**	**0**	**0**	**0**	**51**	**94**	**18**	**30**	**294**	**295**	**623**	**1126**	**1749**
R2				17			1		21	12	66	4416	4481
± s_D	-	-	-	± 4	-	-	± 1	-	± 22	± 13	± 27	± 797	± 777
sim.	**157**	**119**	**0**	**14**	**19**	**188**	**1.6**	**86**	**48**	**24**	**105**	**4070**	**4175**
R4			3.7	28	0.2		0.6				34	4113	4147
± s_D	-	-	± 0.3	± 3	± 0.0	-	± 0.0	-	-	-	± 2	± 244	± 243
sim.	**160**	**125**	**3.7**	**27**	**0.7**	**170**	**0.6**	**86**	**0**	**0**	**34**	**4057**	**4090**
Q_{EF}				28	0.01	1.6	0.7	0.8			36	3	39
± s_D	-	-	-	± 3	± 0.04	± 0.3	± 0.1	± 0.1	-	-	± 5	± 4	± 4
sim.	**0.2**	**0.1**	**3.1**	**28**	**0.8**	**1.4**	**0.7**	**0.8**	**0**	**0**	**34**	**6**	**39**
Q_W				25	0.3			130			34	6272	6306
± s_D	-	-	-	± 2	± 0.0	-	-	± 15	-	-	± 2	± 642	± 642
sim.	**247**	**191**	**0**	**24**	**1**	**259**	**0.7**	**131**	**0**	**0**	**33**	**6213**	**6247**

Table 4.2 **Measurement results of WWTP H-Old**. Average measurements ± standard deviation (s_D) and simulation results (**bold**). The measurements were recorded on the 20th to the 22nd of January 1998.

In the model, particulate material was separated from the effluent ideally. The residual solids concentration in the effluent (X_{EF}), was modelled as a percentile of the RAS concentration. Biological conversions in the RAS were modelled with a non-aerated CSTR placed in the RAS flow. Chemical P precipitation was modelled according to Henze *et al.* (1999). Dosage of $FeCl_3$ was controlled on the average PO_{EF} of 0.8 $gP \cdot m^{-3}$ (table 4.2). During the start-up, no chemical precipitation was applied. This resulted in a wash-out of initially present $FePO_4$ and $Fe(OH)_3$.

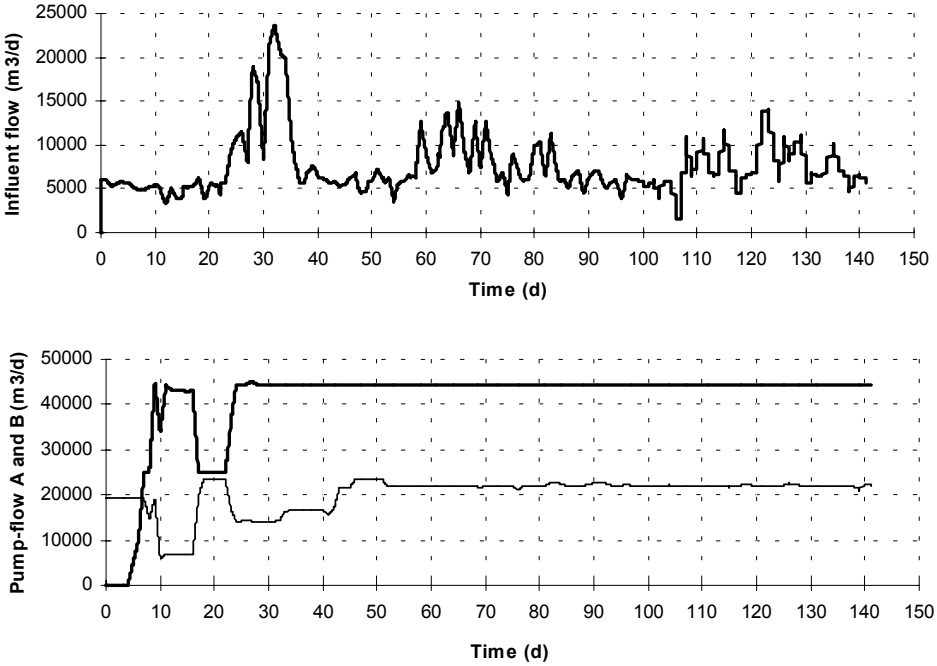

Figure 4.2 Measurement of Q_{IN}, Q_A and Q_B during the start-up. The average dry weather flow was 6855 $m3 \cdot d^{-1}$. During the first 50 days, Q_A (thin line) and Q_B (**bold line**) were operated manually, after which the flows were kept constant. During the start-up, some rain-events occurred.

Model of the new WWTP. The BCFS®-process was modelled as described in chapter 3, according to the flow scheme in fig. 4.1. The actual flow rates Q_A, Q_B and Q_C were modelled, as they largely influenced the first 50 days of the start-up (fig. 4.2). During dry weather conditions, Q_{RAS} was controlled on 8552 $m^3 \cdot d^{-1}$. During rainy weather conditions (Q_{IN} > 8552 $m^3 \cdot d^{-1}$), Q_{RAS} was controlled proportionally to the influent flow (Q_{IN}). This operation resulted in a more or less constant sludge concentration in the process

(fig. 4.3). Measurements of Q_W were not used as these were inaccurate (chapter 3). In stead, the solids concentration in R4 (X_{R4}) was controlled on the actual concentration by regulating Q_W (fig. 4.3). R3, R4 and CL were initialised according to the simulation of the old WWTP (table 4.4). R1, S and R2 were initialised with all concentration set to zero.

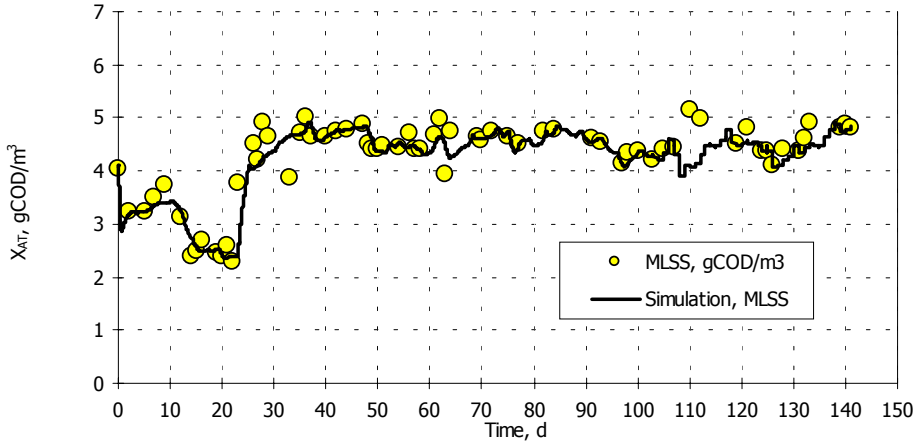

Figure 4.3 **Measurement and simulation of X_{R4} during the start-up.** Dots were measured, the line is simulated. In the model MLSS was controlled on the measured concentration (dots). The drop of concentration during days 10 to 25, was caused by anaerobic sludge retention.

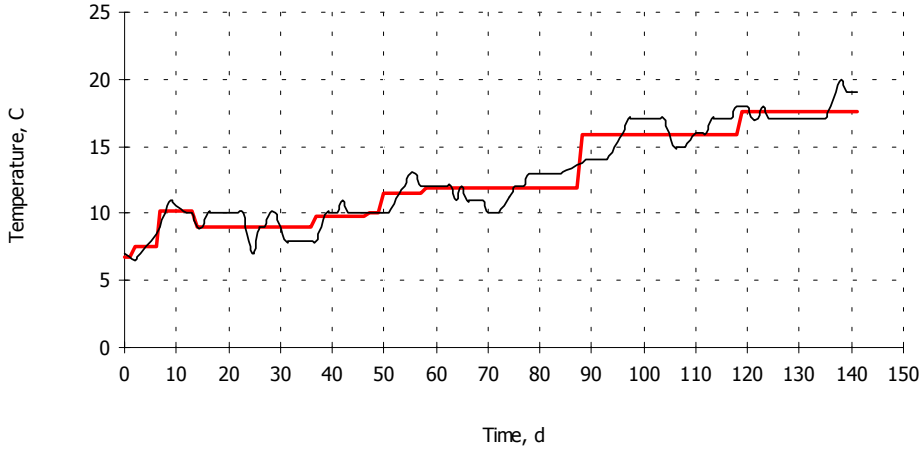

Figure 4.4 **Measured and simulated temperature during the start-up.** The thin line was measured, the **bold line** simulated. Simulation was performed in 10 time-steps, each with an averaged temperature.

4.2.5 Solids retention in the anaerobic reactor

From day 1 to 23, insufficient mixing occurred in R1, which facilitated settling of solids in the 5 meter deep and 2 meter wide plug-flow reactor. During this period, X_{AT} decreased significantly (fig. 4.3). The sharp increase of MLSS on day 23, was caused by installation of new mixers in R1. As these events had a considerable impact on the operation of the WWTP, activated sludge accumulation in R1 was modelled. Therefore, in the model three CSTR's in series with solids retention (740 m^3), were placed parallel to the anaerobic CSTR's. Hereby, the total anaerobic volume was unchanged (1470 m^3). Both modelled flows were mixed and connected to the selector. On simulation-day 23, anaerobic activated sludge retention was deactivated. Hence, we could simulate the sudden release of MLSS into the process.

4.2.6 Modelling temperature

During the start-up, temperature increased significantly. The model showed highly sensitive towards temperature, and therefore it was modelled (fig. 4.5). SIMBA© 3.3+ however, did not allow variable temperature simulations. Therefore, the simulation was performed in 10 time-steps, each step with a different average temperature (fig. 4.4).

The simulations were performed with EBPR temperature coefficients measured by Brdjanovic *et al.* (1998) (θ_{PHA}=0.121, θ_{PP}=0.031, θ_{O2}=0.079 $^oC^{-1}$). The temperature dependency of glycogen formation (θ_{GLY}) was calculated according to eq. 4.1.

$$r_O = \frac{-1}{Y_{PHA/O}} \cdot r_{PHB} + \frac{1}{Y_{PP/O}} \cdot r_{PP} + \frac{1}{Y_{GLY/O}} \cdot r_{GLY} + m_O \cdot C_X \qquad (4.1)$$

Equation 4.1 can be rewritten into eq. 4.2.

$$r_{GLY}(T) = \left[Y_{GLY/O} \times \left(r_O + \frac{-1}{Y_{PP/O}} \cdot r_{PP} + \frac{1}{Y_{PHA/O}} \cdot r_{PHA} + m_O \cdot C_X \right) \right]_{(T=20)} \times \theta_{GLY}^{(T-20)} \qquad (4.2)$$

In eq. 4.2, the observed rates r_O, r_{PP} and r_{PHA} were measured as a function of temperature by Brdjanovic *et al.* (1998). θ_{GLY} could be fitted on the basis of eq. 4.2. Hereby, the contribution of maintenance was neglected. This resulted in a temperature coefficient for glycogen formation of 0.118 $^oC^{-1}$. Figure 5 shows the BioP temperature sensitivity in relation to ASM2(d).

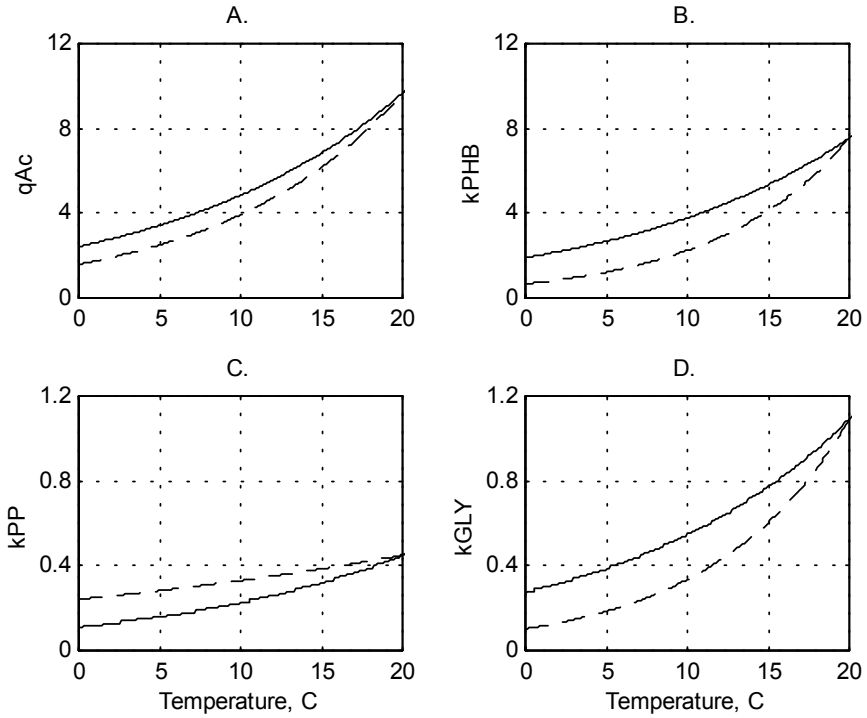

Figure 4.5 BioP temperature dependency. The dependency of the TUD model is shown in dashed lines, of ASM2d in solid lines. On the x-axes temperature is plotted, on the y-axes the maximum rate; (A) Acetate uptake (θ_{Ac}=0.090 °C^{-1}), (B) PHA degradation (θ_{PHA}=0.121 °C^{-1}), (C) PP formation (θ_{PP}=0.031 °C^{-1}) and (D) glycogen formation (θ_{GLY}=0.118 °C^{-1}). The ASM2d temperature coefficient was 0.069 °C^{-1} (Henze *et al.*, 1999).

4.3 Model Calibration and Simulation

4.3.1 Data evaluation

Measurements never are fully accurate. Therefore mass balances never fit completely. In models however, all flows and compounds are balanced. Fitting a model on erroneous data will lead to laborious and unjustified model calibrations. It is therefore essential to check prime data on errors and consistency, before using it in simulations. Hereby especially the SRT is a sensitive operational parameter.

For WWTP H-Old, the SRT was evaluated using the balancing method in chapter 3. On the basis of data from tables 4.1 and 4.2, the overall flow and TP balance, and TP and solids balance over the clarifier were

calculated (fig. 3.3). In the system of four balance equations (n=4), TP_{AT} was unknown (u=1). Therefore the degree of redundancy was 3 (n-u). We chose to evaluate Q_W, Q_{EF} and Q_{RAS}. From the calculations it was shown that all flows could be estimated within their standard deviation (s_D). It was therefore concluded that no gross errors were present. The result of the mass-balance calculations is presented in table 4.3. It is shown that the SRT calculated from the measured flows is considerably smaller than calculated after balancing.

	Unit	Avg. ± s_D	Balanced
Estimated operational data			
Waste Activated Sludge, Q_W	$m^3 \cdot d^{-1}$	452 ± 331	330
Effluent, Q_{EF}	$m^3 \cdot d^{-1}$	5313 ± 2817	5530
Return Activated Sludge, Q_{RAS}	$m^3 \cdot d^{-1}$	11362 ± 3487	10004
Calculated parameters			
Total phosphorus in R4, TP_{AT}	$gP \cdot m^{-3}$	n.d.	85.5
Load Waste activated sludge, ^{L}WAS	$kgCOD_X \cdot d^{-1}$	2835 ± 2370	2050
Sludge Retention Time, SRT	d	12.3 ± 11	16.7

Table 4.3 Data evaluation of WWTP H-Old. Estimation of the SRT. The original flow measurements are shown with standard deviations (s_D).

4.3.2 Calibrating the model of the old WWTP

The initial condition for the start-up was the p.s.s. of the old WWTP. The model was calibrated according to the method in chapter 3. The succeeding calibration steps are described in the following sections.

Step 1. Fitting the solids balance. The solids concentration in the aeration tank (X_{AT}) is mainly determined by the influent X_I/X ratio. Because X_I accumulates in the WWTP, increasing the influent X_I/X ratio results in an increased sludge production (^{L}WAS) and visa versa. In the model, X_{AT} was controlled on 4113 $gCOD_X \cdot m^{-3}$ (table 4.2) by regulating Q_W. To fit Q_W and ^{L}WAS according to the balanced values in table 4.3, the influent X_I/X ratio was adjusted to 0.507. An identical value for X_I/X was found for WWTP Hardenberg (chapter 3).

Step 2. Calibrating nitrification. Nitrification was simulated sufficiently without calibration (table 4.2).

Step 3. Calibrating denitrification. A difference in nitrate measured in the effluent and the RAS flow (NO_{EF} and NO_{RAS} table 4.2), indicated that 3 $gN \cdot m^{-3}$ was denitrified in the RAS volume. This effect was modelled with three CSTR's placed in the RAS flow. By approximation this corresponded

with the actual RAS volume (1050 m^3). Denitrification (^{L}DEN) was calibrated by increasing K_O from 0.2 to 0.7 $gO_2 \cdot m^{-3}$ (table 4.2), which matched the calibrated K_O for WWTP Hardenberg (chapter 3).

Step 4. Calibrating EBPR
The calibrated model of WWTP H-Old calculated absence of PAO's. However an anaerobic phosphate release batch-test, showed some PAO activity. From the maximum phosphate release rate (0.036 $gP \cdot gCOD^{-1} \cdot d^{-1}$), q_{Ac} and Y_{PO}, the initial PAO concentration was calculated to be 33 $gCOD \cdot m^{-3}$. Clearly, this low concentration could be neglected when simulating the old WWTP. However, for the start-up simulation, the initial PAO concentration showed to be sensitive. Therefore, also the initial values for f_{PP}, f_{GLY} and f_{PHA} had to be estimated. From a phosphate release batch-test simulation, the aerobic f_{PP} was estimated to be 0.16 $gP/gCOD_{PAO}$, which matched the value found for WWTP Hardenberg (0.17 $gP/gCOD_{PAO}$, chapter 3). In the batch test simulation, the aerobic fractions f_{GLY} and f_{PHA} were insensitive. These fractions were therefore directly obtained from the simulation of the WWTP (0.38 $gCOD_{GLY}/gCOD_{PAO}$ and 0.02 $gCOD_{PHA}/gCOD_{PAO}$). The simulation results of WWTP H-Old are presented in table 4.4.

4.3.3 Calibrating the Start-up

To simulate the start-up, model calibration was required. Hereby the proposed stepwise method was applied. Whereas this method proved to be quick and simple for p.s.s. calibrations, for dynamic conditions it was laborious, as for each adjusted parameter a complete dynamic (in our case 140-day) simulation run was required. To decrease simulation time, initial calibration were performed with average flows and controller set-points.

Step 1. Fitting the COD_X balance. Mass balancing dynamic systems can be inaccurate. Therefore the SRT of the dynamic system was evaluated differently. Because P is stored in the activated sludge, there is a direct relation between TP_{AT} and the SRT. The SRT during the start-up was therefore evaluated on the basis of the accumulation of TP_{AT} (fig. 4.6). Hereby, the influent X_I/X ratio was set to 0.507, according to the previous simulations. Accumulation of TP_{AT} was predicted sufficiently as was observed from fig. 4.6. This indicated that the SRT was simulated correctly. With the actual Q_A (fig. 4.2) and modelled settling in R1, also X_{R1} was simulated satisfactory (not shown).

component	symbol	unit	p.s.s. of H-Old	final state start-up	p.s.s. of Hdbg
Inert particulate	X_I	$gCOD \cdot m^{-3}$	2828	3620	3550
Solid substrate	X_S	$gCOD \cdot m^{-3}$	63	10	7
Heterotrophic micro-organism's	X_H	$gCOD \cdot m^{-3}$	1091	352	294
Autotrophic micro-organism's	X_A	$gCOD \cdot m^{-3}$	75	52	43
P accumulating organism's	X_{PAO}	$gCOD \cdot m^{-3}$	[1]32.9	531	572
Poly-hydroxyalkanoate	X_{PHA}	$gCOD \cdot m^{-3}$	[2]0.7	13	9
Glycogen	X_{GLY}	$gCOD \cdot m^{-3}$	[2]12.5	265	216
Poly-phosphate	X_{PP}	$gP \cdot m^{-3}$	[1]5.3/[2]5.7	92	98
Iron-hydroxide	X_{MeOH}	$g \cdot m^{-3}$	125	1	n.d.
Iron-phosphate	X_{MeP}	$g \cdot m^{-3}$	160	6	n.d.
Total particulate phosphorous	TP_X	$gP \cdot m^{-3}$	86	148	152
Particulate COD	COD_X	$gCOD \cdot m^{-3}$	4090	4843	4692
Total particulate Kjeldal nitrogen	TKN_X	$gN \cdot m^{-3}$	170	175	171

Table (4.4) Simulated activated sludge compositions. The p.s.s. of the old WWTP was the initial state of the start-up. **[1]** was estimated from a phosphate release batch-test simulation, **[2]** are obtained from a simulation of WWTP Hardenberg (Hdbg). The WWTP was simulated without chemical P precipitation and f_{GLYmax}=0.4.

Step 2a. Calibrating effluent ammonium. In the model nitrification was mainly determined by DO_{R3} and DO_{R4}. DO_{R4} was PI-controlled based on the measured DO profile (fig. 4.7). DO_{R3} was regularly below the measurement detection and therefore less accurate. Moreover, NH_{EF} showed sensitive towards DO_{R3}, as it was in the range of the DO saturation constant ($K_{A,O}$=0.5 $gO_2 \cdot m^{-3}$). Therefore we chose to fit NH_{EF} by calibrating DO_{R3}. Between days 10 and 23, anaerobic digestion of settled X_{R1}, caused a high ammonium loading of the WWTP. During this period, nitrification was calibrated by increasing DO_{R3} to 2 $gO_2 \cdot m^{-3}$. From day 23 and on, with ending of anaerobic activated sludge retention, NH_{EF} was simulated sufficiently with actual DO_{R3}. NH_{EF} peaks on days 60, 85, 110 and 135, were not predicted. Because these peaks did not also occur in R2 (fig. 4.8), it was assumed that these peaks were caused by measurement errors or operational conditions. This however, could not be verified.

Step 2b. Calibrating NH_{R1} and NH_{R2}. After calibrating NH_{EF}, both NH_{R1} (not shown) and NH_{R2} (fig. 4.8) were simulated sufficiently. This was accomplished with the modelled settling of solids in R1, the balanced Q_{RAS} (table 4.3) and measured flows Q_A and Q_B (fig. 4.2).

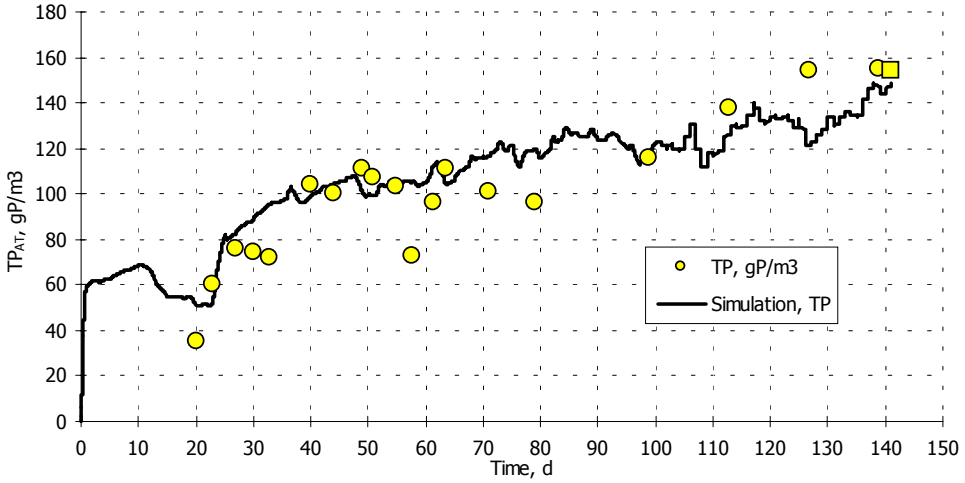

Figure 4.6 Measured and simulated accumulation of TP_{AT}. Dots were measured, the line was simulated. The square at 141 days represents the p.s.s. of WWTP Hardenberg.

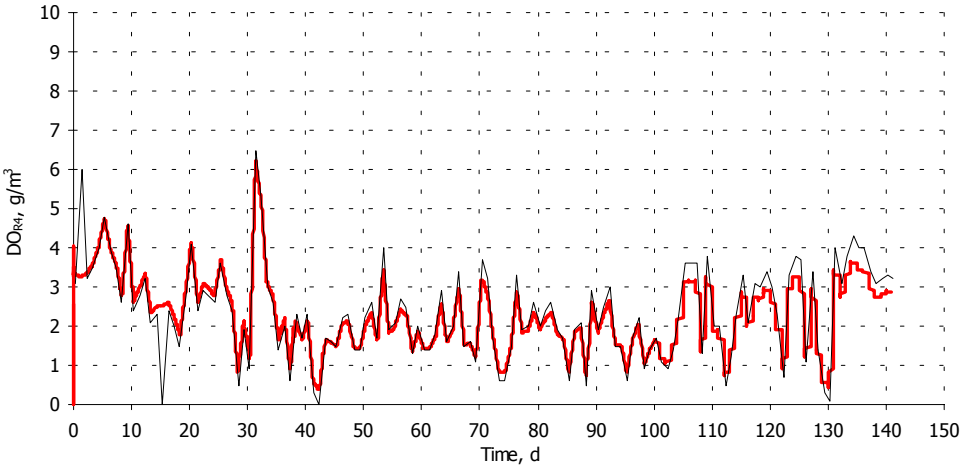

Figure 4.7 Measured and simulated DO_{R4} control. The **bold** line was simulated, the thin line measured. DO_{R2} was measured, however not plotted, as the concentration continuously was below 0.5 $gO_2 \cdot m^{-3}$.

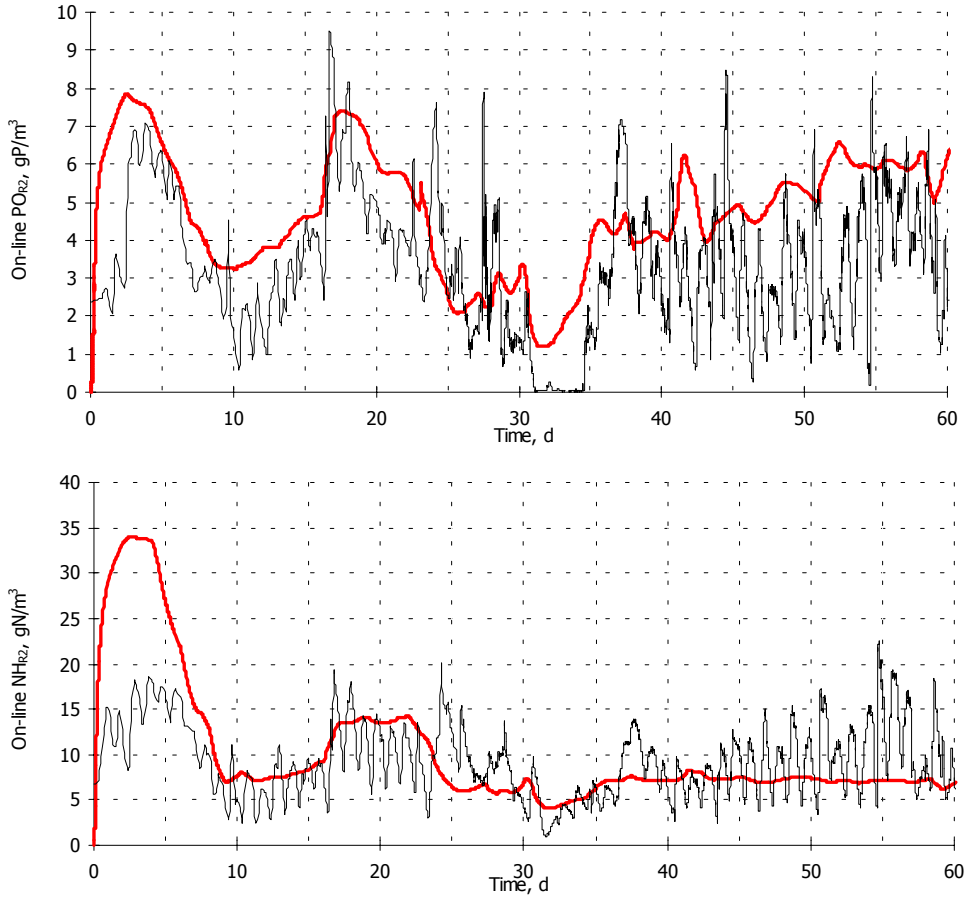

Figure 4.8 **Measured and simulated PO_{R2} and NH_{R2} during the first 60-days.** **Bold** lines represent simulations, thin lines on-line measurements. NO_{R2} was measured, however not plotted, as the concentration continuously was below 0.5 gN·m^{-3}.

Step 3. Fitting the denitrified load. The denitrification rate (^{L}DEN) and nitrate in the effluent (NO_{EF} fig. 4.9) were fitted by increasing K_O according to the method in chapter 3. The same value was found as in the previous simulations (0.7 gO_2·m^{-3}). Denitrification in the RAS volume could not be verified, as NO_{RAS} was not measured regularly.

4.4 BioP Model Evaluation

4.4.1 Sensitivity analysis

On the basis of a dynamic sensitivity analysis the BioP kinetics were evaluated. The sensitivity of k_{GLY}, k_{PP} and k_{PHA} was analysed, as these kinetic parameters are directly related to growth of PAO's (fig. 4.10 and 4.11). In total seven simulations were performed; the default parameter value (k_{GLY}=0.93, k_{PP}=0.45, k_{PHA}=7.55), a 20 % decrease and a 20 % increase of the individual rate values. Hereby, all model distortions were eliminated by applying average flows and controller set-points. The applied temperature was 10 °C, the total simulation time 100 days. In the simulations, only PAO, phosphate in the effluent (PO_{EF}), the anaerobic phosphate concentration (PO_{R1}) and the anaerobic fractions f_{PP} and f_{GLY} and the aerobic fraction f_{PHA} showed sensitive towards the kinetic rates. This is shown in fig. 4.10 (PAO_{AT} a/b/c; PO_{EF} d/e/f; PO_{R1} g/h/i), and fig. 4.11 (f_{PP} j/k/l; f_{GLY} m/n/o; f_{PHA} p/q/r).

4.4.2 Calibrating EBPR

According to the calibration method in chapter 3, EBPR is calibrated last. Anaerobic phosphate release and PP formation are modelled as separate processes. Independent calibration of these processes was therefore possible.

Step 4a. Calibrating anaerobic phosphate release. PO_{R1} (fig. 4.12) is via anaerobic phosphate release, related to growth of PAO's (fig. 4.13). In the model, phosphate release is coupled to storage of PHA via Y_{PO} (0.36 $gP/gCOD_{Ac}$, pH 6.8, Smolders *et al.*, 1994a). PHA is partly utilised for glycogen and PP formation and maintenance. The remaining PHA is available for growth of PAO's. Theoretically, decreasing k_{PP} and k_{GLY} and increasing q_{Ac} should result in more PAO's. In practice however, PP formation is often phosphate limited as usually phosphate in the effluent is low. Growth of PAO's is therefore insensitive towards increasing k_{PP} (fig. 4.10a/g). Decreasing k_{PP} however, immediately results in more phosphate in the effluent (PO_{EF} fig. 4.10d). In a well designed WWTP, PHA formation is limited by the availability of VFA_{IN}. Therefore, growth of PAO will be insensitive for increasing q_{Ac}, however highly sensitive for decreasing q_{Ac}, as this directly affects the storage of PHA.

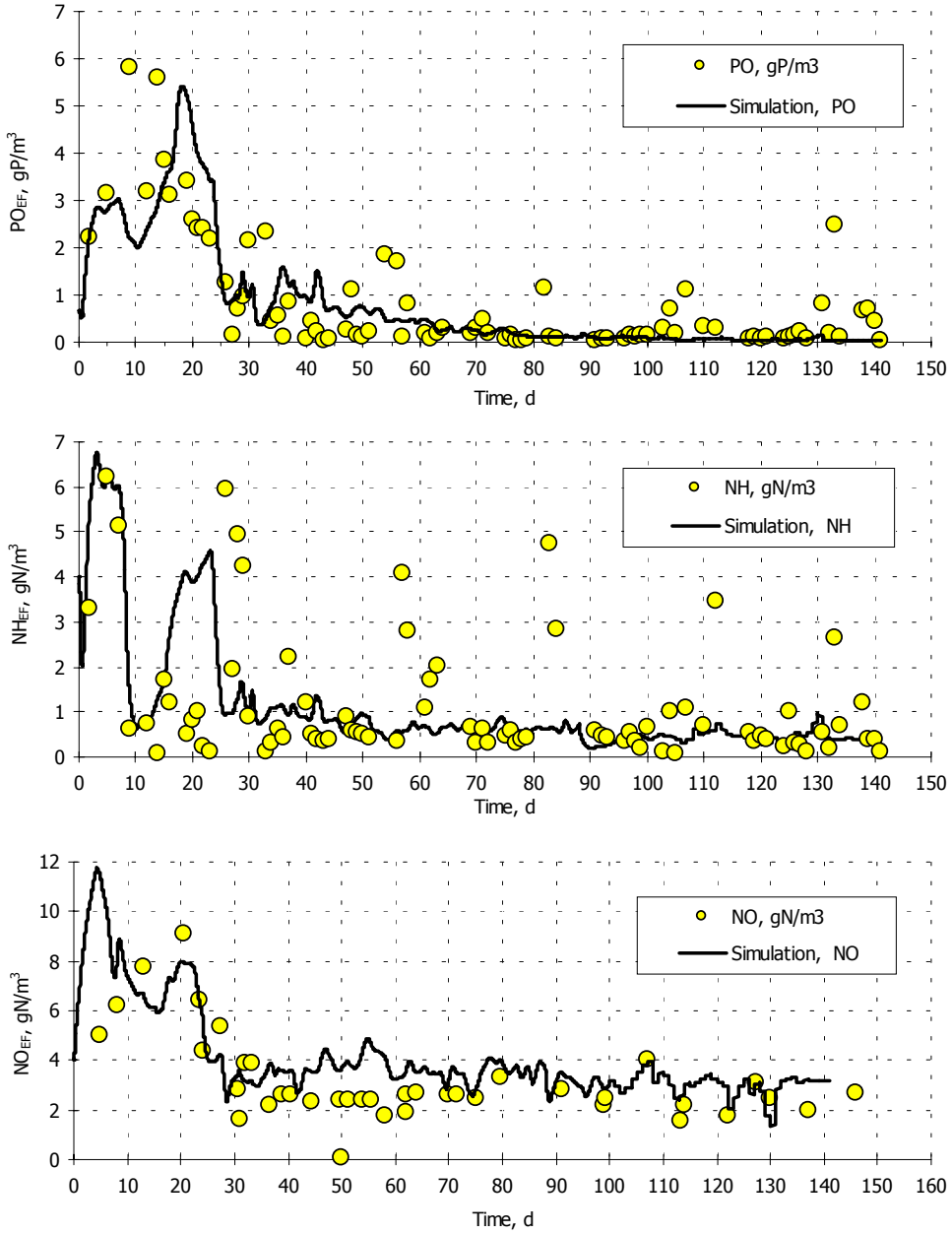

Figure 4.9 **Measured and simulated effluent concentrations.** PO_{EF} (top), NH_{EF} (middle) and NO_{EF} (bottom) during the start-up. Measurements are dots, simulations lines.

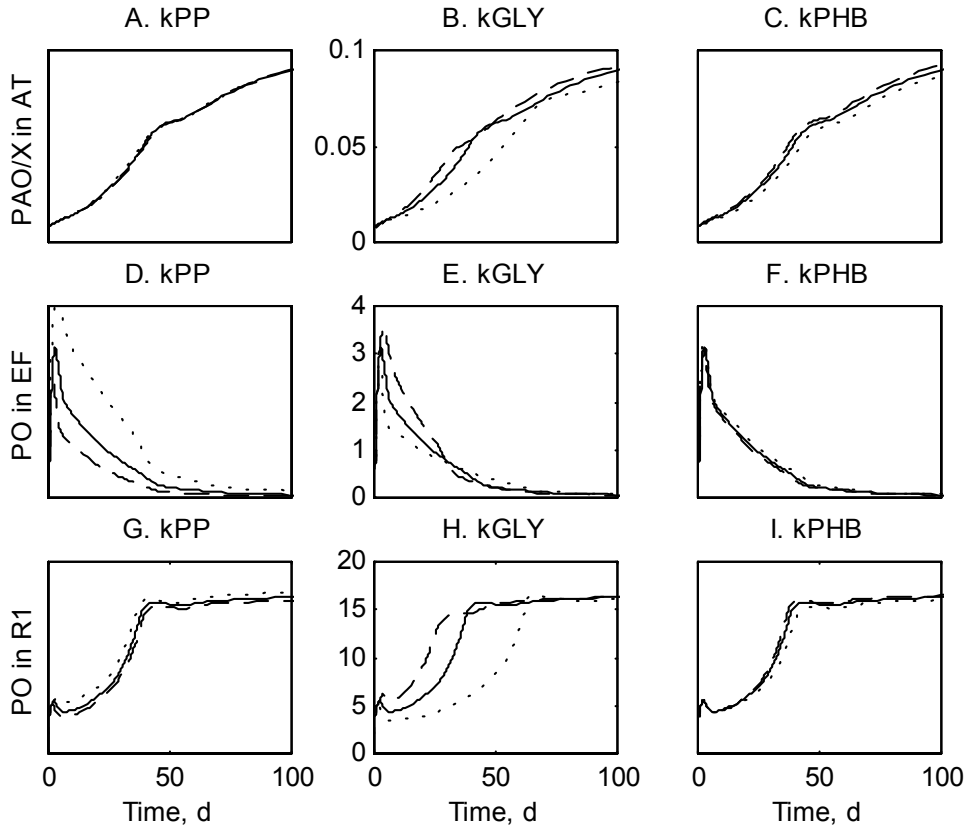

Figure 4.10 Sensitivity of BioP kinetics (A to I). Each fig. represents the effect of a 20 % in- (dotted lines) and decrease (dashed lines) of kinetic rates k_{GLY}, k_{PP} and k_{PHA} on PAO's (a to c), PO_{EF} (d to f) and PO_{R1} (g to i). Solid lines are simulations with default parameter values. The sensitivity analysis was performed with average flows and controller set-points and a temperature of 10 °C.

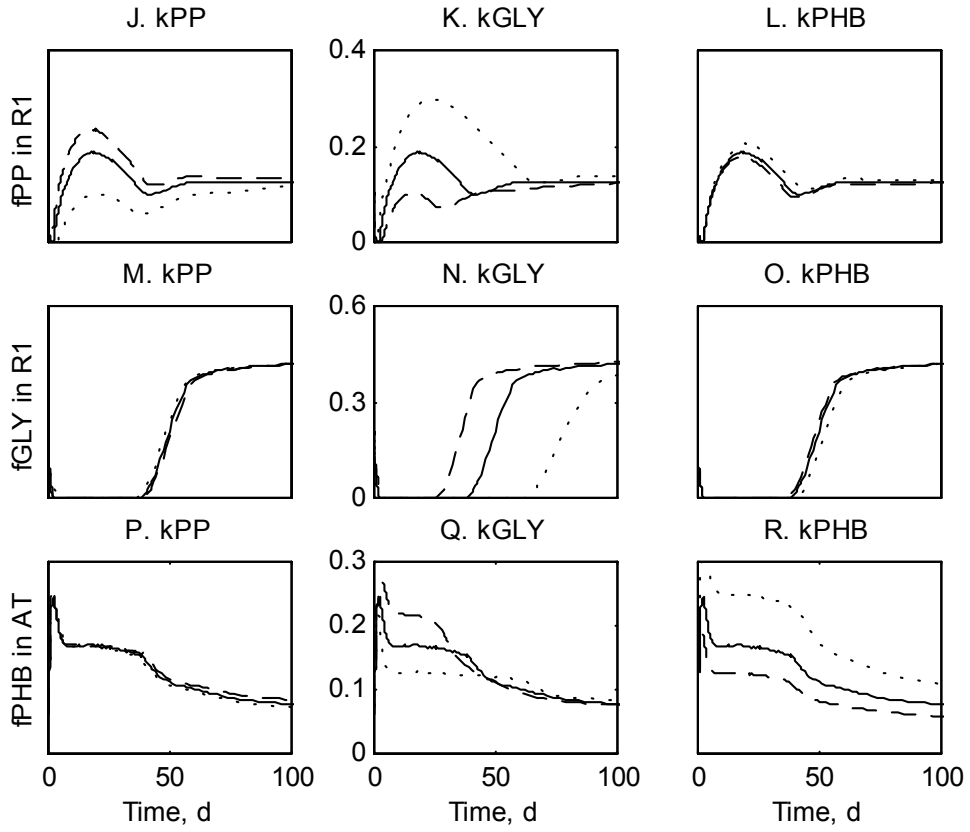

Figure 4.11 Sensitivity of BioP kinetics (J to R). Each fig. represents the effect of a 20 % in- (dotted lines) and decrease (dashed lines) of kinetic rates k_{GLY}, k_{PP} and k_{PHA} on f_{PP} (j to l), f_{GLY} (m to o) and f_{PHA} (p to r). Solid lines are simulations with default parameter values. The sensitivity analysis was performed with average flows and controller set-points and a temperature of 10 °C.

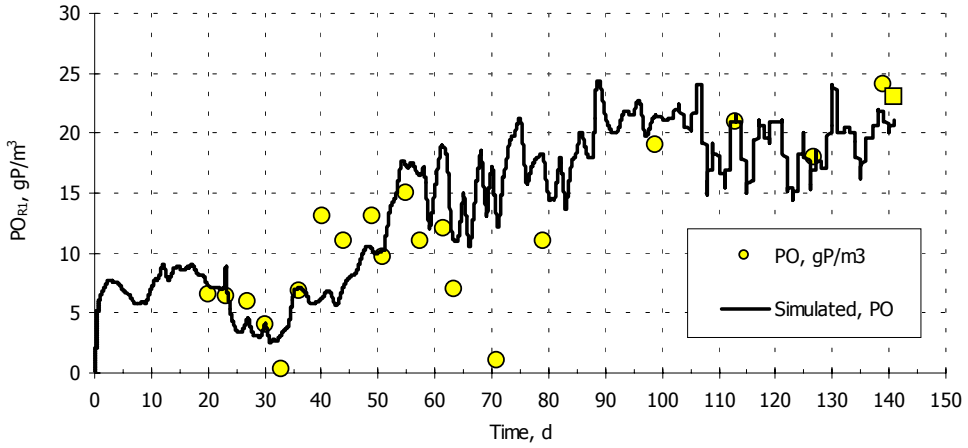

Figure 4.12 Measured and simulated anaerobic phosphate during the start-up. Measurements are dots, the simulation a line. The square at 141 days represents the p.s.s. of the WWTP Hardenberg.

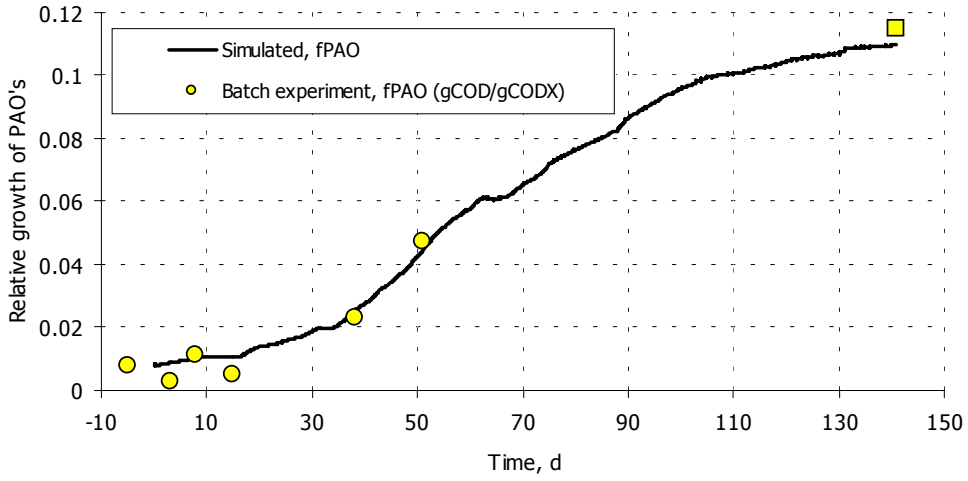

Figure 4.13 Measured and simulated growth of PAO's. Dots were calculated from anaerobic phosphate release batch-tests, the bold line was simulated. The square at 141 days represents the p.s.s. of the WWTP.

Where PHA and PP formation kinetics are well described (Murnleitner *et al.*, 1997, Smolders *et al.*, 1994a/b), glycogen formation kinetics are less certain (Brdjanovic *et al.*, 2000). The model sensitivity towards k_{GLY} was however relative high compared to k_{PP} and q_{Ac} (fig. 4.10). Therefore, we chose to fit growth of PAO's by adjusting k_{GLY}. This was validated on the basis of PO_{R1}. By decreasing k_{GLY} with 15 % to 0.93 $gCOD_{GLY} \cdot gCOD_{PAO}^{-1} \cdot d^{-1}$, acceptable simulation results were obtained (fig. 4.12 and 4.13).

Step 4b. Calibrating anoxic PP formation. To fit anoxic PP formation a unique calibration parameter was required. Sensitivity analysis showed that PP formation was sensitive towards k_{PP}. This however accounted both anoxic and aerobic PP formation. A more specific calibration parameter was the effective saturation constant for nitrate expressed as $g_{PP} \times K_{P,NO}$ (with $K_{P,NO}$=0.5 $gN \cdot m^{-3}$ and reduction factor g_{PP}<1). In the kinetic expression r_{PP}, g_{PP} originates from the observation that PP formation is less sensitive towards DO and nitrate (Murnleitner *et al.*, 1996). During the start-up, NO_{R2} was constantly in the range of $K_{P,NO}$ (0.2 to 0.5 $gN \cdot m^{-3}$). Hence, g_{PP} showed an increased sensitivity. For simulation of WWTP Hardenberg (chapter 3), g_{PP} was determined on 0.25 (-). Simulating the start-up with this value resulted in the PO_{R2} profile presented in fig. 4.8. This profile was established with actual Q_A and Q_B, balanced Q_{RAS} and calibrated NO_{EF} (step 3) and PO_{R1} (step 4a).

4.5 Discussion

The primary goal of the start-up, was to obtain a stable process in the shortest time possible. We were therefore limited to record the WWTP as it was operated. This included calamities, as the start-up was a single event. The scientific goal of the start-up simulation was to evaluate the TUD model kinetics. Hereby, our focus was on long term population dynamics. Therefore sporadic grab sampling was sufficient. For (full-scale) evaluation of short term TUD model kinetics, we refer to chapter 3 and previous studies by van Veldhuizen *et al.* (1999) and Brdjanovic *et al.* (2000).

On the basis of the start-up, the sensitivity of BioP kinetics was evaluated. A similar start-up evaluation was performed by Smolders *et al.* (1995) at lab-scale conditions. From short-cycle SBR experiments, Murnleitner *et al.* (1996) observed that k_{PHA} and k_{PP} were the most sensitive kinetic parameters for BioP. This study shows that during a start-up, k_{GLY} is the most sensitive parameter for growth of PAO's (fig. 4.10b). The modelled glycogen kinetics showed typical on-off dynamics (fig.

4.11 m/n/o). This indicated that glycogen formation is over sensitive (i.e. critical) in the model.

To validate these kinetics, accurate measured data of glycogen, PP and PHA under dynamic conditions are required. In this study these measurements were not performed for two reasons. Firstly, it was expected that high recycle factors in the WWTP would result in small glycogen and PHA gradients. Distinction between anaerobic, anoxic and aerobic glycogen and PHA concentrations would therefor become difficult. Secondly, in full-scale WWTP's PAO's are not the only MO's storing glycogen and PHA. This further affects the measurement accuracy. On the basis thereof, we chose to rely on anaerobic phosphate release batch-tests for the validation of BioP kinetics.

This study showed that during a start-up, glycogen formation is a key process. More (lab-scale) research however, would be needed for an better determination and validation of the glycogen kinetics at start-up conditions. From chapter 3 and this study, it was concluded that under p.s.s. conditions the sensitivity of BioP kinetics is strongly reduced. Therefore the current glycogen kinetics are sufficient for simulation of such conditions.

4.5.1 Influent characterisation

From the influent measurements in January and June, it was observed that seasonal influences were negligible and that dynamics in the influent loads primarily were caused by flow dynamics. This is typical for Dutch sewers, which generally are flat, resulting in concentration and flow dispersion. The start-up was therefore simulated with average dry weather influent loads and measured Q_{IN}, including several rain-events (fig. 4.2). In reality, rain events did cause some variation. However, for the purpose of this study, the influent was simulated sufficiently, as we were mainly interested in long term dynamic effects.

4.5.2 Simulation of the old WWTP

The model of WWTP H-Old was considered adequately calibrated, as the simulation was in agreement with the measurements (tables 4.2 and 4.3). Calibration was done independent of the calibration of WWTP Hardenberg (chapter 3). Nevertheless, both model were fitted with identical parameter values for K_O and X_I/X. It should be emphasised that for both models these parameters were selected on the basis of high sensitivity towards the denitrification rate (^{L}DEN) and the sludge production (^{L}WAS).

4.5.3 Modelling chemical P precipitation

During the start-up simulation, chemical precipitation was inactivated. X_{MeP} therefore acted as an inert fraction that was removed from the WWTP via the WAS in approximately 70 days. During this time, loss of $FePO_4$ (X_{MeP}) was compensated by accumulation of PP. The net accumulation of TP_{AT} was well simulated (fig. 4.6). Neglecting chemical precipitation processes during the start-up was therefore justified.

4.5.4 Modelling anaerobic solids retention

The method that was used to model solids retention in R1 during the first 23 days, was critical. The sudden increase of MLSS on day 23 (approximately 2000 $gCOD \cdot m^{-3}$, fig. 4.3), implicated that 25780 kg MLSS was accumulated in R1. In the model, we assumed this was a gradual process, taking place in the bottom half of the reactor (740 m^3). In 23 days, X_{R1} accumulated to a maximum of 34.8 $kgCOD \cdot m^{-3}$. This concentration corresponded to the measured MLSS in the thickener (32 $kgCOD \cdot m^{-3}$). During anaerobic sludge retention, X_{R1} was subject to hydrolysis, fermentation, lysis and anaerobic maintenance. This caused an increasingly high phosphate and ammonium loading of the WWTP. Our model of the settling process was supported by PO_{R2} and NH_{R2} measurements, as these trends were simulated fairly well (fig. 4.8). The simulated effluent however, did not fully correspond with the measurements (fig. 4.9). PO_{EF} and NH_{EF} peaks on day 20, were caused by an sudden increase of Q_A (fig. 4.2), while PO_{R1} and NH_{R1} were high. At the same time, nitrification and the phosphate uptake rate were low, caused by the reduced MLSS in the WWTP. In an attempt to simulate this effect (step 2a), DO_{R3} was increased to 2 $gO_2 \cdot m^{-3}$. Because there were no other reasonable options to increase aerobic conversions, we chose not to further calibrate the effluent.

4.5.5 Dynamic evaluation of operational conditions

Unlike p.s.s. conditions, a dynamic WWTP does not give the opportunity for detailed evaluation of operational data. The start-up dynamics were in great extent determined by operational conditions. In previous studies it was shown that calibrating model kinetics without gross error detection is inaccurate. However, most operational problems occurred in the first 25 days, after which a proper kinetic evaluation was possible. It showed possible to accurately evaluate the SRT on the basis of accumulation of TP_{AT} (fig. 4.6). k_{GLY} was calibrated on the basis of PO_{R1} and anaerobic phosphate release batch-tests between days 30 and 65 (fig. 4.12 and 4.13). In this period, a maximum sensitivity for k_{GLY} was observed, as growth of

PAO was in an 'exponential' phase (fig. 4.10b/h). Decreasing k_{GLY} 15 % to 0.93 ($gCOD_{GLY} \cdot gCOD_{PAO}^{-1} \cdot d^{-1}$), resulted in a sufficient simulation of PO_{R1} and growth of PAO's. The activated sludge composition was relative insensitive towards the calibrated value of k_{GLY} (table 4.4 and fig. 4.10b/h). This indicated that the WWTP was mainly stoichiometric determined. The start-up was simulated with identical parameter values (X_I/X, K_O and g_{PP}) as for the steady state simulations of the old and new WWTP. This resulted in an adequate simulation of the start-up, as observed in fig. 4.6, 4.8, 4.9, 4.12 and 4.13.

4.5.6 Interpretation of the start-up dynamics

Glycogen kinetics. Simulation of PAO's showed a distinctive delay on day 60 (fig. 4.13). This also was observed in the sensitivity analysis (fig. 4.10a/b/c). Here the delay coincided with an sudden increase of glycogen (fig. 4.11m/n/o). When PO_{EF} becomes limiting (fig. 4.10e), the maximum anaerobic phosphate concentration is reached (PO_{R1} fig. 4.10h). This causes a sudden increase of f_{GLY} to f_{GLYmax} (fig. 4.11n). It could not be answered if this 'on-off' behaviour is realistic, since accurate glycogen measurements were not available.

The strong dynamics of the on-line measurements in fig. 4.9 indicate that the scattered data in fig. 4.12 could be the result of grab sampling. The sudden decrease of PO_{R1} during days 60 to 70 (fig. 4.12) however, could also be explained in the context of the PAO growth lag (fig. 4.13). Sensitivity analysis showed that during the growth lag (fig. 4.10b), anaerobic f_{PP} decreased (fig. 4.11k), induced by a sudden increase of glycogen (fig. 4.11n). Decrease of PO_{R1} also could have been caused by the increased influent supply (fig. 4.2). Neither theories however, could be confirmed.

Modelling a maximum glycogen fraction. The glycogen formation kinetics proposed by Murnleitner *et al.* (1997), allowed unlimited accumulation of glycogen. This especially caused problems at high SRT (Brdjanovic *et al.*, 2000). Modelling f_{GLYmax} showed to be an effective and simple measure to prevent unrealistic glycogen accumulation. In combination with the 'on-off' kinetics the modelled f_{GLYmax} acted as a stoichiometric parameter which determined the p.s.s. glycogen concentration. From the sensitivity analysis (fig. 4.10 and 4.11), it was concluded that all simulations converge to a similar steady state. This strongly supports the conclusion that WWTP's in p.s.s. mainly are determined by model stoichiometry (chapter 3).

Model sensitivity towards the maximum glycogen fraction. Table 4 shows small differences between the activated sludge composition of the final state of the start-up and the p.s.s. of WWTP Hardenberg. These differences are mainly caused by a different value for f_{GLYmax}. For simulation of WWTP Hardenberg the ratio 0.4 was used, whereas the start-up was simulated with a ratio 0.5 ($gCOD_{GLY}/gCOD_{PAO}$, Brdjanovic *et al.*, 1998). The sensitivity of f_{GLYmax} is however low, caused by the relative small glycogen fraction in the activated sludge (4.6 to 5.5 %, table 4.4).

Temperature effects. Simulating the start-up with an average temperature, resulted in an underestimated growth of PAO's. During the start-up, the temperature increased from 6.8 to 17.7 °C (fig. 4.4). The sensitivity of PAO's towards temperature is non linear and relative high (fig. 4.5). Therefore, when modelling BioP, temperature changes should be taken in account.

4.6 Conclusions

On the basis of a start-up simulation of a full-scale WWTP, it was possible to evaluate the (long term growth) kinetics of the metabolic model. A sensitivity analysis showed that the glycogen formation rate and the temperature were most sensitive in the model. By including a temperature profile in the model, simulation results improved significantly. By carefully fitting the glycogen formation, a proper simulation of the start-up and accumulation of PAO's over a 140-day period was possible.

In accordance with previous observations, a high sensitivity towards operational data was observed. This underlines the importance of a proper data evaluation. During the start-up, the sludge retention time could be evaluated accurately on the basis of accumulation of phosphorus in the activated sludge. The start-up could be simulated using identical calibration parameter values for K_O, g_{PP} and X_I/X as for previous simulations.

The glycogen formation rate was found to be sensitive in the model. A maximum glycogen fraction was introduced in the kinetic rate equation for glycogen formation to avoided model instability. With this adjustment, problems relating to unrealistic accumulation of glycogen in the model, as reported in several previous studies, were solved. It was observed that when glycogen formation was not calibrated properly, the value of the maximum glycogen fraction determined the steady state glycogen concentration in the model. The overall model sensitivity of towards this parameter was however low.

This study shows that glycogen formation is a key process during start-up conditions. In the model glycogen formation is sensitive. Therefore a more accurate determination and validation of glycogen formation under start-up conditions is required. For most WWTP's simulations however, the current BioP kinetics are sufficient, as this and previous research showed that the model sensitivity towards BioP kinetics is low under (pseudo) steady state conditions.

References

Alex J., Tschepetzki R. and Bitter U. (1997) SIMBA Simulation of biological waste water treatment. Users manual, Institute of Automation and Communication e. V., Magdeburg.

Brdjanovic D., van Loosdrecht M. C. M., Hooijmans C. M., Alaerts G. J. and Heijnen J. J. (1997) Temperature effects on physiology of biological phosphorus removal. ASCE *Journal of Env. Eng.* **123**(2), 144-154.

Brdjanovic D., Logemann S., van Loosdrecht M. C. M., Hooijmans C. M., Alaerts G. J. and Heijnen J. J. (1998) Influence of temperature on biological phosphorus removal: process and ecological studies. *Water Res.* **32**(4), 1035-1048.

Brdjanovic D., van Loosdrecht M. C. M., Versteeg P., Hooijmans C. M., Alaerts G. J. and Heijnen J. J. (2000) Modeling COD, N and P removal in a full-scale WWTP Haarlem Waarderpolder. *Water Res.* **34**(3), 846-858.

Hellinga C., van der Heijden R. T. J. M., Heijnen J. J., Romein B. and Luyben K. C. A. M. (1992) An improved method for measurement reconciliation and gross error diagnosis for (bio)chemical processes. IFAC-Symp.Ser.10, 235-37.

Henze M., Gujer W., Mino T., Matsuo T., Wentzel M. C., Marais G. v. R. and van Loosdrecht M. C. M. (1999) Activated Sludge Model No.2d, ASM2d. *Water Sci. Technol.* **39**(1), 165-182.

Meijer S. C. F., van Loosdrecht M. C. M. and Heijnen J. J. (2001) Metabolic modelling of full-scale enhanced biological phosphorus removing WWTP's. *Water Res.* **35**(11), 2711-2723.

Murnleitner E., Kuba T., van Loosdrecht M. C. M. and Heijnen J. J. (1997) An integrated metabolic model for the aerobic and denitrifying biological phosphorous removal. *Biotechnol. Bioeng.* 54, 434-450.

Roeleveld P.J and Van Loosdrecht M.C.M. (2001) Experiences with guidelines for wastewater characterisation in The Netherlands. *Wat. Sci. Technol.* **45**(6), 145-156.

Smolders G. L. F., van der Meij J., van Loosdrecht M. C. M. and Heijnen J. J. (1994a) Model of the anaerobic metabolism of the biological phosphorous removal process: stoichiometry and pH influence. *Biotechnol.Bioeng.* **43**(6), 461-470.

Smolders G. L. F., van der Meij J., van Loosdrecht M. C. M. and Heijnen J. J. (1994b) Stoichiometric model of the aerobic metabolism of the biological phosphorus removal process. *Biotechnol.Bioeng.* **44**(7), 837-848.

Smolders G. L. F., Bulstra D. J., Jacobs R., van Loosdrecht M. C. M. and Heijnen J. J. (1995) A metabolic model of the biological phosphorus removal process: Validation during start-up conditions. *Biotechnol.Bioeng.* **48**(3), 234-245.

Van Loosdrecht M.C.M., Brandse F.A. and de Vries A.C. (1998) Upgrading of wastewater treatment processes for integrated nutrient removal – The BCFS®-process. *Wat. Sci. Technol.* **37**(9), 209-217.

Van Loosdrecht M. C. M. and Henze M. (1999) Maintenance, endogeneous respiration, lysis, decay and predation. *Wat. Sci. Technol.* **39**(1), 107-117.

Van Veldhuizen H. M., van Loosdrecht M. C.M. and Heijnen J. J. (1999) Modelling biological phosphorus and nitrogen removal in a full scale activated sludge process. *Water Res.* **33**(16), 3459-3468.

5

Data Verification for Activated Sludge Modelling

Research on activated sludge modelling is mainly directed towards the estimation of model parameters. Model calculations however, rely heavily on accurate determination of operational conditions. This can be difficult, caused by large (full-scale) process flows and the absence of reliable measurements. Therefore, operational data should be verified on (gross) errors before being implemented in model studies. Calibrating a model on erroneous data leads to laborious calibration procedures and moreover, unjustified adaptation of the model (kinetic and stoichiometric) parameters. A simple method for gross error detection is evaluating the mass balance residuals. When there are more measurements than strictly required to solve a system of linear conservation relations (mass balances), data accuracy can be improved using balancing methods. This is referred to as data reconciliation. A reconciled data set is more accurate and is exactly in line with the mass balances of the WWTP. In this chapter we describe a method for gross error detection and data reconciliation. In a case study it is shown how data reconciliation improves the accuracy of the data set and how the use of a balanced data set simplifies the model calibration.

This chapter is largely based upon Meijer *et al.* (2002) *Water. Sci. Technol.* **45**(6), 145-156.

5.1 Introduction

Activated sludge models strongly rely on the accuracy of collected data and measurements of the modelled process. In most WWTP modelling studies, the accuracy of these data is fully relied upon. In stead, much emphasis is put on calibration of kinetic and stoichiometric parameters of the activated sludge model. In previous chapters it was however shown, that WWTP models are more sensitive towards operational data than to most model parameters (chapters 3 and 4). Because measurements are never fully accurate, mass balances never can be closed perfectly. In models however, all flows are balanced. In general, fitting models on erroneous or unbalanced data, will lead to laborious and unjustified model calibration. Therefore, it is essential to check prime data on errors and consistency.

Gross error detection and data reconciliation techniques for biochemical processes have been developed by van der Heijden *et al.* (1994a/b/c). The method was implemented in the free-domain software 'Macrobal' by Hellinga *et al.* (1992). All chemical processes can be described by a combination of linear relations based on mass balances (e.g. COD, N, P). If more measurements are available than required to solve the system, the system is over determined. For such systems gross errors can be detected by evaluating the balance residuals (ε). This is done on the basis of a statistical test. When there is no statistical proof for gross errors, the data can be balanced in a data reconciliation procedure. Finally, this results in a balanced data set without errors and an improved overall accuracy.

Macrobal originally was designed for balancing elements and conversion rates on a molecular level. We applied the program on a process level, balancing the mass flows of the full-scale WWTP Katwoude, situated in the Netherlands and managed by the Dutch water board 'Uitwaterende Sluizen in Hollands Noorderkwartier'. In this chapter it is demonstrated how Macrobal can be used for gross error detection and data reconciliation. It is shown how this simplifies the model calibration and WWTP simulation.

5.2 WWTP Katwoude

5.2.1 Process description

The actual capacity of WWTP Katwoude was 86300 p.e.. The plant had a completely mixed non-aerated selector (R1; 270 m^3), a completely mixed anoxic reactor (R2; 1760 m^3) and a 5 meter deep aerated carrousel reactor (R3; 15840 m^3). Originally the plant was designed for COD and N removal.

However, some BioP activity was observed. Most likely, in summer conditions R1 acted as an anaerobic selection reactor for PAO's. Two surface aerators in R3 controlled oxygen on 1.5 and 0.8 $gO_2 \cdot m^{-3}$ measured on respectively $^3/_5$ and $^4/_5$ of the tank. DO concentration gradients were measured in the longitude, width and depth of the aerobic reactor (not shown). During the whole year, chemical P precipitation was applied in R3 to assure effluent phosphate (PO_{EF}) below 0.5 $gP \cdot m^{-3}$. A natural external recycle from R3 (Q_{R3EX}) supplied R2 with nitrate. Q_{R3EX} was estimated from the superficial flow velocity in R3 (0.37 $m \cdot s^{-1}$) and the cross-section of the passage connecting R2 and R3 (5×1.3 m^2). Four clarifiers were operated in pairs (CL_{12} and CL_{34}). According to the design, flow distribution works FD_1 divided Q_{R3} in favour of CL_{34} with a distribution factor of 0.57. R1 was supplied with RAS by Q_{RS34}, R2 by both Q_{RS12} and Q_{RS34}. FD_2 divided Q_{RS34} in favour of R1 with a distribution factor of 0.543. The waste activated sludge (WAS) from the underflow of CL_{12} (Q_W) was concentrated in two WAS thickeners (TH). The thickened WAS (Q_{TW}) was dewatered by centrifugation (CE) and transported from the WWTP (Q_{DW}). The overflow from the thickener (Q_{OF}) and centrate (Q_{CE}) were recycled to R1. In table 5.1 the hydraulic and operational data are presented. The flow scheme of the WWTP is presented in figure 5.1.

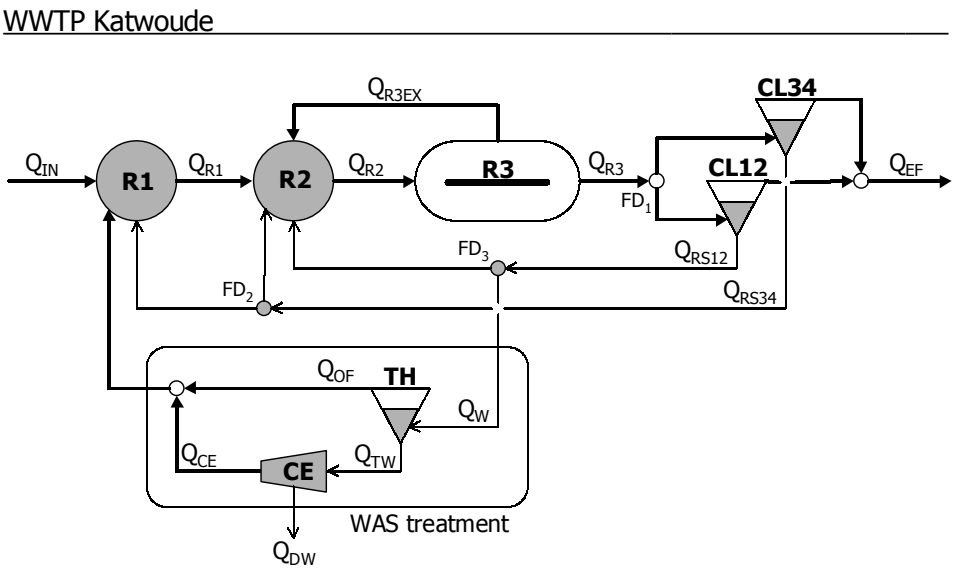

Figure 5.1 Flow scheme of WWTP Katwoude. Bold lines are activated sludge flows. Thin lines are RAS and WAS flows. R1: selector, R2: anoxic reactor, R3: aerated carousel, CL: clarifiers, TH: WAS thickening, CE: dewatering centrifuge and FD: hydraulic flow distribution works.

Flow	Average ± s_D $m^3 \cdot d^{-1}$	Process unit	Volume m^3	Depth m	[3]HRT h
Avg. influent 2000, Q_{24}	13252 ± 5960	Selector, R1	270	3.5	0.2
8-day avg. influent, Q_{IN8}	12380 ± 1270	Denitrification reactor, R2	1760	5.5	0.4
External recycle R3, Q_{R3EX}	[1]207792	Aerated carousel, R3	15840	5.0	7.5
Internal recycle R3, Q_{R3IN}	[2]2077920	Total reactor volume	17870	-	33.5
RAS from CL_{12}, Q_{RS12}	12144 ± 1214	Clarifiers, CL_{12} (2 × 1395 m^3)	2790	-	3.1
RAS from CL_{34}, Q_{RS34}	24960 ± 2496	Clarifiers, CL_{34} (2 × 1399 m^3)	2798	-	2.3
WAS, Q_W	1227 ± 791	Thickeners, TH (2 × 308 m^3)	615	-	12.8
Thickened WAS, Q_{TW}	154 ± 92	Flow distribution factor, FD_1	0.570	-	-
Dewatered WAS, Q_{DW}	14 ± 4	Flow distribution factor, FD_2	0.543	-	-

Table 5.1 Measured operational data and volumes of WWTP Katwoude. [1] estimated from the superficial flow velocity in R3 (0.37 $m \cdot s^{-1}$) and the cross-section of the passage connecting R3 and R2 (1.3×5 m^2). [2] estimated from the superficial flow velocity in R3 (0.37 $m \cdot s^{-1}$) and the cross-section of reactor R3 (13×5 m^2). [3] the HRT was calculated from the balanced flows (Q_{IN8}, Q_{R1}, Q_{R2}, Q_{R3}).

5.2.2 Measurements

The pseudo steady state of WWTP Katwoude was recorded during a 8-day sampling program (the 23rd of February to the 2nd of March 2001). In this period, samples were collected daily from the influent (Q_{IN8}), Q_{R1}, Q_{R2}, Q_{R3}, Q_{RS12} and Q_{RS34} Q_{OF}, Q_{CE} and the effluent (Q_{EF}). The influent, centrate and effluent were 24-hour composite samples, whereas the process internal measurements were grab samples during influent peak flow. The samples were analysed on TCOD, COD_{MF} (COD of the micro-filtrated fraction, 0.45 µ pore diameter, no flocculation), BOD_5 (5 day biological oxygen demand), MLSS (mixed liquor suspended solids), ash fraction of the MLSS, VFA (volatile fatty acids), NH_4^+ (ammonium), NO_3^- (nitrate), TKN (total Kjeldal nitrogen), TP (total phosphorus) and PO_4^{2-} (ortho-phosphate). energy use, pump flow-rates (table 5.1), mixer and aerator operation time and process control measurements were recorded daily. Average measurements of the

8-day sampling program are presented in table 5.3. Also the average measurements over 2000 were collected. These measurements are presented in table 5.2. The average temperature in 2000 was 15 ^{0}C.

	Sampled flow / reactor	Q_{24} $g \cdot m^{-3}$	R3 $g \cdot m^{-3}$	Q_{EF} $g \cdot m^{-3}$	Q_W $kg \cdot d^{-1}$
Meas.	Total COD, TCOD	631 ± 172	n.d.	37.5 ± 7.0	n.d.
Sim.	**X_T+S_T**	**631**	**4662**	**37.5**	**4119**
Meas.	COD particulate, COD_X	n.d.	4628 ± 514	n.d.	4132 ± 910
Sim.	**X_T**	**316**	**4628**	**4.0**	**4118**
Meas.	Total phosphorus, TP	9.2 ± 3.8	112.7 ± 13.0	0.6 ± 0.8	100.6 ± 22
Sim.	**S_{PO} + X_{MeP} + X_{PP} + iP**	**9.2**	**113**	**0.6**	**101.2**
Meas.	Ortho-phosphate	n.d.	n.d.	0.5 ± 0.6	n.d.
Sim.	**S_{PO}**	**3.6**	**0.7**	**0.5**	**0**
Meas.	Precipitated $FePO_4$	n.d.	n.d.	n.d.	n.d.
Sim.	**X_{MeP}**	**0**	**20.3**	**0.0**	**18**
Meas.	Tot. Kjeldalh N, TKN	56 ± 15	274 ± 30	2.6 ± 1.5	244.8 ± 54
Sim.	**S_{NH} + iN**	**56**	**274**	**0.9**	**247**
Meas.	Ammonium	n.d.	n.d.	1.0 ± 1.6	n.d.
Sim.	**S_{NH}**	**37**	**0.7**	**0.7**	**0**
Meas.	Nitrate	n.d.	n.d.	3.2 ± 3.0	n.d.
Sim.	**S_{NO}**	**0**	**3.4**	**3.3**	**0**

Table 5.2 Measurement and simulation results over the year 2000. Average measurements ± s_D. Simulated results and influent data are printed **bold**. The plant was simulated with average influent loads and a temperature of 15 $^{\circ}$C. TP_{R3} was controlled, by regulating Q_W, resulting in a SRT of 19.8 days.

5.2.3 The process model

For all simulations the simulation platform SIMBA© 3.3$^+$ (Alex *et al.*, 1997) was used, operating under Matlab/Simulink© 5.2. In SIMBA© WWTP process models are constructed by connecting CSTR's in a desired configuration. Biological conversions were calculated with the TUD model (appendix III). The WWTP was modelled according to the flow scheme in figure 5.1 and the data in table 5.1. R1 and R2 were each modelled as one CSTR. R3 was modelled as five CSTR's in series, with an internal recycle Q_{R3IN}. Aeration of R3 (OC_{R3}) was modelled with PI control, which regulated DO_{R3} in the first and third CSTR on respectively 1.5 and 0.8 $gO_2 \cdot m^{-3}$. With this set-up, the horizontal DO gradients were approximated. The modelled clarifiers separated solids and water ideally. A small fraction X_{EF} was modelled by a percentile loss of the RAS (0.0005%). Denitrification in the RAS volume was not observed and therefore not modelled. The solids concentration in the AT (X_{R3}) was PI controlled by regulating Q_W. Chemical precipitation of $FePO_4$ was modelled in Q_{R2}. PO_{EF} was PI controlled on 0.5

$gP \cdot m^{-3}$ by regulating the dosage of $FeCl_3$. The model influent was characterised according to Roeleveld and van Loosdrecht (2001). All simulations were performed with a constant influent flow.

	Sampled flow/reactor	Q_{IN8} $g \cdot m^{-3}$	R1 $g \cdot m^{-3}$	R2 $g \cdot m^{-3}$	R3 $g \cdot m^{-3}$	Q_{EF} $g \cdot m^{-3}$
Meas.	TCOD	773 ± 53	n.d.	n.d.	4840 ± 1263	43.7 ± 8.3
Sim.	**$X_T + S_T$**	**773**	**4180**	**4869**	**4845**	**43**
Meas.	COD_X	379 ± 93	3999 ± 222	n.d.	4795 ± 1263	0.0 ± 8.9
Sim.	**X_T**	**380**	**4020**	**4806**	**4805**	**4.1**
Meas.	COD_{MF}	393 ± 41	n.d.	n.d.	44.3 ± 0.6	44.0 ± 0.6
Sim.	**$S_A + S_F + S_I$**	**393**	**160**	**63**	**40**	**40**
Meas.	TP	12.9 ± 4.5	97.1 ± 5.4	n.d.	116.7 ± 6.5	1.8 ± 0.3
Sim.	**$S_{PO} + X_{PP} + iP$**	**12.9**	**98.5**	**116.5**	**116.4**	**1.8**
Meas.	Phosphate	6.4 ± 0.9	5.0 ± 1.4	3.0 ± 0.3	1.8 ± 0.4	1.4 ± 0.2
Sim.	**S_{PO}**	**6.1**	**4.6**	**3.2**	**1.7**	**1.7**
Meas.	TKN	61.7 ± 7.6	n.d.	n.d.	285 ± 32	1.9 ± 0.3
Sim.	**$S_{NH} + iN$**	**61.5**	**248**	**286**	**282**	**2.0**
Meas.	Ammonium	39.9 ± 4.9	14.0 ± 2.2	5.3 ± 1.5	1.0 ± 0.6	0.7 ± 0.6
Sim.	**S_{NH}**	**38.3**	**14.4**	**5.1**	**1.2**	**1.2**
Meas.	Nitrate	0 ± 0	0.7 ± 0.4	0.8 ± 0.6	3.3 ± 1.0	3.2 ± 0.7
Sim.	**S_{NO}**	**0**	**0.54**	**0.4**	**3.3**	**3.5**

Table 5.3 Measurements and simulations of the 8-day sampling program. The plant was sampled daily, at dry weather influent peak flow (8-day average 12380 $m^3 \cdot d^{-1}$). Simulated results and influent data are printed **bold**.

5.2.4 Introducing Macrobal

The free-domain software 'Macrobal' was used for evaluation of operational data. Macrobal originally was designed for balancing chemical elements and conversion rates on a molecular level. In this chapter, the program is used to balance compounds and flows in a full scale WWTP. Operation of Macrobal is explained according to tables 5.4 and 5.5. These tables are drawn up in the Macrobal in and output format. In table 5.4, *n* columns represent the mass balances, with in each balance the concentrations $C_{i,n}$. All empty spaces in the balances represent zeros. Negative concentrations are outflows, positive concentrations are inflows. The balances correspond with the first column of table 5.4, which is indicated as the flow vector Q. This is further specified in table 5.5. The flow vector Q consists of *m* measured and *u* unknown (thus calculated) flows, with a total number of $m+u=i$ elements. The mass balances may relate to individual reactors, groups of reactors or the total WWTP. Ideally, the balances add up to zero,

however caused by measurement errors, balances have residuals (ε_n). For the total system the residuals are calculated according to eq. 5.1.

$$\sum_{i=1}^{i} \overline{Q}_i \times \overline{C}_{i,n} = \overline{\varepsilon}_n \qquad (5.1)$$

A system with *n* balance equations, can be solved if *n=u*. For *n>u* the system is 'over determined'. This is expressed in the 'degree of redundancy', defined as *n-u*. It should be noticed that the degree of redundancy is calculated based on the number of *independent* balance equations.

Balancing data is only useful when no gross errors are apparent. In Macrobal these gross errors are therefore first detected by evaluating the residual (ε) of each balance on the basis of a statistical test (the χ-square distribution). An elaborate description this procedure is found in van der Heijden *et al.* (1994a/b/c). Gross errors are introduced by (i), an incorrect process description (ii), erroneous operational data or (iii), erroneous process measurements. Gross errors in the flow vector can be detected by systematically rejecting measured flows (thus a measured value becomes a unknown value), until the χ-square test is passed. An incorrectly defined balance or measurement error, can be detected by systematically rejecting balances, until the χ-square test is passed.

If $n\text{-}u \geq 1$ and no gross errors are apparent, the system can be balanced. Hereby the residuals (ε_n) are minimised and the standard deviation (s_D) of the balanced operational data are reduced. A high degree of redundancy, results in a high accuracy, i.e. a small s_D.

5.3 Error Detection and Data Reconciliation

5.3.1 Estimation of the SRT

For a reliable simulation, the SRT should be known within 95 % accuracy. This was shown in chapter 3 and by Brdjanovic *et al.* (2000). Therefore the SRT was evaluated on the basis of the TP balance according to chapter 3 and Nowak *et al.* (1999). Primary data indicated the SRT was 20 days. This required an evaluation over approximately 60 days. For the evaluation, average data over the year 2000 was used, which was readily available from the regular WWTP sampling program. The TP balance was calculated over the sludge dewatering (CE) and over the total WWTP. The system of balances is presented in table 5.4. Three out of five flows were measured

(Q_{24}, Q_{TW} and Q_{DW}), leaving two unknown (Q_{CE} and Q_{EF}). TP was measured in Q_{24}, Q_{TW}, Q_{CE} and Q_{EF}. The TP load in the dewatered flow ($^{L}TP_{DW}$) was calculated from the measured sludge production (^{L}WAS). The system of four balance equations (n=4) and two unknown flows (u=2) had a degree of redundancy of two (n-u=2), which allowed error detection and data reconciliation. From the yearly average data, also the COD & N balance was calculated. For these 'open' balances the degree of redundancy was zero (n-u=0), meaning all loads were calculated and no balancing was performed. The net oxygen consumption (OC_{NET} 3607 $kgO_2 \cdot d^{-1}$, table 5.5), calculated from the COD & N balance, was used as a final check on the calibrated model.

Table 5.5 shows the results of the Macrobal calculations. No gross errors were detected in the operational data. Macrobal was able to balance the operational data caused by the large standard deviation (s_D) of Q_{24}. Hereby, the balanced influent flow surprisingly corresponded to the dry weather influent flow (11833 ± 2210 $m^3 \cdot d^{-1}$). Based on this observation, we verified that TP_{IN} was sampled at an average flow rate of 11500 $m^3 \cdot d^{-1}$, which is in correspondence with the balanced Q_{24}. In the reconciled system, all balances were in accordance. From the raw data the SRT was calculated to be 20.0 ± 6.7 days. In the balanced system this was 19.8 ± 4.8 days (17870 m^3 × 112.7 ± 13 $gP \cdot m^{-3}$ divided by 101.5 ± 13 $kgP \cdot d^{-1}$).

5.3.2 Balancing operational data

On the basis of the 8-day sampling program, a system of balances was formulated with the intention to check 7 process flows (Q_{IN8}, Q_{RS12}, Q_{RS34}, Q_{R3EX}, Q_W, Q_{TW} and Q_{DW}) and the flow division by FD_2 on possible errors (table 5.6). According to the flow scheme of the WWTP in figure 5.1 a system of 12 mass balances was formulated. Flows were balanced over R1, R2, R3, CL, TH and CE. Hereby, ammonium was balanced over R1 and R2, and TP was balanced over R1, R2, R3 and CL. On the basis of the relative short hydraulic retention time (HRT), all reactors were assumed to be in a (local) steady state (table 5.1). Q_{IN8} was slightly higher then Q_{24}, caused by minor rain events during the recorded period. Consequently, the sludge production and the net oxygen consumption were not representative and therefore not used. Instead we relied on the SRT evaluation in the previous section.

The system contained 12 balance equations (n=12) and 6 unknown flows (u=6), resulting in a degree of redundancy of n-u=6. On the basis of the original data, we were not able to balance the system within the 75 % confidence level of the χ-square test (table 5.7). Therefore, three measured flows (Q_{RS12}, Q_{RS34} and Q_{R3EX}) were rejected. Recalculating the system with

Q_{RS12}, Q_{RS34} and Q_{R3EX} as unknown (n-u=3), the calculated return flow rates (Q_{RS12} and Q_{RS34}) indicated that flow divider FD_2 was fully directed towards R1. After an inspection at sight this was confirmed. Initially, Q_{R3EX} was estimated from the superficial flow velocity in the carousel reactor (0.37 $m \cdot s^{-1}$). From the balance calculations a lower average flow was expected. This was however not verified in practice. Therefore, in the final calculation Q_{R3EX} was set as unknown. The balanced value for Q_{R3EX} (66750 ± 4500 $m^3 \cdot d^{-1}$) suggests that the average velocity over the depth of the carousel reactor was 0.12 $m \cdot s^{-1}$. The balanced flows are presented in table 5.7.

			n mass balances with elements $C_{i,n}$							
	defined balance		WWTP	CE	WWTP	CE	WWTP	WWTP	WWTP	WWTP
	bal. compound		Flow bal.		TP	TP	COD	TKN	NO_3^-	DO
	unit		-	-	$gP \cdot m^{-3}$	$gP \cdot m^{-3}$	$gCOD \cdot m^{-3}$	$gN \cdot m^{-3}$	$gN \cdot m^{-3}$	$gO_2 \cdot m^{-3}$
flow vector Q with i elements (m measured, u unknown)	Q_{24}	$m^3 \cdot d^{-1}$	1		9.2 ± 3.8		631.3 ± 172	56 ± 15	0 ± 0	
	Q_{EF}	$m^3 \cdot d^{-1}$	- 1		-0.6 ± 0.8		-37.5 ± 7.2	- 2.6 ± 1.5	-3.2 ± 3	
	Q_{TW}	$m^3 \cdot d^{-1}$		1		669 ± 99	- 27468 ± 4077	- 1630 ± 242		
	Q_{CE}	$m^3 \cdot d^{-1}$		- 1		-58 ± 46	2383 ± 1876	141 ± 111		
	Q_{DW}	$m^3 \cdot d^{-1}$	- 1	- 1					-0 ± 0	
	TP_{DW}	$kgP \cdot d^{-1}$			- 1	- 1				
	OC_{COD}	$kgO_2 \cdot d^{-1}$					- 1			- 1
	^{L}NIT	$kgN \cdot d^{-1}$						- 1	1	- 4.57
	^{L}DEN	$kgN \cdot d^{-1}$					- 2.87		- 1	
	OC_{NET}	$kgO_2 \cdot d^{-1}$								1

residuals calculated according to $\sum_{i=1}^{i} \overline{Q}_i \times \overline{C}_{i,n} = \overline{\varepsilon}_n$

Table 5.4 Reconciliation of the year 2000 average measurements. Evaluation of the SRT. CE: balance over the centrifuge, WWTP: balance over the total plant. The last 4 columns are 'open' COD and N balances (OC_{COD}: oxidised COD, ^{L}NIT: nitrified load, ^{L}DEN: denitrified load, OC_{NET}: net oxygen consumption). Empty spaces in the matrix represent zeros.

5.4 Model Calibration and Simulation

After error detection and data reconciliation, we calibrated the model of WWTP Katwoude. Therefore, the calibration method was used as proposed in chapters 3 and 4. First the solids were fitted (TP_X, COD_X and TKN_X) on the basis the average of 2000 (tables 5.2 and 5.5). Next, nitrification, denitrification and EBPR were calibrated on the basis of the 8-day sampling program (tables 5.3 and 5.7). The calculated net oxygen consumption (OC_{NET}) was a final check on the calibrated model (table 5.5).

			Degree of redundancy = 2 No proof for measurement errors based on the χ-square distribution.		
				Measured ± s_D	Balanced ± s_D
flow vector Q with *i* elements (*m* measured, *u* unknown)	Q_{24}	$m^3 \cdot d^{-1}$	measured & bal.	13252 ± 5960	11833 ± 2210
	Q_{EF}	$m^3 \cdot d^{-1}$	calculated	-	11819 ± 2210
	Q_{TW}	$m^3 \cdot d^{-1}$	measured & bal.	153.7 ± 92.3	165.2 ± 31.1
	Q_{CE}	$m^3 \cdot d^{-1}$	calculated	-	151.2 ± 31.4
	Q_{DW}	$m^3 \cdot d^{-1}$	measured & bal.	14 ± 3.8	14 ± 3.8
	$^LTP_{DW}$	$kgP \cdot d^{-1}$	measured & bal.	100.6 ± 22	101.5 ± 10
	OC_{COD}	$kgO_2 \cdot d^{-1}$	calculated	-	1852 ± 10
	^LNIT	$kgN \cdot d^{-1}$	calculated	-	383.9 ± 10
	^LDEN	$kgN \cdot d^{-1}$	calculated	-	346.1 ± 10
	OC_{NET}	$kgO_2 \cdot d^{-1}$	calculated	-	3607 ± 10

Table 5.5 Balancing results of the year 2000 average measurements. Balanced (bal.) operational data according to table 5.4. No gross errors were detected. The results of the data reconciliation are presented in the last column. The result of the COD & N balance is presented in the bottom four rows.

5.4.1 Fitting the sludge production

Step 1. Fitting the model on the TP balance. The model was fitted to the year 2000 balanced loads $^LTP_{IN}$, $^LTP_{EF}$ and $^LTP_{DW}$ (tables 5.4 and 5.5). PO_{EF} was controlled on 0.5 $gP \cdot m^{-3}$ by chemical precipitation. TP_{EF} was calibrated with a percentile loss of solids from the modelled clarifier. For modelling convenience, Q_{DW} was fixed on 14 $m^3 \cdot d^{-1}$ (table 5.5). Hereby, TP_{R3} was controlled on 112.7 $gP \cdot m^{-3}$ (table 5.2) by regulating Q_W, which resulted in $^LTP_{DW}$ of 101.5 $kgP \cdot d^{-1}$. This was in accordance with the balance in table 5.5. Because TP is strongly related to the solid fraction, fitting the model to TP fixes the SRT.

Step 2. Fitting the solids COD_X balance. Because the COD_X balance is a non conserved balance, an incorrect load $^{L}COD_{IN}$ will generally be compensated by OC_{NET} (chapter 3). In the previous section the SRT was fixed according to the TP balance. Hence, the total amount of MLSS in the WWTP was mainly determined by the influent X_I/X ratio, as inert COD (X_I) accumulates in the WWTP. By adjusting the influent X_I/X ratio to 0.798, we fitted the model to the measured TP_X/COD_X ratio of 0.032. Hereby, all model uncertainties related to the production of X_I and the influent characterisation are lumped in the influent X_I/X ratio.

Step 3. Fitting COD_S in the effluent. COD_S in the effluent was fitted by adjusting the influent ratio S_I/S_F from 0.146, calculated according to Roeleveld and van Loosdrecht (2001) to 0.134. Increasing S_I in the influent directly effects the effluent concentration, as S_I is not converted. Hereby, S_A in the influent was not changed, as this model component was directly measured from VFA_{IN}.

Step 4. Fitting the TKN balance. Like COD, TKN is a non conserved compound. An incorrect ^{L}TKN in e.g. Q_{EF} or Q_W, generally will be compensated by OC_{NET} via nitrification, and N_2 production via denitrification. The measured fraction TKN_X/COD_X was 0.059. TKN_X was fitted by increasing the activated sludge fractions iN_{XI} and iN_{XS} to 0.06 gN/gCOD. This resulted in a modelled $^{L}TKN_{DW}$ of 247 $kgN \cdot d^{-1}$ (table 5.2).

5.4.2 Calibrating nitrification, denitrification and BioP

In the previous section, we calibrated X_I/X, S_I/S_F, iN_{XI} and iN_{XS}. nitrification, denitrification and EBPR were calibrated on the basis of the 8-day sampling program (table 5.3). Therefore we used the influent composition (table 5.3), balanced flows (table 5.7) and X_{R3} from the 8-day sampling program. The simulated temperature was 9 ^{0}C.

Step 5. Calibrating the net nitrified load. Strong DO gradients were observed in the depth and width of R3. However, only the gradient in the length of the carousel was measured. DO_{R3} was therefore assumed to be less reliable. To simulate NH_{EF}, the DO set-points in R3 were increased to 2 $gO_2 \cdot m^{-3}$. Hereby, the original aerated volume was not changed (9504 m^3).

Step 6. Calibrating the net denitrified load. The net denitrification (^{L}DEN) was fitted by increasing K_O from 0.2 to 0.3 $gO_2 \cdot m^{-3}$ (chapter 3). This caused effluent nitrate (NO_{EF}) to decrease from 3.7 to 3.2 $gN \cdot m^{-3}$.

Step 7. Calibrating anaerobic phosphate release. From the phosphate balance over R1, the phosphate release in the anaerobic reactor ($^{L}PR_{R1}$) was calculated to be 34 ± 14 $kgP \cdot d^{-1}$. Without calibration, the model

predicted a release of 24 kgP·d^{-1}. Hereby PAO was approx. 1 to 2 % of the total activated sludge. Because the simulated release was within the accuracy of measurement, we chose not to calibrate the phosphate release in R1.

	R1	R2	R3	CL	TH	CE	CL	R1	R1	R2	R2	R3
Flow	Flow balances						TP	TP	NH_4^+	TP	NH_4^+	TP
$m^3 \cdot d^{-1}$							$gP \cdot m^{-3}$	$gP \cdot m^{-3}$	$gN \cdot m^{-3}$	$gP \cdot m^{-3}$	$gN \cdot m^{-3}$	$gP \cdot m^{-3}$
Q_{IN8}	1							12.9 ± 4.5	39.9 ± 4.9			
Q_{R1}	-1	1						-97.14 ± 5.4	-14.02 ± 2.2	97.14 ± 5.4	14.02 ± 2.2	
Q_{R3EX}		1	-1							116.7 ± 6.5	0.99 ± 0.6	-116.7 ± 6.5
Q_{R2}		-1	1							-116.7 ± 6.5	-5.25 ± 1.5	116.7 ± 6.5
Q_{R3}			-1	1			116.7 ± 6.5					116.7 ± 6.5
Q_{RS12}		1		-1			-182.4 ± 4.9			182.4 ± 4.9	0.67 ± 0.6	
Q_{EF}				-1			-1.83 ± 0.5					
Q_{RS34}	1			-1			-141.5 ± 3.8	141.5 ± 3.8	0.67 ± 0.6			
Q_W				-1	1		-182.4 ± 4.9	182.4 ± 4.9				
Q_{OF}	1				-1				27.8 ± 0.6			
Q_{TW}					-1	1		-860.5 ± 112.7				
Q_{CE}	1					-1		183 ± 5.8	80.5 ± 5.3			
Q_{DW}						-1						

Table 5.6 **Data reconciliation of the 8-day measurements.** Evaluation of operational data. Table headings are explained in figure 5.1. The first balances R1, R2, R3, CL, TH and CE are volumetric flow balances. In the following columns TP and ammonium are balanced.

Step 8. Evaluating the net oxygen consumption. A final check on the calibrated model was the simulated net oxygen consumption (OC_{NET} 3594 $kgO_2 \cdot d^{-1}$). This value approximately matched the calculated value (3607 $kgO_2 \cdot d^{-1}$, table 5.5). On the basis the stoichiometric oxygen consumption and the measured energy use for aeration (6569 ± 1319 kWh·d^{-1} or 27.8

kWh/p.e.), an theoretical efficiency of 0.55 kgO_2/kWh is calculated. If an alpha factor is assumed of 0.7 and a deficiency factor of 1.4 (average DO at the aerator 3 $gO_2 \cdot m^{-3}$ and an average temperature of 15 °C), an net efficiency of 1.12 kgO_2/kWh is expected, which is an realistic value.

	First calculation Degree of redundancy = 6 99% confidence of a measurement error based on the χ-square distribution.		Second calculation Degree of redundancy = 5 No proof for measurement error based on the χ-square distribution.		
		Measured ± s_D $m^3 \cdot d^{-1}$		Measured ± s_D $m^3 \cdot d^{-1}$	Balanced ± s_D $m^3 \cdot d^{-1}$
Q_{IN8}	meas. & bal.	12380 ± 1270	meas. & bal.	12380 ± 1270	12800 ± 737
Q_{R1}	calculated	n.d.	calc.	n.d.	38640 ± 2390
Q_{R3EX}	meas. & bal.	[1]207792 ± 20779	meas. & calc.	rejected	66750 ± 4500
Q_{R2}	calculated	n.d.	calculated	n.d.	117300 ± 7270
Q_{R3}	calculated	n.d.	calculated	n.d.	50520 ± 2940
Q_{RS12}	meas. & bal.	[2]23551 ± 2355	meas. & bal.	[3]12144 ± 1214	11880 ± 853
Q_{EF}	calculated	n.d.	calculated	n.d.	12790 ± 737
Q_{RS34}	meas. & bal.	[2]13553 ± 1355	meas. & bal.	[2]24960 ± 2496	24710 ± 1540
Q_W	meas. & bal.	1227 ± 791	meas. & bal.	1227 ± 791	1149 ± 291
Q_{OF}	calculated	n.d.	calculated	n.d.	999 ± 217
Q_{TW}	meas. & bal.	153.7 ± 92.3	meas. & bal.	153.7 ± 92.3	150 ± 75
Q_{CE}	calculated	n.d.	calculated	n.d.	136 ± 75
Q_{DW}	meas. & bal.	14.0 ± 3.8	meas. & bal.	14.0 ± 3.8	14 ± 3.8

Table 5.7 **Balancing results of the 8-day sampling program.** Two calculations were performed. In the first gross errors were detected in Q_{R3EX}, Q_{RS12} and Q_{RS34}. In the second calc. Q_{R3EX} was rejected, and the system could be balanced. [1] estimated from superficial flow velocity (0.37 $m \cdot s^{-1}$). [2] calculated with FD_1 0.57 in favour of CL_{34} FD_2 0.543 in favour of R1. [3] FD_2 set to one.

5.5 Discussion

5.5.1 Balancing conserved compounds

A compound only can be balanced when it is totally recoverable. Most 'conserved' compounds (COD, TN, TOC), have a component in the gaseous phase (respectively O_2, N_2 and CO_2), which generally is not measured. Theoretically this also accounts for volumetric flows, however in practice evaporation of water is negligible. A compound that under normal conditions exclusively is associated with the solid and liquid fractions is phosphorus. P can be recovered from all in and outgoing flows, and therefore is very suitable for balancing purposes. Moreover, TP can be related to the solid fraction (MLSS). This is justified as the activated sludge ratio $TP_X/COD_X/TKN_X$ only changes over a relative long period (3×SRT).

Practical advantages of using TP as a 'balancing compound' are: (i) measuring TP is relative simple, (ii) in WWTP's, TP is generally well above the detection limit and (iii) historical TP measurements are often readily available. In this study, ammonium and phosphate balances were used to evaluate the process. ammonium and phosphate are not conserved and therefore can not be fully recovered. It was however assumed that (i), ammonium was not oxidised in R1 or R2, (ii) ammonification was negligible and (iii), growth of biomass in R1 and or R2 was negligible. These assumptions indicate that balancing ammonium is only valid when the HTR in R1 and R2 is low, and therefore the contribution of these reactions can be neglected. The phosphate balance is less sensitive to biomass growth. This is the direct result of the biomass composition which contains little P ($CH_{2.09}O_{0.54}N_{0.20}P_{0.015}$, Smolders *et al.*, 1994). For the same reason, also hydrolysis and fermentation have reduced effect on the phosphate balance over R1. When phosphate and ammonium are balanced, it must however be realised that the accuracy of the calculations are negatively influenced by these processes.

5.5.2 Calibrating BioP

No PAO activity was simulated with a temperature of 9 ^{0}C. However, if the temperature profile of the preceding year was taken in account, full EBPR was simulated in summer and autumn, whereas some BioP activity was simulated under winter conditions. This showed that the simulated PAO concentration was not only sensitive to the actual temperature, but also to the preceding temperature profile. Simulation of the WWTP at 15 ^{0}C, showed that at least 360 days were needed before PAO's and regular HMO's were in steady state. Because both species competed for the same substrate (VFA), they were limited in their growth. Therefore it took a considerable period before steady state was reached. This is in contrary to AMO's, which if allowed by process conditions, recover in approx. 10 days. It can therefore be concluded that PAO's generally are not in steady state. To avoid laborious and relative inaccurate simulations with variable temperature, it is suggested to experimentally determine the PAO concentration from a anaerobic phosphate release batch-tests. As initial estimation, it is proposed to calculate the anaerobic phosphate release according to eq. 5.2.

$$Q_{IN} \times PO_{IN} + Q_{RS34} \times PO_{RS34} + Q_{CE} \times PO_{CE} + Q_{OF} \times PO_{OF} - Q_{R1} \times PO_{R1} + {}^{L}PR_{R1} = 0 \qquad (5.2)$$

From the phosphate balance over R1, the anaerobic phosphate release $^{L}PR_{R1}$ was calculated to be 34 ± 14 kgP·d^{-1}. On the basis of Q_{R1} = 38640

$m^3 \cdot d^{-1}$, this corresponds with an increase of 0.9 $gP \cdot m^{-3}$ in PO_{R1}. Simulating the model with a yearly temperature profile, $^{L}PR_{R1}$ was calculated to be 24 $kgP \cdot d^{-1}$. This corresponded to a increase of PO_{R1} with 0.6 $gP \cdot m^{-3}$. Both estimated and simulated releases were smaller than the measurement accuracy (PO_{R1}=5.0 ± 1.4 $gP \cdot m^{-3}$, table 5.3). Moreover, in the simulation PAO only made up 2 % of the TCOD. On the basis thereof, further calibration EBPR was not justified.

5.5.3 Calibrating N fractions

The TKN fraction in waste sludge was highly sensitive in the model. Incorrect simulation of TKN in the waste sludge ($^{L}TKN_W$), is compensated by the net oxygen consumption (OC_{NET}) via nitrification and the N_2 production via denitrification. In ASM2d (Henze *et al.*, 1999), it is proposed to use three distinguishable N fractions for the modelled solids (iN_{XI}, iN_{XS} and iN_{BM}) and two for the dissolved compounds (iN_{SF} and iN_{SI}). It is remarked that these values are merely a reference and should experimentally be determined for each situation. iN_{BM} is more or less constant in WWTP's (0.07 gN/gCOD), and therefore should not be calibrated. To fit TKN_X, iN_{XI} is the most sensitive parameter, as X_I usually contributes the most to the activated sludge. In a properly functioning WWTP, X_S will be in the range of 1 to 2 % of the activated sludge. Therefore, only a small error is made when iN_{XI} and iN_{XS} are calibrated simultaneously. Independent calibration of iN_{XI} and iN_{XS}, as proposed by Koch et al. (2000), is not justified as iN_{SF} (iN_{SS}, ASM3p) and iN_{SI} can not be determined with the required accuracy.

In this study ammonium was balanced cover the anaerobic reactor. Therefore S_{NH} in the influent should match the measured influent ammonium concentration. Roeleveld and van Loosdrecht (2001) suggest to calculate S_{NH} according to eq. 5.3.

$$S_{NH} = TKN_{IN} - (iN_{XI} \times X_I + iN_{XS} \times X_S + iN_{BM} \times X_{BM} + iN_{SF} \times S_F + iN_{SI} \times S_I) \quad (5.3)$$

Instead, it is proposed to fit eq. 5.3 to the measured NH_{IN} by adjusting iN_{SF} or iN_{XS} in the model.

5.6 Conclusions

Data evaluation based on linear conservation relations gives insight in basic plant performance. For this information, in practice often complete simulation studies are performed. The use of Macrobal instigates a systematic organisation of raw operational data, whereby information is acquired in the benefit of a proper WWTP evaluation. The extra time invested in data and process evaluation will be saved during calibration, as it takes considerably more effort to fit a model on faulty data.

Macrobal software showed suitable for error detection and reconciliation of operational data and process measurements. Therefore ammonium, TP and flow balances were formulated over several process units. Major errors were detected in three process flows. With the help of balancing methods these errors were corrected.

Model calibration mainly relied on fitting the mass balances that were established in the Macrobal data evaluation. Hereby no stoichiometric or kinetic parameters required calibration.

The balanced data set simplified the model calibration. For the calibration we used the stepwise method proposed in chapters 3 and 4. Hereby, the SRT was fitted according to the overall TP balance, TP_X/COD_X was fitted with the influent X_I/X ratio, TKN_X/COD_X was fitted with iN_{XI} and iN_{XS}, nitrification was fitted by adjusting the DO set-points and denitrification was fitted by increasing K_O.

References

Alex J., Tschepetzki R. and Bitter U. (1997) SIMBA Simulation of biological waste water treatment. Users manual, Institute of Automation and Communication e. V., Magdeburg.

Brdjanovic D., Logemann S., van Loosdrecht M. C. M., Hooijmans C. M., Alaerts G. J. and Heijnen J. J. (1998) Influence of temperature on biological phosphorus removal: process and ecological studies. *Water Res.* **32**(4), 1035-1048.

Brdjanovic D., van Loosdrecht M.C.M., Versteeg P., Hooijmans C.M., Alaerts G.J. and Heijnen J.J. (2000) Modelling COD, N and P removal in a full-scale WWTP Haarlem Waarderpolder. *Water Res.* **34**(3), 846-858.

Henze M., Gujer W., Mino T., Matsuo T., Wentzel M. C. and Marais GvR. and van Loosdrecht M. C. M. (1999) Activated Sludge Model No. 2d, ASM2d. *Wat. Sci. Technol.* **39**(1), 165-182.

Hellinga C. (1992) Macrobal 2.02. Delft University of Technology,. The Netherlands. M.C.M.vanLoosdrecht@TNW.TUDelft.NL. http://www.bt.tudelft.nl/miscell

Koch G., Kuhni M., Gujer W. and Siegrist H. (2000) Calibration and validation of Activated Sludge Model No. 3 for Swiss municipal wastewater. *Water Res.* **34**(14), 3580-3590.

Meijer S. C. F., van Loosdrecht M. C. M. and Heijnen J. J. (2001) Metabolic modelling of full-scale biological nitrogen and phosphorus removing WWTP's. *Water Res.* **35**(11), 2711-2723.

Nowak O., Franz A., Svardal K., Muller V. and Kuhn V. (1999) Parameter estimation for activated sludge models with the help of mass balances. *Water Sci. Technol.* **39**(4), 113-120.

Roeleveld P.J and van Loosdrecht M.C.M. (2001) Experiences with guidelines for wastewater characterization in The Netherlands. *Water Sci. Technol.* **45**(6), 145-156.

Van der Heijden R.T.J.M., Heijnen J.J., Hellinga C., Romein B., Luyben K.Ch.A.M. (1994a) Linear constraint relations in biochemical reaction systems: I. Classification of the calculability and the balanceability of conversion rates. *Biotechnol. Bioeng.* **43**, 3-10.

Van der Heijden R.T.J.M., Romein B., Heijnen J.J., Hellinga C., Luyben K.Ch.A.M. (1994b) Linear constraint relations in biochemical reaction systems: II. Diagnosis and estimation of gross errors. *Biotechnol. Bioeng.* **43**, 11-20.

Van der Heijden R.T.J.M., Heijnen J.J., Hellinga C., Romein B., Luyben K.Ch.A.M. (1994c) Linear constraint relations in biochemical reaction systems: III. Sequencial application of data reconciliation for sensitive detection of systematic errors. *Biotechnol. Bioeng.* **43**, 781-791.

Van Veldhuizen H. M., van Loosdrecht M. C.M. and Heijnen J. J. (1999) Modelling biological phosphorus and nitrogen removal in a full scale activated sludge process. *Water Res.* **33**(16), 3459-3468.

6

Calibration and Validation of the TUD Model

In this chapter the integrated model is evaluated on the basis of a number of lab-scale experiments. This evaluation shows that the integrated metabolic model is suited to describe the concentration dynamics of a wide range of lab-scale SBR and batch experiments using a single set of model parameter values. The full-scale performance of the TUD model, investigated in several previous studies is discussed. Several model improvements were proposed, which are incorporated in the TUD model in this chapter. The major adjustment relates to the glycogen formation kinetics. It is shown that the proposed kinetic equation improves the model performance and simplifies the use of the model. The chapter concludes by discussing some model limitations and modelling considerations.

6.1 Introduction

In previous publications (Murnleitner *et al.*, 1997; Brdjanovic *et al.*, 2000; Wichern *et al.*, 1999), several adjustments of the TUD model were proposed. Some of these changes were never incorporated, some where never properly validated. In this thesis the TUD model was further developed. In chapters 2, 3, 4 and 5 additional model improvements were proposed. In this chapter, the model is tested once more on several lab-scale SBR experiments. In chapters 3, 4 and 5, the model already was tested at full-scale conditions. The goal of this chapter is to complete the model evaluation and to validate the model for full- and lab-scale conditions. To improve the model applicability, the chapter is concluded by discussing the model limitations. These limitations should be considered when the model is applied. The Final version of the TUD model is presented in appendix III.

6.2 Model Improvements

Temperature dependency. BioP temperature dependency was modelled on the basis of the temp. coeff. measured by Brdjanovic *et al.* (1998a). The missing temperature dependency of glycogen formation, was calculated on the basis of eq. 4.2. In the TUD model, all temperature dependent parameters are marked with a superscript ^{T} (appendix III, tables 6a/b/c). In ASM2d, it is considered that the effect of temperature on PAO's and HMO's is identical. In the TUD model, different temp. dependencies are assumed. With changing temperature, this causes the populations of PAO's and HMO's to shift (chapters 4 and 5). In the TUD model, BioP is more sensitive towards temperature compared to ASM2d. In chapters 4 and 5 temperature effects were measured and simulated for two full-scale WWTP's. Notwithstanding promising simulation results in these studies, the modelled temperature dependency should be further founded by experimental data.

Hydrolysis. The hydrolysis rate in the TUD model is a function of the heterotrophic biomass, being the total of X_H + X_{PAO} (chapter 3). This adaptation was made in accordance with the observation of Goel *et al.* (1998 and 1999) that the hydrolysis rate is associated with the total (active) biomass and not solely with X_H. However hydrolysis was identified as a less reliable model process. This is further discussed in section 6.5.3

Limitation of glycogen formation. A practical adjustment to avoid model instability was the introduction f_{GLYmax} in the kinetic rate for glycogen

formation. The value for full-scale conditions was measured by Brdjanovic *et al.* (2000) (0.5 $gCOD_{GLY} \cdot g^{-1}COD_{PAO}$). Different studies show different values for the maximum glycogen fraction. However, at full scale conditions f_{GLYmax} has a limited impact on the overall simulation results. Kinetic limitation of glycogen formation is further discussed in section 6.6.

Limitation of PP formation. Identical to glycogen formation, PP formation was limited to a maximum fraction. The parameter value of f_{PPmax} for full-scale conditions was measured by Wentzel *et al.* (1989) (0.35 $gP_{PP} \cdot g^{-1}COD_{PAO}$). As for f_{GLYmax}, different studies show different values for f_{PPmax}. However, at full scale conditions f_{PPmax} is mostly determined by influent phosphate concentration (PO_{IN}). Limitation by f_{PPmax} will therefore rarely come in effect.

6.3 Lab-Scale Calibration and Validation

We re-evaluated the TUD model on original SBR experiments by Smolders *et al.* (1994a/b and 1995) and Kuba *et al.* (1995) (fig. 6.1 to 6.3). Hereby, similar problems were observed with the glycogen formation (r_{GLY}), as previously reported by Wichern *et al.* (1999) and Brdjanovic *et al.* (2000) and discussed in chapters 3 and 4. All lab experiments were simulated sufficiently, except the A/O SBR experiment with a SRT of 20 days (fig. 6.7). Here, r_{GLY} was highly overestimated (fig. 6.3), and even became higher than PHA degradation. In the model, this resulted in a net conversion of PAO's into glycogen according to eq. 2.22. Hence, the ammonium content of PAO (iN_{BM}) was released in the bulk liquid. Overestimation of r_{GLY} therefore, resulted in a decreased growth and increased ammonium loading. This effected the simulated OC_{NET}.

On the basis of this experiment, the kinetic rate equation for r_{GLY} were redefined according to eq. 6.1. Hereby "typical" kinetic parameter values were used for K_{PO}, K_{Ac} and $K_{NO,}$ which are expected to belong exclusively to lab-scale conditions (appendix III, table 6c). This is further discussed in section 6.7.2.

$$r_{GLY}^{O} = k_{GLY} \cdot \frac{X_{PHA}}{X_{PAO}} \cdot \left\{ 1 - \frac{X_{GLY}/X_{PAO}}{f_{GLY}^{max}} \right\} \cdot \frac{S_O}{K_O + S_O} \cdot X_{PAO} \cdot \qquad (6.1)$$

Eq. 6.1 and the kinetic parameter values in appendix III, table 6c, resulted in the simulations in fig. 6.5, 6.6 and 6.7. In this equation switch

functions are included for X_{PHA}, X_{PP}, S_{NH} and S_{HCO} with a saturation constant value 0.01. After redefinition of the glycogen kinetics, all experiments were described sufficiently. Moreover, an overall improvement was observed compared to the original model (Murnleitner *et al.*, 1997).

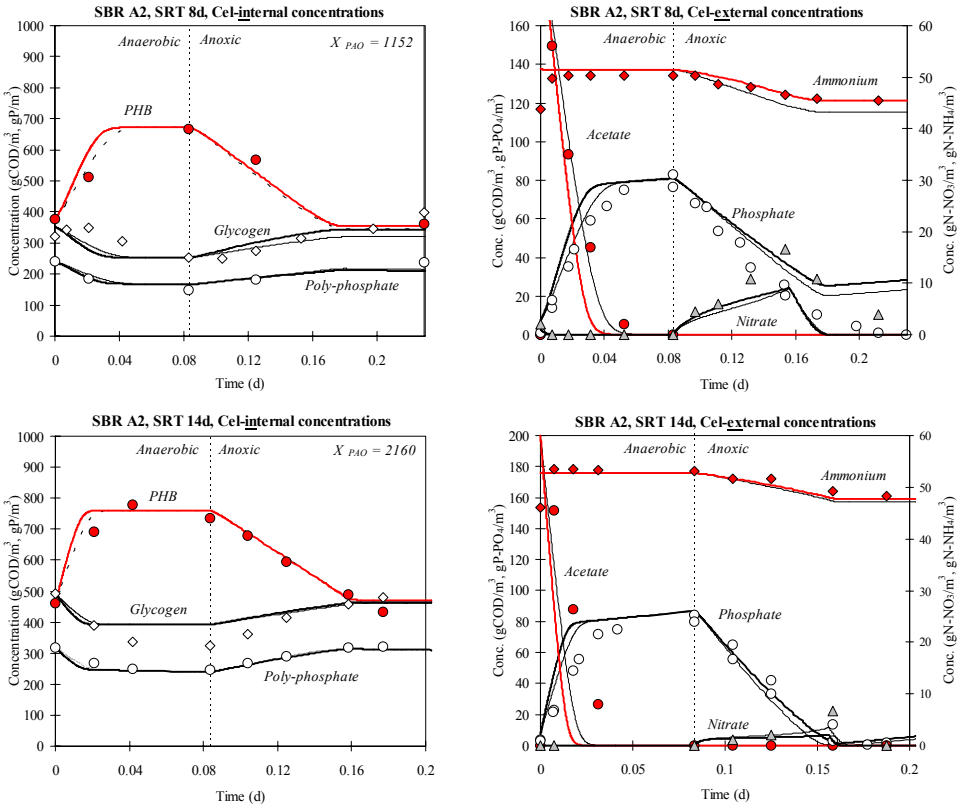

Figure 6.1 A2 SBR experiments by Kuba *et al.* (1996). On the left hand side the cell internal concentrations are shown and on the right, corresponding concentrations in the bulk liquid. In the top experiment the SRT is 8 days, in the bottom 14 days. Thin lines are simulations according to Murnleitner *et al.* (1997). **Bold lines** are the simulations with improved glycogen kinetics.

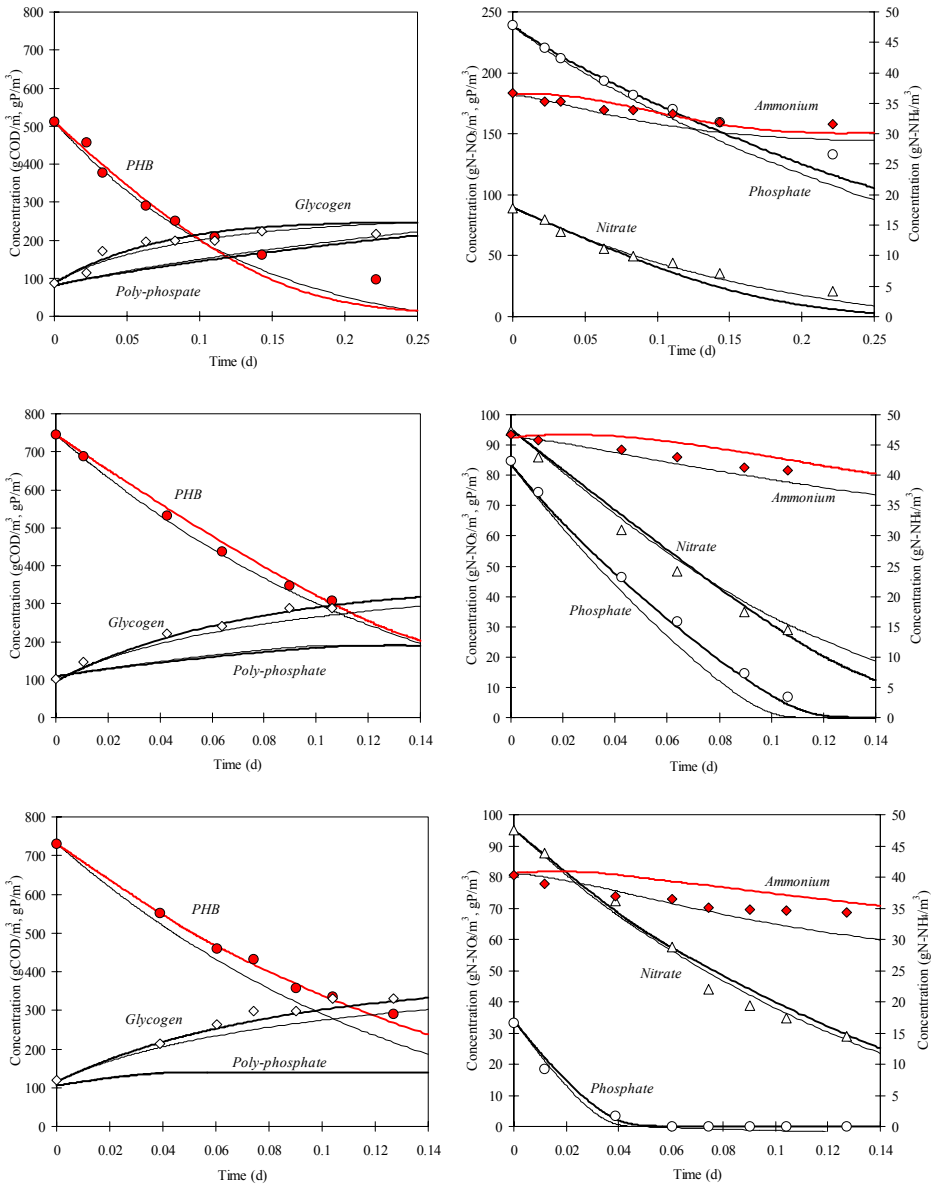

Figure 6.2 **Anoxic batch experiments by Kuba *et al.* (1996).** Cell internal concentrations are shown on the left (PHA, glycogen and PP). The corresponding bulk liquid concentrations are shown on the right (ammonium, nitrate and phosphate). The experiments were performed with decreasing initial phosphate concentrations. Thin lines are simulations according to Murnleitner *et al.* (1997), **Bold lines** are simulations with improved glycogen kinetics.

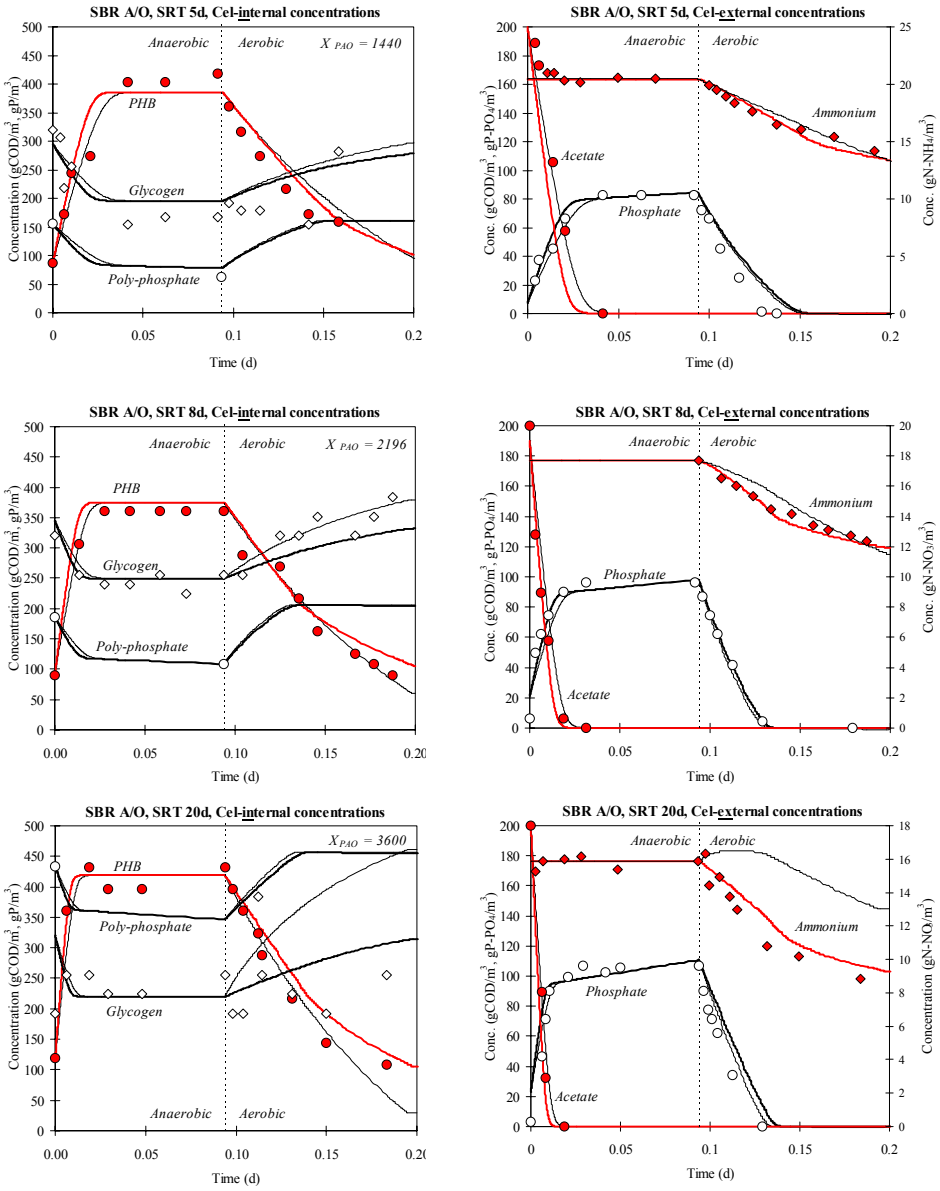

Figure 6.3 **A/O SBR experiments by Smolders *et al.* (1994a/b, 1995b).** Cell internal concentrations are shown on the left (PHA, glycogen and PP). The corresponding bulk liquid concentrations are shown on the right (ammonium, nitrate and phosphate). In the top graphs the SRT is 5 days, in the middle 8 days and in the bottom graphs the SRT is 20 days. Thin lines are simulations according to Murnleitner *et al.* (1997). **Bold lines** are simulations with improved glycogen kinetics.

6.4 Calibration Method

6.4.1 Reconciliation of operational data

Accurate operational data and measurements are a first requirement for a reliable (full-scale) simulation. This was shown chapters 3, 4 and 5 and in previous research by van Veldhuizen *et al.* (1999) and Brdjanovic *et al.* (2000). Therefore, a method for error diagnosis and data reconciliation was developed. The method relies on mass balance calculations and statistical data analysis. The statistical data reconciliation was developed by van der Heijden *et al.* (1994a/b/c) and was made available in the open source software tool 'Macrobal' (Hellinga, 1992). In chapters 3 and 5, the method was tested on two full-scale WWTP's. After evaluation of the input data, the models were fitted without major calibration. Similar experiences were reported by Brdjanovic *et al.* and van Veldhuizen *et al.*.

6.4.2 Calibrating formation of inert material

In chapter 3, it was suggested to calibrate the formation of inert material in the model (X_I and S_I) exclusively based on the influent fractionation. Hereby, the WAS production and effluent S_I concentration are fitted by adjusting respectively the influent ratio's X_I/X and S_I/S_F. Hereby, all errors concerning the influent fractionation and formation of inert material are lumped in the influent. This method showed quick and accurate. However, at the same time it underlines a important limitation of the current activated sludge models, which is the inaptitude of the model to predict the formation of inert matter. This is further discussed in section 6.5.

6.4.3 Calibrating SND

For activated sludge modelling, accurate description of the overall N removal and thereby SND is essential. To accommodate the model to the measured ^{L}DEN, it was proposed to fit ^{L}DEN by adjusting the saturation coefficient for oxygen (K_O, chapter 3). This approach can be interpreted as a black-box model for DO limitation in sludge flocs. Here, K_O is not an intrinsic, but an apparent coefficient, that depends on diffusion gradients in the system. In the TUD model, all saturation coefficients for DO, except for the nitrification process, are replaced by the calibration parameter K_O (0.2 $gO_2 \cdot m^{-3}$). By (upwards) adjusting $K_{O,}$ denitrification in aerobic processes is increased. The need for SND calibration, implies an important model shortcoming. This is further discussed in the next section.

6.5 Model Limitations

6.5.1 Modelling formation of inert material

In general, activated sludge models do not accurately describe the inert COD fractions, i.e. the effluent soluble inert (S_I) and inert particulate activated sludge fraction X_I. This is caused by two model shortcomings; (i) the processes in which S_I and X_I are formed are not well understood and (ii), in the influent characterisation, determination of S_I and X_I is at best an estimate. These problems partly are caused by the definition of inert material as used in current activated sludge models. Nowak *et al.* (1999), showed that the "degree of inertness" of the influent fractions S_I and X_I, is determined by HRT and SRT of the involved WWTP. In time, S_I and X_I will partly degrade. This process is however not taken in account in the model. Inert material is also formed in the activated sludge processes itself. Generally, it is assumed that inert material is dead cell material formed from cell lysis and decay. If the SRT increases, and consequently the biomass growth decreases, cell lysis and decay becomes increasingly important. In other words, the operational conditions strongly influences the model sensitivity for the production of inert material. There are also indications that an important fraction of the biomass can be "dormant", i.e. alive but not active. This dormant fraction is also believed to be influenced by operational conditions like the apparent substrate concentration and the SRT. In activated sludge models no dormant biomass is modelled. Because of these model shortcomings, S_I and X_I require calibration for each simulated system (i.e. operational condition). This should be considered when the model is extrapolated.

6.5.2 Modelling SND

Current activated sludge models do not predict local concentration gradients and diffusion limitations in sludge flocs. Such conditions typically cause SND in aerated reactors (Beccari *et al.*, 1992; Pochana and Keller, 1999a/b). Diffusion limitations in sludge flocs have been related to sludge bulking (Kappeler and Gujer, 1993). Both SND and sludge bulking are important processes in WWTP's. Therefore, better understanding of these processes, would considerably improve the operation of WWTP's.

Pochana and Keller (1999a/b) and Kappeler and Gujer (1993) have proposed different models to describe the diffusion of substrate into sludge flocs. Both models require new assumptions to describe the measurements. In the sludge bulking model of Kappeler and Gujer apparent saturation constants are introduced for bulking and non-bulking micro-organism's. These unknown parameters are a measure for the

diffusion resistance of substrate into sludge flocs and have to be estimated. In the diffusion limitation (SND) model of Pochana and Keller, the (unknown) floc size and density, have to be estimated. As long as these essential data are lacking, such models will not lead to an improvement the model accuracy.

In modelling practice, it is essential to accurately predict SND. All model nitrogen fractions (e.g. S_{NO}, S_{NH}, S_{N2}, iN_{XI}, iN_{XS}, iN_{SF}) are balanced. Therefore, if SND is not simulated correctly also effluent nitrate (NO_{EF}) will be incorrect. In chapter 3 it was therefore suggested fit SND and consequently NO_{EF}, by adjusting the oxygen saturation constant (K_O). This method is a simplified, however effective black box solution to a complicated and not fully understood process. In the TUD model a default value for K_O of 0.2 g $O_2 \cdot m^{-3}$ is proposed according to Henze *et al.* (1999). When K_O is increased, aerobic conversions decrease and simultaneously denitrification increases. If the calibrated value for K_O is high, this could indicate that the anoxic volume of the process is estimated incorrectly, or that in the modelled N balance one or more activated sludge fractions (iN_{XI}, iN_{XS}, iN_{BM}) are estimated incorrectly, as was concluded in chapter 5.

6.5.3 Modelling hydrolysis and fermentation

For reliable simulation of BioP, accurate description of anaerobic substrate (VFA) uptake is vital. Because the exact contribution of anaerobic fermentation and hydrolysis is unknown, the exact VFA uptake can not be determined from measurements. Therefore, in chapter 5, it was proposed to estimate the anaerobic VFA uptake experimentally from the phosphate balance over the anaerobic reactor (eq. 5.2). Based on ^{L}PR and the yield for substrate uptake (Y_{PO}), VFA uptake and PHA formation can be determined. Subsequently, the contribution of anaerobic fermentation and hydrolysis can be estimated from the VFA balance over the anaerobic reactor. In the calibration method it is therefore proposed to fit fermentation and hydrolysis on the basis of these balances.

6.6 Modelling Considerations

6.6.1 Modelling cyclic systems

Despite the kinetic model adjustments, it is shown that the EBPR model still produces (small) errors in the PHA, PP and glycogen concentrations at the end of each simulated cycle (fig. 6.6 and 6.7). Because EBPR is a cyclic process, PHA, PP and glycogen at the end and beginning of each cycle should match (i.e. balance). Miscalculations in the cycle will accumulate in the model. This effect becomes stronger with increasing SRT, as the SRT is

a measure for the number of cycles PAO's encounter before being withdrawn from the system via the WAS. It is our conclusion, that the observations of Brdjanovic *et al.* (2000) were caused by this effect. To simulate a WWTP operated at a SRT of 90 days, they needed to decrease k_{GLY} to a tenth of the default value, which was determined at a SRT of 8 days (Murnleitner *et al.*, 1997). Moreover, in chapter 4 and this study, it was observed that the slightest over- or underestimation of k_{GLY}, resulted in an (unrealistic) accumulation or total depletion of glycogen, which eventually resulted in a total deterioration of PAO's (unpublished results). Therefore it was concluded that this model instability is an intrinsic property of the proposed cyclic kinetic model structure. How this effects the TUD model, is discussed in the following section.

6.6.2 Modelling storage kinetics

It is evident PAO's have a mechanism to balance cell internal storage. We were however, not successful in describing the storage kinetics with the required accuracy. This was mainly because a valid mechanistic description and accurate experimental data were lacking. In line with the metabolic determination of the EBPR yields, it would be possible to relate the kinetic rates of glycogen formation, PP formation and growth of PAO's to the cell internal conversions of ATP and $NADH_2$. Theoretically, this approach could contribute to a better understanding and description of the storage kinetics.

In practice however, accurate determination of glycogen is difficult with existing measurement techniques. f_{GLY} is often overestimated, caused by a general presence of glucose and/or other carbohydrates in micro-organism's (e.g. GAO's). Brdjanovic *et al.* (1998b), therefore developed a bio-essay to determine f_{GLY} in mixed cultures. The accuracy of is method is however not proven in practice. Moreover, it is not suited to measure dynamics conditions. Until reliable data are available on which the model can be validated, precise modelling of glycogen kinetics it is not relevant. Moreover, it was shown that accurate description of glycogen dynamics is not a main requirement for successful application of the model. This especially accounts for simulation of (pseudo) steady state conditions (chapters 3 and 4).

These may seem arguments not to model glycogen at all. There are however two important reasons why glycogen should be included in the model. Firstly, the BioP stoichiometry can only be modelled accurately if all relevant storage compounds are taken in account. This stoichiometry was validated on the basis of the net anaerobic glycogen conversion, which was measured from the relative difference between the anaerobic and aerobic

steady state (fig. 6.1, 6.2 and 6.3). In contrary to absolute glycogen measurements, this can be determined with reasonable accuracy. The validity of this argument is reflected in the solid stoichiometric base of the metabolic BioP model as was reported in previous chapters and studies (Smolders *et al.*, 1994a/b and 1995a; Kuba *et al.*, 1996; Murnleitner *et al.*, 1997; van Veldhuizen *et al.*, 1999; Brdjanovic *et al.*, 2000; Filipe *et al.*, 1999). Secondly, glycogen can potentially become limiting in the EBPR process. The inclusion of glycogen in the model therefore gives the opportunity to (qualitatively) predict such situations (Brdjanovic *et al.*, 1998b).

6.6.3 Kinetic modifications

We recognise the need for a stable and easy applicable model. Therefore a practical modification of the BioP storage kinetics was proposed. Unrealistic accumulation of PP and glycogen was restricted by introducing maximum glycogen (and PP) fractions in the original kinetic expressions (Murnleitner *et al.*, 1997). This approach corresponds to the approach used in ASM2d. Eq. 6.2 shows the restricted rate equation for glycogen formation (appendix III, table 7).

$$r_{GLY}^{O} = k_{GLY} \cdot \frac{X_{PHA}}{X_{GLY}} \cdot \frac{S_O}{K_O + S_O} \cdot X_{PAO} \qquad (6.2)$$

Additionally, eq. 6.2 has model switches for X_{PHA} and f_{GLY} with saturation values of 0.01. Model switches however, only serve the model stability and do not influence the dynamic behaviour of the modelled process rate.

6.6.4 Calibrating the modified storage kinetics

Step 1. Adjustment of k_{GLY}. On the basis of eq. 6.2, it is suggested to fit the steady state glycogen fraction (X_{GLY}/X_{PAO}) by calibrating the maximum glycogen formation rate (k_{GLY}). Theoretically, this is sufficient to simulate EBPR. However, because k_{GLY} is critical in the model, extra measures are needed to stabilise the storage kinetics.

Step 2. Restricting glycogen formation. According to eq. 6.2, glycogen formation stops when f_{GLY} approaches f_{GLYmax}. By limiting the maximum fraction, a "ceiling" is set for the formation of glycogen. The TUD model default value for f_{GLYmax} was measured by Brdjanovic et al. (2000).

Step 3. Forcing glycogen to steady state. By slightly increasing the calibrated value of k_{GLY}, glycogen is forced towards f_{GLYmax} for each simulated cycle. When the maximum fraction is reached, glycogen

formation stops and energy from PHA oxidation is redirected towards growth of PAO's. The increase of k_{GLY} determines the magnitude of the kinetic error that is introduced in the model. However, the larger the increase of k_{GLY}, the faster glycogen reaches steady state. Hereby it should be considered that r_{GLY} never should become higher than r_{PHA}, as this results in a net conversion of PAO's to glycogen, as was observed in fig. 6.7 and discussed in section 6.2.

6.6.5 Sensitivity of the modelled storage kinetics

Practical modifications were proposed to model and calibrate BioP storage kinetics. Hereby, potentially two errors can be made: overestimation of r_{GLY} and incorrect estimation of f_{GLYmax}.

Sensitivity of the maximum glycogen fraction. If, in the second calibration step f_{GLYmax} is overestimated, growth of PAO's is underestimated and visa versa. Hereby, an error is made on the COD balance. However, since the yields of PAO over PHA and glycogen over PHA are very similar ($Y_{O,PHA}$=1.39 $gCOD_{PHA}/gCOD_{PAO}$, $Y_{O,PHA}/Y_{O,GLY}$=1.25 $gCOD_{PHA}/gCOD_{GLY}$), the effect of misinterpretation of f_{GLYmax} on the COD balance is relative small. Therefore also the error in the simulated OC_{NET} and WAS production will be negligible.

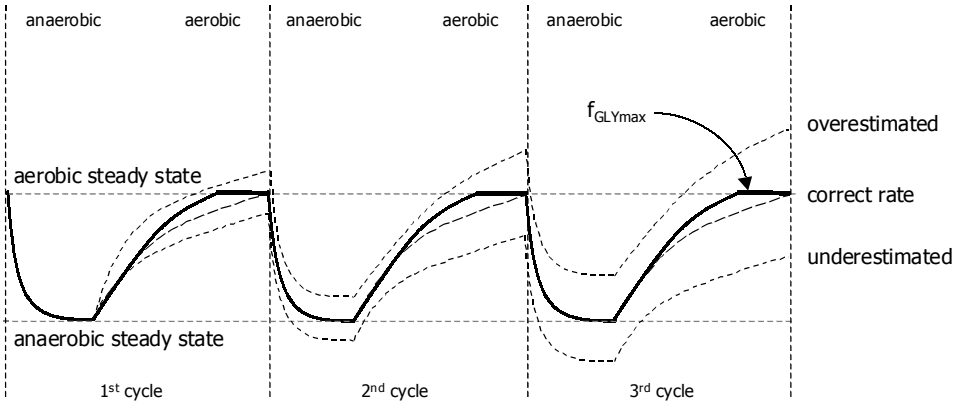

Figure 6.4 **Sensitivity of the modelled cyclic BioP storage kinetics.** Three cycles are shown, each with an anaerobic and aerobic phase. The thin solid line represents the actual dynamics. Dashed lines are the result of a modelled error. This error accumulates for each cycle. Restricting f_{GLY} and overestimating k_{GLY}, results in the **bold** line. This is at the cost of an (non accumulating) error of the dynamics in the aerobic phase.

Sensitivity of the glycogen formation rate. The effect of overestimating k_{GLY} is illustrated in fig. 6.8. Here, anaerobic glycogen consumption is not effected, as this process is stoichiometrically linked the substrate uptake rate (q_{Ac}). Only at the end of the aerobic phase a deviation is observed. Provided that in the simulated WWTP glycogen formation is not kinetically limited, a small overestimation of r_{GLY} in the model does not affect the net glycogen formation. Generally this is the case in full-scale WWTP's were the aerobic phase is designed to accommodate the slower nitrification process.

6.6.6 Including GAO's in the BioP model

Filipe *et al.* (2001a/b), showed that BNR processes often accommodate both PAO's and GAO's. It is suggested that GAO's are out-competed on the basis of the (anaerobic and aerobic) pH. Preliminary results show that increasing pH favours growth of PAO's and contributes to a more stable EBPR process. More insight is however required to establish the precise competition mechanism.

Smolders *et al.* (1994a) and Filipe *et al.* (2001a), observed different yields for anaerobic substrate uptake (Y_{PO}). This difference could be caused by presence of GAO's. However, proper measurements confirming this assumption are lacking. Filipe *et al.* proposed to determine Y_{PO} experimentally. Therefore a batch test with pH control can be used, in which activated sludge is exposed to a pulse of acetate, while measuring the phosphate release (Brdjanovic *et al.*, 1999). From the measured maximum substrate uptake rate q_{Ac} (appendix III, table 6c, Smolders *et al.*, 1994a), also the PAO concentration can be estimated. If a low yield is found in combination with a high PAO concentration, it is likely that other micro-organism's capable of acetate uptake under anaerobic conditions, i.e. GAO's, are present.

If EBPR is negatively affected by presence of GAO's, the metabolic BioP model is inaccurate and therefore GAO's should be modelled. If not, the anaerobic yield for acetate uptake and the PP storage can be calibrated according to the measurements. The model error that is introduced by neglecting GAO's will be small, as the overall stoichiometry of PAO's and GAO's is very similar (Filipe *et al.*, 2001b).

In chapter 4 it was shown that competition between micro-organism's is mainly determined by external factors like temperature and influent variations. In WWTP's, populations therefore generally will not be in steady state. When simulating EBPR systems, it is proposed to estimate the PAO (or GAO) concentration from a batch test, in accordance with Filipe *et al.* (2001b).

6.7 Discussion

6.7.1 A practical approach towards storage kinetics

Generally, modelling research is focussed on improving the performance and broadening the range of application of models. In line with this objective, a kinetic expression for glycogen formation was proposed that was validated for all simulated conditions (eq. 6.1). The introduction of a separate kinetic rate equation specially adapted for full-scale simulations (eq. 6.2), may seem conflicting and therefore undesirable. This research however, clearly showed that glycogen formation kinetics are not properly modelled and understood. The fitted glycogen formation rate (eq. 6.1) in our view suggest an accuracy that can not be met at full-scale conditions. According to the proposed heuristic calibration method (chapter 3), the model was calibrated on the basis of the least reliable processes. For EBPR this was Glycogen formation. Eq. 6.2 is therefore a practical modification which facilitates the calibration and stabilises EBPR dynamics. Previously, it was shown that this simplification is justified, as a result of the strongly reduced sensitivity of the BioP kinetics for most full-scale WWTP's in steady state.

6.7.2 Parameters for full- and lab-scale conditions

The full-scale simulations in the previous chapters were performed with saturation constants for phosphate, nitrate and acetate as proposed in ASM2d (K_{PO}, K_{NO}, K_{Ac} appendix III, table 6b). Smolders *et al.* and Kuba *et al.* showed that for simulation of lab-scale SBR experiments much higher values are required (appendix III, table 6c). Two major differences distinguish full- and lab-scale conditions; (i) the floc size and density and (ii), the bulk concentrations of substrate, DO, nitrate, and phosphate. Under lab-scale SBR conditions, the floc compactness generally is much higher than in most full-scale WWTP's. Moreover, flocs consist almost entirely of PAO's. Therefore, on a lab-scale occurrence of diffusion limitation in flocs is more severe. This results in lower overall conversion rates than expected from the bulk concentrations. In the model, diffusion limitation is expressed in higher saturation constants resulting in the higher values for (K_{PO}, K_{NO} and K_{Ac}). Additionally, slightly different values for q_{Ac} were used to describe A2 and A/O systems (appendix III, table 6c). This was discussed in section 6.6.6. To accommodate both lab- and full-scale conditions, an average value for q_{Ac} was proposed (appendix III, table 6b).

6.8 Conclusions

This and previous lab- and full-scale simulation studies, show that the stoichiometry of the metabolic EBPR model is fully reliable and does not require calibration. This accurate stoichiometry is largely owed to the inclusion of glycogen. With a modified kinetic expression for glycogen formation it showed possible to describe all SBR and batch experiments with a single set of model parameter values (fig. 6.1, 6.2 and 6.3). The parameter values of K_{PO}, K_{NO} and K_{Ac} showed to be different for lab-scale conditions. This is largely explained by operational conditions. Therefore, for these parameters specific lab-scale parameter values were proposed (appendix III, tables 6b and 6c).

A step-wise, balance related model calibration was established to fit the TUD model. It was shown that the method facilitated calibration and improved the model applicability. The method focussed calibration on the least reliable processes, hereby defining the model limitations. An important limitation is the requirement to calibrate the COD, N and P balances for each simulated WWTP.

In previous research problems were reported with the modelled PAO storage kinetics. We concluded that these problems are caused by the cyclic nature of the modelled BioP process. Hereby, repeating simulation cycles cause even the smallest model error to accumulate, resulting in model instability. Practical measures were taken to overcome this modelling problem. Hereby, the model applicability and reliability was improved. It can however be concluded, that the current kinetic model structure is not suited to describe the complex cell-internal mechanism that balances the formation and consumption of PAO storage compounds. More research therefore is needed to determine the precise mechanism. The simplified glycogen formation kinetics however, were sufficient as it was shown in this and previous studies that accurate prediction of glycogen dynamics in full-scale WWTP is often of less interest. Moreover, the sensitivity of the BioP kinetics for most full-scale WWTP's in steady state is strongly reduced.

References

Beccari M, Di Pinto A. C., Ramadori R., Tomei M. C. (1992) Effects of dissolved oxygen and diffusion resistances on nitrification kinetics. *Water. Res.* **26**(8), 1099-1104.

Brdjanovic D., Logemann S., van Loosdrecht M. C. M., Hooijmans C. M., Alaerts G. J. and Heijnen J. J. (1998a) Influence of temperature on biological phosphorus removal: process and ecological studies. *Wat. Res.* **32**(4), 1035-1048.

Brdjanovic D, van Loosdrecht MCM, Hooijmans CM, Alaerts G. J. and Heijnen J. J. (1998b) Bioassay for GLY determination in biological phosphorus removal systems. *Wat. Sci. Tech.* **37**(4-5), 541-547.

Brdjanovic D., van Loosdrecht M. C. M., Hooijmans C. M., Alaerts G. J. and Heijnen J. J. (1999) Innovative methods for sludge characterisation in biological phosphorus removal systems. *Wat. Sci. Tech.* **39**(6), 37-43.

Brdjanovic D., van Loosdrecht M. C. M., Versteeg P., Hooijmans C. M., Alaerts G. J. and Heijnen J. J. (2000) Modeling COD, N and P removal in a full-scale WWTP Haarlem Waarderpolder. *Wat. Res.* **34**(3), 846-858.

Filipe C. D. M. and Daigger G. T. (1999) Evaluation of the capacity of phosphorus-accumulating organisms to use nitrate and oxygen as final electron acceptors: A theoretical study on population dynamics. *Wat. Environ. Res.* **71**(6), 1140-1150.

Filipe C. D. M., Daigger G. T. and Grady C. P. L. (2001a) Stoichiometry and kinetics of acetate uptake under anaerobic conditions by an enriched culture of phosphorus-accumulating organisms at different pHs. *Biotechnol. Bioeng.* **76**(1), 32-43.

Filipe C. D. M., Daigger G. T. and Grady C. P. L. (2001b) pH as a key factor in the competition between GLY-accumulating organisms and phosphorus-accumulating organisms. *Wat. Environ. Res.* **73**(2), 223-232.

Henze M., Gujer W., Mino T., Matsuo T., Wentzel M. C., Marais G. v. R. and van Loosdrecht M. C. M. (1999) Activated Sludge Model No.2d, ASM2d. *Wat. Sci. Tech.* **39**(1), 165-182.

Kappeler J. and Gujer W. (1993) Development of a mathematical model for "aerobic bulking". *Wat. Res.* **28**(2), 303-310.

Kuba T., Wachtmeister A., van Loosdrecht M. C. M. and Heijnen J. J. (1994) Effect of nitrate on phosphorus release in biological phosphorus removal systems. *Wat. Sci. Tech.* **30**(6), 263-269.

Kuba T., Murnleitner E., van Loosdrecht M. C. M. and Heijnen J. J. (1996) A Metabolic Model for Biological Phosphorus Removal by Denitrifying Organisms. *Biotechnol. Bioeng.* **52**(6), 685-695.

Murnleitner E., Kuba T., van Loosdrecht M. C. M. and Heijnen J. J. (1997) An integrated metabolic model for the aerobic and denitrifying biological phosphorous removal. *Biotechnol. Bioeng.* **54**, 434-450.

Nowak O., Svardal K., Franz A. and Kuhn V. (1999b) Degradation of particulate organic matter - A comparison of different model concepts. *Wat. Sci. Tech.* **39**(1), 119-127.

Pochana K., Keller J. and Lant P. (1999a) Model development for simultainious nitrification and denitrification. *Wat. Sci. Tech.* **39(**1), 235–243.

Pochana K. and Keller J. (1999b) Study of factors affecting simultaneous nitrification and denitrification (SND). *Wat. Sci. Tech.* **39(**6), 61–68.

Smolders G. L. F., van der Meij J., van Loosdrecht M. C. M. and Heijnen J. J. (1994a) Model of the anaerobic metabolism of the biological phosphorous removal process: stoichiometry and pH influence. *Biotechnol.Bioeng.* **43**(6), 461-470.

Smolders G. L. F., van der Meij J., van Loosdrecht M. C. M. and Heijnen J. J. (1994b) Stoichiometric model of the aerobic metabolism of the biological phosphorus removal process. *Biotechnol.Bioeng.* **44**(7), 837-848.

Smolders G. L. F., Klop J. M., van Loosdrecht M. C. M. and Heijnen J. J. (1995) A metabolic model for the biological phosphorus removal process: Effect of the sludge retention time. *Biotechnol. Bioeng.* **48**, 222-233.

Van der Heijden R.T.J.M., Heijnen J.J., Hellinga C., Romein B., Luyben K.Ch.A.M. (1994a) Linear constraint relations in biochemical reaction systems: I. Classification of the calculability and the balanceability of conversion rates. *Biotechnol. Bioeng.* **43**, 3-10.

Van der Heijden R.T.J.M., Romein B., Heijnen J.J., Hellinga C., Luyben K.Ch.A.M. (1994b) Linear constraint relations in biochemical reaction systems: II. Diagnosis and estimation of gross errors. *Biotechnol. Bioeng.* **43**, 11-20.

Van der Heijden R.T.J.M., Heijnen J.J., Hellinga C., Romein B., Luyben K.Ch.A.M. (1994c) Linear constraint relations in biochemical reaction systems: III. Sequencial application of data reconciliation for sensitive detection of systematic errors. *Biotechnol. Bioeng.* **43**, 781-791.

Van Veldhuizen H. M., van Loosdrecht M. C. M. and Heijnen J. J. (1999) Modelling biological phosphorus and nitrogen removal in a full scale activated sludge process. *Wat. Res.* **33**(16), 3459-3468.

Wentzel M. C., Dold P. L., Ekama G. A. and Marais G. v. R. (1989a) Enhanced polyphosphate organism cultures in activated sludge. Part III: Kinetic Model. *Water SA*, **15**, 89-102.

Wichern M., Obenaus F. and Rosenwinkel K.-H. (1999) Comparison of the models ASM2d and TU-Delft in simulation praxis, 6. Simba-Anwendertreffen, Magdenburg.

7

ORP Measurements in Activated Sludge; A Literature Review

Introduction of enhanced biological phosphorus removal in conventional COD and nitrogen removing wastewater treatment plants requires specific process design and control to assure process stability. In literature there is a general tendency to more complex control strategies. In practice however, simple controls and control measurements are preferred. A frequently applied control measurement is the Oxidation-Reduction-Potential (ORP). The physical meaning of the ORP measured in activated sludge is however not completely understood. This complicates the determination of appropriate ORP controller set-points. Moreover, drift of ORP measurements in activated sludge is commonly observed. From literature it is concluded that the problems concerning drift and set-point determination are theoretically related, and inherent to ORP measurements in activated sludge. Set-point related ORP control of activated sludge processes therefore is less reliable.

7.1 Introduction

Under operational conditions the performance of WWTP's is largely determined by the applied process control. Especially for a stable BioP process a proper process control is required. In practice, simple controls and control measurements are preferred. Because of it's simplicity, cost effectiveness and 'reliability' the Oxidation-Reduction-Potential (ORP) is a frequently applied control measurement for the control of internal recycle flows, required for BioP. The physical meaning of ORP measurements is however not completely understood. To improve understanding and applicability of ORP measurements, we have reviewed the literature on applications of ORP in activated sludge processes. First the theoretical background is discussed, after handling some common observed practical problems related to ORP measurements. Two major practical problems are discussed: (i) The determination of optimal ORP controller set-points and (ii) the occurrence of electrode potential drift. Where the first often is considered to be a controller optimisation problem, the latter often is indicated as a practical problem related to the implementation and maintenance of ORP-electrodes. It is however shown that both problems are (thermodynamically) related, and typically occur when the ORP is measured in undefined biotic systems (i.e. activated sludge).

7.2 The ORP in Theory

7.2.1 Sequence of redox reactions

In aqueous systems, chemical conversions are determined by the redox (reduction-oxidation) state. In biological active systems (e.g. activated sludge) there is a tendency for high energy yielding conversions to take precedence over less energy yielding conversions. This is translated in a sequence of redox reactions. In the high ORP range, oxidation of organic matter is observed to occur by reduction of O_2. Decreasing ORP is indicative for organic being oxidised with subsequently manganese(IV)oxide (MnO_2), NO_3^-, NO_2 and Fe^{3+} as electron acceptor, followed by fermentation (reduction of organic matter) and reduction of sulphate (SO_4^{2-}) and carbondioxide (HCO_3^-) (Stumm & Morgan, 1984). Since in wastewater treatment plants this sequence can be measured easily, redox potential has been a preferred signal for process control strategies. When controlling WWTP's, generally three redox states are of interest: (i) The aerobic state in which oxygen is the main electron acceptor

(typical ORP value > 0.2 V), (ii) the anaerobic state where organic material (COD) serves as electron acceptor (typical ORP value < -0.05 V) and (iii) an intermediate anoxic state, in which nitrate is the main electron acceptor. Because theoretically the ORP is related to the presence of oxygen and nitrate, it is a potentially useful measurement to detect and control aerobic, anoxic, and anaerobic conditions.

7.2.2 ORP according to the Nernst theory

In general, the redox state is defined as the ability of an aquatic medium to donate or accept electrons or protons. The ORP is the electrical potential measured between a platinum and reference electrode. This potential is induced by the relative easy exchange of electrons and protons at a platinum electrode surface. The measured ORP is determined by the half potential of the platinum intermediated reaction and the half potential of the reference electrode. In theory, the ORP can be calculated according to the Nernst equation (eq. 7.1). Therefore the reaction, concentration of reactants, temperature and pH have to be known.

$$\varepsilon_A = \varepsilon_A^{O'} + 2.3\frac{R \cdot T}{n \cdot F} \cdot \log\left(\frac{[C_{ox}]^{\alpha}}{[C_{red}]^{\gamma}}\right) \text{ for the reaction } \alpha \cdot C_{ox} + n \cdot e \underset{\leftarrow}{\rightarrow} \gamma \cdot C_{red} \qquad (7.1)$$

In eq. 7.1, ε_A is the potential of the half reaction (V), ε^0 the standard electrode potential of the half reaction (V), R the gas constant (8.314 $J \cdot mole^{-1} \cdot K^{-1}$), F the constant of Faraday (96487 $J \cdot V^{-1} \cdot e\text{-}mole^{-1}$) and T the temperature (K). C_{ox} and C_{red} are expressed in molar. The ORP generally is measured with a silver reference electrode (Ag|AgCl, 0.222 V), but also other electrodes, like the calomel electrode are used ($Hg|Hg_2Cl_2$, 0.336 V). In this review, all potentials are relative to the standard hydrogen electrode (0.000 V).

In theory, the ORP for aerobic and anoxic conditions can be calculated, from the oxygen and nitrate half reactions at the electrode surface according to eq. 7.2 and 7.3 (Stumm & Morgan, 1984).

$$\tfrac{1}{4}O_2 + H^+ + e^- \underset{\leftarrow}{\rightarrow} \tfrac{1}{2}H_2O \qquad \varepsilon^{0'} = 0.811 \text{ V} \qquad (7.2)$$

$$\tfrac{1}{5}NO_3^- + \tfrac{6}{5}H^+ + e^- \underset{\leftarrow}{\rightarrow} \tfrac{1}{10}N_2(g) + \tfrac{3}{5}H_2O \qquad \varepsilon^{0'} = 0.746 \text{ V} \qquad (7.3)$$

For pure aquatic systems in thermodynamic equilibrium with pH 7 and T=288 K (15 °C), this yields in the theoretical relations between ORP and dissolved oxygen and nitrate according to eq. 7.4 and 7.5.

$$\mathrm{ORP\ (V)} = 0.348 + 0.0143 \times \log\left(\mathrm{O_2}\right) \tag{7.4}$$

$$\mathrm{ORP\ (V)} = 0.359 + 0.0114 \times \log\left(\mathrm{NO_3^-}\right) \tag{7.5}$$

Here, nitrate is expressed as $gN \cdot m^{-3}$, and oxygen as $gO_2 \cdot m^{-3}$. Eq. 7.4 and 7.5 strongly depend on the pH, as a difference of 0.5 pH units changes the ORP with respectively 0.029 and 0.024V.

7.2.3 Measuring ORP in an undefined aquatic matrix

In aquatic systems with an undefined (chemical and biological) composition, an overall electrode potential is measured. This potential is the net result of all half-reactions of the compounds in the system. When there is no chemical equilibrium, some compounds contribute more to the measured potential then others. This is determined by the "electron exchange density" (e.e.d.), which is a measure for the ease in which electrons exchange at the platinum electrode surface (Bockris and Reddy, 1972). Half reactions with compounds in the gaseous phase generally have a low e.e.d., e.g. nitrate with N_2(g) and oxygen according to eq. 7.2 and 7.3. Heduit *et al.* (1992) and Janssen *et al.* (1998), demonstrated that the e.e.d. is influenced by kinetic rate limitations at platinum electrode surfaces. By polishing and blackening they decreased and increased the electrode surface hereby changing the measured ORP up to 0.350 V. This effect will also occur gradually, certainly in a wastewater environment, leading in the well known potential drift of redox electrodes. Measurements are also influenced by very slow, often mediated conversions of (organic) compounds, which results in an irreversible change of the redox state of the (biotic) medium (Clark, 1960; Stumm & Morgan, 1984).
From the unpredictable nature of ORP measurements in biological aquatic systems, it could be concluded that such measurements are meaningless. Nevertheless, there are multiple studies showing successful application of ORP related control in activated sludge. In multiple studies Simultaneous Nitrification and Denitrification (SND) was controlled on the ORP (de la Ménardiére *et al.*, 1991; Lo *et al.*, 1994; Janssen *et al.*, 1998; Zhao *et al.*, 1999; Fuerhacker *et al.*, 2000). When these studies are compared, different optimal ORP controller set-points are found for similar processes. Where Fuerhacker *et al.* (2000) measured optimal SND in the range of –0.033 to

+0.290 (V), also ranges of +0.200 to +0.400 (V) (de la Ménardiére *et al.*, 1991), +0.250 to +0.350 (V) (Ukita *et al.*, 1990) and +0.040 to +0.180 (V) (Lo *et al.*, 1994) were reported. In the study of Lo *et al.*, biological phosphorus uptake was inhibited at ORP below +0.070 (V).
It is likely these differences were caused by the effects as reported by Heduit *et al.*, Janssen *et al.,* Clark and Stumm & Morgan. The seemingly general occurrence of these kinetic effects, and the low reactivity of oxygen and nitrate at the electrode, in our opinion strongly reduces the reliability of set-point related ORP control. Figure 7.1, is exemplary for the unclear relation between the ORP and the nitrate concentration measured in the activated sludge of WWTP Hardenberg (chapters 3 and 8). The figure shows the theoretical and actual ORP in relation to the measured nitrate concentration (eq. 7.6).

$$ORP_{R3}\ (V) = 0.1098 + 0.0309 \times \log\left(NO_3^-\right) \qquad (7.6)$$

The only similarity is an increased redox potential with increasing nitrate concentration. This makes that qualitatively the redox potential is indicative for the nitrate presence.

7.3 ORP Measurements in Activated Sludge

7.3.1 Relation between ORP and dissolved oxygen

It is generally assumed that under micro-aerophilic conditions the ORP is directly related to the dissolved oxygen. This assumption comes from the observation that the ORP tends to give a strong response to small changes in the dissolved oxygen concentration far below the detection limit of conventional oxygen electrodes (<0.1 $gO_2 \cdot m^{-3}$) (Clark, 1960 and Lie and Welander, 1994). Janssen *et al.* (1998) showed that this assumption does not hold under all circumstances. In an aerated sulphide (HS^-) oxidising system, they measured ORP's below –0.150 V, suggesting that sulphide (ε^0 = -0.140 V) rather then oxygen (ε^0 = 0.811 V) determined the ORP under aerobic conditions. This is caused by the high e.e.d. of sulphide compared to oxygen (Stumm & Morgan, 1984). This observation is supported by Eckert & Truper (1993) who concluded that traces of reductants with high e.e.d. (e.g. HS^- and Fe^{2+}) often determine the measured ORP. Exponential relations between the ORP and dissolved oxygen, as reported by Heduit *et al.* (1992) and Lie and Welander (1994), only hold for an ORP higher then 0.100 V. In this range, trace reductants will mainly be present in oxidised form. Therefore, only under specific conditions that are rarely found in

activated sludge, the measured ORP can be directly related to the nitrate or oxygen concentration.

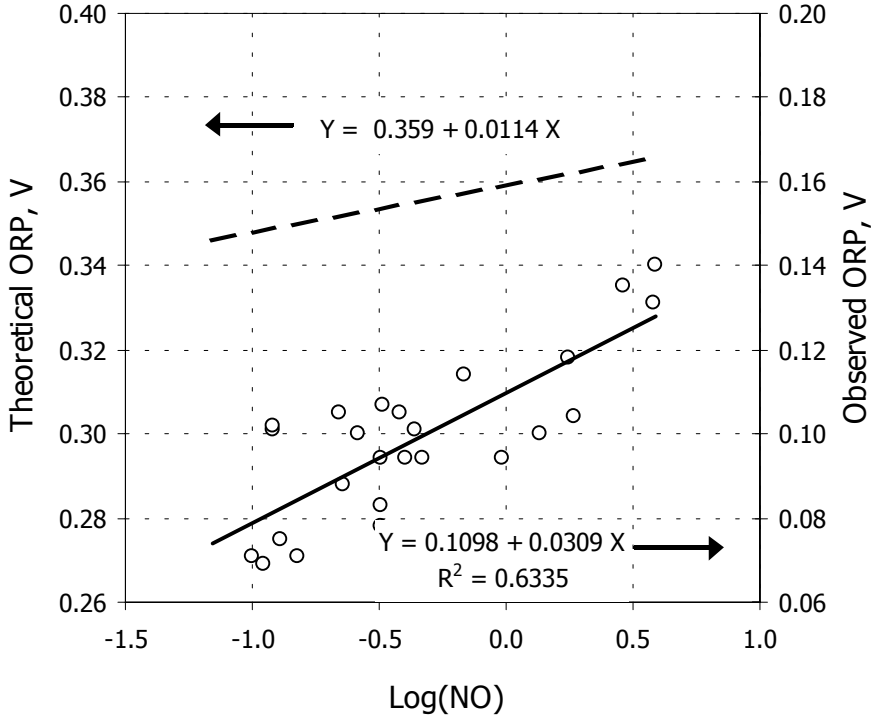

Figure 7.1 Observed and theoretical relation between ORP and NO_3^-. In the fig. nitrate is expressed in $gN \cdot m^{-3}$. On the left y-axis the theoretical relation is plotted according to eq. 7.5 (dashed line). On the right y-axis an observed relation is plotted according to eq. 7.6 (black line).

7.3.2 General relation between ORP and concentration

The conclusion of Eckert & Truper (1993) that traces of reductants rather then the dissolved oxygen or nitrate concentration determines the ORP, is supported by Heduit *et al.* (1992) who, under pH controlled conditions, did not find any effect of nitrate on the ORP measured in a pure abiotic medium. Lie and Welander (1994) even observed an increasing ORP for decreasing nitrate concentrations, totally opposite to the Nernst theory. Heduit *et al.* and Lie and Welander did however find several compounds () with relative high e.e.d. that followed the Nernst theory according to the general eq. 7.7.

$$ORP\ (V) = \alpha + \beta \times \log(C) \qquad (7.7)$$

If in a biotic medium the ORP changes, this results in a shift of the total chemical matrix. Hereby, also compounds with relative low e.e.d. are likely to follow. This results in a general shift of the ORP according to eq. 7.7. This is illustrated in figure 7.2. Here two observed relations are shown between the ORP and phosphate measured in the anaerobic reactor of two EBPR processes. The phosphate concentration in the anaerobic tank is a direct result of phosphate release due to uptake of fermentation products (chapter 2). Whereas under normal conditions phosphate does not relate to the Nernst equation, it is observed that the phosphate concentration follows a general trend according to eq. 7.7. This indicates that an intermediate processes determines the measured redox potential. The shift of the two lines could be caused by drift as well as operational conditions (e.g. supplemental addition of iron). This could however not further be investigated.

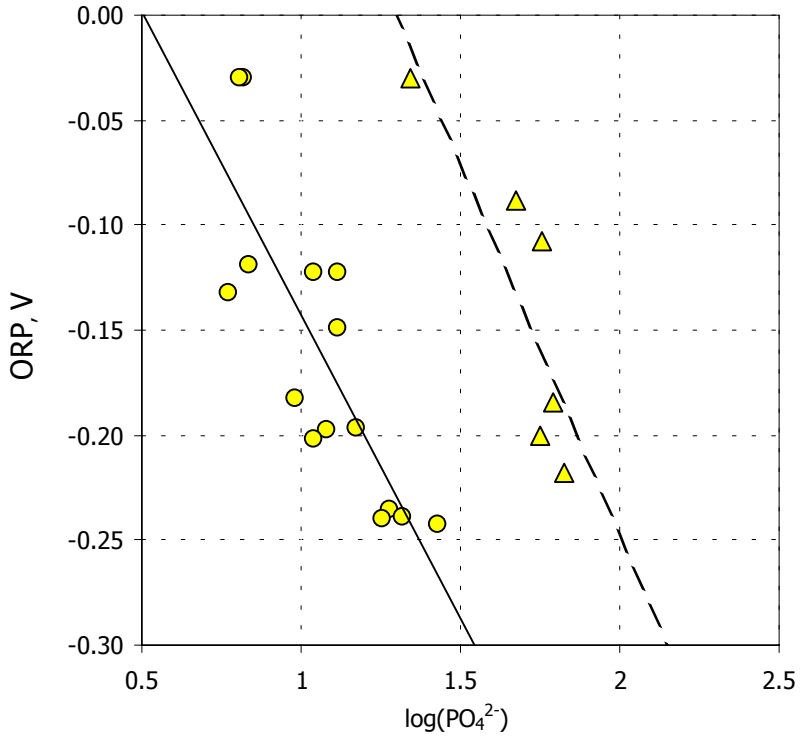

Figure 7.2 Observed relation between ORP and the PO_4^{2-} concentration. Phosphate was measured in $gP \cdot m^{-3}$. Open dots represent measurements in WWTP Hdbg, open diamonds (◇) were measured by de la Ménardiére *et al.* (1991). Both systems could be related according to eq. 7.7 (lines).

In general it is observed that in activated sludge, bulk concentrations and the measured ORP are exponentially related. ORP related control algorithms that include this exponential relation, will therefore have a more gradual and effective control action (Janssen *et al.*, 1998).

7.3.3 Identification of the ORP "braking-point" or "knee"

The characteristic change in slope of the transient ORP profile, commonly referred as the "nitrate braking-point" or "knee", can be used to detect the complete conversion of nitrate. Especially for control of Simultaneous Nitrification and Denitrification in activated sludge processes, ORP braking point detection has shown to be an useful control method (de la Ménardiére *et al.*, 1991; Lo *et al.*, 1994; Brown *et al.*, 1999; Zhao *et al.*, 1999; Fuerhacker *et al.*, 2000). Brown *et al.* (1999) showed that a more accurate detection of the ORP braking-point is achieved on the basis of the first order derivative of the ORP. With ORP braking-point control, complete denitrification has to be achieved for each control-cycle. In contrary to ORP set-point control, braking-point detection is not sensitive for redox-electrode potential drift induced by fouling and interactions with the electrode surface (Clark, 1960; Heduit *et al.*, 1992). The ammonium braking-point, observed when ammonium is completely oxidised, can be accurately observed from the sudden increase in the dissolved oxygen concentration (de la Ménardiére *et al.*, 1991). Using the ORP for this purpose therefore is of less interest.

ORP braking-point control has however two major drawbacks: (i) Braking-point control can only be applied on sequencing batch and pseudo-continuous systems like the Biodenipho process (Arvin *et al.*, 1985), as for continuous systems it leads to strong nitrate and ammonium fluctuations in the effluent and (ii) operating WWTP's at nitrate or oxygen concentrations below the respective saturation constants (i.e. braking-point conditions), causes inefficient use of the system's denitrifying or nitrifying capacity.

7.4 Conclusions

There is an observed exponential relation between the ORP and the bulk concentration of relevant compounds such as oxygen, nitrate or phosphate (the latter only in anaerobic tanks of EBPR plants). Potentially, ORP measurements are therefore useful for process control. However, kinetic effects at the electrode surface cause unpredictable ORP shifts (i.e. electrode potential drift). Moreover, it was concluded that traces of reductants with high e.e.d. (e.g. H_2S and iron) often determine the

measured ORP. These effects, strongly reduce the reliability and accuracy of especially set-point related ORP control. In several studies the first order derivative of the measured ORP, has been used to accurately detect nitrate depletion (ORP braking point detection). In contrary to absolute ORP measurements, braking-point detection does not require set-points and therefore is not sensitive for drift. Braking-point control is however only suited for sequencing batch and pseudo-continuous systems, and causes inefficient use of the system's denitrifying capacity. To control continuos systems using ORP measurements, potentially the first order derivative measurement would be suitable. However a new control strategy should be developed. This is further discussed in the next chapter.

References

Arvin E., Holm-Kristensen G. (1985) Exchange of organics, phosphate and cations between sludge and water in a biological phosphorus and nitrogen removal process. *Wat. Sci. Technol.* **17**(11-12), 147-162.

Baeza J., Gabriel D. and Lafuente J. (1999) Expert supervisory system for a pilot wwtp. *Environmental Modelling and Software* **14**(5), 383-390.

Belanche L., Valdes J. J., Comas J., Roda I. R. and Poch M. (1999) Towards a model of input-output behaviour of wastewater treatment plants using soft computing techniques. *Environmental Modelling and Software* **14**(5), 409-419.

Bockris J. O'M. and Reddy A. K. N. (1972) Modern electrochemistry. Plenum press, New York.

Brown W. A., Cooper D. G., Liss S. N. (1999) Adapting the self-cycling fermentor to anoxic conditions. *Environ. Sci. Technol.* **33**(9), 1458-1463.

Clark W. M. (1960) Oxidation- reduction potentials of organic systems. The Williams & Wilkins company, Baltimore.

De la Ménardiére M., Charpentier J., Vachon A. and Martin G. (1991) ORP as control parameter in a single sludge biological nitrogen and phosphorus removal activated sludge system. *Water SA* **17**(2), 123-132.

Eckert W. and Trüper H. G. (1993) Microbially-related redox changes in a subtropical lake 1. In situ monitoring of the annual redox cycle. *Biogeochem.* **21**, 1-19.

Fuerhacker M., Bauer H., Ellinger R., Sree U., Schmid H., Zibuschka F. and Puxbaum H. (2000) Approach for a novel control strategy for simultaneous nitrification/denitrification in activated sludge reactors. *Water Res.* **34**(9), 2499-2506.

Garcia-Sanz M., Ostolaza J. X. (2000) QFT-control of a biological reactor for simultaneous ammonia and nitrate removal. *System analysis Modelling Simulation* **38**(2), 353-370.

Heduit A. and Thevenot D. R. (1992) Elements in the interpretation of platinum electrode potentials in biological treatment. *Wat. Sci. Technol.* **26**(5-6), 1335-1344.

Janssen A. J. H., Meijer S.C.F., Bontsema J and Lettinga G. (1998) Application of the redox potential for controlling a sulphide oxidising bio-reactor. *Biotechnol. Bioeng.* **60**(2), 147-155.

Lie E. and Welander T. (1994) Influence of dissolved oxygen and oxidation-reduction potential on the denitrification rate of activated sludge. *Wat. Sci. Technol.* **30**(6), 91-100.

Lo C. K., Yu C. W., Tam N. F. Y. and Traynor S. (1994) Enhanced nutrient removal by oxidation-reduction potential (ORP) controlled aeration in a laboratory scale extended aeration treatment system. *Water Res.* **28**(10), 2087-2094.

Menzi S. and Steiner M. (1995) Model-based control for nitrogen-eliminating wastewater treatment plants. IEEE Conference on Control Applications Proceedings 842-847.

Stumm W. and Morgan J. J. (1996) Aquatic chemistry: An introduction emphasising chemical equilibria in natural waters. 3d edition. Wiley, New York.

Wen Ch. H. and Vassiliadis C. A. (1998) Applying hybrid artificial intelligence techniques in wastewater treatment. *Engineering Applications of Artificial Intelligence* **11**(6), 685-705.

Zhao H. Z., Mavinic D. S., Oldham W. K. and Koch F. A. (1999) Controlling factors for simultaneous nitrification and denitrification in a two-stage intermittent aeration process treating domestic sewage. *Water Res.* **33**(4), 961-970.

8

A Case Study; Model Based Process Control Design for Biological Nutrient Removal

In literature, there is a general tendency to complex control strategies for the control of nutrient removing waste water treatment processes. In practice however, simple controls and control measurements are preferred. a relative simple measurement is the oxidation reduction potential (ORP). Previously it was shown that ORP measurements in activated sludge are not reliable. In this chapter this is illustrated in a case study. From this study it was shown that the first order time derivative of the ORP signal can be used to detect depletion and accumulation of oxidative capacity in an activated sludge process. Based on the sign of the first order time derivative of the ORP signal, a feedback control strategy was developed. The control regulated the internal recycle flows of a UCT type WWTP. The performance of this control was first evaluated in a simulation study, after which it was tested at full-scale. As predicted from the simulations, the full-scale control reduced recycle pumping energy without loss of effluent quality.

8.1 Introduction

The introduction of enhanced biological phosphorus removal (EBPR) in conventional COD and N removing wastewater treatment plants (WWTP's) requires a proper process design and reliable control to assure process stability. In literature, there is a general tendency to suggest complex control strategies on the basis of e.g. multi-loop feedback control, fuzzy logic, neural networks, expert systems, real time control or model based control (Menzi *et al.*, 1995; Wen *et al.*, 1998; Baeza *et al.*, 1999; Belanche *et al.*, 1999; Garcia-Sanz *et al.*, 2000). In general these controls rely on multiple (expensive) on-line measurements (e.g. PO_4^{2-}, NO_3^- and NH_4^+). In practice however, often simple controls and measurements are preferred (e.g. Proportional (P) and Proportional-Integral (PI) feedback control and flow and dissolved oxygen (DO) measurements). Because of it's simplicity, cost effectiveness and 'reliability', ORP is a frequently applied control measurement in WWTP's.

As was discussed in chapter 7, ORP measurements in activated sludge are generally not reliable caused by unpredictable electrode potential shifts. This is a problem which arises when the ORP is measured in an undefined biotic matrix (e.g. activated sludge). It was concluded that the time derivative of the ORP signal is not hindered by these effects and therefore could be used to detect accumulation and depletion of oxidative capacity in WWTP's. In this chapter this is illustrated on the basis of a full-scale ORP controlled WWTP. It is concluded that the derivative ORP could be an effective measurement to control recycle rates and reduce pumping energy consumption. Initially, this assumption is tested in a simulation study. A control algorithm is proposed that relies on the first order time derivative of the ORP signal. Eventually, this control is implemented and tested at full-scale.

8.2 Materials and Methods

8.2.1 WWTP Hardenberg

WWTP Hardenberg was a modified UCT (MUCT) -type WWTP (Ekama *et al.*, 1984) according to the BCFS®-design. An elaborate description is found in chapter 3 and in van Loosdrecht *et al.* (1998) and Brandse and de Vries (1998).

WWTP Hardenberg

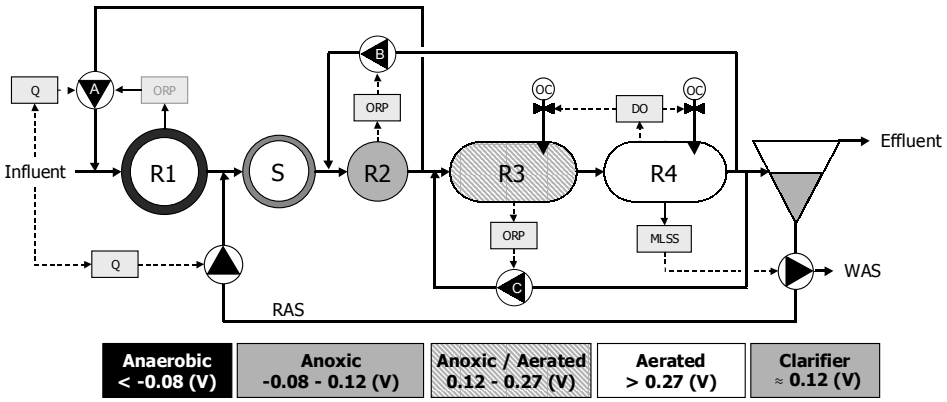

Figure 8.1 **Process control of WWTP Hardenberg.** The grey scales correspond to the redox-states in the legend. **Bold** lines represent the flows, dashed lines the process controls. On-line measurements are printed in boxes; Q_{IN} ($m^3 \cdot d^{-1}$), ORP (V), DO ($gO_2 \cdot m^{-3}$) and MLSS ($g \cdot m^{-3}$). For Q_A, both ORP and influent proportional control was possible. OC_{R3} was activated for $DO_{R4} < 2.5\ gO_2 \cdot m^{-3}$.

Flow	Average. ± s_D $m^3 \cdot d^{-1}$	Process unit	Volume m^3	Depth m	HRT h
Influent, Q_{IN}	6855 ± 2387	Anaerobic reactor, R1	1480	5.0	1.4
Thickener overflow, Q_{OF}	[1]126	Selector reactor, S	740	5.0	0.5
Effluent, Q_{EF}	6738 ± 2516	Pre-anoxic reactor, R2	2290	5.0	0.8
Waste activated sludge, Q_W	243 ± 299	Anoxic/aerobic carousel, R3	4190	2.5	0.9
Recycle A, Q_A	18708 ± 263	Aerated carousel, R4	4190	2.5	0.9
Recycle B, Q_B	35236 ± 334	Clarifiers, CL (2 × 2625 m^3)	5250	-	6.6
Recycle C, Q_C	59174 ± 3021	Total RAS volume	[2]150	-	0.3
Return activated sludge, Q_{RAS}	12126 ± 335				
Internal recycle, Q_{R4IN} and Q_{R3IN}	635040	Total WWTP	18140	-	62.4

Table 8.1 **Measured flows, reactor volumes and depths of the WWTP.** The hydraulic retention time (HRT) of the process units was calculated from the volumes and flows in this table. **[1]** was estimated from grab samples, **[2]** was estimated from denitrification in the return activated sludge (RAS).

The WWTP had an anaerobic reactor with plug-flow characteristics (R1), a selector reactor (S) and anoxic reactor (R2) both completely mixed, followed by two carrousel reactors in line (R3 and R4). Carrousel reactor R3 was alternately aerated, carrousel reactor R4 was continuously aerated. The process contained three recycle flows, Q_A, Q_B and Q_C, and return activated sludge (RAS) from the clarifiers (Q_{RAS}). Q_A, Q_B and Q_C were controlled on three ORP sensors, ORP_{R1}, ORP_{R2} and ORP_{R3} respectively. The lay-out is presented in fig. 8.1. Reactor volumes and operational data are listed in table 8.1. The pseudo steady state (p.s.s.) of the WWPT was recorded during 60-hours (the 23rd to the 25th of June, 1998). Measurements are presented in chapter 3 (tables 3.2 and 3.3).

8.2.2 Process control

Effluent requirements. The WWTP was designed to meet Dutch effluent standards which are; NH_4^+<1 $gN \cdot m^{-3}$, total nitrogen (TN)<10 $gN \cdot m^{-3}$ and total phosphorus (TP)<1 $gP \cdot m^{-3}$.

Control objectives.
Based on these standards, four process requirements were formulated; (i) full nitrification under all circumstances, (ii) a stable P-removal with TP_{EF} < 0.5 $gP \cdot m^{-3}$, (iii) optimal denitrification with TN_{EF} below 10 $gN \cdot m^{-3}$ and (iv) a minimal energy consumption.

These requirements were translated in four control objectives. (1) Maintaining full nitrification by regulating the aeration (OC_{R3} and OC_{R4}). (2) Assuring the anaerobic state in R1 by regulating pump flows Q_A and Q_B. (3) Optimising denitrification in R3 by controlling Q_C. (4) Minimise the energy consumption by regulating OC_{R3}, OC_{R4} and Q_A, Q_B and Q_C.

Controlling nitrification. DO_{R4} was measured on-line and controlled on 2.8 $gO_2 \cdot m^{-3}$ by regulating four surface (brush) aerators. For DO_{R4} < 2.5 $gO_2 \cdot m^{-3}$ (measured 40 meters downstream the second aerator) two surface aerators in R3 were activated. This control was designed to assure full nitrification at influent peak loading.

Controlling the anaerobic state. For a stable EBPR process anaerobic substrate (VFA) uptake by PAO's is essential. VFA uptake is limited in presence of DO and nitrate (i.e. high ORP). In a conventional A/O processes (fig. 1.2), the "anaerobic" reactor R1 is loaded with nitrate from the RAS flow ($^LNO_{RAS}$). This problem is partly solved in the UCT-design, where R1 is loaded with activated sludge from a denitrifying reactor relative low on nitrate. In the UCT-design the anaerobic state is controlled by regulating Q_A. The control span of Q_A is however limited by a minimum

activated sludge concentration in R1 (X_{R1}). In the MUCT and BCFS® design, the anaerobic state is assured by loading R1 with activated sludge from a pre-anoxic reactor (R2). R2 is designed such that the larger part of $^{L}NO_{RAS}$ is denitrified. Hence, nitrate in R2 and the nitrate load from Q_A are constantly low. In the WWTP, X_{R1} was optimised by regulating Q_A, while the anaerobic state in R1 was assured by regulating Q_B. This control provided optimal conditions for growth of PAO's.

Recycle flow control. Q_A, Q_B and Q_C were controlled on the ORP sensors ORP_{R1}, ORP_{R2} and ORP_{R3} respectively (fig. 8.1). The WWTP consisted of 5 reactors in series. Each reactor was operated for a specific redox state. This resulted in sharp gradients of ORP and chemical compounds over the WWTP (chapter 3). Operational experience with three previously built BCFS®-processes (WWTP Holten, 1990; WWTP Genemuiden, 1994 and WWTP Dalfsen, 1996) showed that: (i) Under dry weather influent flow conditions (DWI) the ORP gradient was more or less constant, (ii) a general redox state could be defined for each reactor and (iii) ORP_{R1}, ORP_{R2} and ORP_{R3} were sensitive towards Q_A, Q_B and Q_C, as these flows returned oxidative capacity (i.e. O_2 and NO_3^-). On the basis of these observations, a control-scheme was proposed for WWTP Hardenberg (fig. 8.2) (van Loosdrecht *et al.*, 1998 and Brandse, 2001).

8.2.3 Modelling ORP control

To simulate the process control, the ORP needed to be modelled. From chapter 7, it was concluded that the physical meaning of the ORP measured in activated sludge is unclear. It was also shown, that ORP and the bulk liquid concentration relate according to eq. 7.7. For this study, we fitted the coefficients α and β based on the measured ORP and nitrate concentration at the WWTP Hardenberg. Hereby, it was assumed that nitrate and DO equally contributed to the ORP. This resulted in the empirical relations eq. 8.1 and 8.2.

$$ORP_{R2}\ (V) = 0.026 + 0.045 \times \log(NO_{R2}+DO_{R2}) \qquad (8.1)$$

$$ORP_{R3}\ (V) = 0.066 + 0.045 \times \log(NO_{R3}+DO_{R3}) \qquad (8.2)$$

8.2.4 Simulations

All simulations in this chapter were performed with the validated TUD model (appendix III). For the simulations SIMBA© 3.3+ (Alex *et al.*, 1997) and Matlab/Simulink© 5.2 were used. An elaborate description of the WWTP can be found in chapter 3.

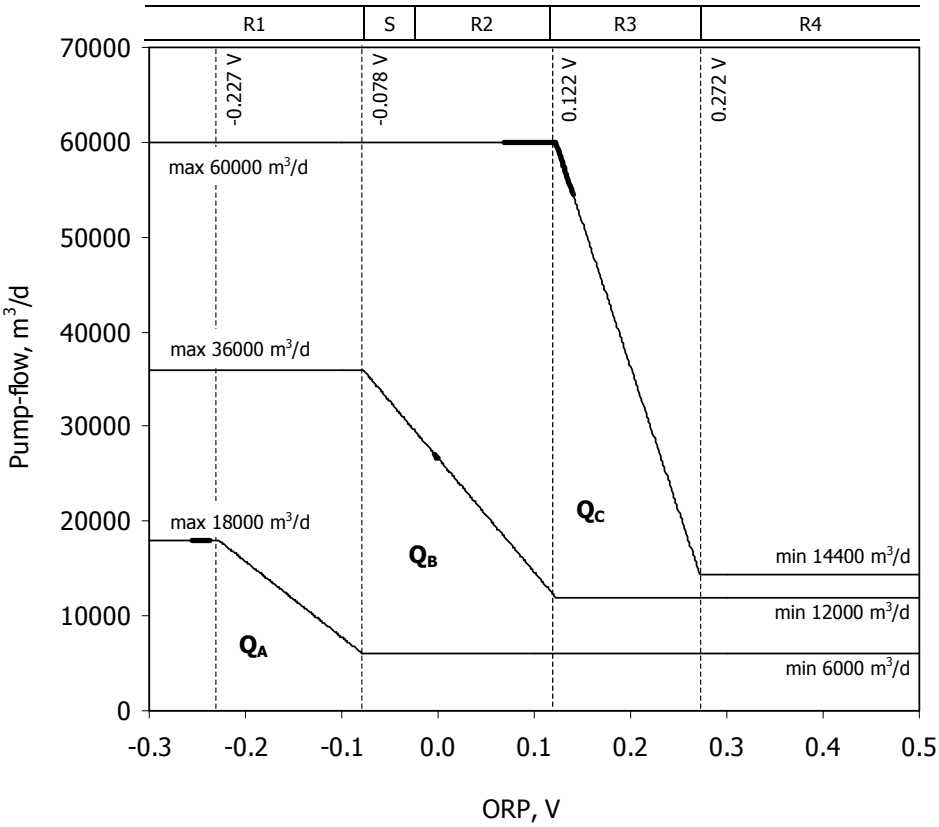

Figure 8.2 ORP control scheme of flow rates Q_A, Q_B and Q_C. The vertical dashed lines separate the ORP ranges (upper x-axes) by which Q_A, Q_B and Q_C are linearly controlled. The **bold** sections of the curves was the measured ORP.

Model adaptations. The internal dynamics of the WWTP were largely determined by the discrete (on-off) control of the aeration of R3 (OC_{R3}). To simulate these dynamics, accurate simulation of the oxygen dynamics in R4 was required. This however, was not achieved. To solve this problem, two model adjustments were made. Firstly the energy input of the aeration of R4 ($^{E}OC_{R4}$) was restricted to a maximum output. Secondly, the on-off control of OC_{R3} was controlled on a threshold of 90 % of this maximum output. This approach proved sufficient to simulate the oxygen dynamics observed in R3.

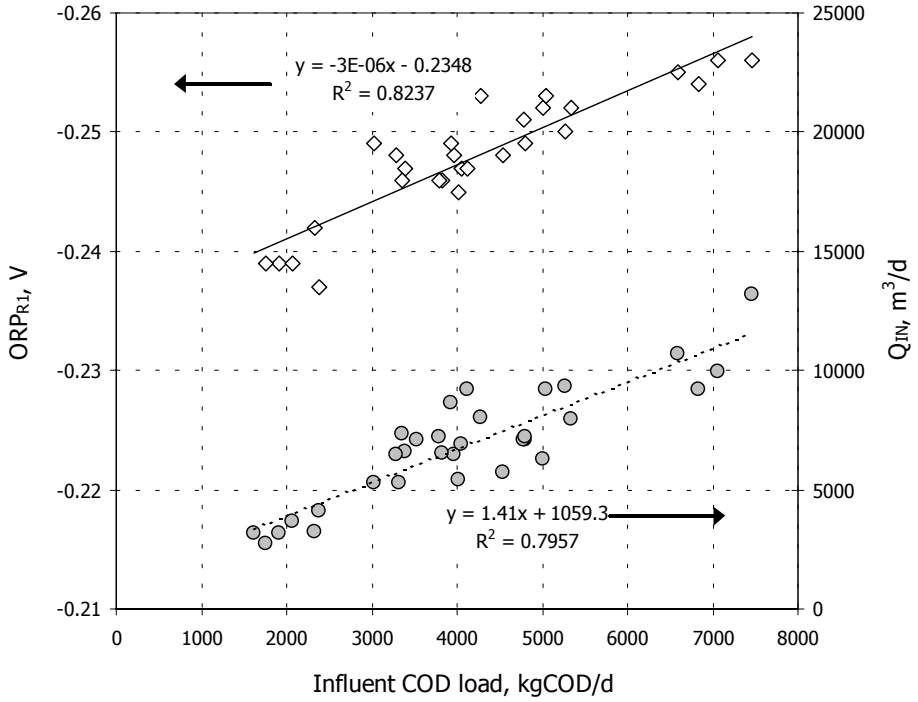

Figure 8.3 **Observed relation between the influent COD load, Q_{IN} and ORP_{R1}.** The left axes shows the relation between ORP_{R1} and the influent COD load, $^{L}COD_{IN}$ (open diamonds ◇). The right axes shows the relation between Q_{IN} and $^{L}COD_{IN}$ (grey dots).

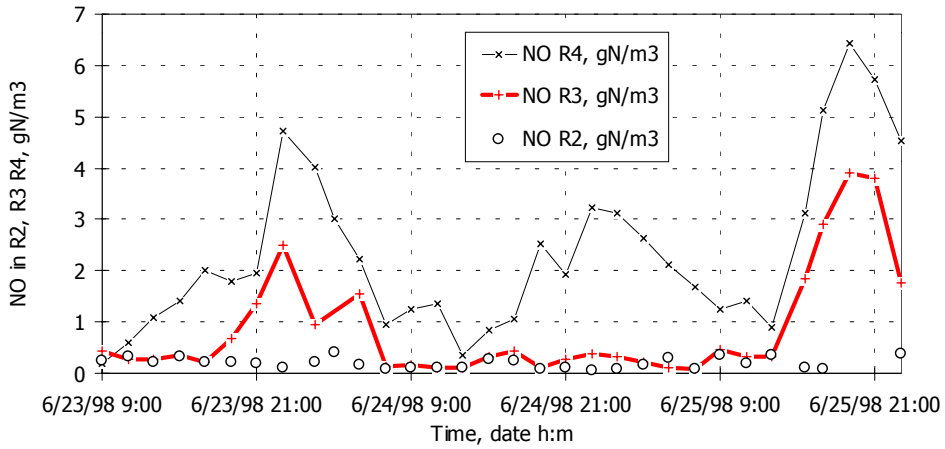

Figure 8.4 **Nitrate profiles in WWTP Hardenberg.** Open dots (o) were measured in R2, the **bold grey line** (+) in R3, and the black line (×) in R4.

8.3 Process Evaluation

Previously it was discussed that ORP set-point control is inaccurate due to unpredictable drift of the ORP signal. In this paragraph, this is illustrated on the basis of an evaluation of the ORP set-point control of WWTP Hardenberg.

8.3.1 Evaluation of control Q_A.

The objective of control of Q_A, was to optimise the activated sludge concentration in the anaerobic reactor (design value X_{R1} = 4 $gCOD_X \cdot m^{-3}$), while minimising the pump flow energy. Originally, Q_A was controlled according to fig. 8.2. This control was formulated on the basis of the observed relation between the ORP and the influent load in fig. 8.3. The measured ORP_{R1} never exceeded –0.227 V, leading in a constantly high flow rate. Q_A was constantly regulated at a maximum rate of 18000 $m^3 \cdot d^{-1}$, resulting in nightly Q_A up to 6 times the influent flow rate. This likely resulted from a drift in the ORP measurement. Neither the second control objective, stabilising EBPR, as the fourth objective, minimising the energy use, were achieved.

8.3.2 Evaluation of control Q_B.

The objective of control Q_B was to supply R2 with nitrate, while maintaining NO_{R2} < 0.5 $gN \cdot m^{-3}$. In the recorded period, the WWTP was under-loaded and therefore also the nitrate loading of R2 was low (fig. 8.4). To fully make use of the denitrification capacity of R2, Q_B was manually set to a maximum flow rate (36000 $m^3 \cdot d^{-1}$). This was mainly caused by the control scheme that was insensitive towards the ORP signal.

8.3.3 Evaluation of control Q_C.

The objective of control Q_C, was to optimise denitrification by regulating flow Q_C, while minimising the energy use. During activation of the aeration in R3 (OC_{R3}), Q_C can be reduced, as DO_{R3} inhibits denitrification. Moreover, under these circumstances nitrate is formed in R3 from nitrification. Fig. 8.5a shows that during ± 65 % of the recorded period, Energy use of Q_C could be reduced. However, during the evaluated period, Q_C was almost constantly at a maximum rate of 60000 $m^3 \cdot d^{-1}$.

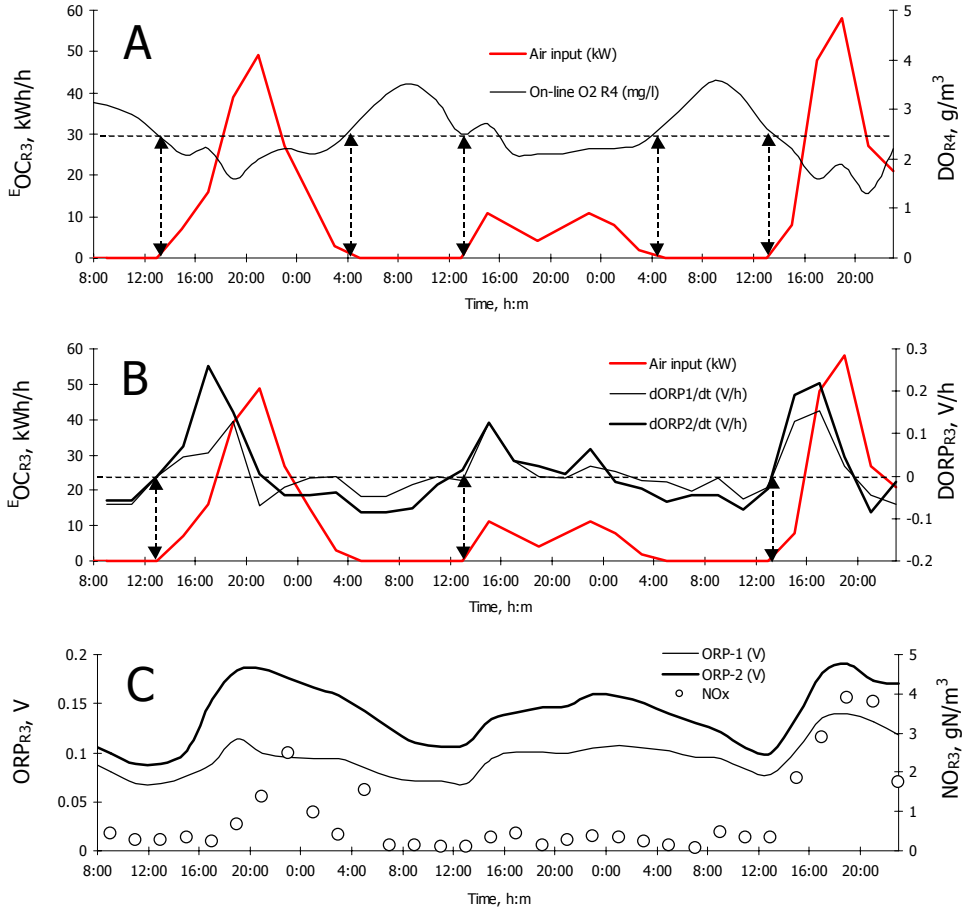

Figure 8.5 **Evaluation of the ORP set-point control.** Fig. A shows OC_{R3} (left axes, **bold grey line**), which is activated for DO_{R4} (right axes, black line) below 2.5 $gO_2 \cdot m^{-3}$ (right axis, dashed line) Vertical arrows indicate OC switching points. Fig. B shows the response of DORP (right axes, solid black lines) on activation of OC_{R3} (left axes, **bold grey line**). Fig. C shows ORP_{R3} (left axes, black lines) and NO_{R3} (right axes, open dots). The two ORP_{R3} measurements are different, caused by electrode potential drift.

Optimal ORP set-points for Q_C. According to fig. 8.2, Q_C was linearly controlled between 0.122 and 0.272 V. Theoretically, Q_C is optimal when nitrate in R3 is approx. 1.5 $gN \cdot m^{-3}$. This optimum is determined by the nitrate saturation concentration for denitrification (0.5 $gN \cdot m^{-3}$, Henze *et al.*, 1999). The ORP signal belonging to this nitrate concentration was estimated from eq. 8.2. This relation is empirical, as it is known that nitrate itself has no or little effect on the measured ORP (Heduit *et al.*, 1992 and Lie and Welander, 1994). From eq. 8.2, the optimal ORP_{R3} threshold was estimated between 0.115 and 0.119 V, (corresponding to NO_{R3} between 1.5 and 2.0 $gN \cdot m^{-3}$). The applied threshold was however 0.122 V (fig. 8.2), which according to eq. 8.2, corresponded to NO_{R3} = 3.2 $gN \cdot m^{-3}$. This shows that the applied ORP control (fig. 8.2) lacks sensitivity towards nitrate as an increase of 1.2 $gN \cdot m^{-3}$ only results in an ORP increase of 0.003 V.

The applied ORP control was insufficient for two reasons. Firstly, it neglected the observed exponential relation between ORP and the bulk liquid concentration (Janssen *et al.*, 1998). Secondly, the ORP set-point control was subject to electrode potential drift. This effect is clearly illustrated in fig. 8.5c. Here two identical ORP_{R3} measurements show a deviation of approximately 0.080 V. On the basis of eq. 8.2, it is obvious that such a potential shift is not acceptable when using set-point related control.

8.4 Alternative Control Strategies

8.4.1 Alternative control measurements

From the previous paragraphs it is apparent that the applied ORP set point control was not functioning properly. Therefore, alternative control strategies should be found. To detect suitable control measurements, the population correlation matrix for the recorded p.s.s. of the WWTP was calculated (table 8.2). The matrix shows all related measurements in the WWTP. In the matrix, 1 is 100 % correlation, correlation's < 0.7 are not shown. The matrix was calculated according to eq. 8.3 (Harnett, 1982).

$$r = \frac{\text{Covariance of x and y}}{(\text{Standard deviation of x})\ (\text{Standard deviation of y})} \qquad (8.3)$$

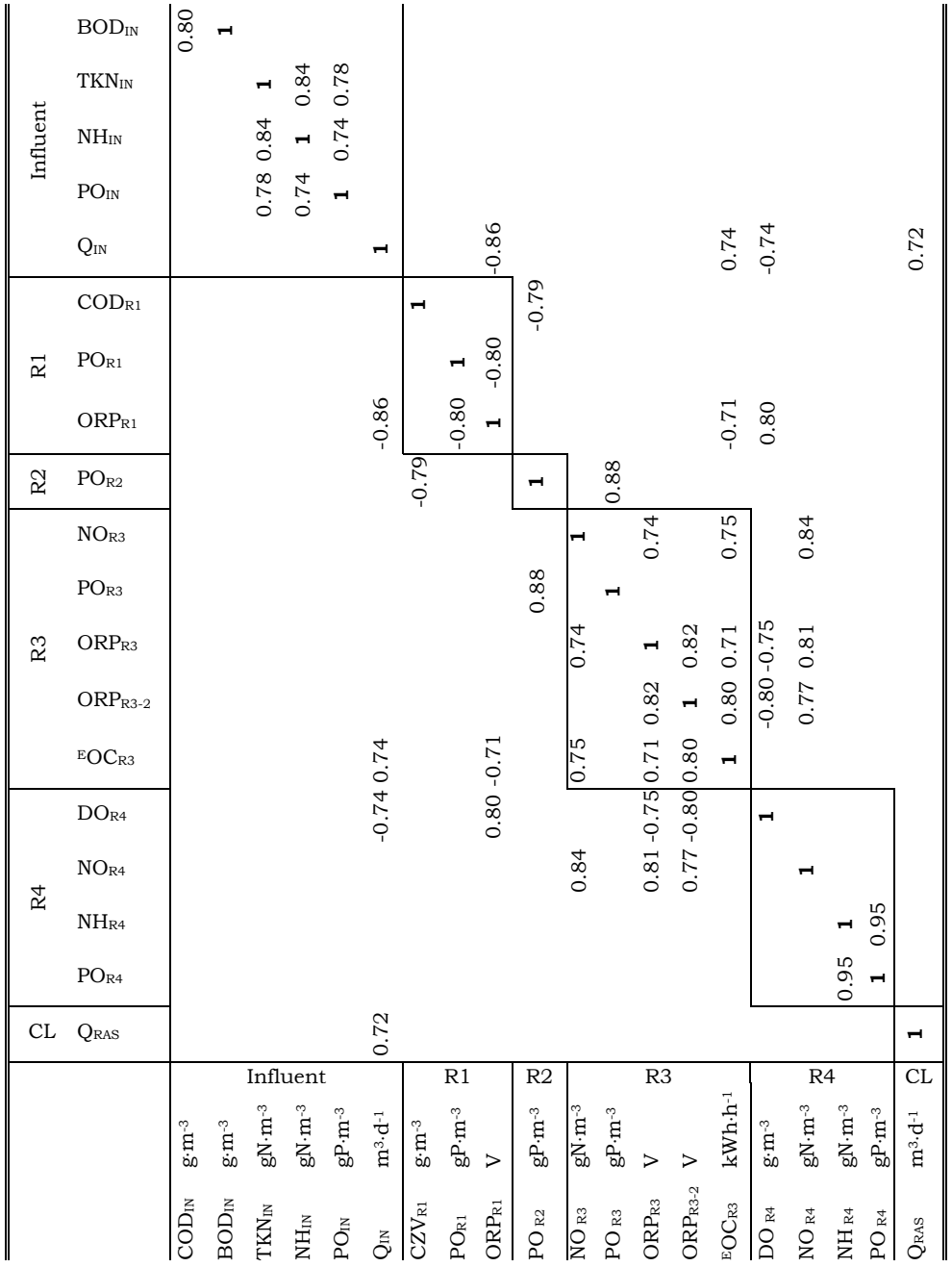

Table 8.2 **Population correlation matrix of all measurements in the WWTP.** Correlation's < 0.7 are not shown, 1 is 100 % correlation. The matrix was calculated according to Harnett, 1982.

In eq. 8.3, x an y represent series of 32 (two-hour average) measurements. The correlation matrix was calculated for 40 data series, of which 20 showed correlation > 0.7. The following was observed:

- The influent flow rate (Q_{IN}) and concentration did not correlate. Dispersion in flat and long sewers and pumping stations, caused the composition to be more or less constant (chapter 3). Consequently, Q_{IN}, the COD load ($^{L}COD_{IN}$) and ammonium load ($^{L}NH_{IN}$) are correlated (fig. 8.3).
- ORP_{R1} was negatively correlated with Q_{IN} and PO_{R1} (fig. 8.3 and 7.3).
- ORP_{R3}, NO_{R3} and OC_{R3} were correlated (fig. 8.5a and 8.5c).
- Control of OC_{R3} caused DO_{R4} to correlate negatively to ORP_{R3} (fig. 8.5a).
- The correlation matrix shows that a wide range of measurements are of potential use for process control. Generally, this is an advantage of compartmentalised WWTP's, over complete mixed processes.

8.4.2 Alternative control of Q_A.

On the basis of the previous observations, an alternative process control is proposed. Table 8.2 and fig. 8.3 show correlation of ORP_{R1}, Q_{IN} and the influent load. We propose to control Q_A proportionally to Q_{IN}. Hereby, Q_A is restricted to 2 times the maximal dry weather influent flow in case of rain weather flow. This simple and reliable control saves energy during low (nightly) influent supply and stabilises the activated sludge concentration in R1 (X_{R1}).

8.4.3 Alternative control of Q_B and Q_C.

In chapter 7 it was concluded that ORP measurements are unreliable caused by electrode potential drift. However, on the basis of the first order time derivative $d\text{ORP}/dt$ (DORP), accurate detection of accumulation and depletion of oxidative capacity in the bulk liquid is possible. Positive DORP indicates oxidative capacity (O_2 or NO_3^-) is consumed faster then supplied. Negative DORP indicates an accumulation of oxidative capacity. Fig. 8.5b shows that DORP is less affected by electrode potential drift. Here, two shifted DORP measurements, responded more or less identical. We therefore developed a control for Q_B and Q_C based on the first order time derivative of the ORP measured in R2 and R3 respectively. This control is further referred to as DORP control.

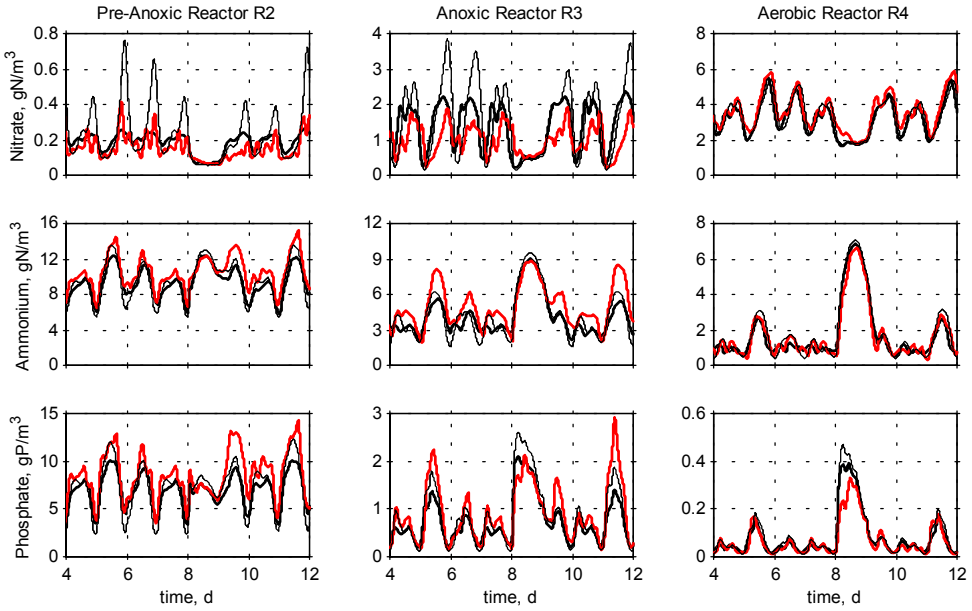

Figure 8.6 Simulation of DORP and PI nitrate control; WWTP performance. Simulation of nitrate (top), ammonium (middle) and phosphate (bottom) in R2 (first column), R3 (second column) and R4 (third column). The **bold black line** represents PI control of NO_{R3} on 2 $gN \cdot m^{-3}$ and NO_{R2} on 0.2 $gN \cdot m^{-3}$. The **bold grey line** represents DORP control. The thin black line is a simulation with constant Q_B and Q_C on respectively 25000 and 31000 $m^3 \cdot d^{-1}$. All simulations were performed with influent proportional control of Q_A.

Development of a DORP control algorithm. Previously the first order time derivative of the ORP signal was identified as an useful control parameter. For effective control of flow rates Q_B and Q_C, a control algorithm was developed. We propose a feedback control that increases the recycle flow rate with quantified steps (K_c m^3/d) for decreasing ORP and visa versa. The controller only uses the sign (positive, negative or zero) of the first order derivative. The control algorithm is shown in eq. 8.4 in it's discrete form.

$$c_n = \frac{K_c}{T} \cdot \left[\frac{\frac{1}{m+1} \cdot \sum_{k=n-m}^{n} \varepsilon_k}{\left| \frac{1}{m+1} \cdot \sum_{k=n-m}^{n} \varepsilon_k \right|} \right] + c_{n-1} \qquad (8.4)$$

T represents the sample interval in n samples per day. The time derivative of the ORP is represented by ε_k (V/d). ε_k theoretically represents the error relative to the controller set-point of zero. In practice however, the set-point will not be reached, caused by the constant distortions of the WWTP. Therefore additionally the control action c_n (m^3/d) was limited by minimal and maximal controller outputs (i.e. minimal and maximal rates of the flows Q_C and Q_B). With the simulated control, small rounding errors caused high frequency noise in the calculated time derivative of the ORP (ε_k). Because this caused control instability, a moving average was used to smoothen this signal. Also in practice application of a moving average showed useful. The moving average is included in the control algorithm in eq. 8.4. To reduce simulation time, the controller output was smoothened. This adjustment was however not required in the practical test. A schematic design of the DORP control algorithm is shown in fig. 8.6.

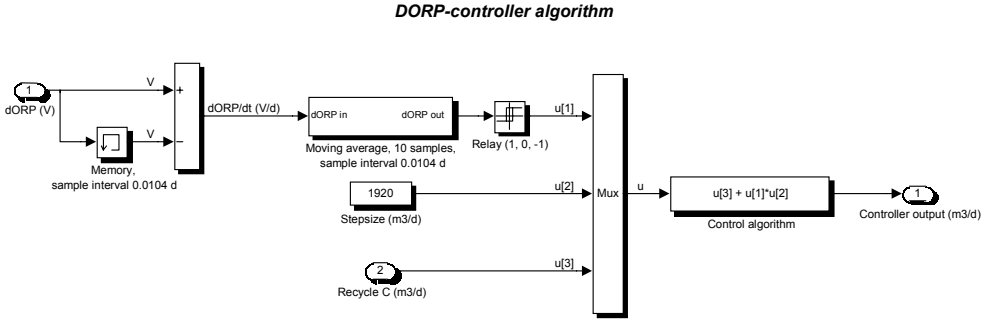

Figure 8.7 The proposed DORP control algorithm. Control parameters are the sample interval (d), step-size ($m^3 \cdot d^{-1}$) and maximum and minimum recycle rates ($m^3 \cdot d^{-1}$). The relay converts DORP to –1, 0 or +1.

Potentially derivative feedback control can cause process instability (Stephanopoulos, 1984). However, in the WWTP there is a strong increasing ORP gradient which is counteracted by the recycle flows. The natural tendency of the process to maintain this ORP gradient, damps the dynamics caused by the control action, and therefore prevents process instability. Theoretically, derivative feedback control will not be able to totally eliminate process disturbances. However, a properly tuned DORP controller should be able to damp a dynamic influent flow (e.g. day and night fluctuations).

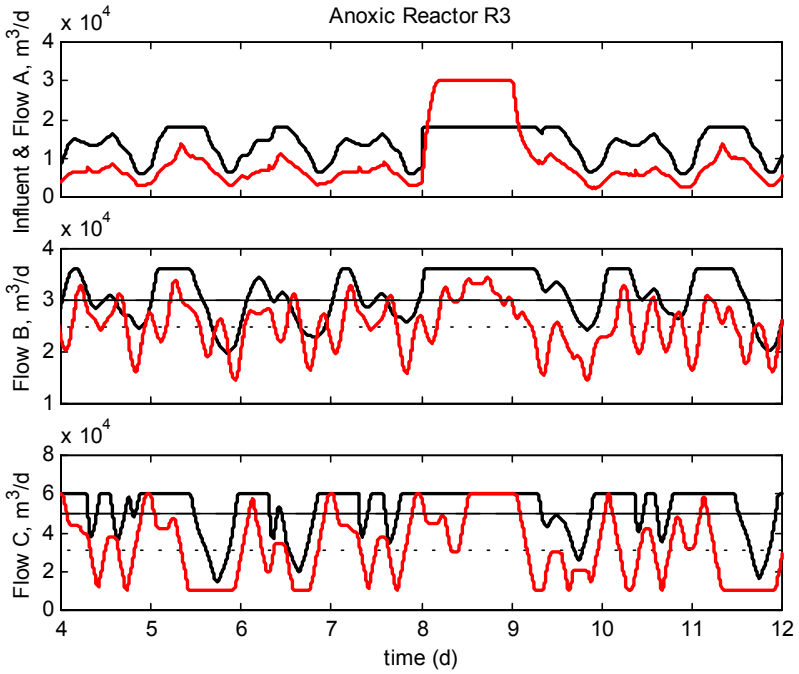

Figure 8.8 **Simulation of PI and DORP control; controller performance.** The top graph shows the Q_{IN} (**bold grey line**) and proportional control of Q_A (**bold black line**). The middle and bottom graphs show PI nitrate (**bold black lines**) and DORP control (**bold grey line**) of Q_B and Q_C. On days 8 and 9 RWI conditions were simulated. For Q_B and Q_C the average of the control outputs is presented as a horizontal lines (PI solid and DORP dashed lines).

8.4.4 Model based control evaluation

The proposed control strategy was evaluated on the basis of a benchmark simulation study. Default conditions were simulated with constant Q_A, Q_B and Q_C according to table 8.1. Two controls were tested; DORP control of Q_B and Q_C and PI nitrate control of Q_B and Q_C. For both simulations influent proportional control of Q_A was applied. PI control theoretically approaches the optimal controlled situation. Hereby, nitrate was controlled on 0.2 and 2 $gN \cdot m^{-3}$ in R2 and R3 respectively.

Simulation conditions. All simulations were performed on the basis of the calibrated simulated pseudo steady state (p.s.s) of WWTP Hardenberg (chapter 3). For 12 days, dry weather conditions were simulated. On days 8 and 9, the performance was tested with rainy weather. Rainy weather influent flow was modelled as 4 times the dry weather influent flow (27200

$m^3 \cdot d^{-1}$), with all concentrations diluted 3 times. This dilution factor was measured at the WWTP.

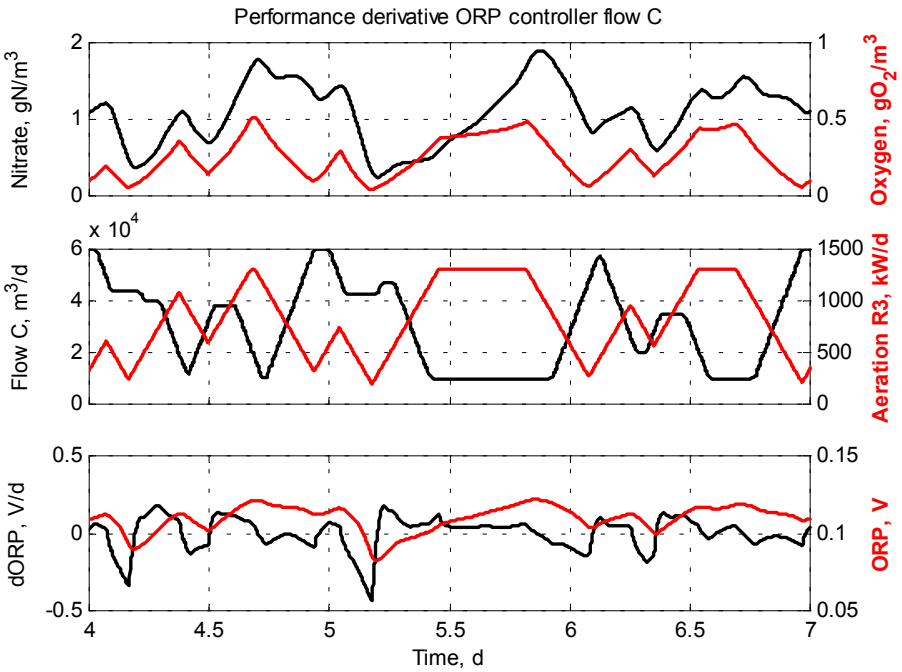

Figure 8.9 **Simulation of DORP control of Q_C.** The **bold** lines correspond to the left axes, **bold grey** lines to the right axes. The top fig. shows NO_{R3} and DO_{R3}. The middle fig. shows Q_C and OC_{R3}. The bottom fig. shows the ORP_{R3} simulated according to eq. 8.2 and $DORP_{R3}$.

Simulation results. The simulation results are presented in fig. 8.7, 8.8 and 8.9. DORP control meets the required control objectives. Fig. 8.7 shows that the effluent quality (i.e. R4) for the three control strategies is similar. Nitrate in R2 is maintained below 0.5 $gN \cdot m^{-3}$ for both PI and DORP control, reaching the second control objective. For the uncontrolled simulation, a serious deterioration of P-removal was predicted Fig. 8.8 shows that DORP control saves approx. 30 and 45 % on energy consumption of pumps B and C.

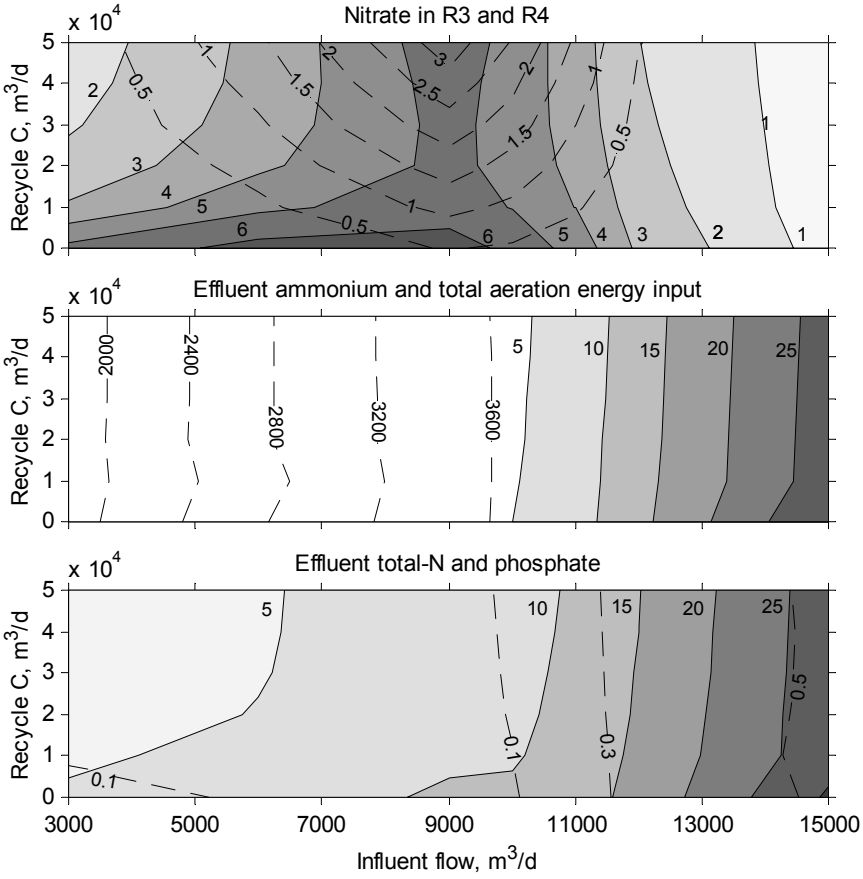

Figure 8.10 Simulated influence of Q_C on the WWTP performance. Grey scales represent nitrate in the aerated reactor R3 (top), ammonium (middle) and the total nitrogen concentration (bottom). Dashed lines represent nitrate in the alternated aerated reactor R3 (top), aeration energy input (middle) and effluent phosphate (bottom).

Controller stability. In a practical test, high-frequency disturbances caused large peaks in the calculated DORP. This resulted in instability of the control. Therefore, the ORP was filtered with a moving average over 40 measurements (sample interval 0.72 minutes). Consequently, a time lag of 0.72×40=28.8 minutes was introduced. Potentially this can cause process instability (Stephanopoulos, 1984). However, by defining minimum and maximum controller outputs (Q_B, 12000 to 36000 and Q_C, 10000 to 60000

$m^3 \cdot d^{-1}$, fig. 8.2) and choosing appropriate controller gains (fig. 8.6), it was possible to control the ORP in a relative small range (fig. 8.9).

8.4.5 Impact of Q_C on the WWTP performance

Before DORP control of Q_C was implemented at full-scale, the possible impact on the plant performance was evaluated based on a series of steady state simulations. In total 48 simulations were performed, in which Q_C was varied between 0 and 50000 $m^3 \cdot d^{-1}$ and Q_{IN} between 3000 and 15000 $m^3 \cdot d^{-1}$. During the simulations aeration in R3 was adjusted to accommodate full nitrification. The result of the simulations is shown in the contour plots in fig. 8.10. Grey scales represent nitrate in R4 (top), effluent ammonium (middle) and effluent total nitrogen (bottom). For Q_{IN} > 9000 $m^3 \cdot d^{-1}$, the maximum aeration capacity is reached (3700 $kWh \cdot d^{-1}$). This causes the contour lines to become more or less vertical, indicating that under these conditions effluent quality is mainly determined by Q_{IN} (i.e. the influent ammonium and COD load). The figure also shows that for Q_{IN} < 9000 $m^3 \cdot d^{-1}$, the net denitrification can be optimised by increasing Q_C. Generally, it can be concluded that control of Q_C should optimise denitrification in R3 under dry weather conditions, whereas under rainy weather conditions the control should restrict the energy consumption of Q_C (^EQ_C). Fig. 8.10 shows that the general sensitivity towards Q_C is low. However, poor control of Q_C can lead to an increase of nitrate in the effluent up to 5 $gN \cdot m^{-3}$. Theoretically the optimal control of Q_C should follow the contour line of nitrate in R3 at 1.5 $gN \cdot m^{-3}$ (fig. 8.10, top graph, dashed lines).

Potentially on-off control of the aeration in R3 produces more nitrate then can be supplied by Q_C. Fig. 8.10 (top graph, dashed lines) shows that the optimum for Q_C decreases when Q_{IN} increases. This is mainly caused by increasing aeration of R3. The less efficient recycle of nitrate with Q_C is however favoured over alternated aeration. Firstly, aeration causes inhibition of denitrification in R3. Secondly, aeration causes oxidation of COD which therefore is no longer available denitrification.

8.4.6 Full scale implementation of DORP control

On the basis of the promising simulations, the control scheme was tested at full-scale on WWTP Hardenberg. During a two week period, the controller was fine-tuned by adjusting the sample interval (0.0104 d) and the control output step size (1920 $m^3 \cdot d^{-1}$). The performance of DORP control was recorded during the 20th to the 23rd of December 2001. In the third day, a rain event occurred starting on the 21st of December on 22:00 h. The results of this test are shown in fig. 8.11. Table 8.3 shows the plant efficiency before and after implementation of DORP control.

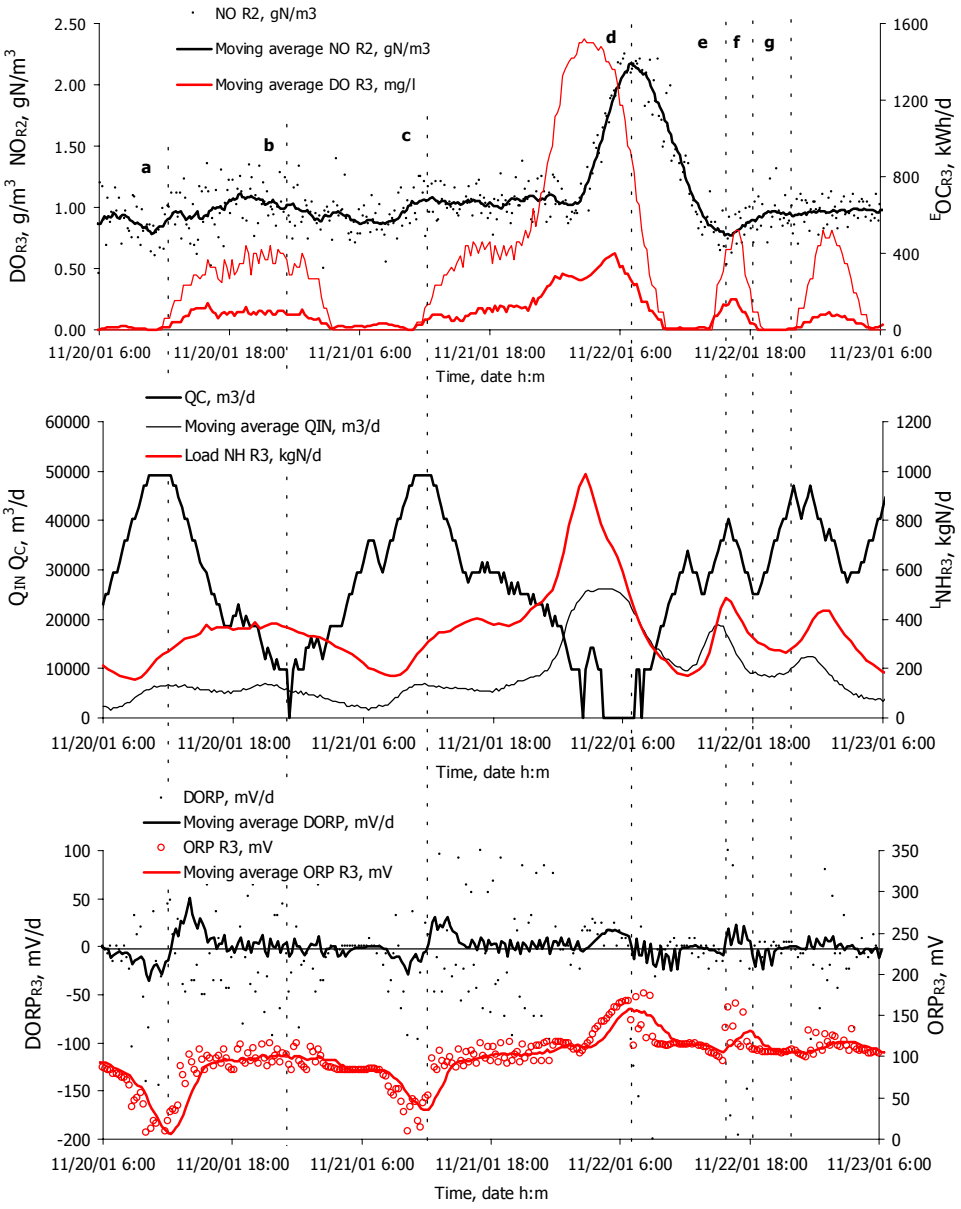

Figure 8.11 Full-scale test of DORP control of flow Q_C. 7 periods a to g are distinguished. On top, the aeration energy input ${}^{E}OC_{R3}$ (kWh·d^{-1}), oxygen in R_3 (DO_{R3}, g·m^{-3}) and nitrate in R_2 (NO_{R2}, gN·m^{-3}) is shown. In the middle the ammonium load in the influent (${}^{L}NH_{IN}$, kgN·d^{-1}), Q_{IN} and Q_C (m^3·d^{-1}) are shown. In the bottom ORP_{R3} (mV) and the DORP (mV·d^{-1}) are shown.

Dry weather performance. The dry weather performance of DORP control was evaluated based on periods a to d (fig. 8.11). In periods a and c, Q_C was increased as a result of decreasing ORP. This was associated with, (i) a decreased influent COD load (i.e. Q_{IN}), (ii) decreasing ammonium load ($^LNH_{IN}$), (iii) shutting–down aeration in R3 and (iv) decreasing nitrate in R3 (NO_{R3}) by decreasing nitrification and increasing denitrification in R3. In periods b and d, Q_C was decreased as a result of increasing ORP_{R3}. This was associated with (i) an increasing influent COD load, (ii) increasing $^LNH_{IN}$, (iii) activation of the aeration and (iv) increasing NO_{R3} caused by increasing nitrification and decreasing denitrification. Table 8.3 shows that the overall plant performance did not change with introduction of DORP control. However, the energy use of recycle C was reduced with approx. 50 % compared to the reference situation.

1 of 2					WWTP efficiency				
		Rainfall	Q_{IN}	Q_C	COD	BOD	TKN	TP	TSS
		mm	$m^3 \cdot d^{-1}$	$m^3 \cdot d^{-1}$			%		
06/11/01	Reference	3	5524	59174	94.4	99.3	97.6	95.1	98.4
13/11/01	Reference	9	6727		92.2	98.4	95.7	83.8	97.3
20/11/01	DORP	0	5242	[1]29496	92.7	99.1	96.9	93.3	98.0
21/11/01	DORP	0.1	4929		91.6	99.0	95.2	n.d.	96.7
22/11/01	DORP	10	14748	n.d.	92.8	98.9	95.0	n.d.	98.6

2 of 2	Effluent loads								
	$^LCOD_{EF}$	$^LBOD_{EF}$	$^LTKN_{EF}$	$^LNH_{EF}$	$^LNO_{EF}$	$^LTN_{EF}$	$^LTP_{EF}$	$^LPO_{EF}$	$^LMLSS_{EF}$
	kgCOD·	kgCOD·	$kgN \cdot d^{-1}$	$kgN \cdot d^{-1}$	$kgN \cdot d^{-1}$	$kgN \cdot d^{-1}$	$kgP \cdot d^{-1}$	$kgP \cdot d^{-1}$	$kg \cdot d^{-1}$
06/11/01	221	11	12	0.7	16	28	3	1.7	28
13/11/01	262	20	18	1.6	27	45	7	6.3	40
20/11/01	278	16	14	0.5	17	31	4	1.9	26
21/11/01	281	15	20	0.5	16	36	n.d.	2.3	44
22/11/01	767	44	49	6	68	117	n.d.	11.8	74

Table 8.3 Effect of DORP control on Q_C. On 6 and 13 November the plant was operated with ORP set-point control. On 20 to 22 November Q_C was controlled with DORP control. On 22 November a rain event occurred. [1] average value over 20 and 21 November 2001.

Rainy weather performance. The third day of the test period, a rain event occurred (fig. 8.11, periods *d* to *g*). In periods *d* and *f*, Q_C was decreased as result of increasing ORP_{R3}. This was associated with (i) an increased influent load (i.e. Q_{IN}), (ii) increasing $^LNH_{IN}$, (iii) activation of the aeration in R3 and (iv) increase of nitrate in R3 caused by increasing nitrification and

decreasing denitrification. In periods *e* and *g*, Q_C was increased as result of decreasing ORP_{R3}. This was associated with (i) a diluted influent, (ii) decreasing $^{L}NH_{IN}$, (iii) shutting–down of the aeration and (iv) decrease of NO_{R3} caused by decreasing nitrification and increasing denitrification. From the effluent loads in table 8.3 it can be calculated that the process meets the requirement of full nitrification and denitrification under rainy weather conditions (NH_{EF} 0.4 $gN \cdot m^{-3}$, TN_{EF} 7.9 $gN \cdot m^{-3}$).

8.5 Discussion

8.5.1 Evaluation of the BNR performance

Fig. 8.10 (middle graph, dashed lines) shows that nitrification is limited by the maximum oxygen input in R3 and R4 ($kgO_2 \cdot d^{-1}$). The net oxygen input ($^{E}OC_{NET}$) was modelled according to the original plant design on a maximum of 3700 $kWh \cdot d^{-1}$ (6 surface aerators). With an estimate alpha-factor of 0.65, an efficiency is calculated of 1.89 kgO_2/kWh. For Q_{IN} > 7000 $m^3 \cdot d^{-1}$, the maximum ammonium loading of the WWTP was reached. Hereby NH_{EF} exceeded 1 $gN \cdot m^{-3}$ caused by a limited aeration capacity. For Q_{IN} >10000 $m^3 \cdot d^{-1}$, effluent nitrate exceeded 10 $gN \cdot m^{-3}$ due to limited denitrification capacity. P-removal was not negatively influenced by increasing influent loading. Effluent phosphate only exceeded the limit of 0.5 $gP \cdot m^{-3}$ for an influent flow approx. twice the designed flow rate (14000 $m^3 \cdot d^{-1}$), which illustrates the excellent BioP capacity of the BCFS®-design.

8.5.2 Controlling BNR

The correlation matrix in table 8.2, shows that there are multiple possibilities to control MUCT-type WWTP's. We propose a control based on Q_{IN}, DO_{R4}, ORP_{R2} and ORP_{R3}. These measurements are all proven in practice, cheap, low on maintenance and reliable. The applied algorithms rely on continuos single loop feedback P-, PI- and DORP control. All used controls are relative simple in operation and application. The success of this approach, largely is determined by the WWTP plug-flow characteristics. The strong natural ORP gradient over the WWTP stabilised the control actions. In large extent, the designed configuration, volumes, and recycle rates determined the effluent quality. The process control merely optimised the near optimal operational conditions, in particular the energy use of the WWTP.

8.5.3 Modelling the ORP

ORP was modelled on the basis of observed relations between ORP and the total of the nitrate and oxygen concentration (eq. 8.1 and 8.2). These empirical relations are different for each specific situation, due to by undefined changes in the chemical matrix of the activated sludge (e.g. by dosage of $FeCl_3$). For accurate simulation of the ORP, eq. 8.1 and 8.2 are insufficient. There are however, several arguments that justify our approach.

In this study, precise estimation of α (eq. 7.7) is of less interest, as the absolute value of the ORP does not influence the first order derivative. The value of β (eq. 7.7) mainly determines the dynamics of the simulated (derivative) ORP. The DORP control algorithm (eq. 8.4) however, only uses the sign (+1, 0, –1), and not the absolute value of the derivative. This reduces the sensitivity of β. Moreover, in practice this approach causes DORP to be less sensitive towards changing electrode dynamics caused by e.g. augmentation of the ORP electrode.

8.5.4 Evaluation of the control strategy

Controller stability. Fig. 8.7, 8.8 and 8.9 show the simulated performance of PI and DORP control. DORP control is stable, however more dynamic then PI control (fig. 10, middle and bottom graph). Additional stability of DORP control is provided by restriction of the controller output. On the basis of fig. 8.10 (top graph, dashed lines), Q_C was restricted to a minimum of 10000 $m^3 \cdot d^{-1}$. The maximum was 60000 $m^3 \cdot d^{-1}$. However, for Q_{IN} < 6000 $m^3 \cdot d^{-1}$, this flow rate was to small to optimise denitrification in R3. For control of Q_B, simulation showed that the average nitrate concentration in R2 was mainly determined by the maximum rate of Q_B. This flow rate was chosen on the basis of the designed volume of R2 and the activated sludge concentration in the WWTP. Additionally, the total daily controller output was limited to 3 times the maximum of Q_C (60000 $m^3 \cdot d^{-1}$), by choice of the step-size and sample time according to eq. 8.5.

$$\text{total daily controller output} = \frac{\text{step-size } (m^3/d)}{\text{sample-time (d)}} = \frac{1920}{0.0104} = 1.8\times10^5 \ \frac{m^3/d}{d} \qquad (8.5)$$

In the simulations the total daily controller output could be increased to 8 times the maximum of Q_C, without losing stability. Hereby, the controller dynamics increased, resulting in a higher average control output. This did

not improve the performance of the WWTP, but increased the energy consumption with approx. 20 %.

Controller performance. Fig. 8.7 shows that all simulated scenario's result in similar phosphate and nitrogen removal. Because the WWTP was low loaded, the performance was near optimal. Without recycle control, the second control objective, maintaining NO_{R2} < 0.5 $gN \cdot m^{-3}$, is not reached (fig. 8.7). This is expressed in a decreased PAO concentration and potential lower P-removal capacity. If under uncontrolled circumstances (i.e. the current situation at the WWTP) the influent loading is increased, the model predicts complete deterioration of BioP, caused by distortion of the anaerobic state of R1. In a recent evaluation of the uncontrolled WWTP, deterioration of the P-removal capacity was actually observed. Simulations show that control of Q_B based on DORP is a good alternative for PI control, as both result in a stable EBPR.

Energy savings. Fig. 8.8 and 8.9 show that DORP control of Q_C reduces pump energy with approx. 50 % (30 $kWh \cdot d^{-1}$). This was mainly accomplished by decreasing Q_C while aeration of R3 was activated (fig. 8.9, middle graph). High DO_{R3} inhibits denitrification, which makes recycling of nitrate unnecessary. PI control however, maintains NO_{R3} continuously on 2 $gN \cdot m^{-3}$, also when the aeration is activated. Compared to DORP control, this leads to a 66 % higher flow rate of Q_C (fig. 8.8), without improving effluent quality. The energy saving of approx. 20 % (50 $kWh \cdot d^{-1}$) on Q_B with DORP control was an additional effect, as the primary objective was to maintain a stable P-removal process (i.e. nitrate in R2 < 0.5 $gN \cdot m^{-3}$).

DORP versus PI control. In a benchmark study, DORP was compared to PI control. It was assumed that PI control approached optimal process conditions. In practice however, measuring the ORP has several advantages over analytical on-line measurement of nitrate: (i) it was shown that DORP control reduces the energy use in respect to PI control, (ii) ORP measurements are simple, reliable and low on maintenance, (iii) on-line nitrate measurement equipment is expensive with high operating costs and (iv), it is questionable if measurement of NO_{R2} below 0.5 $gN \cdot m^{-3}$, as required for control of Q_B, is reliable. Since this study showed that PI and DORP control result in similar WWTP performance, DORP control was preferred.

8.5.5 Model based control design

DORP control was developed, evaluated and implemented at full-scale, fully relying on model predictions. The simulated controller dynamics, control parameters, WWTP performance and energy savings, all were

validated in practice. As predicted by the model, full-scale DORP control was stable. Initially, the controller was operated with a step-size of 1920 $m^3 \cdot d^{-1}$ and a sample-time of 0.0104 d. These parameters were in accordance with the simulation. The energy saving of 50 % on Q_C was predicted by the model. Also the controller dynamics were largely in accordance with the measurements. The main observed difference between the measured controller output (fig. 8.11, middle graph) and the simulated output (fig. 8.8 and 8.9), was largely caused by smoothening the pumping flow rate in the model, by means of a moving average. This was done to reduce model calculation time. From these results, we conclude that our approach towards modelling the ORP was justified. While it is our general opinion that quantitative model predictions are not fully reliable. This study shows that modelling can be a powerful tool for process optimisation and controller design, provided a properly calibrated model is used.

8.6 Conclusions

Previously it was concluded that ORP set-point control is inaccurate due to unpredictable electrode potential drift. This was illustrated in a case study of a full-scale WWTP with ORP set-point control. A statistical evaluation of the WWTP performance, showed that the first order time derivative of the ORP signal was suitable for control of the internal recycle flows. In a simulation study this was confirmed. Similar performance was observed for derivative ORP control and control based on on-line nitrate measurements. The derivative control however is far more simple. Moreover, in practice it is more reliable and cheaper in implementation and operation. On the basis of hereof a control scheme was proposed for UCT-type WWTP's, based on measurements of the influent flow, oxygen concentration and the ORP. The applied control algorithms relied on continuos single loop feedback proportional control. The controls are relative simple in operation and cheap in application. The success of this approach, largely is determined by the UCT process and it's plug-flow characteristics. The controls merely optimised the operational conditions. Hereby especially the BioP process stability was improved and the energy consumption of the recycle flows decreased.

The proposed derivative ORP control was developed, evaluated and implemented at full-scale, fully relying on model simulations. The simulated controller dynamics, control parameters, WWTP performance and energy savings all were validated in practice. This shows that, provided a properly calibrated model is used, modelling can be a powerful tool for process optimisation and controller design.

References

Alex J., Tschepetzki R. and Bitter U. (1997) SIMBA Simulation of biological waste water treatment. Users manual, Institute of Automation and Communication e. V., Magdeburg.

Baeza J., Gabriel D. and Lafuente J. (1999) Expert supervisory system for a pilot WWTP. *Environmental Modelling and Software* **14**(5), 383-390.

Belanche L., Valdes J. J., Comas J., Roda I. R. and Poch M. (1999) Towards a model of input-output behaviour of wastewater treatment plants using soft computing techniques. *Environmental Modelling and Software* **14**(5), 409-419.

Brandse F. A. and de Vries A. C. (1998) Werkwijze voor het zuiveren van afvalwater. Dutch patent, 1003711, 17p.

Brandse F. A. personal communication (2001)

Ekama G. A., Marais G. v. R., Siebritz I. P. (1984) Biological excess phosphorus removal. Theory, design and operation of nutrient removal activated sludge processes, Water Research Commission, Pretoria, South Africa, 7, 1-32.

Garcia-Sanz M., Ostolaza J. X. (2000) QFT-control of a biological reactor for simultaneous ammonia and nitrate removal. *System analysis Modelling Simulation* **38**(2), 353-370.

Henze M., Gujer W., Mino T., Matsuo T., Wentzel M. C. and Marais GvR. and van Loosdrecht M. C. M. (1999) Activated Sludge Model No. 2d, ASM2d. *Wat. Sci. Technol.* **39**(1), 165-182.

Harnett D. L. (1982) Statistical methods. Addison-Wesley Publishing Company, Reading Massachusetts.

Heduit A. and Thevenot D. R. (1992) Elements in the interpretation of platinum electrode potentials in biological treatment. *Wat. Sci. Technol.* **26**(5-6), 1335-1344.

Janssen A. J. H., Meijer S.C.F., Bontsema J and Lettinga G. (1998) Application of the redox potential for controlling a sulphide oxidising bio-reactor. *Biotechnol. Bioeng.* **60**(2), 147-155.

Lie E. and Welander T. (1994) Influence of dissolved oxygen and oxidation-reduction potential on the denitrification rate of activated sludge. *Wat. Sci. Technol.* **30**(6), 91-100.

Meijer S. C. F., van Loosdrecht M. C. M. and Heijnen J. J. (2001) Metabolic modelling of full-scale enhanced biological phosphorus removing WWTP's. *Water Res.* **35**(11), 2711-2723.

Menzi S. and Steiner M. (1995) Model-based control for nitrogen-eliminating wastewater treatment plants. IEEE Conference on Control Applications Proceedings 842-847.

Stephanopoulos G. (1984) Chemical process control: An introduction to theory and practice. Prentice-Hall, Inc., Englewood Cliffs, New Jersey (696p.)

Van Loosdrecht M.C.M., Brandse F.A. and de Vries A.C. (1998) Upgrading of wastewater treatment processes for integrated nutrient removal – The BCFS®-process. *Wat. Sci. Technol.*. **37**(9), 209-217.

Van Veldhuizen H. M., van Loosdrecht M. C.M. and Heijnen J. J. (1999) Modelling biological phosphorus and nitrogen removal in a full scale activated sludge process. *Water Res.* **33**(16), 3459-3468.

Wen Ch. H. and Vassiliadis C. A. (1998) Applying hybrid artificial intelligence techniques in wastewater treatment. *Engineering Applications of Artificial Intelligence* **11**(6), 685-705.

9

Conclusions and Outlook

9.1 Conclusions

9.1.1 Model validation

Based on this and previous research it was concluded that the stoichiometric basis of the metabolic BioP model is reliable. The model was extrapolated from a lab-scale development to full-scale conditions without calibration of the stoichiometric parameters. The high accuracy of the BioP stoichiometry was largely owed to the metabolic modelling approach. In this approach all relevant storage polymers (PP, PHA and glycogen) are included. Model sensitivity analysis showed that the stoichiometry was sensitive under all conditions. Accurate determination therefore was possible. At (pseudo) steady state conditions however, it was observed that the model sensitivity towards the modelled kinetics was low. Calibration of the model kinetics under these conditions therefore is inaccurate. During simulation of a start-up of a full-scale wastewater treatment process, a strong increase of the modelled kinetics was observed. From this study, it was possible to accurately calibrate of the BioP storage kinetics. Also the temperature dependency of the BioP process could be validated accurately in the start-up simulation. Problems with the glycogen storage kinetics, as reported in several previous publications were solved by adjusting of the glycogen formation kinetics.

In the here presented research, the model was tested on four full-scale wastewater treatment processes including a full-scale start-up of a nutrient removing wastewater treatment plant. For all simulations only minor model calibrations were required to simulate effluent and process internal concentrations correctly. Using the same model, eight lab-scale experiments were described with a single parameter value set. Therefore it can be concluded that the TUD model is validated for full and lab-scale conditions.

9.1.2 Glycogen kinetics

In previous research problems were reported with the modelled PAO storage kinetics. It is concluded that these problems are caused by the cyclic nature of the BioP process and how this is translated in the model. If a cyclic system is not accurately balanced, model errors will accumulate, eventually resulting in model instability. Practical measures were taken to overcome this modelling problem. This improved the model reliability and applicability. It is however concluded, that the current kinetic model structure is not suited to describe the complex cell-internal mechanism that balances the formation and consumption of cell-internal storage compounds. More research is needed to determine this mechanism. From

the model evaluation it is however concluded that the current (glycogen formation) kinetics are sufficient to simulate most full-scale wastewater treatment processes. Firstly, it was shown that accurate prediction of glycogen dynamics in full-scale wastewater treatment processes is of less interest. Moreover, the model sensitivity of the BioP kinetics for most full-scale (pseudo) steady state conditions is low.

9.1.3 Data evaluation

Operational data, in particular the sludge retention time, largely determined the model simulations. A high model sensitivity towards operational data (e.g. process flows and volumes) and input data (e.g. the simulated influent) was observed. In practice however, these data often contain (gross) errors. After a proper data evaluation and error correction, all simulated full-scale wastewater treatment plants could be simulated without major model calibration. It is therefore concluded that evaluation of operational data should is important. If the operational data can not be properly determined, calibration of this data should be considered in favour of calibration of the model parameters.

Data evaluation based on linear conservation relations, gave insight in the performance of the investigated wastewater treatment plant. Important operational conditions like the sludge retention time, the conversion of COD, nitrification and denitrification rates, the oxygen consumption etc., could be determined. In the full-scale plant evaluation studies, this information showed highly useful for process optimisation purposes.

With the help of balancing methods, errors in several full-scale operational data sets could be detected and corrected. For this purpose the software tool Macrobal was introduced. Firstly, the use of Macrobal facilitated the organisation of raw plant data, giving insight in the data and the required measurements for a proper plant evaluation. Macrobal also effectively detected gross and statistical errors in the evaluated data sets. Finally, it was shown that with the help of Macrobal data sets can be reconciled. Hereby all measurements in the data set are balanced. Calibrating a model on balanced data showed to be accurate and effective. It is concluded that a data evaluation and balancing procedure increases the model reliability. Moreover, a proper data evaluation prevents that the model is wrongfully fitted on faulty data.

9.1.4 Model calibration

A step-wise calibration method was developed, that strongly relied on the mass balances calculated in the data evaluation procedure. To fit the balances in the model, calibration parameters were selected from the least

reliable processes in the model. From the model evaluation it was concluded that these processes were the formation of inert material, simultaneous nitrification and denitrification, fermentation, anaerobic hydrolysis, and glycogen formation. By selecting all calibration parameters from these specific processes, the model uncertainty was largely lumped in these processes. This resulted in a better definition of the model uncertainty, which on it's turn increased the model applicability and thereby, reliability. The calibration method was tested on two full-scale wastewater treatment processes. The method showed to be quick and straightforward. Calibration iteration loops could be minimised. The operational conditions that were calculated from the data evaluation procedure were useful a final check on the calibrated model.

9.1.5 Model based process control design

With renewed insights in data evaluation, model calibration and model accuracy, the model was extrapolated and used for dynamic process control design. For wastewater treatment processes often simple controls and measurements are preferred. Therefore, the oxidation-reduction- or redox-potential is a frequently applied control measurement. It was however shown, that redox-measurements in activated sludge are not reliable. From literature it was concluded that this is caused by kinetically induced drift of the redox-signal as a result of the specific conditions in activated sludge. Set-point related redox-control therefore is not reliable. On the basis thereof, a new control strategy was developed that relied on the first order time derivative of the redox-signal. Based on the derivative redox-signal accumulation and depletion of oxidative capacity (i.e. oxygen and nitrate) in activated sludge can be detected. The derivative signal is however is less affected by drift then absolute redox-measurements.

Based on these conclusions a control strategy was developed in which the internal recycle flows of a nutrient removing wastewater treatment plant are controlled based on the first order time derivative redox-signal. This strategy was evaluated in a full-scale case study. Firstly the control was simulated. The simulations showed that the proposed control matched on-line nitrate control. Hereafter the derivative redox-control was implemented and tested at a full-scale wastewater treatment plant. The implementation fully relied on the simulated control parameters and dynamics. During three months the control was tested. Only minor control adjustments were required. The measurements and simulations showed similar trends. As was predicted in the simulation study, energy consumption of the main recycle was reduced with 50% without effecting the effluent quality.

It is the authors belief that quantitatively, the model extrapolating is not fully reliable. However, the study showed that modelling is a powerful tool for process optimisation and control design, provided that the operational data is properly evaluated, the model is properly calibrated and the model uncertainties are defined and well-understood. It is hereby emphasised that testing new control concepts in a dynamic simulation environment, is the closest to reality after reality itself. Moreover, dynamic simulation facilitates quick model development and evaluation, for a fraction of the costs and with minimal risk.

9.2 Outlook

This research has shown that the kinetic model structure that describes the cell-internal storage mechanism of BioP organisms is not sufficient. Further research would be needed to elucidate and model the mechanism in which BioP organisms balance their cell-internal storage. From a theoretical point of view, this could be interesting. In practice however, further refining the glycogen kinetics would not contribute much to the full-scale performance of the model, since it was shown that the effect of glycogen on the overall wastewater treatment process is small.

A topic that does require extra attention is modelling of simultaneous nitrification and denitrification. This is an important process in full-scale wastewater treatment processes. Especially in carrousel systems it largely contributes to the net denitrification. As long as this process is not properly understood and modelled, heuristic design methods will be required. Simultaneous nitrification and denitrification is typically caused by oxygen gradients, insufficient mixing and sludge stratification. It is known that these processes can be modelled more accurate with multidimensional flow and diffusion models. Combining these models with the activated sludge model could lead to a better description of the processes that cause simultaneous nitrification and denitrification. Wastewater treatment process designs could benefit from such a combined model.

Like simultaneous nitrification and denitrification the formation of inert and inactive cell material in activated sludge systems should be investigated with more detail. Currently heuristic methods (models) are required to predict the sludge formation. A better knowledge concerning the formation of inert material would highly contribute to the performance of activated sludge models and wastewater treatment process design in general.

Finally, more effort is required to introduce activated sludge models in the practice of wastewater treatment plant design. Current design methods strongly rely on heuristically determined design parameters (e.g. BOD sludge loading, influent BOD/N ratio, etc.). For the design of COD and N removing wastewater treatment plants this method is sufficient. However, for the design of BioP systems, the method lacks accuracy. The BioP model therefore, is a major improvement over existing design methods. Moreover, activated sludge models can be used for dynamic optimisation of treatment plants and the development of process control. However, the complexity of dynamic modelling remains a obstacle for a large scale introduction of activated sludge models for design purposes. More attention therefore is needed for the development of better, and more important, more easy applicable simulation software.

Appendix I

De ontwikkeling van een nieuwe generatie rioolwaterzuiveringsinstallaties

met dank aan Niko Baaijens

De conventionele chemische en biologische methoden om rioolwater te zuiveren van de meststoffen stikstof (N) en fosfaat (P) zijn kostbaar en inefficiënt. Mede door onderzoek verricht aan de vakgroep bioproces-technologie in Delft is er een nieuw biologisch zuiveringsproces ontworpen op basis van zogenaamde Denitrificerende Fosfaat Bacteriën (DPB). Het nieuwe proces is als eerste toegepast door het Waterschap Groot Salland (WGS). In de moderne rioolwaterzuiveringsinstallatie te Hardenberg wordt het in Delft ontwikkelde zuiveringsproces al enkele jaren succesvol toegepast.

Het nieuwe zuiveringsproces heeft de hoofdletters BCFS meegekregen die staan voor Biologisch Chemisch Fosfaat en Stikstof. De nieuwe groep bacteriën in het BCFS-proces, verwijdert gelijktijdig N en P uit het rioolwater. Dat gebeurt in de praktijk efficiënter dan met bestaande chemische en/of biologische zuiveringsmethoden.

De basis voor het BCFS-proces is gelegd door onderzoekers van de TU Delft in het Kluyverlaboratorium voor Biotechnologie. Zij hebben de metabole werking van de bacterie doorgrond en in een wiskundig model ondergebracht. Op basis van dit model wordt het nu mogelijk kleinere en betrouwbaardere rioolwaterzuiverings-installaties (rwzi's) met een vooraf bepaalde verwerkingscapaciteit te ontwerpen, te bouwen en te beheren.

Dit artikel is grotendeels gebaseerd op Baaijens (2002) *ChemPress* **36**(2)

Het principe van biologische zuivering

Het principe van de BCFS-zuivering berust op de omzetting van vuil in bacteriën. De bacteriën 'verademen' het vuil waarbij de organische verbindingen worden omgezet in CO_2, water en nieuwe bacteriën. Tijdens de groei vormen de bacteriën kolonies in de vorm van zwevende vlokken die door bezinking van het water kunnen worden gescheiden. Dit proces is vergelijkbaar met het decanteren van een goede wijn waarbij de wijn wordt uitgeschonken zonder de droesem op de bodem van de fles in beroering te brengen. Om een effectief zuiveringsproces te kunnen ontwerpen is het nodig de omzettingsprocessen in actief-slib op een wiskundige manier te beschrijven naar hun complexe ecologische, biologische en metabolische samenhangen. Zuiveringsprocessen worden meestal als een 'black box' beschreven zoals in het algemeen toegepaste actief-slib model nr. 1 (ASM-1) waarin de omzetting van organische stof en stikstof (nitrificatie en denitrificatie) is beschreven. Met de komst van ASM-1 werd het mogelijk zuiveringsprocessen op de computer te simuleren.

Figuur 0.1 Luchtfoto van de rioolwaterzuiveringsinstallatie Ommen. In de ronde, in compartimenten verdeelde reactoren wordt het rioolwater gezuiverd. De bacteriën worden van het water gescheiden in de nabezinker. In de inzet: rwzi Ommen in aanbouw met daarnaast het oude zuiveringsproces.

Modelleren van fosfaatbacteriën

Bio-P oftewel de biologische fosfaatverwijdering kan met de black box-benadering niet goed worden beschreven. Bio-P berust op een ingewikkeld samenspel van cel-intern opgeslagen polymeren en de afwisseling tussen beluchte en onbeluchte fasen in het zuiveringsproces.

Het ontbreken van goede ontwerpcriteria voor biologische fosfaat-verwijdering heeft tot gevolg dat vrijwel alle bestaande zuiveringsmethoden voor biologische fosfaatverwijdering te kort schieten in doelmatigheid en stabiliteit. Het chemische alternatief: de binding van fosfaat met ijzerzouten wordt daarom nog steeds toegepast.

De black box-benadering schiet te kort omdat daarmee alléén bestaande processen gesimuleerd kunnen worden. In de praktijk blijkt dat de nieuwe fosfaatbeesten zich moeilijk in dat model laten inpassen, voornamelijk vanwege hun ingewikkelde interne stofwisseling. Als model is daarom gekozen voor een metabole netwerkstructuur afkomstig uit de biotechnologie van het Kluyverlaboratorium. Toegepast op de fosfaat bacteriën is dat redelijk succesvol gebleken.

Als een zuiveringsmechanisme zoals bio-P niet goed wordt begrepen, betekent dit dat het proces allerlei onzekerheden in zich heeft en met intuïtie en ervaringswijsheid moet worden gevolgd en aangepast. Een dergelijk systeem kan zeker niet onmiddellijk geoptimaliseerd aan het werk worden gezet. Het is altijd 'net niet goed genoeg' ontworpen en dat betekent dat achteraf correcties moeten plaats vinden wat kan neerkomen op het introduceren van chemische methoden waarmee de biologische verwijderingscapaciteit wordt verstoord, zoniet vernietigd. Dit betekend dat als het systeem 'net niet goed genoeg' biologisch werkt, je 'net niks hebt'. Hierdoor wordt in de praktijk zuiveringen vaak veel groter en duurder gemaakt dan nodig is.

Metabole modellering

Bij het Delftse onderzoek naar biologische fosfaatverwijdering is de nieuwe groep Denitrificerende fosfaat (P) Bacteriën (DPB) diepgaand onderzocht. De DPB-bacteriën verwijderen zeer efficiënt gelijktijdig nitraat en fosfaat uit afvalwater. Hierbij wordt uit nitraat (NO_3) het onschuldige stikstofgas (N_2) gevormd en wordt fosfaat in grote hoeveelheden opgeslagen in de bacteriecel als poly-fosfaat (PP). Deze bacteriën groeien relatief langzaam. Desondanks kunnen ze de concurrentie met sneller groeiende soorten aan door hun vermogen zonder aanwezigheid van zuurstof voedingsstoffen in de cel op te slaan als poly-acetaat (PHA).

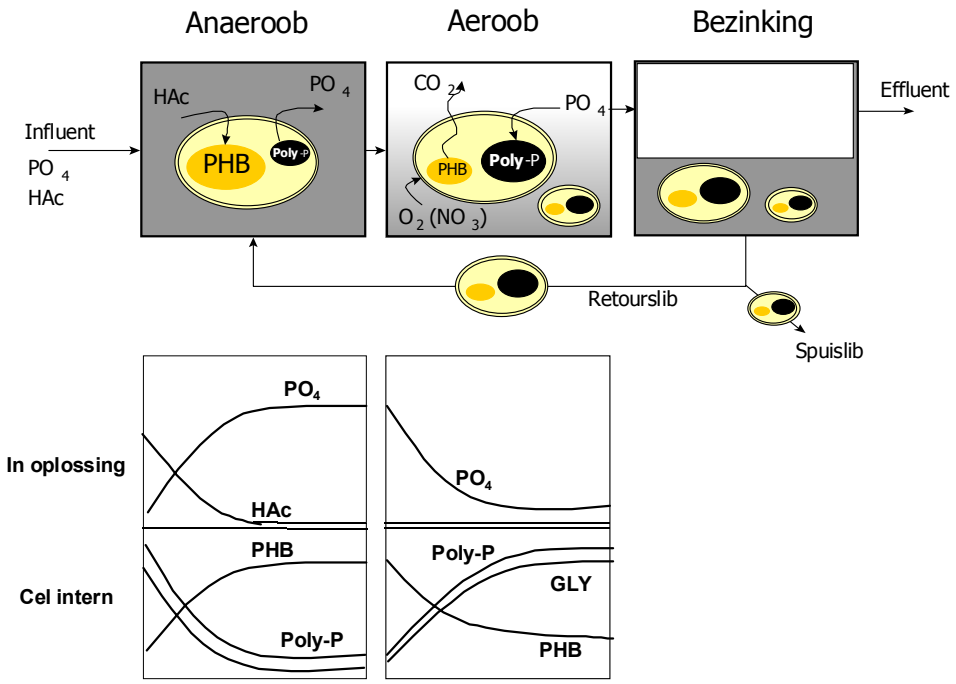

Figuur 0.2 In de eerste anaërobe reactor wordt voeding (HAc, acetaat) opgenomen door fosfaatbacterien en opgeslagen als PHB (of PHA). De cel kan dit alleen als er energie wordt vrijgemaakt door de afbraak van poly-fosfaat (poly-P). In de reactor stijgt hierdoor de fosfaatconcentratie sterk. In de tweede reactor wordt het opgeslagen PHB verademt (met nitraat of zuurstof. Fosfaat wordt hierbij door de bacteriën opgeslagen. Bacteriën worden gescheiden van de waterfase door bezinking en opnieuw naar de eerste reactor gebracht. De netto fosfaatverwijdering verloopt via de afvoer van het spuislib.

Al in een vroeg stadium van het onderzoek is samenwerking gezocht met Waterschap Groot Salland. Dit schap beheert de rioolwaterzuivering Holten waarin op toevallige wijze meetbare denitrificerende biologische fosfaatverwijdering plaats vond. Uit de toetsing van het TU Delft fosfaatmodel in de praktijk is gebleken dat de metabole modeleringstechniek een werkbare methode is waarmee zowel experimenten op laboratoriumschaal (2 liter) als op volle schaal (ruim 3.5 miljoen liter in Holten), goed kunnen worden beschreven zonder optredende schaalproblemen.

Hardenberg is het langst lopende BCFS-project dat voor onderzoek nog steeds erg interessant is. Het ecosysteem dat hier werkzaam is, groeit vanzelf. Het systeem is open. Het verandert en het past zich voortdurend

aan aan de bacteriën in het rioolwateraanbod en aan bacteriën die vanuit de lucht worden aangevoerd. De fosfaatbeesten reageren daarop door zich te her-rangschikken. Er gaat een tijd overheen voordat het ecosysteem zich aanpast en uitbalanceert. De historie van zo'n proces kan in Hardenberg over een aantal jaren worden overzien en geëvalueerd.

Hoog rendement

De biologische rioolzuiveringsinstallatie in Hardenberg van WGS heeft een capaciteit van 1715 kubieke meter per uur (41 miljoen liter per dag) en bestaat uit vijf zuiveringsbakken en drie recirculatiesystemen van actief-slib. Met deze configuratie wordt in één procesgang een verwijderings-rendement van ruim 90 procent voor fosfaat èn stikstof gehaald en is de hoeveelheid zuiveringsslib dat moet worden afgevoerd 10 tot 20 procent lager. Het gebruik van chemicaliën als aluminiumchloride kan tot een minimum beperk blijven, wat veel scheelt in de kosten en tegelijk het milieu spaart.

De vijf bakken zijn de anaërobe zone met de strippertank, de contactbak, de anoxische zone (met de nieuwe bacteriën), de wisselreactor en de oxische reactor. De gelijktijdige fosfaat- en stikstofverwijdering vindt plaats in de anoxische bak. Hier gebruiken de bacteriën fosfaat als nutriënt (voedingsstof) om nitraat uit het water te verwijderen.

Al in 1990 is het Zuiveringsschap West-Overijssel, de voorloper van WGS, begonnen met deze biologisch-chemische zuivering volgens de Delftse methode. Dit gebeurde op de rwzi in Holten. Met de nieuwe biologische zuiveringsmethoden zijn tussen 1994 en 1998 deelaspecten beproefd op de rwzi's in Genemuiden, Dalfsen en Steenwijk.

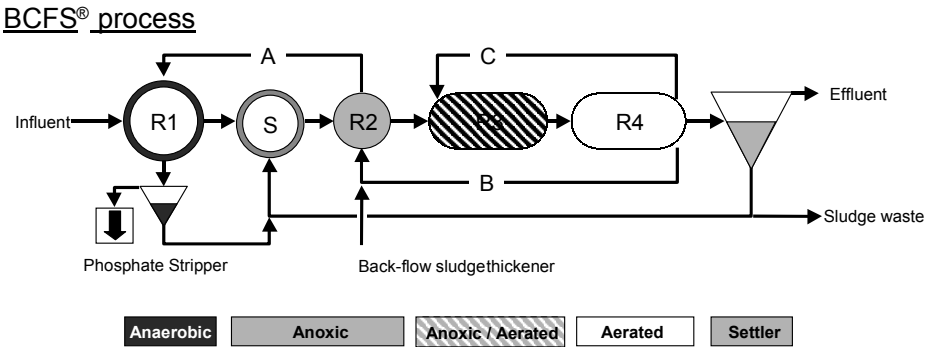

Figuur 0.3 Het BCFS proces. Door de interne recirculatie wisselen anaërobe, anoxische en aërobe condities elkaar af.

Praktijkvoordelen

BCFS is geoptimaliseerd voor de efficiënte denitrificerende fosfaatverwijdering. Ook is er een mogelijkheid om fosfaat op een efficiënte manier terug te winnen uit het rioolwater. Uit het Delftse fosfaatmodel is gebleken dat voor een stabiel bio-P proces een sterk gecompartimenteerde opbouw de voorkeur heeft. In de praktijk is bewezen dat een dergelijke opbouw compacte groei van bacteriën bevordert, wat de bezinkbaarheid van het slib sterk verbetert. Voor het BCFS-proces kunnen daarom de nabezinkers, de karakteristieke ronde bakken die vaak het grootste deel van de beschikbare oppervlakte beslaan, flink kleiner worden uitgevoerd.

Een ander voordeel van een gecompartimenteerde opbouw is de mogelijkheid om het proces te regelen en optimaliseren. Goede en betrouwbare procesregelingen worden belangrijker met de heersende tendens om rwzi's niet meer continu te bemannen en mogelijk zelfs op afstand te monitoren en te beheren.

Het TU Delft procesmodel voorziet een geheel nieuw, inmiddels gepatenteerd regelconcept op basis van goedkope, betrouwbare en gemakkelijk te onderhouden procesmetingen. Met succes is deze regeling direct van de ontwerptafel toegepast op volle schaal zonder tussenkomst van vaak kostbare en tijdrovende semi-volle schaalexperimenten.

Appendix II

Notation and Abbreviations

α ..... fit coefficient for linear equation
$\alpha_1,\alpha_2,\alpha_3$ ..... efficiency for PP synthesis (metabolic parameter)
β ..... fit coefficient for linear equation
δ ..... ATP formation per $NADH_2$ (metabolic parameter)
ε ..... mass balance residual
ε ..... phosphate uptake efficiency (metabolic parameter)
ε^0 ..... standard potential of a half reaction
ε_A ..... potential of a half reaction
η_{PNO}..... anoxic PAO reduction factor (model parameter)
θ_{GLY} ..... temperature coefficient for glycogen formation
θ_{O2} ..... temperature coefficient for oxygen consumption
θ_{PHA} ..... temperature coefficient for PHA formation (model parameter)
θ_{PP}..... temperature coefficient for PP formation (model parameter)
κ ..... ATP for biomass polymerisation (metabolic parameter)
A/O ..... cyclic anaerobic/aerobic (-process)
A2..... cyclic anaerobic/anoxic (-process)
A2/O ..... cyclic anaerobic/anoxic/aerobic (-process)
Ag|AgCl..... silver reference electrode redox half reaction
AMO ..... active autotrophic nitrifying micro-organism
ASM..... activated sludge model (-1, -2, -2d, -3, -3p)
ATP..... metabolic energy intermediate (chemical compound)
BCFS® ..... biological and chemical P and N (-process)
BioP..... enhanced biological phosphorus (-removal, -model, -process)
BNR..... biological nutrient (P and N) removal
BOD_5 ..... 5-day biological oxygen demand (composition measurement)
CE ..... centrifuge (process unit)
$CL_{1,2}$ ..... clarifier 1 and 2 (process unit)
$CL_{3,4}$ ..... clarifier 3 and 4 (process unit)

CO_2 ..... carbon dioxide (chemical compound)
COD ..... chemical oxygen demand (composition measurement)
COD_{MF} ..... micro-filtrated COD fraction (composition measurement)
COD_S ..... soluble COD fraction
COD_X ..... particulate COD fraction
CSTR ..... complete mixed stirred tank reactor (-model)
C_X ..... active biomass concentration
DEN_{NET} ..... net denitrification in the WWTP
DEN_{R2} ..... denitrification in reactor 2
DEN_{R3} ..... denitrification in reactor 3
DEN_{R4} ..... denitrification in reactor 4
DO ..... dissolved oxygen (on-line measurement)
DO_{R3} ..... dissolved oxygen in reactor 3
DO_{R4} ..... dissolved oxygen in reactor 4
DORP..... derivative oxidation-reduction-potential (-control)
$DORP_{R3}$ ..... derivative of the ORP in reactor 3
$DORP_{R4}$ ..... derivative of the ORP in reactor 4
$d\text{ORP}/dt$ ..... first order derivative of the ORP
dp ..... relative change of parameter
dy .....relative change of model output
$^{E}OC_{NET}$ ..... net aeration energy consumption
$^{E}OC_{R3}$ ..... energy consumption for aeration in reactor 3
$^{E}OC_{R4}$ ..... energy consumption for aeration in reactor 3
$^{E}Q_A$ ..... pumping energy consumption for flow A
$^{E}Q_B$ ..... pumping energy consumption for flow B
$^{E}Q_C$ ..... pumping energy consumption for flow C
EBPR ..... enhanced biological phosphorus removal
e.e.d. ..... electron exchange density
e.g. ..... for instance, for example
eq. ..... equation
F ..... constant of Faraday (96487 $J \cdot V^{-1} \cdot e\text{-}mole^{-1}$)
FD ..... flow distribution works (process unit)
FD_1 ..... flow distribution works 1 (process unit)
FD_2 ..... flow distribution works 2 (process unit)
$FeCl_3$ ..... iron-chloride (chemical compound)
$Fe(OH)_3$ ..... iron-hydroxide (chemical compound)
Fe^{2+} ..... iron in reduced form (chemical compound)
FeO^{+} ..... iron in reduced form (chemical compound)
$FePO_4$ ..... iron-phosphate precipitant (chemical compound)
f_{GLY} ..... glycogen fraction relative to PAO (model parameter)
f_{GLYmax} ..... maximum PAO glycogen fraction (model parameter)

fig. ..... figure
f_{PHA}..... PHA fraction relative to PAO (model parameter)
f_{PP} ..... poly-phosphate fraction relative to PAO (model parameter)
GAO..... glycogen accumulating micro-organism
g_{PP}..... oxygen and nitrate affinity reduction (model parameter)
Hdbg..... Hardenberg, the Netherlands (WWTP)
H-Old..... Hardenberg-Old, the Netherlands (WWTP)
$Hg|Hg_2Cl_2$..... redox half reaction for calomel reference electrode
Hltn ..... Holten, the Netherlands (WWTP)
HMO ..... active heterotrophic micro-organisms
Hrlm ..... Haarlem Waarderpolder, the Netherlands (WWTP)
HS^- ..... sulphide (chemical compound)
HRT ..... hydraulic retention time
i..... total number of elements
i.e. ..... id est, in other words
IAWQ ..... International Association for Water Quality (IWA)
iN_{BM} ..... nitrogen fraction in active biomass (model parameter)
iN_{SF} ..... nitrogen fraction of S_F (model parameter)
iN_{SF} ..... nitrogen fraction of S_F (model parameter)
iN_{SI}..... nitrogen fraction of S_I (model parameter)
iN_{XI} ..... nitrogen fraction of X_I (model parameter)
iN_{XS}..... nitrogen fraction of X_S (model parameter)
IWA..... International Water Association (former IAWQ)
$K_{A,O}$ ..... oxygen affinity constant for nitrifiers (model parameter)
$K_{A,P}$ ..... PO affinity const. for nitrifiers (model parameter)
K_{Ac} ..... affinity constant for acetate (model parameter)
k_{GLY}..... maximum glycogen storage rate (model parameter)
k_h..... maximum hydrolysis rate (model parameter)
$K_{H,O}$..... oxygen affinity const. for heterotrophs (model parameter)
K_{NO} ..... nitrate affinity constant (model parameter)
K_O..... oxygen affinity constant (model parameter)
K_P ..... phosphate affinity constant (model parameter)
$K_{P,O}$ ..... oxygen affinity constant for PAO (model parameter)
k_{PP} ..... maximum PP storage rate (model parameter)
Ktwd ..... Katwoude, the Netherlands (WWTP)
^LDEN ..... denitrified load, kgN/d
$^LDEN_{RAS}$ ..... denitrified in the return activated sludge volume, kgN/d
^LNIT ..... nitrified load, kgN/d
$^LNO_{RAS}$..... nitrate load in the return activated sludge flow
$^LPR_{R1}$..... phosphate load released in reactor 1, kgP/d
$^LTP_{EF}$..... total phosphate load in the effluent, kgP/d

$^{L}TP_{DW}$ ..... total phosphate load in the dewatered WAS, kgP/d
$^{L}TP_{IN}$ ..... total phosphate load in the influent, kgP/d
$^{L}TKN_{W}$ ..... load total Kjeldalh N in the waste activated sludge, kgN/d
^{L}WAS ..... waste activated sludge production, kg/d
m ..... measured value
m_{ATP} ..... ATP requirement for maintenance (metabolic parameter)
MLSS ..... mixed liquor suspended solids (composition measurement)
MnO_2 ..... manganese in reduced form (chemical compound)
m_O, m_{PHA} ..... maintenance rate (metabolic parameter)
m_{OC} ..... oxygen consumption for maintenance (model parameter)
MUCT ..... modified university of Cape Town (-process)
N ..... nitrogen (chemical element)
n ..... number of mass balances
N_2 ..... dissolved dinitrogen gas (chemical compound)
$NADH_2$ ..... metabolic intermediate (chemical compound)
n.d. ..... no data, not determined
NH_4^+ ..... ammonium (chemical compound)
NH_{EF} ..... ammonium in effluent
NH_{IN} ..... ammonium in influent
NH_{IN2} ..... ammonium in secondary inflow
NH_{R2} ..... ammonium in reactor 2
NH_{R4} ..... ammonium in reactor 4
NO_3^- ..... nitrate (NO_3 + NO_2) (composition measurement)
n-u ..... degree of redundancy
O_2 ..... dissolved oxygen, DO (chemical compound)
OC ..... oxygen consumption, aeration, kgO_2/d
OC_{COD} ..... oxygen consumption for COD removal, kgO_2/d
OC_{NET} ..... net oxygen consumption, kgO_2/d
ORP ..... oxidation-reduction-potential (on-line measurement)
ORP_{R2} ..... oxidation-reduction-potential in reactor 2
ORP_{R3} ..... oxidation-reduction-potential in reactor 3
p ..... parameter
P ..... phosphorus (chemical element)
P ..... proportional (-control)
p.e. ..... person equivalent
P/Ac ..... ratio of phosphate release over acetate uptake
P/O ..... ratio of phosphate release over maintenance OC
PAO ..... phosphate accumulating micro-organism
PHA ..... poly-hydroxyalkanoate (chemical compound)
PHB ..... poly-hydroxybuterate (chemical compound)
PI ..... proportional-integral (-control)

PO_4^{2-} ..... ortho-phosphate (chemical compound)
PO_{IN} ..... phosphate in influent
PO_{R1} ..... phosphate in reactor 1
PO_{R2} ..... phosphate in reactor 2
PP ..... poly-phosphate (chemical compound)
Q_A ..... recycle pump flow A
q_{Ac} ..... maximum anaerobic acetate uptake rate (model parameter)
Q_B ..... recycle pump flow B
Q_C ..... recycle pump flow C
Q_{CE} ..... thickened activated sludge flow to CE
Q_{CENT} ..... centrate flow from CE
Q_{DW} ..... dewatered waste activated sludge flow
Q_{EF} ..... effluent flow
q_{fe} ..... maximum fermentation rate (model parameter)
$\vec{Q}_i$ ..... flow vector
Q_{IN} ..... influent flow
Q_{IN2} ..... secondary inflow
$q_{NO,Ac}$ ..... maximum anoxic acetate uptake rate (model parameter)
Q_{OF} ..... overflow thickener
Q_{R3} ..... natural overflow reactor 3
Q_{R3EX} ..... external carrousel recycle flow from reactor 3
Q_{R3IN} ..... internal carrousel flow reactor 3
Q_{R4IN} ..... internal carrousel flow reactor 4
Q_{RAS} ..... return activated sludge flow
Q_{RS12} ..... return activated sludge flow from clarifiers 1 and 2
Q_{RS34} ..... return activated sludge flow from clarifiers 1 and 2
Q_{TW} ..... thickened waste activated sludge flow
Q_W ..... waste activated sludge flow
R ..... gas constant (8.314 $J \cdot mole^{-1} \cdot K^{-1}$)
R1 to R4 ..... anaerobic, anoxic or aerobic reactor (process unit)
RAS ..... return activated sludge (recycled from clarifier underflow)
redox ..... reduction-oxidation
r_{GLY} ..... observed glycogen formation rate
r_O ..... observed oxygen consumption rate
r_{PHB} ..... observed poly-hydroxyalkanoate formation rate
r_{PP} ..... observed poly-phosphate formation rate
r_X ..... observed biomass growth rate
s ..... parameter sensitivity
S ..... selector reactor (process unit)
$S_?$ ..... soluble organic matter ($S_A + S_F + S_I$)
SBR ..... sequential batch reactor (process unit)

s_D..... standard deviation
S_I ..... soluble inert fraction (model compound)
S_I/S_F..... influent ratio soluble inert and fermentable substrate
sim. ..... simulated, simulation
S_{N2} ..... dissolved nitrogen gas (model compound)
SND..... simultaneous nitrification and denitrification
S_{NH}..... ammonium (model compound)
S_{NO}..... nitrate concentration (model compound)
S_O ..... oxygen concentration (model compound)
SO_4^{2-} ..... sulphate (chemical compound)
SRT..... sludge retention time
p.s.s..... pseudo steady state
T..... temperature
^{T}..... temperature dependent model parameter
TCOD..... totalchemical oxygen demand (composition measurement)
TH ..... thickener (process unit)
TKN ..... total Kjeldalh nitrogen (composition measurement)
TN..... total nitrogen (TKN + NO)
TOC ..... total organic carbon (composition measurement)
TP ..... total phosphorus (composition measurement)
TP_{AT} ..... total phosphorus in aeration tank
TP_{CENT} ..... total phosphorus in centrate
TP_{EF} ..... total phosphorus in effluent
TP_{IN}..... total phosphorus in influent
TP_{IN2} ..... total phosphorus in secondary inflow
TP_{OF} ..... total phosphorus in thickener overflow
TP_{R1} ..... total phosphorus in reactor 1
TP_{R4} ..... total phosphorus in reactor 4
TP_{RS34}..... total phosphorus in RAS from clarifiers 3 and 4
TP_W ..... total phosphorus in waste activated sludge
TP_X ..... total phosphorus in particulate matter
TUD ..... Delft university of technology (-model)
TUDM ..... technical university of Delft integrated metabolic BioP model
u..... unknown value, calculated value
UCT ..... university of Cape Town (-process)
VFA ..... volatile fatty acid (composition measurement)
VSS ..... volatile suspended solids (composition measurement)
WAS..... waste activated sludge (removed from settler underflow)
WWTP..... wastewater treatment plant
$X_?$ ..... particulate matter, suspended solid matter
X_{AT}..... particulate matter in the aeration tank

X_{BM} ..... active biomass (X_{PAO} + X_A + X_H)
X_{EF} ..... mixed liquor suspended solids in effluent
X_H ..... active heterotrophic biomass (model compound)
X_I ..... inert particulate matter (model compound)
X_I/X ..... influent fraction inert particulate of total particulate
X_{IN} ..... mixed liquor suspended solids in influent
X_{MeOH} ..... particulate metal-hydroxide (model compound)
X_{MeP} ..... particulate metal-phosphate (model compound)
X_{PAO} ..... phosphorus accumulating organisms (model compound)
X_{PHA} ..... poly-hydroxyalkanoate (model compound)
X_{QA} ..... mixed liquor suspended solids in pump flow A
X_{R1} ..... mixed liquor suspended solids in reactor 1
X_{R4} ..... mixed liquor suspended solids in reactor 4
X_S ..... particulate substrate (model compound)
X_W ..... mixed liquor suspended solids in waste activated sludge
y ..... model output
$Y_{a/b}$ ..... yield a over b
$Y_{AN,PO}$ ..... anaerobic yield for acetate uptake (model parameter)
$Y_{NO,PO}$ ..... anoxic yield for acetate uptake (model parameter)
$Y_{O,GLY}$ ..... yield for aerobic glycogen formation (model parameter)
$Y_{O,PHA}$ ..... yield for aerobic PHA formation (model parameter)
< ..... smaller then
> ..... larger then

Appendix III

The Integrated Metabolic Activated Sludge Model

Description of the model compounds

In the model, soluble components are indicated with $S_?$, particulate components with $X_?$. Only soluble components carry an ionic charge. The $X_?$ fractions are assumed to be associated with the activated sludge, whereas $S_?$ fractions can only be transported with the water phase.

Soluble ($S_?$) compounds.

S_O Dissolved oxygen ($gO_2 \cdot m^{-3}$). Dissolved oxygen can directly be measured and is subject to gas exchange. On the COD balance oxygen accounts for –1 g $COD \cdot g^{-1}O_2$.

S_F Readily biodegradable fermentable organic substrate ($gCOD \cdot m^{-3}$). This fraction of the biodegradable substrate is readily available for Heterotrophic organisms. S_F is converted to S_A in the fermentation process. S_F does not have an ionic charge.

S_A Volatile fatty acids, VFA ($gCOD \cdot m^{-3}$). VFA can directly be measured. It is assumed all lower fatty acids (C_2 to C_5) are available as S_A. The ionic charge is -1/64. The TOC/COD ratio of S_A is 0.4 gC/gCOD. In the bio-P process S_A is stored under anaerobic conditions as PHA.

S_{NH} Ammonium plus ammonia ($NH_3 + NH_4^+$, $gN \cdot m^{-3}$). Ammonium can directly be measured. For the balance of the ionic charge (+1/14 mole) S_{NH} is assumed to be all N_{H4}^+.

S_{NO} Nitrate plus nitrite ($NO^{3-} + NO^{2-}$, $gN \cdot m^{-3}$). For all stoichiometric calculations S_{NO} is assumed to be NO_3^- only. The charge of S_{NO} is

equal to –1/14 mole. On the COD balance nitrate accounts for -2.86 gCOD· g^{-1}N.

S_{N2} Di-nitrogen ($gN \cdot m^{-3}$) formed in the denitrification process. In the model di-nitrogen accumulates in the liquid and can be used as a measure for the total denitrified load.

S_{PO} Inorganic soluble phosphorus, primary ortho phosphate ($gP \cdot m^{-3}$). For the balance of the ionic charge it is assumed that S_{PO} consists of 50% $H_2PO_4^-$ and 50% HPO_4^{2-} and therefore has an electric charge of -1.5/31 mole.

S_I Inert soluble organic material ($gCOD \cdot m^{-3}$). S_I is assumed to be non biodegradable. Generally S_I is a part of the influent. As in the default of ASM2d, in the TUDP model no S_I is formed in the hydrolysis process (f_{SI}=0). In low loaded activated sludge plants the effluent soluble organic fraction ($S_A+S_F+S_I$) largely consists of S_I.

S_{HCO} Alkalinity of the wastewater (mole $HCO_3^- \cdot m^{-3}$). Alkalinity is used to approximate the conservation of ionic charge (equal to -1 mole) in biological reactions. Alkalinity is introduced in order to predict possible low pH conditions, which might inhibit some biological processes.

Particulate ($X_?$) compounds

X_I Inert particulate organic material ($gCOD \cdot m^{-3}$). Under normal operational conditions this organic fraction is not biodegraded. X_I may be a part of the influent. In the process X_I flocculates into the activated sludge. Also X_I may be formed in the process from lysis of heterotrophic and autotrophic organisms. X_I is assumed to contain a fraction ammonium (iN_{XI}) and phosphate (iP_{XI}).

X_S Slowly biodegradable particulate substrate ($gCOD \cdot m^{-3}$). This substrate must undergo cell external hydrolysis to S_F before being available as substrate. X_S may be part of the influent whereas it also may be formed in the process from lysis of heterotrophic and autotrophic organisms. X_S is assumed to contain a fraction ammonium (iN_{XS}) and phosphate (iP_{XS}).

X_H Heterotrophic organisms ($gCOD \cdot m^{-3}$). These organisms represent the general heterotrophic population. X_H grows aerobically, whereas most a large fraction of X_H also can use nitrate as an electron acceptor (i.e. denitrification). X_H grows on both S_A and S_F. No cell-internal storage is modelled. X_H is assumed to contain a fraction ammonium (iN_{BM}) and phosphate (iP_{BM}). These fractions are equal for all biomass fractions (i.e. X_H, X_{PAO} and X_A).

X_{PAO} Phosphate accumulating organisms ($gCOD \cdot m^{-3}$). PAO's represent the heterotrophic population that under anaerobic conditions stores Poly-Hydroxyalcanoates (X_{PHA}). Under denitrifying and aerobic conditions PAO's use PHA as substrate for growth while storing poly-phosphate (X_{PP}) and glycogen (X_{GLY}). All processes related to PAO's are based on metabolic descriptions of the cell internal processes. The state of reduction of X_{PAO} is assumed to be 0.334 $gC \cdot gCOD^{-1}$.

X_{PP} Poly-phosphate ($gP \cdot m^{-3}$). This is a cell-internal storage product of PAO's. It is assumed only to be associated with PAO's, however not included in the latter's mass. It forms part of the particulate phosphorus and may be analytically observed. For stoichiometric considerations, poly-phosphate is assumed to have the composition of $(K_{0.33}Mg_{0.33}PO_3)_n$. Since the model does not account for K^+ and Mg^{2+}, poly phosphate is represented as $(HPO_3)_n$. An electric charge of $-1/31$ must be included to compensate for this term.

X_{PHA} Cell-internal storage of poly-hydroxyalkanoates in PAO's ($gCOD \cdot m^{-3}$). This storage compound is only associated with PAO's. It is however not included in the mass of PAO's. X_{PHA} can not be directly be related to analytically measured PHA values, as also non PAO's are known to accumulate PHA. Therefore X_{PHA} is only a functional component required for modelling biological phosphorus removal. For stoichiometric considerations, X_{PHA} is assumed to have the composition of Poly-Hydroxy-Buterate $(C_4H_6O_2)_n$. The state of reduction of X_{PHA} is assumed to be 0.334 $gC \cdot gCOD^{-1}$.

X_{GLY} Cell-internal storage of glycogen in PAO's ($gCOD \cdot m^{-3}$). This storage compound is only associated with PAO's. It is however not included in the mass of PAO's. X_{GLY} can not be directly be related to analytically measured glycogen values, as also non PAO's are known to accumulate glycogen. Therefore X_{GLY} is only a functional component required for modelling biological phosphorus removal. For stoichiometric considerations, X_{GLY} is assumed to have the composition of $(C_6H_{10}O_5)_n$. The state of reduction of X_{GLY} is assumed to be 0.375 $gC \cdot gCOD^{-1}$.

X_A Autotrophic nitrifying organisms ($gCOD \cdot m^{-3}$). Nitrifying organisms are responsible for nitrification. They are obligate aerobic, chemo-litho-autotrophic. It is assumed that nitrifiers oxidise ammonium (S_{NH}) directly to nitrate (S_{NO}). Nitrite (NO_2^-) as intermediate compound is not considered in the model.

X_{TSS} Total Suspended Solids ($g \cdot m^{-3}$). TSS is an analytical measurement typically followed on a day to day basis by plant operators. X_{TSS} is calculated in the model from the model stoichiometry. It is not a

balanced compound and therefore relies on the TSS fractions (i_{TSS}) of the particulate compounds ($X_?$) and X_{TSS} in the influent.

Description of the Modelled Processes

(1-3) Hydrolysis ($r_H^{AN}, r_H^{O}, r_H^{NO}$, $gCOD_{XS} \cdot d^{-1}$). In these three process the particulate bio-degradable substrate X_S is converted to soluble substrate (S_F). The hydrolysis process is dependent on the electron donor (oxygen or nitrate). Under anoxic and anaerobic conditions the hydrolysis rate is reduced according to the reduction factors η_{NO} and η_{fe}. In the TUDP model hydrolysis is a function of the total heterotrophic population ($X_H + X_{PAO}$).

(4) Aerobic heterotrophic growth (r_{SF}^{O}, $gCOD_{XH} \cdot d^{-1}$) on readily biodegradable fermentable organic substrate (S_F). In presence of oxygen X_H grows on S_F. The formation of storage products (PHA) by regular heterotrophs (X_H) is not modelled.

(5) Aerobic heterotrophic growth (r_{SA}^{O}, $gCOD_{XH} \cdot d^{-1}$) on Volatile Fatty Acids (S_A). In presence of oxygen (S_O) as electron acceptor X_H grows on VFA (S_A). The formation of storage products (PHA) by regular heterotrophs is not modelled.

(6) Anoxic heterotrophic growth (r_{SF}^{NO}, $gCOD_{XH} \cdot d^{-1}$) on readily biodegradable fermentable organic substrate (S_F). The same process as aerobic growth (process 5) except nitrate (S_{NO}) serves as the main electron acceptor. It is not clear weather all heterotrophs are capable of denitrification. Experimentally a reduced anoxic activity is observed compared to aerobic conditions. This is expressed with a reduction factor (η_{NO}) in the kinetic rate equation.

(7) Anoxic heterotrophic growth (r_{SA}^{NO}, $gCOD_{XH} \cdot d^{-1}$) on Volatile Fatty Acids (S_A). The same as for aerobic growth (process 6) except nitrate serves as the main electron acceptor. It is not clear weather all heterotrophs are capable of denitrification. Experimentally a reduced anoxic activity is observed compared to aerobic conditions. This is expressed with a reduction factor (η_{NO}) in the kinetic rate equation.

(8) Anaerobic fermentation (r_{fe}^{AN}, $gCOD_{SF} \cdot d^{-1}$). Anaerobic formation of Volatile Fatty Acids (S_A) from readily biodegradable fermentable organic substrate (S_F). The process is induced by regular heterotrophic organisms (X_H). In most plants anaerobic conditions are relative short. Therefore in the degradation of particulate

substrate to VFA ($X_S \rightarrow S_F \rightarrow S_A$), anaerobic fermentation ($S_F \rightarrow S_A$) is often the limiting process.

(9) Heterotrophic Lysis (r_{HL}, $gCOD_{XH} \cdot d^{-1}$). Lysis of regular heterotrophs (X_H) to particulate substrate (X_S) and particulate inert material (X_I). In the model the concepts of lysis (processes 9 and 21) is used for the regular heterotrophs, whereas the maintenance concept (processes 11 and 15) is used for phosphate accumulating bacteria (X_{PAO}).

(10) Anaerobic uptake of Volatile Fatty Acids by PAO's (r_{SA}^{AN}, $gCOD_{SA} \cdot d^{-1}$). VFA is taken up under anaerobic conditions and stored as PHA (X_{PHA}). The energy needed for this process is provided from the conversion of cell-internally stored glycogen (X_{GLY}) and poly-phosphate (X_{PP}). Hereby, PAO's release large amounts of ortho-phosphate (S_{PO}). The yield of S_A taken up and X_{PHA} formed (Y_{PHA}) is a function of the pH.

(11) Anaerobic maintenance (r_M^{AN}, $gP \cdot d^{-1}$). In absence of an electron acceptor cell-internal stored poly-phosphate (X_{PP}) is converted to ortho-phosphate (S_{PO}) yielding in energy that used for cell maintenance.

(12) Anoxic uptake of Volatile Fatty Acids by PAO's (r_{SA}^{NO}, $gCOD_{SA} \cdot d^{-1}$). VFA is taken up under anoxic conditions and stored as PHA (X_{PHA}). The energy needed for this process is provided from the conversion of cell-internally stored poly-phosphate (X_{PP}), which is released by PAO's as ortho-phosphate (S_{PO}). No glycogen is used in this process.

(13) Aerobic consumption of PHA (r_{PHA}^{O}, $gCOD_{XPHA} \cdot d^{-1}$). Growth of PAO's on cell internally stored PHA (X_{PHA}). The net growth of PAO is assumed to be a function of the PHA degradation, poly-phosphate formation and glycogen formation. In reality PHA is used for glycogen and poly-phosphate formation and growth. In the model however, X_{PHA} is converted to X_{PAO}, whereas Glycogen (X_{GLY}) and poly-phosphate (X_{PP}) are only formed from X_{PAO}. As a result of this mathematical description, processes 13, 14 and 15 can not be read independently.

(14) Aerobic poly-phosphate formation (r_{PP}^{O}, $gP \cdot d^{-1}$). Ortho-phosphate (S_{PO}) is aerobically taken up by X_{PAO} and cell-internally stored as poly-phosphate (X_{PP}). This process is much faster then nitrification, and therefore rarely limiting in wwtp's. Under aerobic and anoxic conditions X_{PP} and X_{GLY} are restored to provide the anaerobic uptake of substrate (S_A).

(15) Aerobic glycogen formation (r_{GLY}^{O}, $gCOD_{XGLY} \cdot d^{-1}$). In presence of an electron acceptor (S_O), X_{PHA} is partly converted to glycogen (X_{GLY}).

Under aerobic and anoxic conditions X_{PP} and X_{GLY} are restored to provide the anaerobic uptake of substrate (S_A).

(16) Aerobic maintenance (r_M^O, $gCOD_{XPAO} \cdot d^{-1}$). In the maintenance concept PHA is oxidised yielding in energy for cell maintenance. This is mathematically described by the oxidation of X_{PAO} with oxygen (S_O). The formation of inert material (X_I or S_I) from processes like decay, predation and lysis are reconciled in the model via the process yields.

(17) Anoxic PHA degradation (r_{PHA}^{NO}, $gCOD_{XPHA} \cdot d^{-1}$). Oxidation PHA (X_{PHA}) with nitrate (X_{NO}) as the main electron acceptor. It is not clear whether all PAO's are capable of denitrification. Experimentally a reduced denitrification rate is observed compared to aerobic conditions. In the model this is expressed with a reduction factor (η_{NO}) in the kinetic rate equation. As a result of the mathematical description of the metabolic model, processes 17, 18 and 19 can not be read independently.

(18) Anoxic poly-phosphate formation (r_{PP}^{NO}, $gP \cdot d^{-1}$). Ortho-phosphate (S_{PO}) is stored as poly-phosphate (X_{PP}) by X_{PAO} with nitrate (S_{NO}) as the main electron acceptor. As for the anoxic PHB degradation (process 16), the anoxic poly-phosphate formation rate is reduced with a factor η_{NO} compared to aerobic conditions (process 13).

(19) Anoxic formation of glycogen (r_{GLY}^{NO}, $gCOD_{XGLY} \cdot d^{-1}$). In presence of nitrate (S_{NO}), X_{PHA} is partly converted to glycogen (X_{GLY}). X_{GLY} is restored to provide reduction equivalents and energy in the anaerobic uptake of substrate (S_A). As for the anoxic PHB degradation (process 16), the anoxic glycogen formation is reduced with the a factor η_{NO} compared to aerobic conditions (process 14).

(20) Anoxic maintenance (r_M^{NO}, $gCOD_{XPAO} \cdot d^{-1}$). Maintenance of PAO's analogue to aerobic maintenance (process 15) with nitrate (X_{NO}) as the main electron acceptor.

(21) Autotrophic growth (r_A^O, $gCOD_{XA} \cdot d^{-1}$). Autotrophic growth of nitrifying organisms (X_A) in which the energy yielding reaction is the oxidation of ammonium (X_{NH}) to nitrate (X_{NO}) with oxygen (S_O)as the main electron acceptor and CO_2 as the carbon source for biomass formation.

(22) Autotrophic lysis (r_{AL}, $gCOD_{XA} \cdot d^{-1}$). Lysis of autotrophic nitrifying organisms (X_A) yielding in inert material (X_I) and particulate substrate (X_S).

Model Stoichiometry

The model stoichiometry is presented table 1 according to the matrix notation for chemical reactions proposed by Petersen (1965). In the matrix, horizontally 22 processes are represented, the 18 modelled compounds are ordered vertically. The composition (COD, TOC/COD, N, P, charge and TSS) of the compounds is listed in table 2. Multiplication of a row from the stoichiometric matrix with a row from the composition matrix gives a composition balance, which adds up to zero when summarised horizontally. The stoichiometric coefficients ($c_{?,1..22}$, table 4) are derived from the composition balances. The composition factors are listed in table 2.7, the stoichiometric parameters in table 2.8. The yields and maintenance factors of the metabolic model are derived from the P/O (δ) ration being the amount ATP produced from $NADH_2$ and the ATP use for maintenance (m_{ATP}) (tables 5 and 6b). These parameters therefore can not be calibrated individually.

Model Kinetics

The kinetic rate equations of the TUD model are presented in table 7. The kinetic parameters are listed in tables 6a/b/c. The best fit for the lab-scale SBR systems was obtained with the kinetic parameters in table 6c and the kinetic rate for glycogen formation in equation 2.24. For the simulation of full-scale conditions we propose to use the simplified glycogen formation rate equation in table 2.10 and the kinetic parameters in table 6a. For the calibration of the glycogen formation rate we suggest to use the tree-step method as proposed in this chapter.

← Process			Component →	1 S_O gO_2/m^3	2 S_F $gCOD/m^3$	3 S_A $gCOD/m^3$	4 S_{NH} gN/m^3	5 S_{NO} gN/m^3	6 S_{N2} gN/m^3
1	r_h^O	Aerobic Hydrolysis	$gCOD_{XS}/d$		$1-f_{SI}$		$c_{N,1}$		
2	r_h^{NO}	Anoxic Hydrolysis	$gCOD_{XS}/d$		$1-f_{SI}$		$c_{N,1}$		
3	r_h^{AO}	Anaerobic Hydrolysis	$gCOD_{XS}/d$		$1-f_{SI}$		$c_{N,1}$		
Regular Heterotrophic Organisms X_H									
4	r_{SF}^O	Aerobic Growth on S_F	$gCOD_{XH}/d$	$-(1/Y_H-1)$	$-1/Y_H$		$c_{N,4}$		
5	r_{SA}^O	Aerobic Growth on S_A	$gCOD_{XH}/d$	$-(1/Y_H-1)$		$-1/Y_H$	$c_{N,5}$		
6	r_{SF}^{NO}	Anoxic Growth on S_F	$gCOD_{XH}/d$		$-1/Y_H$		$c_{N,6}$	$-\frac{(1/Y_H-1)}{2.86}$	$\frac{(1/Y_H-1)}{2.86}$
7	r_{SA}^{NO}	Anoxic Growth on S_A	$gCOD_{XH}/d$			$-1/Y_H$	$c_{N,7}$	$-\frac{(1/Y_H-1)}{2.86}$	$\frac{(1/Y_H-1)}{2.86}$
8	r_{fe}^{AN}	Fermentation	$gCOD_{SF}/d$		-1	1	$c_{N,8}$		
9	r_{HL}	Heterotrophic Lysis	$gCOD_{XH}/d$				$c_{N,9}$		
Phosphorus Accumulating Organisms X_{PAO}									
10	r_{SA}^{AN}	Anaerobic Storage of S_A	$gCOD_{SA}/d$			-1			
11	r_M^{AN}	Anaerobic Maintenance	gP/d						
12	r_{SA}^{NO}	Anoxic Storage of S_A	$gCOD_{SA}/d$			-1		$-\frac{(1-Y_{SA}^{NO})}{2.86}$	$\frac{(1-Y_{SA}^{NO})}{2.86}$
13	r_{PHA}^{NO}	Anoxic PHA Consumption	$gCOD_{PHA}/d$				$c_{N,13}$	$-\frac{(1-1/Y_{PHA}^{NO})}{2.86}$	$\frac{(1-1/Y_{PHA}^{NO})}{2.86}$
14	r_{PP}^{NO}	Anoxic Storage of poly-P	gP/d				$c_{N,14}$	$-\frac{(1/Y_{PP}^{NO})}{2.86}$	$\frac{(1/Y_{PP}^{NO})}{2.86}$
15	r_{GLY}^{NO}	Anoxic Glycogen Formation	$gCOD_{GLY}/d$				$c_{N,15}$	$-\frac{(1/Y_{GLY}^{NO}-1)}{2.86}$	$\frac{(1/Y_{GLY}^{NO}-1)}{2.86}$
16	r_M^{NO}	Anoxic Maintenance	$gCOD_{PAO}/d$				$c_{N,16}$	$-1/2.86$	$1/2.86$
17	r_{PHA}^O	Aerobic PHA Consumption	$gCOD_{PHA}/d$	$1/Y_{PHA}^O-1$			$c_{N,17}$		
18	r_{PP}^O	Aerobic Storage of poly-P	gP/d	$-1/Y_{PP}^O$			$c_{N,18}$		
19	r_{GLY}^O	Aerobic Glycogen Formation	$gCOD_{GLY}/d$	$1-1/Y_{GLY}^O$			$c_{N,19}$		
20	r_M^O	Aerobic Maintenance	$gCOD_{PAO}/d$	-1			$c_{N,20}$		
Autotrophic Nitrifying Organisms X_A									
21	r_A^O	Autotrophic Growth	$gCOD_{XA}/d$	$1-4.57/Y_A$			$c_{N,21}$	$1/Y_A$	
22	r_{AL}	Autotrophic Lysis	$gCOD_{XA}/d$				$c_{N,22}$		

↓ Composition		Component →	1 S_O gO_2	2 S_F gCOD	3 S_A gCOD	4 S_{NH} gN	5 S_{NO} gN	6 S_{N2} gN
1	COD	gCOD	-1	1	1		-2.86	…
2	TOC/COD	gC/gCOD		…	0.4			
3	Nitrogen	gN		$i_{N,SF}$	$i_{N,SA}$	1	1	1
4	Phosphorus	gP		$i_{P,SF}$	$i_{P,SA}$			
5	Ionic charge	mole			-1/64	+1/14	-1/14	
6	TSS	g						

Table 1. Stoichiometric matrix and component composition matrix.

7	8	9	10	11	12	13	14	15	16	17	18
S_{PO}	S_I	S_{HCO}	X_I	X_S	X_H	X_{PAO}	X_{PP}	X_{PHA}	X_{GLY}	X_A	X_{TSS}
gP/m^3	$gCOD/m^3$	$mole/m^3$	$gCOD/m^3$	$gCOD/m^3$	$gCOD/m^3$	$gCOD/m^3$	gP/m^3	$gCOD/m^3$	$gCOD/m^3$	$gCOD/m^3$	g/m^3
$c_{P,1}$	f_{SI}	$c_{e,1}$		-1							$c_{TSS,1}$
$c_{P,1}$	f_{SI}	$c_{e,1}$		-1							$c_{TSS,1}$
$c_{P,1}$	f_{SI}	$c_{e,1}$		-1							$c_{TSS,1}$
$c_{P,4}$		$c_{e,4}$			1						$c_{TSS,4}$
$c_{P,5}$		$c_{e,5}$			1						$c_{TSS,5}$
$c_{P,6}$		$c_{e,6}$			1						$c_{TSS,6}$
$c_{P,7}$		$c_{e,7}$			1						$c_{TSS,7}$
$c_{P,8}$		$c_{e,8}$									$c_{TSS,8}$
$c_{P,9}$		$c_{e,9}$	$f_{XI,H}$	$1- f_{XI,H}$	-1						$c_{TSS,9}$
Y_{PO}^{AN}		$c_{e,10}$					$-Y_{PO}^{AN}$	Y_{SA}^{AN}	$1-Y_{SA}^{AN}$		$c_{TSS,10}$
1		$c_{e,11}$					-1				$c_{TSS,11}$
Y_{PO}^{NO}		$c_{e,12}$					$-Y_{PO}^{NO}$	Y_{SA}^{NO}			$c_{TSS,12}$
$c_{P,13}$		$c_{e,13}$				$1/Y_{PHA}^{NO}$		-1			$c_{TSS,13}$
$c_{P,14}$		$c_{e,14}$				$-1/Y_{PP}^{NO}$	1				$c_{TSS,14}$
$c_{P,15}$		$c_{e,15}$				$-1/Y_{GLY}^{NO}$			1		$c_{TSS,15}$
$c_{P,16}$		$c_{e,16}$				-1					$c_{TSS,16}$
$c_{P,17}$		$c_{e,17}$				$1/Y_{PHA}^{O}$		-1			$c_{TSS,17}$
$c_{P,18}$		$c_{e,18}$				$-1/Y_{PP}^{O}$	1				$c_{TSS,18}$
$c_{P,19}$		$c_{e,19}$				$-1/Y_{GLY}^{O}$			1		$c_{TSS,19}$
$c_{P,20}$		$c_{e,20}$				-1					$c_{TSS,20}$
$c_{P,21}$		$c_{e,21}$								1	$c_{TSS,21}$
$c_{P,22}$		$c_{e,22}$	$f_{XI,A}$	$1- f_{XI,A}$						-1	$c_{TSS,22}$

7	8	9	10	11	12	13	14	15	16	17	18
S_{PO}	S_I	S_{HCO}	X_I	X_S	X_H	X_{PAO}	X_{PP}	X_{PHA}	X_{GLY}	X_A	X_{TSS}
gP	gCOD	mole	gCOD	gCOD	gCOD	gCOD	gP	gCOD	gCOD	gCOD	g
	1		1	1	1	1		1	1	1	
	...		...	...	...	0.334 (α)		0.334	0.375	...	
	$i_{N,SI}$		$i_{N,XI}$	$i_{N,XS}$	$i_{N,XH}$	$i_{N,BM}$				$i_{N,BM}$	
1	$i_{P,SI}$		$i_{P,XI}$	$i_{P,XS}$	$i_{P,XH}$	$i_{P,BM}$	1			$i_{P,BM}$	
-1.5/31		-1					-1/31				
			$i_{TSS,XI}$	$i_{TSS,XS}$	$i_{TSS,BM}$	$i_{TSS,BM}$	$i_{TSS,PP}$	$i_{TSS,PHA}$	$i_{TSS,GLY}$	$i_{TSS,BM}$	1

S_{NH} (gN·m^{-3})	S_{PO} (gP·m^{-3})
$c_{N,1} = i_{N,XS} - i_{N,SI} \cdot f_{SI} - i_{N,SF} \cdot (1 - f_{SI})$	$c_{P,1} = i_{P,XS} - i_{P,SI} \cdot f_{SI,H} - i_{P,SF} \cdot (1 - f_{SI,H})$
$c_{N,4} = i_{N,SF} / Y_H - i_{N,BM}$	$c_{P,4} = i_{P,SF} / Y_H - i_{P,BM}$
$c_{N,5} = -i_{N,BM}$	$c_{P,5} = -i_{P,BM}$
$c_{N,6} = i_{N,SF} / Y_H - i_{N,BM}$	$c_{P,6} = i_{P,SF} / Y_H - i_{P,BM}$
$c_{N,7} = -i_{N,BM}$	$c_{P,7} = -i_{P,BM}$
$c_{N,8} = i_{N,SF}$	$c_{P,8} = i_{P,SF}$
$c_{N,9} = i_{N,BM} - i_{N,XI} \cdot f_{XI,H} - i_{N,XS} \cdot (1 - f_{XI,H})$	$c_{P,9} = i_{P,BM} - i_{P,XI} \cdot f_{XI,H} - i_{P,XS} \cdot (1 - f_{XI,H})$
$c_{N,10} = 0$	$c_{P,10} = Y_{PO}^{AN}$
$c_{N,11} = 0$	$c_{P,11} = 1$
$c_{N,12} = 0$	$c_{P,12} = Y_{PO}^{NO}$
$c_{N,13} = -i_{N,BM} / Y_{PHA}^{NO}$	$c_{P,13} = -i_{PBM} / Y_{PHA}^{NO}$
$c_{N,14} = i_{N,BM} / Y_{PP}^{NO}$	$c_{P,14} = i_{P,BM} / Y_{PP}^{NO} - 1$
$c_{N,15} = i_{N,BM} / Y_{GLY}^{NO}$	$c_{P,15} = i_{P,BM} / Y_{GLY}^{NO}$
$c_{N,16} = i_{N,BM}$	$c_{P,16} = i_{P,BM}$
$c_{N,17} = -i_{N,BM} / Y_{PHA}^{O}$	$c_{P,17} = -i_{P,BM} / Y_{PHA}^{O}$
$c_{N,18} = i_{N,BM} / Y_{PP}^{O}$	$c_{P,18} = i_{P,BM} / Y_{PP}^{O} - 1$
$c_{N,19} = i_{N,BM} / Y_{GLY}^{O}$	$c_{P,19} = i_{P,BM} / Y_{GLY}^{O}$
$c_{N,20} = i_{N,BM}$	$c_{P,20} = i_{P,BM}$
$c_{N,21} = -i_{N,BM} - 1/Y_A$	$c_{P,21} = -i_{P,BM}$
$c_{N,22} = i_{N,BM} - i_{N,XI} \cdot f_{XI,A} - i_{N,XS} \cdot (1 - f_{XI,A})$	$c_{P,22} = i_{P,BM} - i_{P,XI} \cdot f_{XI,A} - i_{P,XS} \cdot (1 - f_{XI,A})$

Table 3a. Stoichiometric coefficients for S_{NH} and S_{PO}.

S_{HCO} (mole·m^{-3})	X_{TSS} (g·m^{-3})
$c_{e,1} = c_{N,1}/14 - c_{P,1}\cdot(1.5/31)$	$c_{TSS,1} = -i_{TSS,XS}$
$c_{e,4} = c_{N,4}/14 - c_{P,4}\cdot(1.5/31)$	$c_{TSS,4} = i_{TSS,BM}$
$c_{e,5} = c_{N,5}/14 - c_{P,5}\cdot(1.5/31) + 1/(64\cdot Y_H)$	$c_{TSS,5} = i_{TSS,BM}$
$c_{e,6} = c_{N,6}/14 - c_{P,6}\cdot(1.5/31) + (1/Y_H - 1)/(14\cdot 2.86)$	$c_{TSS,6} = i_{TSS,BM}$
$c_{e,7} = c_{N,7}/14 - c_{P,7}\cdot(1.5/31) + (1/Y_H - 1)/(14\cdot 2.86) + 1/(64\cdot Y_H)$	$c_{TSS,7} = i_{TSS,BM}$
$c_{e,8} = c_{N,8}/14 - c_{P,8}\cdot(1.5/31) - 1/64$	$c_{TSS,8} = 0$
$c_{e,9} = c_{N,9}/14 - c_{P,9}\cdot(1.5/31)$	$c_{TSS,9} = i_{TSS,XI}\cdot f_{XI,H} + i_{TSS,XS}\cdot(1-f_{XI,H}) - i_{TSS,BM}$
$c_{e,10} = -Y_{PO}^{AN}\cdot(1.5/31) + 1/64 + Y_{PO}^{AN}/31$	$c_{TSS,10} = i_{TSS,PP}\cdot(-Y_{PO}^{AN}) + i_{TSS,PHA}\cdot Y_{SA}^{AN} + i_{TSS,GLY}\cdot(1-Y_{SA}^{AN})$
$c_{e,11} = -1.5/31 + 1/31$	$c_{TSS,11} = -i_{TSS,PP}$
$c_{e,12} = -Y_{PO}^{NO}\cdot(1.5/31) + 1/64 + Y_{PO}^{NO}/31 + \left(1-Y_{SA}^{NO}\right)/(14\cdot 2.86)$	$c_{TSS,12} = i_{TSS,PP}\cdot(-Y_{PO}^{NO}) + i_{TSS,PHA}\cdot Y_{SA}^{NO}$
$c_{e,13} = c_{N,13}/14 - c_{P,13}\cdot(1.5/31) - (1/Y_{PHA}^{NO} - 1)/(14\cdot 2.86)$	$c_{TSS,13} = i_{TSS,BM}/Y_{PHA}^{NO} - i_{TSS,PHA}$
$c_{e,14} = c_{N,14}/14 - c_{P,14}\cdot(1.5/31) + 1/(14\cdot 2.86\cdot Y_{PP}^{NO}) - 1/31$	$c_{TSS,14} = -i_{TSS,BM}/Y_{PP}^{NO} + i_{TSS,PP}$
$c_{e,15} = c_{N,15}/14 - c_{P,15}\cdot(1.5/31) + (1/Y_{GLY}^{NO} - 1)/(14\cdot 2.86)$	$c_{TSS,15} = -i_{TSS,BM}/Y_{GLY}^{NO} + i_{TSS,GLY}$
$c_{e,16} = c_{N,16}/14 - c_{P,16}\cdot(1.5/31) + 1/(14\cdot 2.86)$	$c_{TSS,16} = -i_{TSS,BM}$
$c_{e,17} = c_{N,17}/14 - c_{P,17}\cdot(1.5/31)$	$c_{TSS,17} = i_{TSS,BM}/Y_{PHA}^{O} - i_{TSS,PHA}$
$c_{e,18} = c_{N,18}/14 - c_{P,18}\cdot(1.5/31) - 1/31$	$c_{TSS,18} = -i_{TSS,BM}/Y_{PP}^{O} + i_{TSS,PP}$
$c_{e,19} = c_{N,19}/14 - c_{P,19}\cdot(1.5/31)$	$c_{TSS,19} = -i_{TSS,BM}/Y_{GLY}^{O} + i_{TSS,GLY}$
$c_{e,20} = c_{N,20}/14 - c_{P,20}\cdot(1.5/31)$	$c_{TSS,20} = -i_{TSS,BM}$
$c_{e,21} = c_{N,21}/14 - c_{P,21}\cdot(1.5/31) - 1/(14\cdot Y_A)$	$c_{TSS,21} = -i_{TSS,BM}$
$c_{e,22} = c_{N,22}/14 - c_{P,22}\cdot(1.5/31)$	$c_{TSS,22} = i_{TSS,XI}\cdot f_{XI,A} + i_{TSS,XS}\cdot(1-f_{XI,A}) - i_{TSS,BM}$

Table 3b. Stoichiometric coefficients for S_{HCO} and X_{TSS}.

Table 4. Component composition factors belonging to the composition matrix (table 1, bottom).

Component composition factors i_N, i_P and i_{TSS}					
1	Nitrogen content of inert soluble COD, S_I	$i_{N,SI}$	0.01	$gN \cdot g^{-1}COD_{SI}$	Henze *et al.*, 1999; ASM2d
2	Nitrogen content of soluble substrate, S_F	$i_{N,SF}$	0.03	$gN \cdot g^{-1}COD_{SF}$	"
3	Nitrogen content of inert particulate COD, X_I	$i_{N,XI}$	0.03	$gN \cdot g^{-1}COD_{XI}$	This thesis
4	Nitrogen content of particulate substrate, X_S	$i_{N,XS}$	0.03	$gN \cdot g^{-1}COD_{XS}$	Henze *et al.*, 1999; ASM2d
5	Nitrogen content of biomass, X_H, X_{PAO}, X_{AUT}	$i_{N,BM}$	0.07	$gN \cdot g^{-1}COD_{BM}$	"
6	Phosphorus content of inert soluble COD, S_I	$i_{P,SI}$	0	$gP \cdot g^{-1}COD_{SI}$	"
7	Phosphorus content of soluble substrate, S_F	$i_{P,SF}$	0.01	$gP \cdot g^{-1}COD_{SF}$	"
8	Phosphorus content of inert particulate COD, X_I	$i_{P,XI}$	0.01	$gP \cdot g^{-1}COD_{XI}$	"
9	Phosphorus content of particulate substrate, X_S	$i_{P,XS}$	0.01	$gP \cdot g^{-1}COD_{XS}$	"
10	Phosphorus content of biomass, X_H, X_{PAO}, X_{AUT}	$i_{P,BM}$	0.02	$gP \cdot g^{-1}COD_{BM}$	"
11	Ratio Total Suspended Solids to X_I	$i_{TSS,XI}$	0.75	$gTSS \cdot g^{-1}COD_{XI}$	"
12	Ratio Total Suspended Solids to X_S	$i_{TSS,XS}$	0.75	$gTSS \cdot g^{-1}COD_{XS}$	"
13	Ratio Total Suspended Solids to biomass X_H, X_{PAO}, X_{AUT} $(CH_{2.09}O_{0.54}N_{0.2}P_{0.015})_n$	$i_{TSS,BM}$	0.90	$gTSS \cdot g^{-1}COD_{BM}$	Smolders *et al.*, 1994b
14	Ratio Total Suspended Solids to X_{PP} $(Mg^{2+}_{1/3}K^{+}_{1/3}PO_3)_n$	$i_{TSS,PP}$	3.23	$gTSS \cdot g^{-1}P_{PP}$	Smolders *et al.*, 1994a
15	Ratio Total Suspended Solids to X_{PHA} $(C_4H_6O_2)_{1/4}$	$i_{TSS,PHA}$	0.6	$gTSS \cdot g^{-1}COD_{PHA}$	Doi, 1990
16	Ratio Total Suspended Solids to X_{GLY} $(C_6H_{10}O_5)_{1/6}$	$i_{TSS,GLY}$	0.84	$gTSS \cdot g^{-1}COD_{GLY}$	Stryer, 1975
17	Ratio COD to Oxygen (S_O)	$i_{COD,O}$	-1	$gCOD \cdot g^{-1}O_2$	
18	Ratio COD to Nitrate (S_{NO})	$i_{COD,NO}$	-2.86	$gCOD \cdot g^{-1}N_{SNO}$	

Table 5. Stoichiometric parameters.

Hydrolysis of Particulate Substrate					
1	Fraction of inert COD generated in hydrolysis	f_{SI}	0	$gCOD_{SI} \cdot g^{-1}COD_{(XH+XPAO)}$	Henze *et al.*, 1999; ASM2d
Regular Heterotrophic Organisms X_H					
1	Heterotrophic yield for growth on substrate	Y_H	0.63	$gCOD_{XH} \cdot g^{-1}COD$	"
2	Fraction of inert COD generated in biomass lysis	$f_{XI,H}$	0.10	$gCOD_{XI} \cdot g^{-1}COD_{XH}$	"
Autotrophic Nitrifying Organisms X_A					
1	Autotrophic yield for growth	Y_A	0.24	$gCOD_{XA} \cdot g^{-1}N_{SNH}$	"
2	Fraction of inert COD generated in biomass lysis	$f_{XI,A}$	0.10	$gCOD_{XI} \cdot g^{-1}COD_{XA}$	"
Phosphorus Accumulating Organisms X_{PAO}					
1	ATP produced per NADH or P/O ratio	δ	1.85	mole ATP·mole^{-1}NADH	Smolders *et al.*, 1994b
2	Observed biomass ratio TOC over COD	α	0.334	$gC_{PAO} \cdot g^{-1}COD_{PAO}$	"
4	Anaerobic yield for phosphate release	Y_{PO}^{AN}	$0.184 \times pH - 0.94 \approx 0.35$	$gP_{SPO} \cdot g^{-1}COD_{SA}$	Smolders *et al.*, 1994a
5	Yield for anaerobic formation of PHA from S_A	Y_{SA}^{AN}	1.50	$gCOD_{PHB} \cdot g^{-1}COD_{SA}$	"
6	Observed yield for anoxic phosphate release	Y_{PO}^{NO}	0.23	$gP_{SPO} \cdot g^{-1}COD_{SA}$	Kuba *et al.*, 1994
7	Yield for anoxic formation of PHA from S_A	Y_{SA}^{NO}	$\frac{(8.3 \cdot Y_{PO}^{NO} - 4.9 + 8 \cdot \delta)}{9 \cdot \delta} \approx 0.71$	$g\ COD_{PHB} \cdot g^{-1}COD_{SA}$	This thesis
8	Anoxic yield for degradation of X_{PHB}	Y_{PHA}^{NO}	$\frac{19 + 3 \cdot \delta/\alpha}{4 + 9 \cdot \delta} \approx 1.72$	$g\ COD_{PHB} \cdot g^{-1}COD_{PAO}$	+* Murnleitner *et al.*, 1997
9	Anoxic yield for formation of X_{GLY}	Y_{GLY}^{NO}	$\frac{12.6 + 2 \cdot \delta/\alpha}{9 + 6 \cdot \delta} \approx 1.18$	$g\ COD_{GLY} \cdot g^{-1}COD_{PAO}$	"
10	Anoxic yield for formation of X_{PP}	Y_{PP}^{NO}	$\frac{57 + 9 \cdot \delta/\alpha}{28 + 4 \cdot \delta} \approx 3.02$	$g\ P_{PP} \cdot g^{-1}COD_{PAO}$	"
11	Aerobic yield for degradation of X_{PHB}	Y_{PHA}^{O}	$\frac{9.4 + 3 \cdot \delta/\alpha}{2 + 9 \cdot \delta} \approx 1.39$	$g\ COD_{PHB} \cdot g^{-1}COD_{PAO}$	+ Murnleitner *et al.*, 1997
12	Aerobic yield for formation of X_{GLY}	Y_{GLY}^{O}	$\frac{12.6 + 4 \cdot \delta/\alpha}{9 + 12 \cdot \delta} \approx 1.11$	$g\ COD_{GLY} \cdot g^{-1}COD_{PAO}$	"
13	Aerobic yield for formation of X_{PP}	Y_{PP}^{O}	$\frac{57 + 18 \cdot \delta/\alpha}{28 + 4 \cdot \delta} \approx 4.42$	$g\ P_{PP} \cdot g^{-1}COD_{PAO}$	+* Murnleitner *et al.*, 1997

* Parameters containing typesetting errors in *Henze et al.*, 1999 (ASM2d).
+ Parameters containing rounding errors in Murnleitner *et al.* (1996) and van Veldhuizen *et al.* (1999).

Table 6a. Kinetic parameters for Hydrolysis, X_H and X_A.

Hydrolysis of Particulate Substrate					
1	Hydrolysis rate [(T)]	k_h	$3.0 \times e^{(0.0406 \cdot (T-20))}$	$gCOD_{XS} \cdot g^{-1}COD_{(XH+XPAO)} \cdot d^{-1}$	Henze *et al.*, 1999; ASM2d
2	Anoxic hydrolysis reduction factor	η_{NO}	0.8	-	This thesis
3	Anaerobic hydrolysis reduction factor	η_{fe}	0.2	-	Henze *et al.*, 1999; ASM2d
4	Saturation / inhibition coefficient for oxygen	K_O	0.2	$gO_2 \cdot m^{-3}$	"
5	Saturation / inhibition coefficient for nitrate	K_{NO}	0.5	$gN_{SNO} \cdot m^{-3}$	"
6	Saturation coefficient for particulate COD [(T)]	K_X	$0.1 \times e^{(-0.110 \cdot (T-20))}$	$gCOD_{XS} \cdot g^{-1}COD_{(XH+XPAO)}$	"
Heterotrophic Micro-Organism's X_H					
1	Maximum heterotrophic growth rate [(T)]	μ_H	$6.0 \times e^{(0.069 \cdot (T-20))}$	$gCOD_{XH} \cdot g^{-1}COD_{XH} \cdot d^{-1}$	"
2	Maximum fermentation rate [(T)]	q_{fe}	$3.0 \times e^{(0.069 \cdot (T-20))}$	$gCOD_{SF} \cdot g^{-1}COD_{XH} \cdot d^{-1}$	"
3	Heterotrophic decay rate [(T)]	b_H	$0.4 \times e^{(0.069 \cdot (T-20))}$	$gCOD_{XH} \cdot g^{-1}COD_{XH} \cdot d^{-1}$	"
4	Reduction factor for denitrification	η_{NO}	0.8	-	"
5	Saturation / inhibition coefficient for oxygen	K_O	0.2	$gO_2 \cdot m^{-3}$	"
6	Saturation coefficient for growth on S_F	K_F	4.0	$gCOD_{SF} \cdot m^{-3}$	"
7	Saturation coefficient for fermentation of S_F	K_{fe}	20.0	$gCOD_{SF} \cdot m^{-3}$	* Gujer *et al.*, 1995; ASM2
8	Saturation coefficient for growth on Acetate	K_{Ac}	4.0	$gCOD_{SA} \cdot m^{-3}$	Henze *et al.*, 1999; ASM2d
9	Saturation / inhibition coefficient for nitrate	K_{NO}	0.5	$gN_{SNO} \cdot m^{-3}$	"
10	Saturation coef. for Ammonium (nutrient)	K_N	0.05	$gN_{SNH} \cdot m^{-3}$	"
11	Saturation coefficient for Phosphate (nutrient)	K_P	0.01	$gP_{SPO} \cdot m^{-3}$	"
12	Saturation coefficient for alkalinity (HCO_3^-)	K_{HCO}	0.1	$moleHCO_3^- \cdot m^{-3}$	"
Autotrophic Micro-Organism's X_A					
1	Autotrophic growth rate [(T)]	μ_A	$1.0 \times e^{(0.105 \cdot (T-20))}$	$gCOD_{XA} \cdot g^{-1}COD_{XA} \cdot d^{-1}$	"
2	Autotrophic decay rate [(T)]	b_A	$0.15 \times e^{(0.110 \cdot (T-20))}$	$gCOD_{XA} \cdot g^{-1}COD_{XA} \cdot d^{-1}$	"
3	Saturation coefficient for oxygen	$K_{A,O}$	0.5	$gO_2 \cdot m^{-3}$	"
4	Saturation coefficient for Ammonium	K_{NH}	1.0	$gN_{SNH} \cdot m^{-3}$	"
5	Saturation coefficient for Phosphate (nutrient)	K_P	0.01	$gP_{SPO} \cdot m^{-3}$	"
6	Saturation coefficient for alkalinity (HCO_3^-)	K_{HCO}	0.5	$moleHCO_3^- \cdot m^{-3}$	"

[(T)] Temperature dependant parameters and their reference.
* Parameters containing typesetting errors in *Henze et al.*, 1999 (ASM2d).

Table 6b. Kinetic parameters for X_{PAO}.

Phosphorus Accumulating Organisms X_{PAO}					
1	Maximum anaerobic acetate uptake rate (T)	q_{Ac}	$8.0 \times e^{(0.090 \cdot (T-20))}$	$gCOD_{SA} \cdot g^{-1}COD_{PAO} \cdot d^{-1}$	This thesis; (T) Brdjanovic et al., 1998
2	Anaerobic maintenance rate (T)	m_{AN}	$0.05 \times e^{(0.069 \cdot (T-20))}$	$gP_{PP} \cdot g^{-1}COD_{PAO} \cdot d^{-1}$	Smolders et al., 1995; (T) Murnleitner et al.. 1997
3	Maximum anoxic acetate uptake rate (T)	q_{Ac}^{NO}	$1.5 \cdot q_{Ac} \times e^{(0.090 \cdot (T-20))}$	$gCOD_{SA} \cdot g^{-1}COD_{PAO} \cdot d^{-1}$	Kuba et al., 1994; (T) Brdjanovic et al., 1998
4	PHA degradation rate (T)	k_{PHA}	$5.51 \times e^{(0.121 \cdot (T-20))}$	$gCOD_{PHA} \cdot g^{-1}COD_{PAO} \cdot d^{-1}$	This thesis; (T) Brdjanovic et al., 1998
5	Glycogen formation rate (T)	k_{GLY}	$0.93 \times e^{(0.118 \cdot (T-20))}$	$gCOD_{GLY} \cdot g^{-1}COD_{PAO} \cdot d^{-1}$	This thesis
6	Poly-phosphate formation rate (T)	k_{PP}	$0.10 \times e^{(0.031 \cdot (T-20))}$	$gP_{PP} \cdot g^{-1}COD_{PAO} \cdot d^{-1}$	Murnleitner et al., 1997; (T) Brdianovic et al.. 1998
7	Observed oxygen consumption for	m_{OC}	0.096	$gO_2 \cdot g^{-1}COD_{PAO} \cdot d^{-1}$	Smolders *et al.*, 1994b
8	Aerobic maintenance rate (T)	m_O	$\frac{3 \cdot \delta \cdot m_{OC}}{3.2 + \delta/\alpha} \approx 0.06 \times e^{(0.069 \cdot (T-20))}$	$gCOD_{PAO} \cdot g^{-1}COD_{PAO} \cdot d^{-1}$	+° Murnleitner et al., 1997
9	Anoxic maintenance rate (T)	m_{NO}	$\frac{6 \cdot \delta \cdot m_{OC}}{6.3 + \delta/\alpha} \approx 0.09 \times e^{(0.069 \cdot (T-20))}$	$gCOD_{PAO} \cdot g^{-1}COD_{PAO} \cdot d^{-1}$	‘’
10	Saturation reduction factor for PP formation	g_{PP}	0.22	-	Murnleitner *et al.*, 1997
11	Reduction factor for denitrifying P removal	η_{NO}	0.8	-	This thesis
12	Saturation coefficient for poly-P formation	K_{PO}	1.0	$gP_{SPO} \cdot m^{-3}$	‘’
13	Saturation coefficient for growth on acetate	K_{Ac}	4.0	$gCOD_{SA} \cdot m^{-3}$	Henze *et al.*, 1999; ASM2d
14	Saturation / inhibition coefficient for nitrate	K_{NO}	0.5	$gN_{SNO} \cdot m^{-3}$	‘’
15	Saturation / inhibition coefficient for	K_O	0.2	$gO_2 \cdot m^{-3}$	‘’
16	Saturation coefficient for f_{PHA}	K_{fPH}	0.2	$gCOD_{PHA} \cdot g^{-1}COD_{PAO}$	This thesis
17	Saturation coeff. for Phosphate (nutrient)	K_P	0.02	$gP_{SPO} \cdot m^{-3}$	‘’
18	Saturation coefficient for NH_4 (nutrient)	K_N	0.05	$gN_{SNH} \cdot m^{-3}$	‘’
19	Maximum poly-phosphate fraction of PAO’s	$f_{...}^{max}$	0.35	$gP_{PP} \cdot g^{-1}COD_{PAO}$	Wentzel *et al.*, 1989
20	Maximum glycogen fraction of PAO’s	$f_{...}^{max}$	0.5	$gCOD_{GLY} \cdot g^{-1}COD_{PAO}$	Brdjanovic *et al.*, 1998
21	Saturation coefficient for poly-P	K_{PP}	0.01	$gP_{PP} \cdot m^{-3}$	Switch
22	Saturation coefficient for glycogen	K_{GLY}	0.01	$gCOD_{GLY} \cdot m^{-3}$	‘’
23	Saturation coefficient for PHA	K_{PHA}	0.01	$gCOD_{PHA} \cdot m^{-3}$	‘’
24	Saturation coefficient for f_{GLY}	$K_{fGL...}$	0.01	$gCOD_{GLY} \cdot g^{-1}COD_{PAO}$	‘’
25	Saturation coefficient for f_{PP}	K_{fPP}	0.01	$gCOD_{PP} \cdot g^{-1}COD_{PAO}$	‘’
26	Saturation coefficient for alkalinity (HCO_3^-)	K_{HCO}	0.01	$moleHCO_3^- \cdot m^{-3}$	‘’

+ Parameters containing rounding errors in Murnleitner *et al.* (1996) and van Veldhuizen *et al.* (1999).
° Parameters containing typesetting errors in van Veldhuizen *et al.* (1999).
(T) Temperature dependant parameters including their reference.

	Process	Kinetic Rate Equation ($r_?$)	Switch function (on / off)
Hydrolysis of Particulate Substrate X_S			
1	Aerobic Hydrolysis ($gCOD_{XS} \cdot d^{-1}$)	$r_h^O = k_h \cdot \frac{X_S/(X_H + X_{PAO})}{K_X + X_S/(X_H + X_{PAO})} \cdot (X_H + X_{PAO})$	
2	Anoxic Hydrolysis ($gCOD_{XS} \cdot d^{-1}$)	$r_h^{NO} = \eta_{NO} \cdot k_h \cdot \frac{X_S/(X_H + X_{PAO})}{K_X + X_S/(X_H + X_{PAO})} \cdot \frac{S_{NO}}{K_{NO} + S_{NO}} \cdot (X_H + X_{PAO})$	$\cdot \frac{K_O}{K_O + S_O}$
3	Anaerobic Hydrolysis ($gCOD_{XS} \cdot d^{-1}$)	$r_h^{AN} = \eta_{fe} \cdot k_h \cdot \frac{X_S/(X_H + X_{PAO})}{K_X + X_S/(X_H + X_{PAO})} \cdot (X_H + X_{PAO})$	$\cdot \frac{K_O}{K_O + S_O} \cdot \frac{K_{NO}}{K_{NO} + S_{NO}}$
Heterotrophic Micro-Organisms X_H			
4	Aerobic Growth on S_F ($gCOD_{XH} \cdot d^{-1}$)	$r_{SF}^O = \mu_H \cdot \frac{S_F}{S_A + S_F} \cdot \frac{S_F}{K_F + S_F} \cdot \frac{S_O}{K_O + S_O} \cdot X_H$	$\cdot \frac{S_{NH}}{K_N + S_{NH}} \cdot \frac{S_{PO}}{K_P + S_{PO}} \cdot \frac{S_{HCO}}{K_{HCO} + S_{HCO}}$
5	Aerobic Growth on S_A ($gCOD_{XH} \cdot d^{-1}$)	$r_{SA}^O = \mu_H \cdot \frac{S_A}{S_A + S_F} \cdot \frac{S_A}{K_A + S_A} \cdot \frac{S_O}{K_O + S_O} \cdot X_H$	$\cdot \frac{S_{NH}}{K_N + S_{NH}} \cdot \frac{S_{PO}}{K_P + S_{PO}} \cdot \frac{S_{HCO}}{K_{HCO} + S_{HCO}}$
6	Anoxic Growth on S_F ($gCOD_{XH} \cdot d^{-1}$)	$r_{SF}^{NO} = \eta_{NO} \cdot \mu_H \cdot \frac{S_F}{S_A + S_F} \cdot \frac{S_F}{K_F + S_F} \cdot \frac{S_{NO}}{K_{NO} + S_{NO}} \cdot X_H$	$\cdot \frac{K_O}{K_O + S_O} \cdot \frac{S_{NH}}{K_N + S_{NH}} \cdot \frac{S_{PO}}{K_P + S_{PO}} \cdot \frac{S_{HCO}}{K_{HCO} + S_{HCO}}$
7	Anoxic Growth on S_A ($gCOD_{XH} \cdot d^{-1}$)	$r_{SA}^{NO} = \eta_{NO} \cdot \mu_H \cdot \frac{S_A}{S_A + S_F} \cdot \frac{S_A}{K_A + S_A} \cdot \frac{S_{NO}}{K_{NO} + S_{NO}} \cdot X_H$	$\cdot \frac{K_O}{K_O + S_O} \cdot \frac{S_{NH}}{K_N + S_{NH}} \cdot \frac{S_{PO}}{K_P + S_{PO}} \cdot \frac{S_{HCO}}{K_{HCO} + S_{HCO}}$
8	Fermentation of S_F ($gCOD_{SF} \cdot d^{-1}$)	$r_{fe}^{AN} = q_{fe} \cdot \frac{S_F}{K_{fe} + S_F} \cdot X_H$	$\cdot \frac{K_O}{K_O + S_O} \cdot \frac{K_{NO}}{K_{NO} + S_{NO}} \cdot \frac{S_{HCO}}{K_{HCO} + S_{HCO}}$
9	Heterotrophic Lysis ($gCOD_{XH} \cdot d^{-1}$)	$r_{HL} = b_H \cdot X_H$	

Table 7a. Kinetic rate equations.

	Process	Kinetic Rate Equation ($r_?$)	Switch function (on / off)
Phosphorus Accumulating Organisms X_{PAO}			
10	Anaerobic storage of S_A ($gCOD_{SA} \cdot d^{-1}$)	$r_{SA}^{AN} = q_{Ac} \cdot \frac{S_A}{K_A + S_A} \cdot X_{PAO}$	$\cdot \frac{K_O}{K_O + S_O} \cdot \frac{K_{NO}}{K_{NO} + S_{NO}} \cdot \frac{X_{GLY}}{K_{GLY} + X_{GLY}} \cdot \frac{X_{PP}}{K_{PP} + X_{PP}}$
11	Anaerobic Maintenance ($gP \cdot d^{-1}$)	$r_M^{AN} = m_{AN} \cdot X_{PAO}$	$\cdot \frac{K_O}{K_O + S_O} \cdot \frac{K_{NO}}{K_{NO} + S_{NO}} \cdot \frac{X_{PP}}{K_{PP} + X_{PP}}$
12	Anoxic storage of S_A ($gCOD_{SA} \cdot d^{-1}$)	$r_{SA}^{NO} = q_{Ac}^{NO} \cdot \frac{S_A}{K_A + S_A} \cdot \frac{S_{NO}}{K_{NO} + S_{NO}} \cdot X_{PAO}$	$\cdot \frac{K_O}{K_O + S_O} \cdot \frac{X_{PP}}{K_{PP} + X_{PP}}$
13	Anoxic PHA consumption ($gCOD_{XPHA} \cdot d^{-1}$)	$r_{PHA}^{NO} = \eta_{NO} \cdot k_{PHA} \cdot \frac{X_{PHA}/X_{PAO}}{K_{fPHA} + X_{PHA}/X_{PAO}} \cdot \frac{S_{NO}}{K_{NO} + S_{NO}} \cdot X_{PAO}$	$\cdot \frac{K_O}{K_O + S_O} \cdot \frac{S_{NH}}{K_N + S_{NH}} \cdot \frac{S_{PO}}{K_P + S_{PO}} \cdot \frac{S_{HCO}}{K_{HCO} + S_{HCO}}$
14	Anoxic storage of PP ($gP \cdot d^{-1}$)	$r_{PP}^{NO} = \eta_{NO} \cdot k_{PP} \cdot \frac{X_{PAO}}{X_{PP}} \cdot \frac{S_{PO}}{K_{PO} + S_{PO}} \cdot \frac{S_{NO}}{g_{PP} \cdot K_{NO} + S_{NO}} \cdot X_{PAO}$	$\cdot \frac{K_O}{K_O + S_O} \cdot \frac{X_{PHA}}{K_{PHA} + X_{PHA}} \cdot \frac{f_{PP}^{max} - X_{PP}/X_{PAO}}{K_{fPP} + (f_{PP}^{max} - X_{PP}/X_{PAO})}$
15	Anoxic Glycogen formation ($gCOD_{XGLY} \cdot d^{-1}$)	$r_{GLY}^{NO} = \eta_{NO} \cdot k_{GLY} \cdot \frac{X_{PHA}}{X_{GLY}} \cdot \frac{S_{NO}}{K_{NO} + S_{NO}} \cdot X_{PAO}$	$\cdot \frac{K_O}{K_O + S_O} \cdot \frac{X_{PHA}}{K_{PHA} + X_{PHA}} \cdot \frac{f_{GLY}^{max} - X_{GLY}/X_{PAO}}{K_{fGLY} + (f_{GLY}^{max} - X_{GLY}/X_{PAO})}$
16	Anoxic Maintenance ($gCOD_{XPAO} \cdot d^{-1}$)	$r_M^{NO} = m_{NO} \cdot \frac{S_{NO}}{K_{NO} + S_{NO}} \cdot X_{PAO}$	$\cdot \frac{K_O}{K_O + S_O}$
17	Aerobic PHA consumption ($gCOD_{XPHA} \cdot d^{-1}$)	$r_{PHA}^{O} = k_{PHA} \cdot \frac{X_{PHA}/X_{PAO}}{K_{fPHA} + X_{PHA}/X_{PAO}} \cdot \frac{S_O}{K_O + S_O} \cdot X_{PAO}$	$\cdot \frac{S_{NH}}{K_N + S_{NH}} \cdot \frac{S_{PO}}{K_P + S_{PO}} \cdot \frac{S_{HCO}}{K_{HCO} + S_{HCO}}$
18	Aerobic storage of PP ($gP \cdot d^{-1}$)	$r_{PP}^{O} = k_{PP} \cdot \frac{X_{PAO}}{X_{PP}} \cdot \frac{S_{PO}}{K_{PO} + S_{PO}} \cdot \frac{S_O}{g_{PP} \cdot K_O + S_O} \cdot X_{PAO}$	$\cdot \frac{X_{PHA}}{K_{PHA} + X_{PHA}} \cdot \frac{f_{PP}^{max} - X_{PP}/X_{PAO}}{K_{fPP} + (f_{PP}^{max} - X_{PP}/X_{PAO})}$
19	Aerobic Glycogen formation ($gCOD_{XGLY} \cdot d^{-1}$)	$r_{GLY}^{O} = k_{GLY} \cdot \frac{X_{PHA}}{X_{GLY}} \cdot \frac{S_O}{K_O + S_O} \cdot X_{PAO}$	$\cdot \frac{X_{PHA}}{K_{PHA} + X_{PHA}} \cdot \frac{f_{GLY}^{max} - X_{GLY}/X_{PAO}}{K_{fGLY} + (f_{GLY}^{max} - X_{GLY}/X_{PAO})}$
20	Aerobic Maintenance ($gCOD_{XPAO} \cdot d^{-1}$)	$r_M^{O} = m_O \cdot \frac{S_O}{K_O + S_O} \cdot X_{PAO}$	
Autotrophic Nitrifying Organisms X_A			
21	Autotrophic growth ($gCOD_{XA} \cdot d^{-1}$)	$r_A^{O} = \mu_A \cdot \frac{S_{NH}}{K_{NH} + S_{NH}} \cdot \frac{S_O}{K_O + S_O} \cdot X_A$	$\cdot \frac{K_{PO}}{K_P + S_{PO}}$
22	Autotrophic Lysis ($gCOD_{XA} \cdot d^{-1}$)	$r_{AL} = b_A \cdot X_A$	

Table 7b. Kinetic rate equations.

Table 6c. Kinetic parameters used for the simulation of lab-scale A2 and A/O SBR systems.

Phosphorus Accumulating Organisms X_{PAO}					
1[a]	Maximum anaerobic acetate uptake rate [(T)] A/O SBR system	q_{Ac}	$9.67 \times e^{(0.090 \cdot (T-20))}$	$gCOD_{SA} \cdot g^{-1}COD_{PAO} \cdot d^{-1}$	Smolders *et al.*, 1995b; [(T)] Brdjanovic *et al.*, 1998
1[b]	Maximum anaerobic acetate uptake rate [(T)] A2 SBR system	q_{Ac}	$4.3 \times e^{(0.090 \cdot (T-20))}$	$gCOD_{SA} \cdot g^{-1}COD_{PAO} \cdot d^{-1}$	Kuba *et al.*, 1996; [(T)] Brdjanovic *et al.*, 1998
1[c]	Maximum anaerobic acetate uptake rate [(T)] best fit A2 and A/O SBR system	q_{Ac}	$6.4 \times e^{(0.090 \cdot (T-20))}$	$gCOD_{SA} \cdot g^{-1}COD_{PAO} \cdot d^{-1}$	Murnleitner *et al.*, 1997; [(T)]Brdjanovic *et al.*, 1998
1[d]	Maximum anaerobic acetate uptake rate [(T)] best fit lab- and full-scale conditions	q_{Ac}	$8.0 \times e^{(0.090 \cdot (T-20))}$	$gCOD_{SA} \cdot g^{-1}COD_{PAO} \cdot d^{-1}$	This thesis; [(T)] Brdjanovic et al., 1998
2	Glycogen formation rate [(T)] best fit A2 and A/O SBR system	k_{GLY}	$5.83 \times e^{(0.118 \cdot (T-20))}$	$gCOD_{GLY} \cdot g^{-1}COD_{PAO} \cdot d^{-1}$	This thesis
3	Saturation coefficient for poly-P formation A2 and A/O SBR system	K_{PO}	3.1	$gP_{SPO} \cdot m^{-3}$	Murnleitner *et al.*, 1997
4	Saturation coefficient for growth on acetate A/O SBR system	K_{Ac}	32	$gCOD_{SA} \cdot m^{-3}$	Smolders et al., 1995a
5	Saturation / inhibition coefficient for nitrate A2 and A/O SBR system	K_{NO}	1.4	$gN_{SNO} \cdot m^{-3}$	Murnleitner *et al.*, 1997

Summary

Theoretical and Practical Aspects of Modelling Activated Sludge Processes

by S.C.F. Meijer

The main objective of activated sludge research is to understand and master the biological processes and interactions in activated sludge systems. For this purpose, a dynamic activated sludge model was developed. Models generally are used for research and educational purposes, to facilitate communication and allow the focusing on aspects of interest. Activated sludge models describe the physiology and ecological interactions of several groups of micro-organisms in an aquatic medium (the activated sludge). In practice, application of activated sludge models will facilitate the development of more efficient wastewater treatment processes.

In the field of domestic wastewater treatment, there is an increasing requirement to improve effluent quality for the benefit of receiving surface waters. Additionally, it is required to minimise energy consumption and reduce the use of chemicals in the treatment process. Research at the department of bio-engineering of the Delft university of technology has shown that biological phosphorus removal in wastewater treatment contributes to a more efficient nitrogen and phosphorus removal. Hereby energy consumption and the use of chemicals are reduced considerably. Since 1990, a metabolic model describing this process was developed. This largely was done in the framework of the task group for modelling activated sludge systems of the International Association for Water Quality (IAWQ). The metabolic model, is a mathematical description of the cell-internal metabolism of the total microbial population capable of biological phosphorus removal. In previous research it was shown that the metabolic modelling approach leads to a more consistent model with less model parameters.

In this particular research the focus was on the performance of the integrated metabolic BioP model at full-scale conditions. In previous publications, the model was tested on three full-scale wwtp's. Although the first results were promising, several questions arose concerning the reliability of the model, especially of the model kinetics. It was concluded that the applicability of the model was rather poor, and that a structured method for model calibration was required. Moreover, the necessity was shown for a method to organise, evaluate and correct large quantities of operational (input) data used for modelling.
To gain experience with the integrated model, the model was tested under a range of lab- and full-scale conditions. Hereby, a goal was to identify the bottlenecks in modelling full-scale wastewater treatment processes. A major bottleneck was the model calibration. It was intended to find a more straightforward and practical method to calibrate the model. Furthermore, a goal was to specify the model reliability, and make more explicit under which conditions and for what purposes the model should and should not be used. In the evaluation process, the model was refined were needed. Also possibilities were investigated to simplify and reduce the model and hereby improve the practical applicability of the model. Eventually, the goal was to improve the model as a tool for the development, design and optimisation of wastewater treatment plants.

Introducing the Metabolic BioP Model

Chapter 2 starts with a literature overview of the development of the metabolic BioP model. The metabolic model is rather different from other activated sludge models. Therefore the model structure and development is discussed in detail. Also the model stoichiometry and kinetics are discussed. The main purpose of this chapter is to give insight in the metabolic modelling concept, as this is required for a proper application. The chapter concludes by discussing the integration of the metabolic BioP with ASM2d. The integrated model will be further investigated in this research.

Simulating a Full-Scale WWTP at Steady-State

In chapter 3 a full-scale biological nutrient removing wastewater treatment process (WWTP) was simulated. The model output matched the data of the real WWTP with only minor parameter adjustments. A stepwise calibration method was proposed, in which three model parameters were calibrated. These parameters related to less accurate processes in the model. From the evaluation it was concluded that the modelled inert influent fraction and anoxic sludge fraction require calibration for each simulated

wastewater treatment process. Also it was observed that under steady state conditions the sensitivity of the model kinetics was low. This generally will apply to all WWTP's at (pseudo) steady state. Calibrating model kinetics under these conditions is therefore less accurate. Operational plant conditions were evaluated based on mass balance calculations. The phosphorus balance showed useful to evaluate the sludge retention time of the system. Because all compounds on the phosphorous balance can be recovered, errors in the operational data become apparent. Errors in operational data strongly effect the model reliability. This data therefore should be checked on consistency or be considered in model calibration.

Simulating the Start-up of a Full-Scale WWTP

In chapter 3, it was shown that wastewater treatment plants simulated at (pseudo) steady state have a low kinetic sensitivity. An increased sensitivity of the model kinetics was expected at start-up conditions. Therefore a full-scale start-up was evaluated in a simulation study. A kinetic sensitivity analysis showed that the model converged to identical steady states, disregarding the kinetic parameter values. This observation underlined that the BioP process is largely determined by stoichiometry. The sensitivity analysis showed that the glycogen formation rate and the temperature were most sensitive in the model. By including a temperature profile in the model, simulation results improved significantly. It was shown that in the metabolic model growth is mainly determined by the glycogen formation rate. By carefully fitting this process, good simulation results were obtained. The glycogen formation rate was found to be highly sensitive in the model. A maximum glycogen fraction was introduced to avoided model instability. With this practical adjustment, unrealistic accumulation of glycogen in the model could be avoided.

Introducing a Data Verification Procedure

Research on activated sludge modelling is mainly directed towards the estimation of model parameters. Model calculations however, rely heavily on accurate determination of operational conditions. This can be difficult, caused by large (full-scale) process flows and the absence of reliable measurements. Therefore, operational data should be verified on (gross) errors before being implemented in model studies. Calibrating a model on erroneous data leads to laborious calibration procedures and moreover, unjustified adaptation of the model (kinetic and stoichiometric) parameters. A simple method for gross error detection is evaluating the mass balance residuals. When there are more measurements than strictly

required to solve a system of linear conservation relations (mass balances), data accuracy can be improved using balancing methods. This is referred to as data reconciliation. A reconciled data set is more accurate and is exactly in line with the mass balances of the WWTP. In this chapter we describe a method for gross error detection and data reconciliation. In a case study it is shown how data reconciliation improves the accuracy of the data set and how the use of a balanced data set simplifies the model calibration.

Model Validation

In chapter 6, the integrated model is evaluated on the basis of a number of lab-scale experiments. This evaluation shows that the integrated metabolic model is suited to describe the concentration dynamics of a wide range of lab-scale SBR and batch experiments using a single set of model parameter values. The full-scale performance of the TUD model, investigated in several previous studies is discussed. Several model improvements were proposed, which are incorporated in the TUD model in this chapter. The major adjustment relates to the glycogen formation kinetics. It is shown that the proposed kinetic equation improves the model performance and simplifies the use of the model. The chapter concludes by discussing some model limitations and modelling considerations.

A Case Study; Model Based Process Control Design

In chapters 7 and 8 the validated model is used for the development of a control strategy. The introduction of enhanced biological phosphorus removal in conventional wastewater treatment plants requires specific process design and control to assure process stability. In literature there is a general tendency to more complex control strategies and measurements. In practice however, simple controls and measurements are preferred. A frequently applied control measurement is the Oxidation-Reduction-Potential (ORP). The physical meaning of the ORP measured in activated sludge is however not completely understood. This complicates the determination of appropriate ORP controller set-points. Moreover, drift of ORP measurements in activated sludge is commonly observed. From literature it is concluded that the problems concerning drift and set-point determination are related, and inherent to ORP measurements in activated sludge. Set-point related ORP control of activated sludge processes therefore is less reliable. In chapter 8 this is illustrated in a case study. From the case study it was concluded that the first order time derivative of the ORP signal can be used to detect depletion and accumulation of

oxidative capacity in activated sludge. Based on the sign of the first order time derivative of the ORP signal, a feedback control strategy was developed. The control regulated the internal recycle flows of a nutrient removing wastewater treatment plant. The performance of this control was first evaluated in a simulation study, after which it was tested at full-scale. As predicted from the simulations, the full-scale control reduced recycle pumping energy without loss of effluent quality.

Samenvatting

Theoretische en Praktische Aspecten van het Modelleren van Actief-Slibprocessen

door S.C.F. Meijer

Door een verscherpte regelgeving betreffende lozingen op oppervlaktewater is er sprake van een toenemende vraag naar rioolwaterzuiveringsinstallaties met een verbeterde effluentkwaliteit. Een aanvullende eis is dat het energieverbruik en de toediening van chemicaliën voor het zuiveren van rioolwater worden geminimaliseerd. Onderzoek aan de vakgroep Bioprocestechnologie van de Technische Universiteit Delft heeft uitgewezen dat met denitrificerende biologische fosfaatverwijdering een beter effluent kan worden verkregen, terwijl tegelijkertijd minder energie en chemicaliën worden gebruikt. Sinds 1990 wordt in deze onderzoeksgroep gewerkt aan de ontwikkeling van een metabool model van het biologische fosfaatverwijderingsproces (het BioP proces). Middels het modelonderzoek kan een beter begrip worden verkregen van de biologische omzettingen die plaats vinden in de zogenaamde actief-slibsuspensie in rioolwaterzuiveringen. Het onderzoek is grotendeels uitgevoerd in samenwerking met de IAWQ (International Association for Water Quality, het huidige IWA).

Het metabole model voor biologische fosfaatverwijdering is een mathematische beschrijving van het celinterne metabolisme van BioP bacteriën. In eerder onderzoek is aangetoond dat een metabole beschrijving van het BioP proces leidt tot een compacter en meer consistent model dan bij een reguliere (black box) modellering. Het metabole model is ontwikkeld op basis van laboratoriumexperimenten. Om het model ook in de praktijk toe te kunnen passen is in dit onderzoek het model getest op een aantal rioolwaterzuiveringsinstallaties (rwzi's). Het doel van het onderzoek was om knelpunten te ondekken in de modellering. Een aspect dat hierbij is onderzocht, is de mogelijkheid procesdata te controleren op fouten. Een ander onderzoeksaspect was de kalibratie van

het model. De bestaande methodiek blijkt in de praktijk te ingewikkeld en omslachtig. Door een verbeterde kalibratie kan bovendien de betrouwbaarheid van het model worden verbeterd. Een meer algemeen doel van dit onderzoek was de modellering te structureren om zodoende de toepassing van het model te vergemakkelijken.

Een beschrijving van het metabole modelleringsconcept

In het tweede hoofdstuk van dit proefschrift wordt de ontwikkeling van het metabole model beschreven. Het metabole modelleringsconcept wijkt sterk af van de reguliere actief-slibmodellering. Het is bovendien nodig om enige kennis van de modelstructuur te hebben alvorens het model kan worden toegepast. Het hoofdstuk begint met een overzicht van de eerdere publicaties op het gebied van metabole BioP modellering. Vervolgens wordt de modelstructuur besproken. Hierbij komt zowel de modelstoichiometrie als de modelkinetiek aan bod. Het hoofdstuk sluit af met een de beschrijving van de integratie van het BioP model met het actief-slibmodel (ASM2). Dit geïntegreerde model is het onderwerp van het verdere onderzoek en is beschreven in appendix III van deze dissertatie.

Simulatie van een rwzi in een stabiele operationele toestand

In hoofdstuk 3 van dit proefschrift wordt de simulatie beschreven van een rioolwaterzuiveringsinstallatie (rwzi) in een stabiele operationele toestand. De studie betrof het zogenaamde MUCT proces. Dit is een nutriënten verwijderend proces dat is geoptimaliseerd voor denitrificerende biologische fosfaatverwijdering. Zonder grote aanpassingen van de modelparameters kon de rwzi worden gesimuleerd. Drie processen moesten aanvullend worden gekalibreerd. Dit was nodig om simultane nitrificatie en denitrificatie en de vorming van de inerte slibfractie te kunnen beschrijven. Uit deze studie is gebleken dat deze processen niet afdoende worden beschreven met de huidige actief-slibmodellen. Er kon worden geconcludeerd op basis van deze en eerdere studies dat de stoichiometrie van het model betrouwbaar is. Deze stoichiometrie, ontworpen aan de hand van laboratoriumexperimenten, kon zonder enige aanpassing worden toegepast voor de simulatie van praktijkschaal rwzi's. Uit de simulatie van een rwzi in een stabiele operationele toestand bleek dat onder deze condities de modelkinetiek minder gevoelig is. Een nauwkeurige evaluatie van deze kinetiek was hierdoor niet mogelijk. De studie toonde aan dat de nauwkeurigheid van operationele data, met name de slibleeftijd en het debiet van de interne processtromen, in grote mate de betrouwbaarheid van het model bepaalden. Dit vertaalde zich in een grote modelgevoeligheid

voor deze operationele (invoer-) data. In deze studie konden enkele fouten in de operationele data worden opgespoord middels de berekening van de fosfaatbalans. Deze balans kan in theorie altijd worden gesloten. Hierdoor worden fouten in de operationele data zichtbaar. Omdat dergelijke fouten de modeluitkomst sterk beïnvloeden, wordt aangeraden deze data te verifiëren. In het geval dat dit niet mogelijk is, wordt aanbevolen het model te kalibreren op basis van de minder betrouwbare operationele data, in plaats van de modelstoichiometrie en kinetiek te kalibreren.

Simulatie van een opstart van een praktijkschaal rwzi

In hoofdstuk 3 is aangetoond dat de kalibratie van de modelkinetiek op basis van een rioolwaterzuiveringproces in een stabiele operationele toestand niet goed mogelijk is. Het was de verwachting dat de kinetische modelgevoeligheid sterk zou toenemen tijdens een opstart van een rwzi. In hoofdstuk 4 is daarom een opstart bestudeerd van een praktijkschaal zuivering. In een periode van 140 dagen is gevolgd hoe het actief-slib uit een conventionele zuivering zich transformeerde naar een actief-slibsuspensie die het vermogen vertoonde op een biologische wijze fosfaat te verwijderen. Deze overgang is gesimuleerd met het BioP model. Tijdens een modelgevoeligheidsanalyse werd waargenomen dat, ondanks de ingestelde waardes van de modelkinetiek, het model naar een identieke stabiele toestand convergeerde. Deze waarneming onderschrijft de eerdere conclusie dat het BioP proces grotendeels wordt bepaald door de stoichiometrie. Uit dezelfde gevoeligheidsanalyse kwam naar voren dat de glycogeenvorming en de temperatuur de meest gevoelige parameters waren voor de beschrijving van de opstart. Door een temperatuurprofiel in de modellering op te nemen werd een veel betere simulatie verkregen. In deze studie is aangetoond dat de groei van BioP bacteriën in het metabole model voornamelijk wordt bepaald door de vormingsnelheid van glycogeen. Door deze snelheid nauwkeurig af te stellen, kon een goede simulatie worden verkregen. De glycogeenvormingsnelheid was echter zeer gevoelig in het model waardoor bij een verkeerde afstelling modelinstabiliteit kon ontstaan. Door de kinetische vergelijking voor de glycogeenvorming te begrenzen, kon dit worden voorkomen.

Foutdiagnostiek en evaluatie van de data

In hoofdstukken 3 en 4 is geconcludeerd dat de modelnauwkeurigheid sterk afhangt van de betrouwbaarheid van de operationele invoerdata. Deze data moeten daarom worden gecontroleerd op fouten. In hoofdstukken 3 en 4 is hiervoor een aanzet gegeven middels massabalansberekeningen. In hoofdsul 5 wordt een meer verfijnde

methode toegepast, gebaseerd op programmatuur voor data-evaluatie. De data-evaluatie methodiek is getest op een praktijkschaal rwzi. Het gebruik van de programmatuur vereiste een systematische organisatie van de benodigde operationele gegevens. In de praktijk bleek het hierdoor mogelijk optimaal gebruik te maken van de informatie uit de data. De extra tijd die moest worden geïnvesteerd in de data-evaluatie kon ruimschoots worden terugverdiend bij het kalibreren van het model aangezien het aanzienlijk lastiger is een model passend te maken op incorrecte meetgegevens. De evaluatie van de data is uitgevoerd op basis van verschillende massabalansberekeningen. Er werden hierbij meerdere inconsequenties gevonden in de dataset. Middels de voorgestelde methode bleek het goed mogelijk de dataset te balanceren. Na deze correctie verliep de kalibratie van het model aanzienlijk eenvoudiger. Bovendien kon de rioolwaterzuivering met een hogere nauwkeurigheid worden gesimuleerd.

Modelvalidatie

In hoofdstuk 6 wordt het BioP model geëvalueerd op basis van een aantal laboratoriumexperimenten. De simulatie van de experimenten toonde aan dat het model bruikbaar was voor de beschrijving van uiteenlopende condities. Hierbij hoefden de modelparameters niet te worden aangepast. Ook wordt in hoofdstuk 6 de effectiviteit van het model onder praktijkschaal-condities geëvalueerd. Dit gebeurt naar aanleiding van de bevindingen in dit proefschrift en voorafgaande publicaties. Op basis hiervan worden verschillende modelaanpassingen voorgesteld, waarvan de belangrijkste betrekking hebben op de glycogeenvormingskinetiek. Er wordt aangetoond dat met de voorgestelde kinetische verbeteringen de betrouwbaarheid en het gebruiksgemak van het model wordt verbeterd. Het hoofdstuk sluit af met een bespreking van een aantal tekortkomingen in het model.

Een voorbeeldstudie van de toepassing van het model voor het ontwerp van een procesregeling

In hoofdstukken 7 en 8 wordt het gevalideerde model gebruikt bij het ontwerp van een procesregeling. Om de groei van BioP bacteriën in een conventionele rioolwaterzuivering mogelijk te maken is een goede procesregeling nodig die de stabiliteit van de biologische fosfaatverwijdering kan waarborgen. In de wetenschappelijke literatuur zijn veel voorbeelden te vinden van regelstrategieën die zijn gebaseerd op ingewikkelde en kostbare metingen. In de praktijk is er echter behoefte aan betrouwbare regelingen die gebruik maken van simpele metingen. Om deze reden wordt vaak gebruikt gemaakt van regelingen op basis van de redox-

potentiaal. Dit is een eenvoudige en goedkope meting. De fysische betekenis van redox-metingen in actief-slib is echter niet geheel duidelijk. Het is hierdoor lastig de juiste instellingen (redox-setpoint) te kiezen voor de procesregeling. Ook wordt in de praktijk vaak een onverklaarbare verschuiving in de tijd waargenomen van het redox-signaal. Op basis van de wetenschappelijke literatuurstudie kan worden vastgesteld dat de problematiek rond het vaststellen van de regelaarinstellingen en de waargenomen potentiaalverschuiving zijn gerelateerd en worden veroorzaakt door hetzelfde fysische verschijnsel. Dit probleem lijkt inherent te zijn aan redox-metingen in actief-slib. De toepassing van redox-metingen voor procesbesturing is hierdoor minder betrouwbaar. In hoofdstuk 8 wordt dit aangetoond bij de evaluatie van de werking van een praktijkschaal rioolwaterzuivering bestuurd op basis van meerdere redox-metingen. Tijdens dezelfde evaluatie is gebleken dat de eerste orde tijdsafgeleide van het redox-signaal bruikbaar was om de toename of vermindering van oxidatieve capaciteit (bijvoorbeeld zuurstof en nitraat) in actief-slib vast te stellen. Gebruikmakend van dit afgeleide signaal is vervolgens een procesregeling ontworpen. Deze regeling was bedoeld om de interne recirculatiestromen in een rioolwaterzuivering te sturen. Deze regeling is gesimuleerd in het actief-slibmodel. Op basis van positieve simulatieresultaten is de regeling toegepast op de praktijkschaal zuivering. Zoals de simulaties voorspelden, kon een aanzienlijke energiebesparing worden gerealiseerd op het recirculatiedebiet.

Personalia

Sebastiaan (Bas) Carel Fred Meijer, de auteur van dit proefschrift, werd geboren op 5 februari 1969 te Leiden. Na het voltooien van het Havo aan het Haags Montessori Lyceum in 1986, een baan in de horeca in 1987, en het behalen van het Vwo-diploma aan de dag- en avondscholengemeenschap Boerhaave te Leiden, is hij in 1989 begonnen aan een studie Scheikunde aan de Rijksuniversiteit Leiden. In 1991 vond deze een vervolg in een studie Milieutechnologie aan de Landbouwuniversiteit Wageningen, alwaar hij in 1996 het ingenieurs-diploma heeft behaald. Het afstudeeronderzoek betrof een procesregeling voor een biologisch sulfide oxiderend systeem op basis van de Redox-potentiaal. Dit onderzoek werd gedeeltelijk uitgevoerd bij de vakgroep Meet-, regel- en systeemtechniek onder begeleiding van Pâques BV en Heineken Technical Services. In 1996, heeft de auteur tijdens een stage bij het waterschap Veluwe het Bio-Deniphoproces gemodelleerd zoals toegepast op de rioolwaterzuivering Ede. Na een korte carrière als taxichauffeur in de regio Leiden is de auteur in 1997 begonnen aan een promotieonderzoek aan de Technische Universiteit Delft. Het onderzoek betrof de modellering van de biologische zuivering van huishoudelijk afvalwater en werd uitgevoerd aan de vakgroep Bio-procestechnologie van de faculteit Technische Natuurwetenschappen. De inhoud van dit onderzoek is beschreven in deze dissertatie. Sinds september 2002 is Bas Meijer werkzaam als adviseur water en reststoffen bij het ingenieurs- en adviesbureau Grontmij NV in De Bilt. In deze hoedanigheid werkte hij in deeltijd bij het waterschap De Dommel en heeft hij het als gastdocent vak dynamische modellering gedoceerd aan het IHE te Delft.

Publicaties

Gedurende de carrière van Bas Meijer zijn verschillende publicaties verschenen van zijn hand en heeft hij een substantiële bijdrage geleverd aan publicaties van anderen. Dit zijn, in chronologische volgorde:

Janssen A. J. H., Meijer S. C. F., Bontsema J. and Lettinga G. (1998) Application of the redox potential for controlling a sulphide oxidising bio-reactor. Biotechnol. Bioeng. 60(2), 147-155.

Greben M. A., Meijer S. C. F, Van Veldhuizen H. M. and R. Schemen. (2000) Modelleren van biologische fosfaatverwijdering in rwzi Ursem. H2O 33(19) 99-101.

Van Veldhuizen H. M., Greben M. A., Meijer S. C. F. and Van Loosdrecht M. C. M. (2000) Application of models with biological phosphorus removal in activated sludge systems. Conference proceeding on Wastewater and EU-Nutrient Guidelines. 289p, 68-73.

Meijer S. C. F., van Loosdrecht M. C. M. and Heijnen J. J. (2001) Metabolic modelling of full-scale biological nitrogen and phosphorus removing WWTP's. Water Res. 35(11), 2711-2723.

Hao X., van Loosdrecht M. C. M., Meijer S. C. F., J. J. Heijnen and Qian Y. (2001a) Model Based Evaluation of denitrifying dephosphatation in a two-sludge system. J. of Envir. Engrg. 127(2), 112-118.

Hao X., van Loosdrecht M. C. M., Meijer S. C. F., J. J. Heijnen and Qian Y. (2001b) Model Based Evaluation of two BNR processes – UCT and A2N. Wat. Res. 35(12), 2851-2860.

Meijer S. C. F., van der Spoel H., Heijnen J. J. and van Loosdrecht M. C. M. (2001) error diagnostics and data reconciliation for activated sludge modelling using linear conservation relations. Activated Sludge Modelling Fifth Kollekolle Seminar, Denmark, 10- 12 September 2001, 193-204.

Meijer S. C. F., van der Spoel H., Susanti S., Heijnen J. J. and van Loosdrecht M. C. M. (2002a) Error diagnostics and data reconciliation for activated sludge modelling using mass balances. Water Sci. Technol. 25(6), 145-156.

Meijer S. C. F., van Loosdrecht M. C. M. and Heijnen J. J. (2002b) Oxidation-Reduction-Potential controlled biological nutrient removal. IWA Conference on Automation in Water Quality Monitoring, Vienna, Austria May 21-22, 2002, 271-280.

Meijer S. C. F., van Loosdrecht M. C. M. (2002c) Octrooi procesregeling voor biologische verwijdering van fosfaten en nitraten op basis van redox-potentiaalmetingen. (octrooinummer 165 893).

Meijer S. C. F., van Loosdrecht M. C. M. and Heijnen J. J. (2002d) Modelling the start-up of a full-scale biological nitrogen and phosphorus removing WWTP's. Water Res. 36, 4667-4682.

Meijer S. C. F., Majoor E., van der Wijk J., van Loosdrecht M. C. M. and Heijnen J. J. (submitted) Oxidation-Reduction-Potential controlled biological phosphorus and nitrogen removal.

Meijer S. C. F., van Hooff C. (2002) Het geheim van plaatbeluchting. H2O 35(25/26) 38-39.

Nawoord

Utrecht, 21 maart 2004

Voor u ligt het resultaat van vele dagen en nachtelijke uren werk. Medio 2002 was dit proefschrift bijna af. Nu, bijna twee jaar later schrijf ik dit nawoord. Morgen kan het naar de drukker worden gebracht (bedankt Ton). De afgelopen twee jaar zijn intensief geweest. Een nieuwe baan, nieuwe collega's, een nieuwe stad, een nieuw huis, samenwonen met Irenka, een detachering bij het waterschap, nog meer nieuwe collega's, en natuurlijk het proefschrift. Na het relatief rustige bestaan als onderzoeker in Delft heb ik dit ervaren als een ware achtbaan. Met name de laatste maanden, waarin ik het proefschrift heb afgerond, leken eindeloos. Terugblikkend op deze periode besef ik dat ik veel heb geleerd. Ik ziet het als een voorecht als ingenieur het vak te kunnen beoefenen waar ik al die jaren voor heb geleerd. Dat ik daarbij mijn ingewikkelde modellen niet (altijd) nodig heb en vaak toekan met gezond verstand en een stukje kladpapier was wel een verassing. Bij het ontwikkelen de onmisbare praktische kijk waren er altijd de collega's van Grontmij die mij op het rechte pad konden brengen. Daarvoor wil ik hen bedanken.

De periode in het Kluiverlaboratorium in Delft heb ik als zeer bijzonder ervaren. Dankzij de losse stijl van begeleiden door Mark en Sef was er altijd de ruimte zelf invulling te geven aan het onderzoek. Ook op momenten dat ik er zelf geen licht meer in zag, was daar altijd Sef met zijn immer optimistische en enthousiaste benadering en Mark met zijn nimmer aflatende stroom van ideeën. De werkbesprekingen met hen zal ik niet snel vergeten.

Graag wil ik al mijn oud-collega's bedanken voor de bijzonder prettige atmosfeer in het Kluyverlaboratorium en met name mijn kamergenoten Merle, Cristian en Antonio. Zonder de Zuid-Europese lunch in de universiteitsaula was mijn dag niet compleet.

Gedurende mijn jaren als promovendus was er altijd een warme belangstelling voor mijn wetenschappelijke vorderingen. Dit heeft bijgedragen aan mijn inspiratie en hiermee aan de kwaliteit van dit proefschrift. Graag wil ik iedereen in mijn omgeving hiervoor bedanken.

Soms ging de interresse verder dan alleen het stellen van vragen. Graag wil ik Hens bedanken voor zijn suggesties voor hoofdstuk 7 en Dirk voor zijn aanmoediging om een datum aan te vragen.

Zonder paranimfen is een promotie niet compleet. Merle en Menno, alvast bedankt voor de morele steun (en het recht zetten van de overheadprojector).

Als laatste wil ik mijn afstudeerbegeleider Albert Janssen bedanken zonder wiens lichtende voorbeeld ik waarschijnlijk nooit was gaan promoveren…

Bas Meijer